A thesis submitted for the degree of
Doctor of Philosophy in Mechanical Engineering at the
Académie universitaire Wallonie-Europe
University of Liège, Liège, Belgium
Faculty of Applied Sciences

Patient-Specific Modeling of Extracorporeal Life Support Therapy

By **HABRAN Simon**, Chemical Engineer

Supervised by DAUBY Pierre, Ph.D.

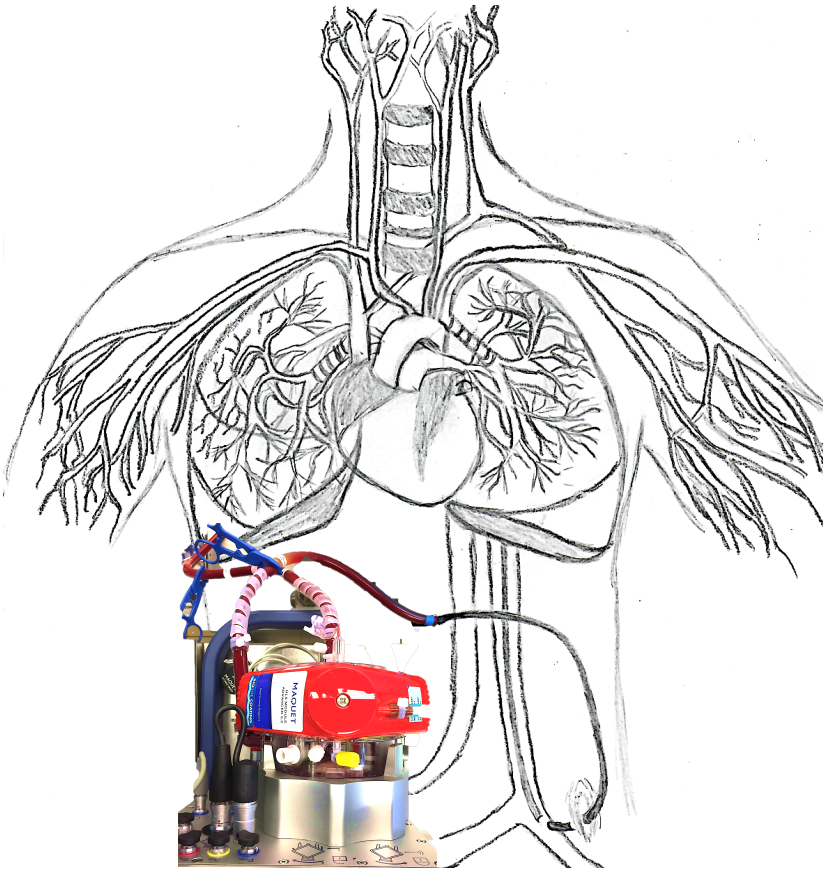

May 2018

"Declare the past, diagnose the present, foretell the future"
Hippocrates

The present dissertation has been evaluated by the jury members:

Prof. P. C. Dauby (supervisor),
University of Liège, Liège, Belgium

Dr T. Desaive,
University of Liège, Liège, Belgium

Dr P. Morimont,
CHU de Liège, Liège, Belgium

Prof. B. Lambermont,
CHU de Liège, Liège, Belgium

Dist. Prof. J. G. Chase,
University of Canterbury, Christchurch, New Zealand

Prof. D. Toye,
University of Liège, Liège, Belgium

Prof. J.-P. Ponthot,
University of Liège, Liège, Belgium

The research described in the present dissertation was financially supported by the Belgian National Funds for Scientific Research, F.R.S.-FNRS (PDR T.1058.14) in the context of the research project *MoCA* (Modeling of Cardiopulmonary Assistance).

Acknowledgements

The present work has been made possible by several collaborations and I would like to take the opportunity to thank some of them whose contributions were essential for the realization of this thesis.

First, Pierre Dauby, my supervisor, for suggesting me an interesting project including a Ph.D. thesis. He gave me my first professional opportunity which was full of stimulating experiences: public presentations, scientific writings, clinical trials and many others. I also thank him for his constant support and his wise advices. Thanks to his contribution, I have improved my scientific skills such as providing meticulous reports and giving unambiguous presentations.

Thomas Desaive, the head of the GIGA − in silico medicine department, for his permanent availability. He helped me many times for exploiting and analyzing experimental and clinical data. In addition, I thank him for revising all my writings.

Philippe Morimont and Bernard Lambermont, intensive care doctors from the Liège University Hospital (CHU), for enlightening me about medical concepts. They were always available for giving a medical point of view on the results.

Nathalie Janssen and Jean-paul Cheramy, employees of the CHU who have an important part in the animal experiments. Nathalie Janssen is a surgeon who placed all the medical tools in the cardiopulmonary system of the pigs. Jean-paul Cheramy is a lab technician who helped us several times for technical and logistical issues.

The perfusionist team from the Liège University Hospital, especially Théo Amand, Marc Lagny, Philippe Amabili, Dominique Hella, Francine Blaffart and Jonathan Goffoy, for sharing all their knowledge on extracorporeal life support and for introducing me to the intensive care unit of the CHU. With their collaboration, I was able to observed real patients assisted by an extracorporeal life support. This experience was very enriching for this study.

Sarah, Vincent, Antoine, Hatim and Ramin, my colleagues, for making the office a place of scientific discussions but also a place to live in harmony.

Finally, my family, my betrothed Hiba and my friends for their support and interest in my research. In particular, I wish to thank Emile, my nephew, for appearing in our world during the last year of my doctoral training. His cute little face helped me to put things into perspective during the difficult moments of finishing a doctoral thesis.

Résumé

Les assistances cardio-respiratoires extracorporelles, souvent désignées par l'abréviation anglophone ECLS (*ExtraCorporeal Life Support*), sont déjà largement utilisées dans de nombreux hôpitaux. Ces assistances permettent de subvenir aux besoins vitaux de patients souffrant de maladies respiratoires et/ou cardio-vasculaires sévères. Cependant, les cliniciens restent encore confrontés à plusieurs problèmes liés à l'utilisation de ces appareils médicaux et certaines améliorations des approches thérapeutiques associées seraient souhaitables.

Dans cette thèse, nous développons des modèles mathématiques simplifiés des systèmes respiratoire et cardiovasculaire couplés à un modèle d'ECLS. La plupart des paramètres qui apparaissent dans la description sont déterminés à partir de données cliniques et les modèles proposés sont donc patient-spécifiques. Ces modèles permettent de tester in silico diverses options thérapeutiques et devraient donc permettre au clinicien d'optimiser l'utilisation de l'ECLS.

Dans notre travail, une première validation des modèles mathématiques a été réalisée à l'aide de données expérimentales obtenues à partir de modèles animals sur le cochon. Ensuite, une seconde validation a été réalisée en utilisant des données cliniques. Les résultats obtenus sont très prometteurs et constituent une perspective encourageante dans le développement d'un outil qui permettra une utilisation des ECLS plus efficace et adaptée à chaque patient.

Abstract

Extracorporeal life support (ECLS) is already widely used for helping patients suffering from acute heart and/or lung pathologies. However, clinicians still face several issues with the use of ECLS and improvements of the associated therapeutic approaches in ICU would be beneficial.

In this thesis, mathematical models of the respiratory and cardiovascular systems coupled with a model of the ECLS are developed. Most parameters of the description are determined from clinical data and the models are thus patient-specific. Such models allow one to test in silico different therapeutic options and should thus help the clinicians to optimize the use of ECLS.

In our work, a first validation of our mathematical models has been performed using experimental data obtained on animal models with pigs. Then a second validation was carried out using clinical data. The obtained results are promising and provide an encouraging first step towards the development of a medical tool that will allow a more efficient and personalized use of ECLS in ICU.

Contents

List of Figures

List of Tables

List of Symbols and Abbreviations

Symbol	Unit	Meaning
Cardiovascular system		
A_h	ml^{-1}	Exponential parameter of the EDPVR equation
$A_{Sl,h}$	$\mathrm{s} \cdot \mathrm{ml}^{-2}$	Coefficient of the linear term of parameter A_h
$A_{0,h}$	ml^{-1}	Coefficient of the independent term of parameter A_h
B_h	mmHg	Pre-exponential parameter of the EDPVR equation
B_1	s^{-2}	First parameter of the cardiac driver function. This parameter does not depend on the cardiac period.
$B_{1,T}$	s^{-2}	First parameter of the cardiac driver function. This parameter depends on the cardiac period.
β	1	Parameter used for the correlation between the parameter $B_{1,T}$ and the cardiac period
C_1	s	Second parameter of the cardiac driver function. This parameter does not depend on the cardiac period.
$C_{1,T}$	s	Second parameter of the cardiac driver function. This parameter depends on the cardiac period.
CO	ml/s	Cardiac output
$\overline{\Delta\overline{P}_a/\overline{P}_a}$	1	Mean of the relative difference between the $\overline{P}_a$ simulated with the mathematical model and the corresponding experimental data.
$\overline{\Delta PP_a/PP_a}$	1	Mean of the relative difference between the PP_a simulated with the mathematical model and the corresponding experimental data.
$\overline{\Delta\overline{P}_v/\overline{P}_v}$	1	Mean of the relative difference between the $\overline{P}_v$ simulated with the mathematical model and the corresponding experimental data.

$\frac{\Delta \max_{\mathrm{T}}(V_h)}{\max_{\mathrm{T}}(V_h)}$	1	Mean of the relative difference between the $\max_{\mathrm{T}}(V_h)$ simulated with the mathematical model and the corresponding experimental data.
$\overline{\Delta SV/SV}$	1	Mean of the relative difference between the SV simulated with the mathematical model and the corresponding experimental data.
$\Delta_1 A_h/A_h$	1	Relative variation of parameter A_h for a variation of $Q_d = 1$ l/min.
$\Delta_1 E_a/E_a$	1	Relative variation of parameter E_a for a variation of $Q_d = 1$ l/min.
$\Delta_1 E_h/E_h$	1	Relative variation of parameter E_h for a variation of $Q_d = 1$ l/min.
$\Delta_1 SBV/SBV$	1	Relative variation of parameter SBV for a variation of $Q_d = 1$ l/min.
$\Delta_1 R_s/R_s$	1	Relative variation of parameter R_s for a variation of $Q_d = 1$ l/min.
$\Delta_3 A_h/A_h$	1	Relative variation of parameter A_h for a variation of $Q_d = 3$ l/min.
$\Delta_3 E_a/E_a$	1	Relative variation of parameter E_a for a variation of $Q_d = 3$ l/min.
$\Delta_3 E_h/E_h$	1	Relative variation of parameter E_h for a variation of $Q_d = 3$ l/min.
$\Delta_3 SBV/SBV$	1	Relative variation of parameter SBV for a variation of $Q_d = 3$ l/min.
$\Delta_3 R_s/R_s$	1	Relative variation of parameter R_s for a variation of $Q_d = 3$ l/min.
$\mathbf{e}$	$[m \times 1]$	Fictive error on the measurements. m is the number of measurements for one extracorporeal blood flow.
e_1	1	Error on $\overline{P}_a$
e_2	1	Error on PP_a
e_3	1	Error on $\overline{P}_v$
e_4	1	Error on $\max_{\mathrm{T}}(V_h)$ (error on SV in the appendix).
E_a	mmHg/ml	Elastance of the arteries
E_h	mmHg/ml	Slope of the ESPVR equation. This parameter defined the contractility of the heart.
$E_{Sl,a}$	$\mathrm{mmHg \cdot s \cdot ml^{-2}}$	Coefficient of the linear term of parameter E_a
$E_{Sl,h}$	$\mathrm{mmHg \cdot s \cdot ml^{-2}}$	Coefficient of the linear term of parameter E_h
$E_{0,a}$	mmHg/ml	Coefficient of the independent term of parameter E_a
$E_{0,h}$	mmHg/ml	Coefficient of the independent term of parameter E_h
E_v	mmHg/ml	Elastance of the veins
EF	1	Ejection fraction of the left ventricle

$e(t)$	1	Cardiac driver function
ϕ_{LVOT}	cm	Diameter of the left ventricular outflow tract
γ	1	Parameter used for the correlation between the parameter $C_{1,T}$ and the cardiac period
H(x)	1	Heaviside function
HR	s^{-1}	Heart rate
$\max_T(V_h)$	ml	Maximum blood volume in the heart (diastolic volume in the left ventricle)
$\mathbf{p}$	$[5 \times 1]$	Vector containing the 5 parameters of the cardiovascular model
$\mathbf{p}^*$	$[5 \times 1]$	Vector containing the 5 parameters of the cardiovascular model and their values minimized the error function Φ
P_a	mmHg	Blood pressure in the arteries
$\overline{P}_a$	mmHg	Mean blood pressure in the arteries
PP_a	mmHg	Pulse blood pressure in the arteries
P_{atm}	mmHg	Atmospheric pressure
P_{ed}	mmHg	End-diastolic pressure in the heart
P_{es}	mmHg	End-systolic pressure in the heart
P_h	mmHg	Blood pressure in the heart
P_{pump}	mmHg	Hydraulic pressure in the pump
P_X	mmHg	Hydraulic pressure in the accumulation chamber
P_v	mmHg	Blood pressure in the veins
$\overline{P}_v$	mmHg	Mean blood pressure in the veins
Ψ	1	Error function used for the identification of the cardiovascular system
Q_i	ml/s	Blood flow crossing the input valve of the heart
Q_o	ml/s	Blood flow crossing the output valve of the heart
Q_{pump}	ml/s	Water flow ejected from the pump
Q_s	ml/s	Systemic blood flow
Q_X	ml/s	Water flow in the accumulation chamber
SV	ml	Stroke volume
R_i	$\text{mmHg} \cdot \text{s/ml}$	Resistance of the input valve
R_o	$\text{mmHg} \cdot \text{s/ml}$	Resistance of the output valve
R_s	$\text{mmHg} \cdot \text{s/ml}$	Systemic resistance
$R_{Sl,s}$	$\text{mmHgs}^2 \cdot \text{ml}^{-2}$	Coefficient of the linear term of parameter R_s
$R_{0,s}$	$\text{mmHg} \cdot \text{s/ml}$	Coefficient of the independent term of parameter R_s
SBV	ml	Stress blood volume
SBV_{Sl}	s	Coefficient of the linear term of parameter SBV
SBV_0	ml	Coefficient of the independent term of parameter SBV
$\sigma_{\overline{P}_a}$	mmHg	Measurement error on $\overline{P}_a$
$\sigma_{\overline{P}_v}$	mmHg	Measurement error on $\overline{P}_v$
σ_{PP_a}	mmHg	Measurement error on PP_a
$\sigma_{\max_T(V_h)}$	ml	Measurement error on $\max_T(V_h)$

σ_{SV}	ml	Measurement error on SV
T	s	Cardiac period
V_h	ml	Heart blood volume
V_s	ml	Stressed volume
$V_{s,a}$	ml	Stress blood volume in the arteries
$V_{s,h}$	ml	Stressed blood volume in the heart
$V_{s,v}$	ml	Stressed blood volume in the veins
V_u	ml	Unstressed volume
$V_{u,h}$	ml	Unstressed blood volume in the heart
V_X	ml	Water volume in the accumulation chamber
VTI	cm	Velocity time integral across the left ventricular outflow tract
$\mathbf{y^{data}}$	$[m \times n]$	Matrix containing the different experimental data used for the identification of the cardiovascular system. m is the number of measurements for one extracorporeal blood flow and n is the number of extracorporeal blood flows used for the identification.
$\mathbf{y^{model}}$	$[m \times n]$	Matrix containing the different hemodynamic values simulated by the cardiovascular model. m is the number of the hemodynamic values used for the identification for one extracorporeal blood flow. n is the number of extracorporeal blood flows used for the identification.
Respiratory system		
α_{O_2}	ml_{O_2}/ml/mmHg	Solubility coefficient of O_2 in blood plasma
α_{CO_2}	ml_{CO_2}/ml/mmHg	Solubility coefficient of CO_2 in blood plasma
$avDCO_2$	ml_{CO_2}/ml	Arterial-venous CO_2 difference (the difference between O_2 concentrations in the arteries and veins)
$avDO_2$	ml_{O_2}/ml	Arterial-venous O_2 difference (the difference between O_2 concentrations in the arteries and veins)
C_{a,CO_2}	(ml_{CO_2}/ml)	Total CO_2 concentration in the arteries
C_{a,O_2}	(ml_{O_2}/ml)	Total O_2 concentration in the arteries
C_{Hb}	(ml_{Hb}/ml)	Hemoglobin concentration
C_{CO_2}	(ml_{CO_2}/ml)	Total CO_2 concentration
C_{l,CO_2}	(ml_{CO_2}/ml)	Total CO_2 concentration in the lungs (pulmonary capillaries)
C_{l,O_2}	(ml_{O_2}/ml)	Total O_2 concentration in the lungs (pulmonary capillaries)
C_{O_2}	(ml_{O_2}/ml)	Total O_2 concentration
C_{Pl,CO_2}	(ml_{CO_2}/ml)	Total CO_2 concentration in blood plasma
C_{ra,CO_2}	(ml_{CO_2}/ml)	Total CO_2 concentration in the right atrium
C_{ra,O_2}	(ml_{O_2}/ml)	Total O_2 concentration in the right atrium
C_{v,CO_2}	(ml_{CO_2}/ml)	Total CO_2 concentration in the veins
C_{v,O_2}	(ml_{O_2}/ml)	Total O_2 concentration in the veins

D_{Hb}	1	Dilution factor of the hemoglobin when the ECLS is switched on
$\Delta C_{Hb}/C_{\mathrm{Hb}}$	1	Relative variation of the hemoglobin concentration between the baseline situation and the ECLST
$\Delta f_s/f_s$	1	Relative variation of the pulmonary shunt between the baseline situation and the change of the ventilator settings
$\overline{\Delta P_{\mathrm{CO}_2}}$	mmHg	Mean of the difference between the PCO_2 simulated with the mathematical model and the corresponding experimental data.
$\lvert\overline{\Delta P_{\mathrm{CO}_2}}\rvert$	mmHg	Absolute value of the mean of the difference between the PCO_2 simulated with the mathematical model and the corresponding experimental data.
$\overline{\Delta P_{\mathrm{CO}_2}/P_{\mathrm{CO}_2}}$	1	Mean of the relative difference between the PCO_2 simulated with the mathematical model and the corresponding experimental data.
$\lvert\overline{\Delta P_{\mathrm{CO}_2}/P_{\mathrm{CO}_2}}\rvert$	1	Absolute value of the mean of the relative difference between the PCO_2 simulated with the mathematical model and the corresponding experimental data.
$\overline{\Delta P_{\mathrm{O}_2}}$	mmHg	Mean of the difference between the PO_2 simulated with the mathematical model and the corresponding experimental data.
$\lvert\overline{\Delta P_{\mathrm{O}_2}}\rvert$	mmHg	Absolute value of the mean of the difference between the PO_2 simulated with the mathematical model and the corresponding experimental data.
$\overline{\Delta P_{\mathrm{O}_2}/P_{\mathrm{O}_2}}$	1	Mean of the relative difference between the PO_2 simulated with the mathematical model and the corresponding experimental data.
$\lvert\overline{\Delta P_{\mathrm{O}_2}/P_{\mathrm{O}_2}}\rvert$	1	Absolute value of the mean of the relative difference between the PO_2 simulated with the mathematical model and the corresponding experimental data.
$\Delta\dot{V}_A/\dot{V}_A$	1	Relative variation of the alveolar ventilation between the baseline situation and the change of the ventilator settings
$\Delta\dot{V}_E/\dot{V}_E$	1	Relative variation of the minute ventilation between the baseline situation and the change of the ventilator settings
F_{I,CO_2}	1	Inspired fraction of CO_2
F_{I,O_2}	1	Inspired fraction of O_2
F_{L,CO_2}	1	CO_2 volume fraction in the lungs (alveoli)
F_{L,O_2}	1	O_2 volume fraction in the lungs (alveoli)
f_r	s^{-1}	Respiratory frequency
f_s	1	Fraction of the pulmonary blood flow crossing the pulmonary shunt

$(f_s)_{Baseline}$	1	Fraction of the pulmonary blood flow crossing the pulmonary shunt during baseline situation
$(f_s)_{PV}$	1	Fraction of the pulmonary blood flow crossing the pulmonary shunt after the change of the ventilator settings
$k_{\mathrm{HCO_3}}$	$(\mathrm{ml_{CO_2}/ml})$	Correction term which is introduced to compensate for variations between individuals in standard HCO_3 concentration
$K_{\mathrm{HCO_3}}$	1	Equilibrium constant of the CO_2 hydratation/dehydratation reaction
$MR_{\mathrm{CO_2}}$	$\mathrm{ml_{CO_2}/s}$	Global production of CO_2 by metabolism
$MR_{\mathrm{O_2}}$	$\mathrm{ml_{O_2}/s}$	Global production of O_2 by metabolism
$\mathrm{PCO_2}$	mmHg	CO_2 partial pressure
$\mathrm{PH_2O}$	mmHg	H_2O partial pressure
$P_{I,\mathrm{CO_2}}$	mmHg	Inspired CO_2 partial pressure
$P_{I,\mathrm{O_2}}$	mmHg	Inspired O_2 partial pressure
$P_{L,\mathrm{CO_2}}$	mmHg	CO_2 partial pressure in the air contained in the lungs (alveoli)
$P_{L,\mathrm{O_2}}$	mmHg	O_2 partial pressure in the air contained in the lungs (alveoli)
$\mathrm{PN_2}$	mmHg	N_2 partial pressure
$\mathrm{PO_2}$	mmHg	O_2 partial pressure
Q_a	ml/s	Alveolar perfusion
Q_c	ml/s	Capillary perfusion
Q_p	ml/s	Pulmonary blood flow
Q_s	ml/s	Systemic blood flow
RQ	1	Respiratory quotient
$Sat_{\mathrm{O_2}}$	1	Saturation of hemoglobin with O_2
S	$\mathrm{mmHg^{-1}}$	Empiric parameter which accounts for the Bohr effect
τ_{HL}	s	Transport delay from the heart (right atrium) to the lungs (pulmonary capillaries)
τ_{LT}	s	Transport delay from the lungs (pulmonary capillaries) to the tissues
τ_{TH}	s	Transport delay from the tissues to the heart (right atrium)
$\dot{V}_A$	ml/s	Alveolar ventilation
$\left(\dot{V}_A\right)_{Baseline}$	ml/s	Alveolar ventilation during baseline situation
$\left(\dot{V}_A\right)_{PV}$	ml/s	Alveolar ventilation after the change of the ventilator settings
V_{Dead}	ml	Dead space volume
$\dot{V}_E$	ml/s	Minute ventilation
V_E	ml	Respiratory volume
$V_{L,\mathrm{CO_2}}$	$\mathrm{ml_{CO_2}}$	Effective volume of CO_2 in the lungs
$\dot{V}_{L,\mathrm{CO_2}}$	$\mathrm{ml_{CO_2}/s}$	CO_2 extraction in the lungs

V_{L,O_2}	$\mathrm{ml}_{\mathrm{O}_2}$	Effective volume of O_2 in the lungs
$\dot{V}_{L,\mathrm{O}_2}$	$\mathrm{ml}_{\mathrm{O}_2}$/s	O_2 supply in the lungs
V_T	ml	Tidal volume
V_{T,CO_2}	$\mathrm{ml}_{\mathrm{CO}_2}$	Effective volume of CO_2 in the tissues
V_{T,O_2}	$\mathrm{ml}_{\mathrm{O}_2}$	Effective volume of O_2 in the tissues
V_{TB}	ml	Total blood volume
χ_{HL}	1	Blood volume ratio in the blood vessels located between the heart (right atrium) and the lungs (pulmonary capillaries)
χ_{LT}	1	Blood volume ratio in the blood vessels located between the lungs (pulmonary capillaries) and the tissues
χ_{TH}	1	Blood volume ratio in the blood vessels located between the tissues and the heart (right atrium)
ECLS system		
D_{CO_2}	$\mathrm{ml}_{\mathrm{CO}_2}$/s/mmHg	Global CO_2 diffusion coefficient across the synthetic membrane for the ECLS model Mod 1
D_{O_2}	$\mathrm{ml}_{\mathrm{O}_2}$/s/mmHg	Global O_2 diffusion coefficient across the synthetic membrane for the ECLS model Mod 1
D'_{CO_2}	$\mathrm{ml}_{\mathrm{CO}_2}$/s/mmHg	Global CO_2 diffusion coefficient across the synthetic membrane for the ECLS model Mod 2
D'_{O_2}	$\mathrm{ml}_{\mathrm{O}_2}$/s/mmHg	Global O_2 diffusion coefficient across the synthetic membrane for the ECLS model Mod 2
D_{s,CO_2}	$\mathrm{ml}_{\mathrm{CO}_2}$/s/mmHg/cm^2	CO_2 diffusion coefficient across the synthetic membrane
D_{s,O_2}	$\mathrm{ml}_{\mathrm{O}_2}$/s/mmHg/cm^2	O_2 diffusion coefficient across the synthetic membrane
C_{in,CO_2}	$\mathrm{ml}_{\mathrm{CO}_2}$/ml	CO_2 concentration at the inlet cannula
C_{in,O_2}	$\mathrm{ml}_{\mathrm{O}_2}$/ml	O_2 concentration at the inlet cannula
C_{m,CO_2}	$\mathrm{ml}_{\mathrm{CO}_2}$/ml	CO_2 concentration in blood along the synthetic membrane
C_{m,O_2}	$\mathrm{ml}_{\mathrm{O}_2}$/ml)	O_2 concentration in blood along the synthetic membrane
C_{out,CO_2}	$\mathrm{ml}_{\mathrm{CO}_2}$/ml	CO_2 concentration at the outlet cannula
C_{out,O_2}	$\mathrm{ml}_{\mathrm{O}_2}$/ml	O_2 concentration at the outlet cannula
f_d	1	Fraction of the systemic blood flow entering the inlet cannula
F_{D,CO_2}	1	CO_2 volume fraction in the gas leaving the extracorporeal device
F_{D,O_2}	1	O_2 volume fraction in the gas leaving the extracorporeal device
F_{ID,CO_2}	1	CO_2 volume fraction in the gas entering the extracorporeal device
F_{ID,O_2}	1	O_2 volume fraction in the gas entering the extracorporeal device

F_{M,CO_2}	1	CO_2 volume fraction in the gas along the synthetic membrane
F_{M,O_2}	1	O_2 volume fraction in the gas along the synthetic membrane
k_{recir}	s/ml	Parameter of the recirculation equation in function of the extracorporeal blood flow.
P_{D,CO_2}	mmHg	CO_2 partial pressure in the gas leaving the extracorporeal device
P_{D,O_2}	mmHg	O_2 partial pressure in the gas leaving the extracorporeal device
P_{m,CO_2}	mmHg	CO_2 partial pressure in blood along the synthetic membrane
P_{M,CO_2}	mmHg	CO_2 partial pressure in the gas along the synthetic membrane
P_{m,O_2}	mmHg	O_2 partial pressure in blood along the synthetic membrane
P_{M,O_2}	mmHg	O_2 partial pressure in the gas along the synthetic membrane
P_{out,CO_2}	mmHg	CO_2 partial pressure at the outlet cannula
P_{out,O_2}	mmHg	O_2 partial pressure at the outlet cannula
R_{recir}	1	Fraction of the recirculation in the extracorporeal blood flow
Q_d	ml/s	Extracorporeal blood flow
S_m	cm^2	Exchange surface of the membrane
τ_{IN}	s	Transport delay from the right atrium to the ECLS
τ_{OUT}	s	Transport delay from the ECLS to the right atrium
$\dot{V}_D$	ml/s	Gas flow crossing the ECLS
V_d	ml	Volume in the blood side of the ECLS
V_D	ml	Volume in the gas side of the ECLS
V_{IN}	ml	Volume of the extracorporeal circulation transporting blood from the patient to the ECLS
V_{OUT}	ml	Volume of the extracorporeal circulation transporting blood from the ECLS to the patient
X	1	Nondimensional 1-D coordinate along the synthetic membrane

Abbreviation	Meaning
ARDS	Acute respiratory distress syndrome
BSA	Body surface area
BTPS	Body temperature and ambient pressure, water satured
CHU	French abbreviation of *Centre Hospitalier Universitaire*
Clinical trial R	Retrospective clinical trial of patients assisted by a vv-ECLS
Clinical trial S	Clinical trial of patients assisted by a $ECCO_2RD$ and following a stringent protocol (Supernova study).
COPD	Chronic obstructive pulmonary disease
CO_2	Carbon dioxide
$ECCO_2RD$	Extracorporeal CO_2 removal device
$ECCO_2RT$	Extracorporeal CO_2 removal therapy
ECLS	Extra-corporeal life support
ECLST	Extra-corporeal life support therapy
ECMO	Extracorporeal membrane oxygenation
EDPVR	End-diastolic pressure volume relationship
ESPVR	End-systolic pressure volume relationship
Experiments A	Experiments carried out on pigs suffering from ARDS
Experiments H	Experiments carried out on "healthy" pigs
H^+	Hydrogen ion or proton
Hb	Hemoglobin
HCO_3^-	Bicarbonate ion or hydrogen carbonate ion
ICU	Intensive care unit
LVOT	Left ventricular outflow tract
Mod 1	ECLS model when the the geometry is reduced to one dimension and when the gas and blood flows are in opposite direction
Mod 2	ECLS model when the gas and liquid compartments are considered as perfectly mixed.
Mod 3	ECLS model when the hypothesis of equilibrium between blood and gas is considered.
MSFP	Mean circulatory filling pressure
O_2	Oxygen
PV loop	Pressure-volume loop
STPD	Standard temperature and ambient pressure, water dry
va-ECLS	Venoarterial extra-corporeal life support
vv-ECLS	Venovenous extra-corporeal life support

Chapter 1

Introduction

1.1 Extracorporeal life support

Extracorporeal life support (ECLS) is used to help patients suffering from acute heart failure and/or acute lung pathologies. When the heart and/or the lungs of such patients are not capable of ensuring the vital functions (O_2 and CO_2 gas exchanges in the blood and the circulation of blood), ECLS is used to support the main tasks of these organs until patient recovery. Such devices are now commonly used already been used many times all around the world since the first ECLS therapy was performed in 1971 [99]. However, even if new technologies have contributed to several improvements of the different components of the ECLS (components size reduction, efficacy and hemocompatibility improvements), the side effects and the complications related to the use of an ECLS remain high [99]. Therefore, a better understanding of ECLS is necessary to develop new therapeutic approaches, and at the end increase the patient safety.

The ECLS can be set up in different configurations according to the pathology of the patient. If the patient has a severe heart pathology, or a severe cardiopulmonary pathology, the clinicians use the ECLS in the venoarterial configuration whereas if the patient has a pulmonary disorder without heart failure, such as an acute respiratory distress syndrome (ARDS), the ECLS is rather used in the venovenous configuration. These two main configurations have numerous distinct properties and the therapeutic approaches are thus different. Therefore, the venoarterial ECLS (va-ECLS) and the venovenous ECLS (vv-ECLS) are studied separately in this dissertation.

1.1.1 Venoarterial ECLS (va-ECLS)

The standard configuration of a va-ECLS for an adult is the following: the cannula extracting the venous blood is inserted into the femoral vein and placed just below the junction of the right atrium and the inferior vena cava, while the cannula reinjecting the extracorporeal blood flow is inserted into the femoral artery and placed in the aortic arch. One of the main issues that clinicians have to deal with is the weaning of va-ECLS. Indeed, since this configuration takes a fraction of the systemic blood flow in the veins and rejects it in the arteries, the va-ECLS "hides" the true hemodynamics of the heart by decreasing the preload and increasing the afterload. Consequently, the medical team has to perform weaning tests by decreasing the extracorporeal blood flow to approximately 0.5 l/min. With this small extracorporeal blood flow, the interaction of the va-ECLS with the heart is much smaller and the real hemodynamics of the heart can be evaluated by measuring the mean arterial pressure, the ejection fraction in the left ventricle and the velocity time integral [4]. However, small blood flows in the ECLS increase the risk of coagulation and the concentration of heparin must be increased during the weaning tests. The drawback of heparin is the risk of hemorrhages, one of the main complications of ECLS.

1.1.2 Venovenous ECLS (vv-ECLS)

The standard configuration of a vv-ECLS for an adult is the following: the cannula extracting the venous blood is inserted into the femoral vein and placed just below the junction of the right atrium and the inferior vena cava, while the cannula reinjecting the extracorporeal blood flow is inserted into the right internal jugular vein and placed in the superior vena cava. This configuration does not directly influence the hemodynamics of the heart since the vv-ECLS extracts and reinjects the blood almost at the same location of the cardiovascular system. The important features of the vv-ECLS are thus an adequate O_2 supply and an adequate CO_2 removal. Nowadays, the ECLS settings to achieve these goals are empirically chosen by the clinicians after the ECLS is switched on. A different approach would consist in estimating the optimal settings of the vv-ECLS before inserting the cannulae, which could be useful to improve the therapeutic strategy. In particular, a new kind of vv-ECLS has recently been developed: the extracorporeal CO_2 removal device ($ECCO_2RD$). $ECCO_2RD$ has already been used for patients suffering from moderate ARDS ($Pa_{O_2}/F_{I,O2} > 100$ mmHg [31], where Pa_{O_2} is the arterial partial pressure in O_2 and $F_{I,O2}$ is the inspired oxygen fraction) or chronic obstructive pulmonary disease (COPD) [75, 11, 30, 110, 1, 104]. This device is characterized by a small extracorporeal blood flow and it could be helpful to estimate the quantity of CO_2 removal. With this information, the medical team could decide if this new technology can be used for a specific patient.

1.2 Approach

The study developed in this thesis aims to predict the physiological response of patients assisted by ECLS. To achieve this goal, this dissertation develops a mathematical model of the cardiovascular system connected to a va-ECLS and a mathematical model of the respiratory system connected to a vv-ECLS. Then, the parameters of the mathematical models are estimated with the measurements available in the intensive care unit (ICU). This parameter identification thus turns clinical data into patient-specific parameters.

1.2.1 Mathematical models

Mathematical models are used to represent complex systems in order to improve the knowledge of such systems in different situations. The models also try to predict the behavior of the system for a specific situation. The cardiovascular and the respiratory systems are very complex, but the models developed in this study are quite simplified with the aim to be identifiable with the available measurements in the ICU and to obtain small computation times. Therefore, *lumped* models of the cardiovascular system connected to a va-ECLS and of the respiratory system connected to a vv-ECLS are used in this study. These models consist in gathering different components of a system together in several "boxes". The use of such mathematical models to improve health care in the ICU becomes increasingly demanded and many similar models are currently developed to provide personalised model-based cares (a review on these questions is proposed in [22]).

Cardiovascular model connected to a va-ECLS Many cardiovascular models have already been developed in literature [18, 107, 86, 105, 67, 21, 47, 95, 97, 17] but only a few have studied the interaction between a va-ECLS and the cardiovascular system. Broomé *et al.* [17] have built such a mathematical model but their model is very complex (32 compartments for the cardiovascular system and 1 ECLS compartment) and many parameters cannot be identified with the data available in the ICU. Their model is thus very hard to be made patient-specific. On the other hand, a minimal model of the cardiovascular system was proposed by Pironet *et al.* [89] and shown identifiable in ICU. The purpose of our work is to complement this latter model by an additional compartment describing the va-ECLS [44].

Respiratory model connected to a vv-ECLS Scientists have already developed several mathematical models of the respiratory system to describe lung and tissues gas exchanges [37, 113, 9] but these models rarely take into account pulmonary gas exchange abnormalities like ARDS and COPD. Some authors have proposed to model these pathologies

by including a perfusion/ventilation mismatch [54] or by decreasing the diffusion across the alveolar capillary membrane [93]. On top of this, very few authors have developed models of the respiratory system connected to an ECLS [14, 116, 74, 72]. The models of Walter *et al.* [116] and Brendel *et al.* [14] describe lung, tissues and ECLS gas exchanges but to account for gas exchange abnormalities in the lung, these authors introduce two purely empirical parameters. An appropriate description of gas exchange abnormalities is of paramount importance in this work and parameters with a clear physiological interpretation are introduced to describe these abnormalities. Moreover, the goal of the authors cited above is different from ours since they use their models in a control algorithm designed to maintain appropriate long-term gas contents of the blood, while our approach will help clinicians determining the best settings of an ELCS before it is used [42, 43, 45].

1.2.2 Parameter identifications

To obtained a patient-specific model, parameters have be identified from measurements commonly available in the ICU. The word *patient-specific* means that the mathematical models can be adapted to each patient and these models provide different results according to the specific clinical conditions of the patient. However, clinical data are extremely limited and several parameters cannot be identified even if the mathematical models are simplified. Moreover, the model parameters should be uniquely identified from the measurements to turn clinical data into patient-specific parameters [89]. Consequently, the parameter identification is a delicate but essential procedure in order to develop personalised model-based care.

1.3 Goals

This study has several objectives and 5 mains goals can be enumerated:

1. Developing a simple model of the cardiovascular system connected to a va-ECLS and a simple model of the respiratory system connected to a vv-ECLS.

2. Estimating the parameters of the models with the aim of being as much patient-specific as possible.

3. Testing and validating the 2 models with animal experiments. For the cardiovascular model connected to a va-ECLS, the tests are performed during the weaning tests from this device. For the respiratory model connected to a vv-ECLS, the tests are performed during the first hours of an extracorporeal life support therapy (ECLST).

4. Testing and validating the 2 models with clinical retrospective data. For the cardiovascular model connected to a va-ECLS the tests are performed during the weaning of this device. For the respiratory model connected to a vv-ECLS the tests are performed during the first hours of an ECLST.

5. Developing medical tools in order to help clinicians to improve their therapeutic approach. These tools will provide a personalised therapy.

The goals 1, 2, 3, and 4 are respectively developed in Part II, Part III, Part IV and Part V of this thesis. The last goal is in fact a long-term follow-up of our study and a first approach is introduced in Chapter 12.

1.4 Thesis organization

This thesis is divided into 5 main parts, each of them briefly introduced below.

Part I describes the cardiovascular and respiratory systems and introduces the usefulness and the key features of ECLS. The understanding of this medical background is useful for the next parts of the thesis. This part is divided into 2 chapters: Chapter 2 and Chapter 3 for, respectively, the description of the cardiopulmonary system and the ECLS.

Part II describes the modeling of the cardiovascular and respiratory systems and the ECLS. This part is divided into 2 chapters. Chapter 4 introduces the different compartments of the cardiovascular model connected to a va-ECLS, which are the arteries, the veins, the heart and the ECLS. Chapter 5 introduces the different compartments of the respiratory model connected to a vv-ECLS, which are the tissues, the lungs and the ECLS.

Part III presents the parameter identification for both models and is divided into 2 chapters: Chapter 6 for the cardiovascular model and Chapter 7 for the respiratory model.

Part IV describes the use of the models to simulate the cardiovascular system connected to a va-ECLS and the respiratory system connected to a vv-ECLS. This part compares the mathematical simulations with data obtained from pig experiments, with the aim to validate the mathematical model. Chapter 8 describes the validation of the cardiovascular model during the weaning tests from a va-ECLS while Chapter 9 describes the validation of the respiratory model during the first hours of an ECLST.

Part V is similar to Part IV except that the simulations are compared to clinical data obtained in the ICU. Chapter 10 describes the validation of the cardiovascular model during the weaning tests from a va-ECLS in the ICU while Chapter 11 describes the validation of the respiratory model during the first hours of an ECLST in the ICU. The last chapter presents conclusions and discusses a future approach to improve the use of ECLS in the ICU.

Part I

Medical background

The first part of this thesis introduces the elementary concepts in the medical field which are essential to understand our study. This part is composed of two chapters; Chapter 2 and Chapter 3. Chapter 2 describes the physiology of the cardiopulmonary system. The basic functionnings of the heart, the vessels and the lungs are explicated. Chapter 3 discusses the usefulness of extracorporeal circulations in intensive care unit. The main components and the different applications of these devices are also described in this chapter.

Chapter 2

Physiological background

Before modeling complex physiological systems such as the cardiovascular system, a good understanding of these systems is necessary. Therefore, this chapter gives a brief introduction of the cardiovascular and respiratory physiologies. Since the cardiovascular model and the respiratory model described in the following chapters are macroscopic models, the physiological descriptions will be limited to a macroscopic study; a molecular or a cellular study is not necessary. In addition, a macroscopic description of the blood chemistry is also provided in this chapter.

2.1 Cardiovascular system

The cardiovascular system is composed of two main systems: the heart and the vascular system. The heart can be considered as a pump and the vascular system can be considered as the pipes transporting blood. The description of these two systems is given in this section.

2.1.1 Physiology of the heart

The heart is a complex pump which draws blood in and rejects it following a cardiac cycle. The different components and the mechanisms of this pump are described below.

Anatomy

The heart has four cardiac chambers: the left and right ventricles and the left and right atria (Figure 2.1). All cardiac chambers are subject to contraction and the corresponding work is delivered by the cardiac muscle also called myocardium. The left and right ventricles are separated by the intraventricular septum. Therefore, the two ventricles actually work like two independent pumps. The left and right atria are located just before the left

and right ventricles respectively and, when they contract, they fill the ventricles actively. The atria thus act like a weak primer pump. These two cardiac chambers are separated from the ventricles by tricuspid valve and mitral valve for the right side and the left side of the heart respectively. In addition to these two valves, the heart has a pulmonary valve at the entrance of the pulmonary artery and an aortic valve at the entrance of the aorta. These four valves force blood to circulate in one direction. Indeed, when the blood flow crosses a valve in the right direction (see the arrows in Figure 2.1) this valve is opened, otherwise, it is closed. Figure 2.1 also illustrates the veins and the arteries which are directly connected to the heart. While blood enters the right atrium from the inferior and superior vena cava and goes out from the right ventricle towards the pulmonary artery, blood enters the left atrium from pulmonary vein and goes out from the left ventricle towards the aorta.

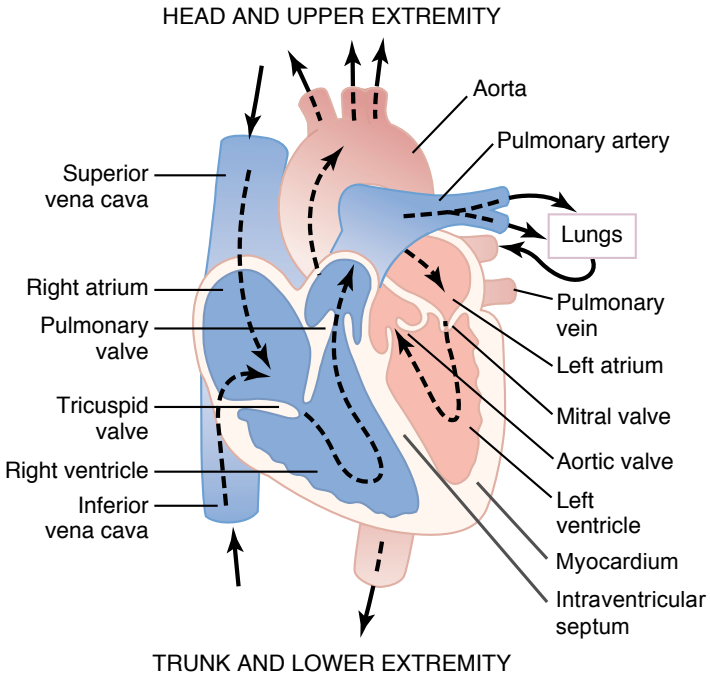

Figure 2.1 – Anatomy of the heart and the blood circulation through the heart chambers and the heart valves [46].

Cardiac cycle

For every cardiac beat, the heart follows a cycle which can be divided into 6 main steps [46] (Figure 2.2):

1. Isovolumic contraction of the ventricles: for this step, all cardiac valves are closed while the myocardium is contracting. Consequently, the pressure in the ventricular

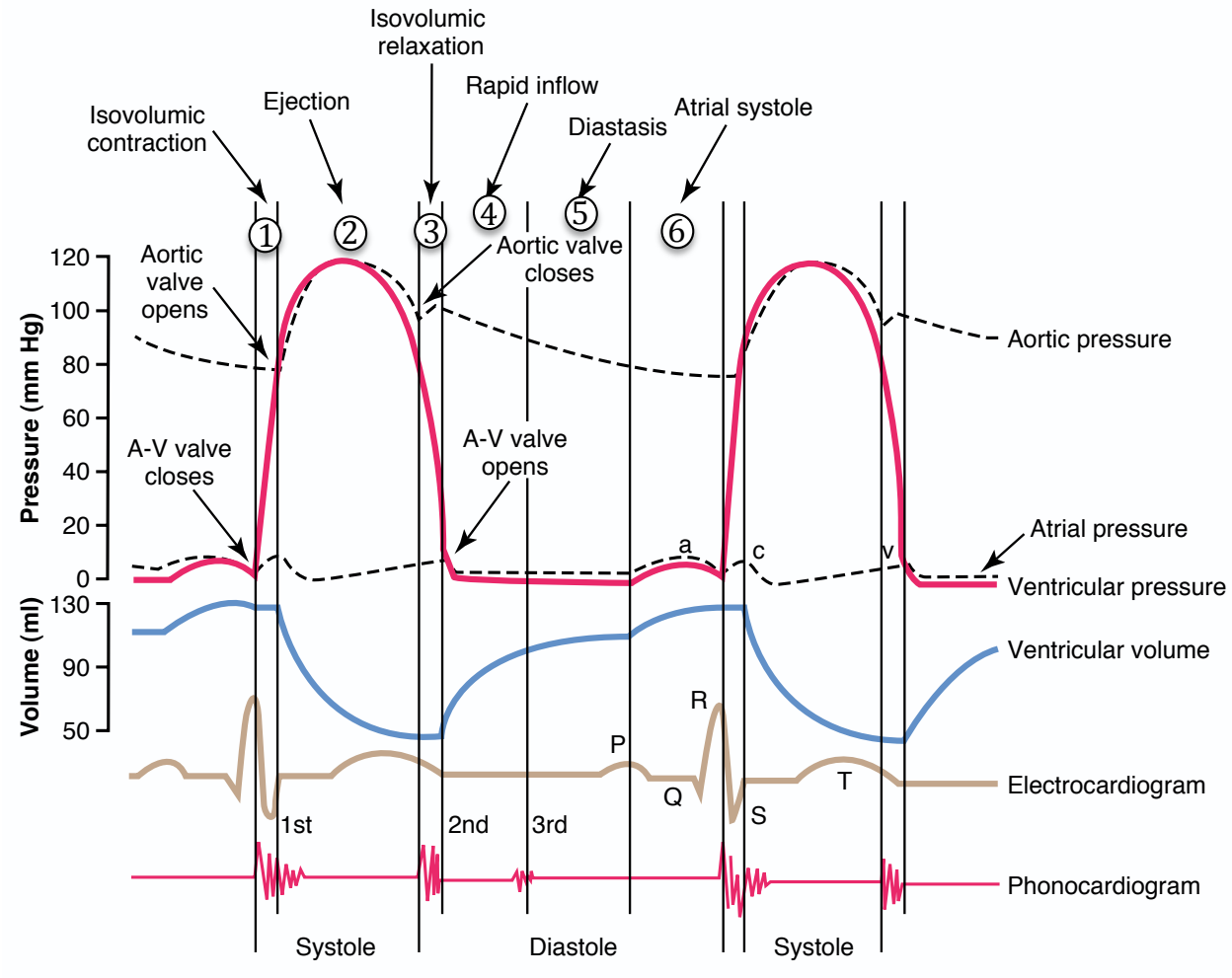

Figure 2.2 – Cardiac cycle for left ventricle. The figure depict changes in left arterial pressure, left ventricular pressure, aortic pressure, ventricular volume, the electrocardiogram and the phonocardiogram [46].

chambers increases.

2. Ejection of blood from the ventricles: the contraction continues and the pressure in the ventricles becomes larger than in the aorta for the left ventricle and than in the pulmonary artery for the right ventricle. So, the aortic valve and the pulmonary valve open and blood goes out of the ventricles. As a result, the volume in the ventricles decreases during this step.

3. Isovolumic relaxation of the ventricles: all cardiac valves are closed and the myocardium relaxes. Consequently, the pressure in the ventricular chambers decreases.

4. Rapid inflow in the ventricles: the pressure in the ventricles becomes lower than in the atria and blood enters the ventricles. Hence, the volume in the ventricles

increases during this step.

5. Diastasis of the ventricles: the blood flow in the ventricles decreases, the heart is subject to very small changes during this step.

6. Atrial systole: the atria contract and the ventricles are filled actively. After that, the isovolumic contraction of the ventricles occurs and the cardiac cycle starts again.

The aortic pressure, the left ventricular pressure and volume for the 6 steps are depicted in Figure 2.2. These values correspond to an adult in a physiological situation. The two panels at the bottom of Figure 2.2 describe the electric cardiac activity (electrocardiogram) and the sounds made by the heart (phonocardiogram). This information will not be discussed in this work.

2.1.2 Important physiological parameters of the heart

Stroke volume, heart rate and cardiac output

The value of the cardiac output (CO) is of paramount importance and is often estimated in the ICU. The CO stands for the quantity of blood which is ejected by the heart during one minute and it is thus equal to [60]:

$$CO = SV \cdot HR \ , \tag{2.1}$$

where SV is the stroke volume and HR is the heart rate (the number of cardiac cycle during one minute). The stroke volume stands for the volume ejected from the ventricle during one single beat. This volume is equal to the difference between the end-diastolic volume (corresponding to the volume at the end of step 6 in Figure 2.2) and the end-systolic volume (corresponding to the volume at step 3 in Figure 2.2). For a human of 70 kg at rest, the standard values of the end-diastolic volume, the end-systolic volume and the heartbeat are equal to 120 ml, 50 ml and 80 beats/min respectively [46]. Therefore, the standard stroke volume and cardiac output are equal to 70 ml and 5.6 l/min respectively.

Pressure-volume loop

The pressure-volume loop (PV loop) is certainly one of the most important data to characterizing the behavior of the heart. Figure 2.3 represents the different steps of the cardiac cycle on the PV loop: first, the vertical line when the ventricle volume is the largest corresponds to the isovolumic contraction of the ventricles, second, the PV loop shows a large decrease in the ventricular volume corresponding to the ejection of blood, third, the vertical line when the ventricle volume is the smallest corresponds to the isovolumic relaxation

and, finally, the PV loop shows a large increase in the ventricular volume corresponding to the filling of the ventricle. Therefore, the preload, the afterload and the ventricle contractility can be analyzed using the PV loop [61] and these concepts are briefly described below.

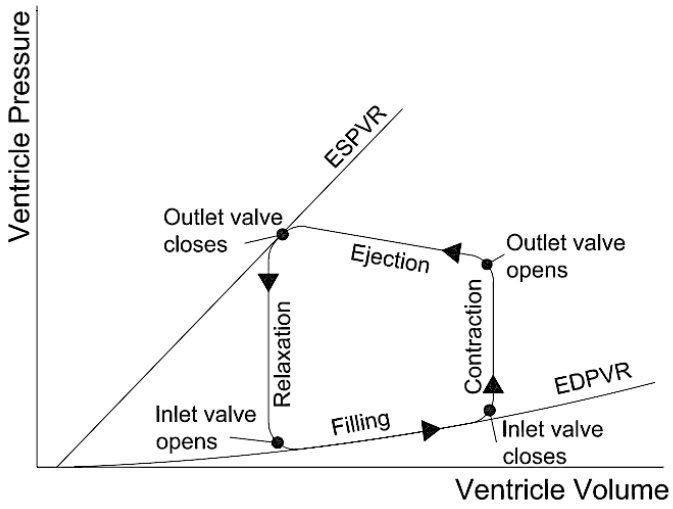

Figure 2.3 – Pressure-volume loop [106]

Preload is the ability of the heart to fill up and is characterized by the compliance of the heart. The compliance is an intrinsic property of the heart. However, the preload also depends on extrinsic property of the heart such as the venous return. If the venous return increases, more blood enters the ventricles and the preload is increased. Graph A in Figure 2.4 shows how the PV loop changes when the preload increases or decreases. When the preload increases, whereas the end-systolic volume is unchanged, the end-diastolic volume increases and, therefore, the stroke volume increases. The relationship between end-diastolic pressure and end-diastolic volume is of paramount importance and the abbreviation EDPVR, which stands for End-Diastolic Pressure Volume Relationship, is used (Figure 2.3 and Figure 2.4).

Afterload describes the resistance to blood ejection. Afterload is an extrinsic property of the heart and is influenced by several vascular properties such as the systemic resistances. For example, if the systemic resistances increase, the afterload increases since it is harder to eject blood out of ventricles. Graph B in Figure 2.4 shows how the PV loop changes when afterload increases or decreases. When afterload increases, whereas the end-diastolic volume is unchanged, the end-systolic volume increases and, therefore, the stroke volume decreases. The end-systolic pressure also increases when afterload increases.

Ventricle contractility is the ability of ventricles to contract and is an intrinsic property of the heart. Therefore, the ventricle contractility does not change with the preload or with the afterload. This contractility can be estimated with several PV loops: it is equal to the slope of the straight line named ESPVR (Figure 2.3 and Figure 2.4). ESPVR is the abbreviation of End-Systolic Pressure Volume Relationship and this straight line is tangent to the PV loop corresponding to the end of the ventricle contraction (Figure 2.3). For different afterloads, the ventricle contractility is unchanged and Figure 2.4 shows that the different PV loops are tangent to the ESPVR. If the ventricle contractility increases, the slope of the ESPVR increases and, for a same afterload and preload, whereas the end-diastolic volume is unchanged, the end-systolic volume decreases and the stroke volume thus increases.

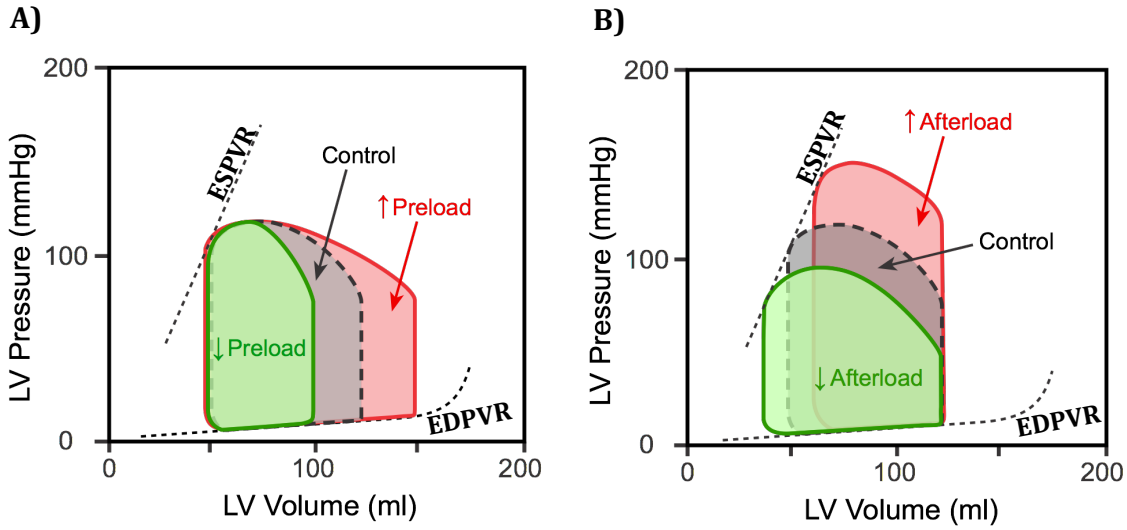

Figure 2.4 – Effect of preload (graph A) and afterload (graph B) on the pressure-volume loops [61].

However, these 3 properties of the heart are not independent effects [61] since the cardiovascular system is a closed loop. Hence, the different PV loops in Figure 2.4 are rarely observed in real life. For example, if preload decreases, the ventricles eject less blood and the blood flow in the arteries decreases. Consequently, the blood pressure in the arteries decreases and afterload is thus diminished.

Elastance and compliance of the ventricles

The ability of the ventricles to expand when blood enters these cardiac cavities is really important for the preload of the heart. This feature of the heart can be estimated with the diastolic compliance or the diastolic elastance of the ventricles. These two parameters describe a passive behavior of the ventricles. The diastolic compliance $C_{diastole}$ of a ventricle

is the measure of its aptitude to expand under an increase in an external pressure [62] and the following relation is written:

$$C_{diastole} = \left(\frac{\partial V}{\partial P}\right)_{diastole} . \tag{2.2}$$

This compliance is not constant during all the diastolic period, it is larger for small pressure and smaller for larger pressure. The diastolic elastance $E_{diastole}$ is the inverse of the compliance and the following relation can be written:

$$E_{diastole} = \left(\frac{\partial P}{\partial V}\right)_{diastole} . \tag{2.3}$$

Like the compliance, the elastance is not constant during all the diastolic period; it is smaller for small pressure and larger for larger pressure. The EDPVR curve in Figure 2.3 represents the evolution of the ventricle pressure as a function of its volume during the diastolic period. The slope of this curve increases and thus confirms the evolution of the elastance values.

The preload influences directly the end-diastolic volume and therefore the stroke volume. The larger the preload, the larger the volume ejected by the ventricles. However, the relation between the stroke volume and the preload is not linear. When the ventricles are overfilled, the muscular fibres are too stretched and the myocardium cannot contract efficiently [33]. This effect is well known under the name of Frank-Starling curve. Figure 2.5 represents this curve and highlights two different zones: one at low preload where the stroke volume increases linearly with the preload and one at high preload where the stroke volume is nearly constant with the preload.

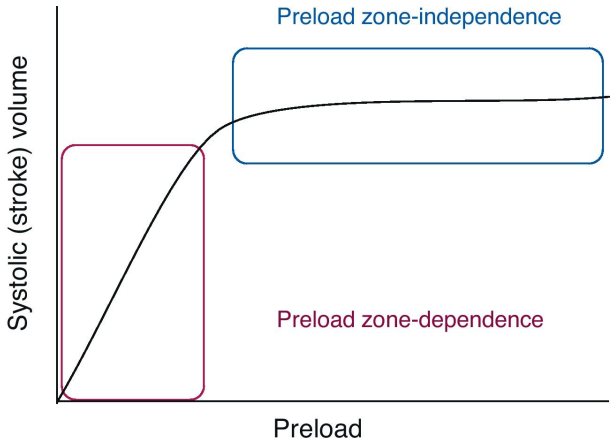

Figure 2.5 – Frank-Starling curve [33].

2.1.3 Physiology of the vascular system

The blood circulation

Thanks to the cardiac cycle, blood is transported across blood vessels toward the body tissues. This circulation ensures the adequate supplies of various molecules to the organism. A particularly important molecule is oxygen (O_2) and Figure 2.6 represents blood vessels in red when blood is rich in oxygen and in blue when blood is poor in oxygen. Indeed, blood is oxygenated in the lungs and the oxygenated blood releases the O_2 molecules in all tissues which are used for their metabolism. The circulation of blood in the whole body is quite complex but after some simplifications, this transport can be divided into 11 main processes [119] (Figure 2.6):

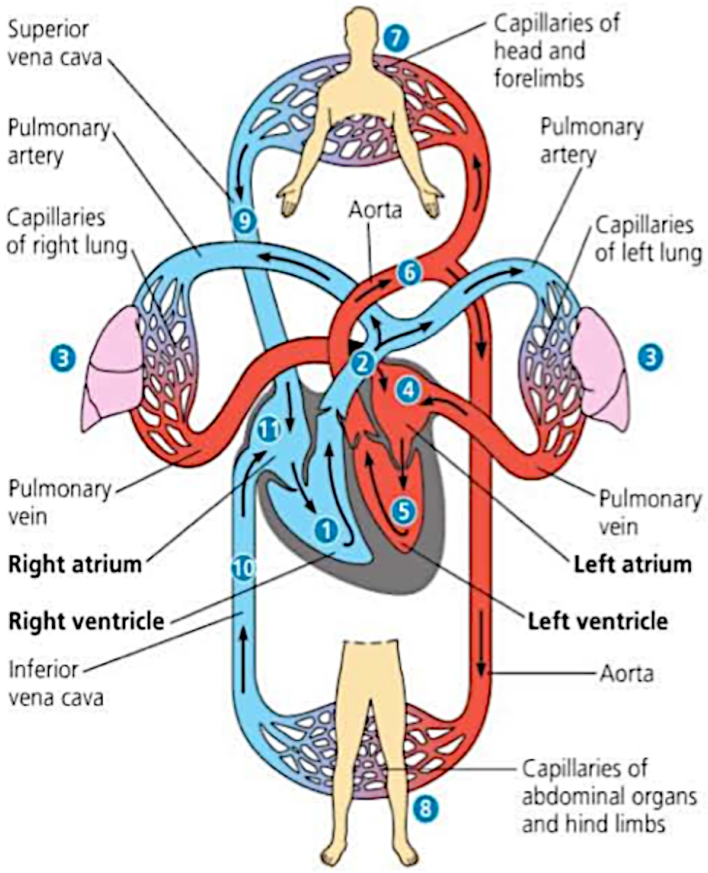

Figure 2.6 – The blood circulation in the circulatory system [119]

1. Blood enters the right ventricle and gets out of this chamber through the pulmonary artery.

2. The pulmonary artery is divided into 2 arteries: the left pulmonary artery, which goes to the left lung, and the right pulmonary artery, which goes to the right lung.

3. In the lungs, gas exchanges take place in the pulmonary capillaries: O_2 is delivered to blood and carbon dioxide (CO_2) is released.

4. In the right and left pulmonary veins, the oxygen enriched blood is transported back to left atrium.

5. Blood enters the left ventricle and then is ejected through the ascending aorta.

6. After the ascending aorta, one part of blood goes to the head and upper limbs and the other part goes to the abdominal organs and lower limbs.

7. Oxygen is released and carbon dioxide is extracted in the capillaries of head and lower limbs.

8. Oxygen is released and carbon dioxide is extracted in the capillaries of abdominal organs and upper limbs.

9. Blood crosses the superior vena cava to go to the right atrium.

10. Blood crosses the inferior vena cava to go to the right atrium.

11. Blood enters the right atrium and, then, goes into the right ventricle (the cycle starts again).

Steps 1 to 4 are commonly named the pulmonary circulation while steps 5 to 11 define the systemic circulation.

The blood vessels

The blood circulation is carried out by blood vessels. These vessels have different shapes and macro-molecular structures according to their locations and functions in the vascular system. In the systemic circulation, 7 main types of blood vessels can be distinguished [60, 46] (Figure 2.7 and Table 2.1):

- The aorta: is located just after the left ventricle and this large artery dampens the pulsatile pressure thanks to its elastic membrane. The main function of the aorta is of course to distribute blood toward the different arterial systems.

- Arteries: transport blood to the different tissues of the body. As in the aorta, blood is under high pressure in the arteries and, consequently, they have a strong vascular wall. Small arteries are able to constrict but it is mainly the arterioles which play this function.

- Arterioles: are small vessels (Table 2.1) which are able to constrict. Thanks to these vessels, the arterial blood pressure is controled and the blood flow is regulated in response to the tissue needs. For example, if the activity of one organ increases, the arterioles located near this organ will dilate and the other arterioles will constrict. Consequently, these vessels need strong muscular walls and are innervated by autonomic nerves.

- Capillaries: are microscopic vessels. However the total cross section is large (Table 2.1) since the number of capillaries is huge. Their membrane is very thin and it is permeable to water and other small molecules such as CO_2 and O_2. Therefore, the function of these vessels is to participate in gas exchanges.

- Venules: collect blood from the capillaries. Like the arterioles, venules are able to constrict and their membrane contains muscular cells. These vessels can thus control the capillary blood pressure and the venous blood volume.

- Veins: collect blood from the venules. Their major roles are to store and to regulate blood volume by decreasing or increasing their diameter. A large fraction of the blood volume is stored in the systemic veins ($\approx 60\%$ [23]).

- Venae cavae: are the 2 final venous vessels (inferior vena cava and superior vena cava). These vessels collect blood from the venules and transport it back to the right atrium.

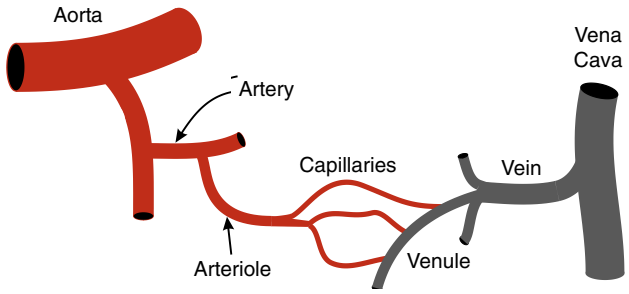

Figure 2.7 – Major types of blood vessels in the systemic circulation [60].

The pulmonary circulation is analogous to the systemic circulation; there are also arterioles, capillaries and venules. The pulmonary arteries are analogous to the aorta in the pulmonary circulation and the pulmonary veins are analogous to the venae cavae in the pulmonary circulation.

Table 2.1 – Characteristics (diameter, total cross-sectional area and function) of the different types of the blood vessels in the systemic circulation [60, 46].

Vessel type	Diameter (mm)	Cross-sectional area (cm^2)	Function
Aorta	25	2.5	Pulse dampening and distribution
Arteries	$0.2 - 4.0$	20	Distribution and resistance
Arterioles	$0.01 - 0.20$	40	Resistance (pressure/flow regulation)
Capillaries	$0.006 - 0.010$	2500	Exchange
Venules	$0.01 - 0.20$	250	Exchange, collection and capacitance
Veins	$0.2 - 5.0$	80	Capacitance (blood volume)
Venae Cavae	35	8	Collection

2.1.4 Important physiological parameters of the vascular system

Pressures and volumes

Pressures and volumes are not only important parameters for the heart (see section 2.1.2) but also for the whole cardiovascular system. Figure 2.8 represents the normal blood pressures in the different vascular vessels. In the aorta and in the large arteries, the blood pressure is pulsatile because of the contraction of the left ventricle; the maximum pressure is around 120 mmHg and the minimum pressure is around 80 mmHg. In small arteries, their membrane is less elastic and the blood pressure becomes less pulsatile. In the arterioles, the blood pressure decreases drastically since these vessels have a small diameter. From the capillaries to the venae cavae, the blood pressure decreases progressively and reaches a blood pressure near 0 mmHg in the venae cavae [46]. For the pulmonary circulation, the same blood pressure evolution is observed but with much lower values in the pulmonary arteries. However, the blood pressure in the pulmonary veins is larger than in the systemic veins. Indeed, the pulmonary circulation has a much smaller vascular network than the systemic circulation and the pressure drop is thus much smaller in the pulmonary circulation.

Figure 2.9 represents the percentage of the total blood volume in the different parts of the circulatory system. The vessels under low pressures (veins and venules) in the systemic circulation have the largest percentage (around 64%). This result corresponds to the vascular function of these vessels: storing the blood volume. The other vessels of the systemic circulation (arteries, arterioles and capillaries) have a percentage around 10%. Since the pulmonary circulation has a much smaller vascular network, the percentage in this circulation is small (less than 10%).

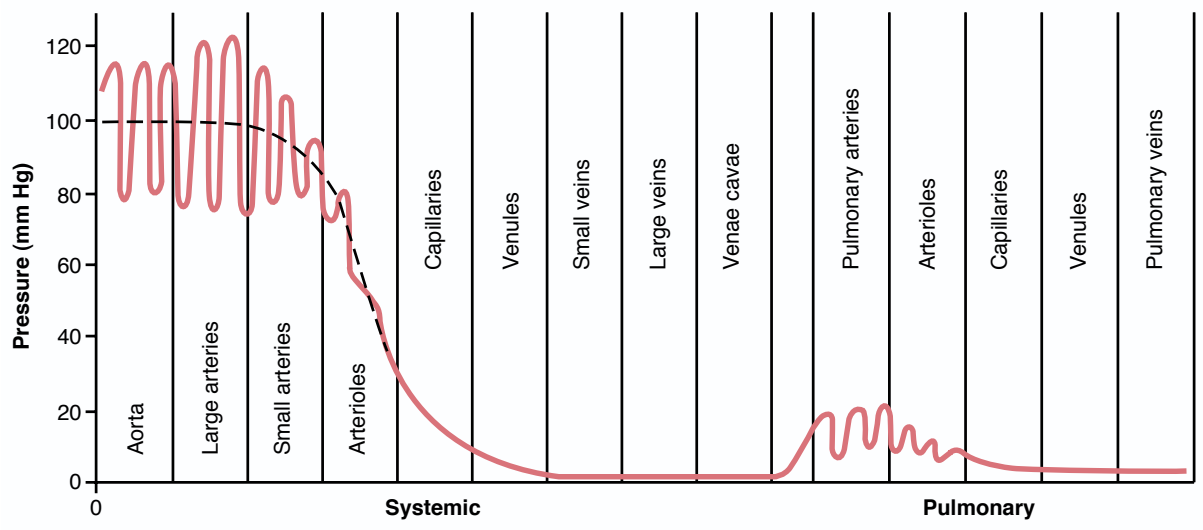

Figure 2.8 – Normal blood pressure in the different vascular vessels [46].

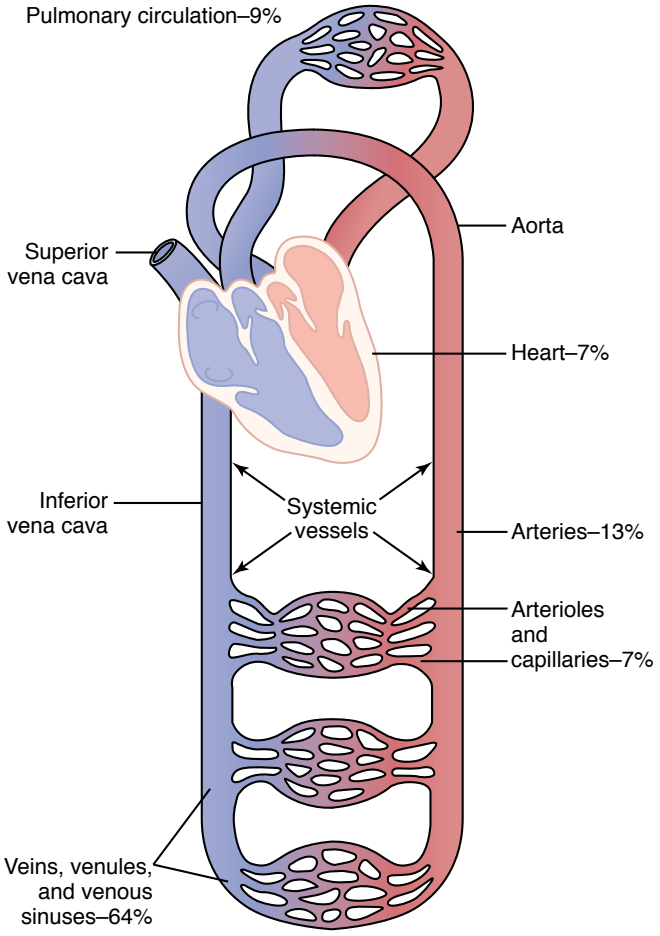

Figure 2.9 – Distribution of blood (in percentage of the total blood volume) in the different parts of the circulatory system [46].

Elastance and compliance

Elastance and compliance are also important parameters of the vascular system (the elastance and compliance have been already discussed for the ventricles in section 2.1.2). The relation between pressures and volumes is simpler for the vascular system since they are passive elements and the pressure and volume variations are smaller. The approximation of a constant elastance or a constant compliance is often used for the vascular vessels. Therefore, the following equation can be written [60]:

$$\Delta V = C \cdot \Delta P \tag{2.4a}$$

$$= \frac{1}{E} \cdot \Delta P \ . \tag{2.4b}$$

The compliance is much larger in the veins than in the arteries. Indeed, the veins must dilate easily (the volume in the veins increases for a small increase in blood pressure in the veins) in order to store the venous blood. For example, standard compliance values for an adult are equal to about 100 ml/mmHg for the systemic veins and about 1 ml/mmHg for the arteries [105].

Blood flow and resistance

Thanks to pressure gradients between the different vessels (Figure 2.8), blood can flow from one vessel to another vessel having a lower blood pressure. If the inertial flows are neglected, the blood flow Q between two locations is equal to [60, 57]:

$$Q = \frac{\Delta P}{R} \ , \tag{2.5}$$

where ΔP is the difference between the blood pressure in the upstream part and the blood pressure in the downstream part and R is the resistance in the section limited by the two considered parts. The resistance increases very much (to the power 4, see Poiseuille's equation [118]) when the diameter of the vessels decreases. Therefore, the resistance is very high for the small vessels. For example, the global resistance of the vascular system surrounded the tissues is around 0.95 $\text{mmHg} \cdot \text{s} \cdot \text{ml}^{-1}$ for a healthy adult whereas the resistance in the aorta is around 0.03 $\text{mmHg} \cdot \text{s} \cdot \text{ml}^{-1}$ [105].

2.2 Blood chemistry

The blood chemistry is very complex; a large number of different molecules are present in this fluid and a lot of chemical reactions are involved [94]. However, since this research focuses on respiration, we will describe mainly the oxygen and carbon dioxide reactions.

2.2.1 Oxygen

O_2 can be dissolved in blood plasma but this quantity alone would not be sufficient for the metabolism of all cells [46]. In fact, the majority ($\approx$ 97% [46]) of O_2 in blood is complexed with hemoglobin, a protein present in abundance in the erythrocytes (there are several millions of hemoglobin molecules in each erythrocyte). The hemoglobin has 4 domains (2 α and 2 β) and each domain can bind a molecule of O_2 [46]. The oxidation of the hemoglobin occurs using an iron molecule which is localized on the heme of each domain. An erythrocyte, the four domains of the protein and the heme are illustrated in Figure 2.10.

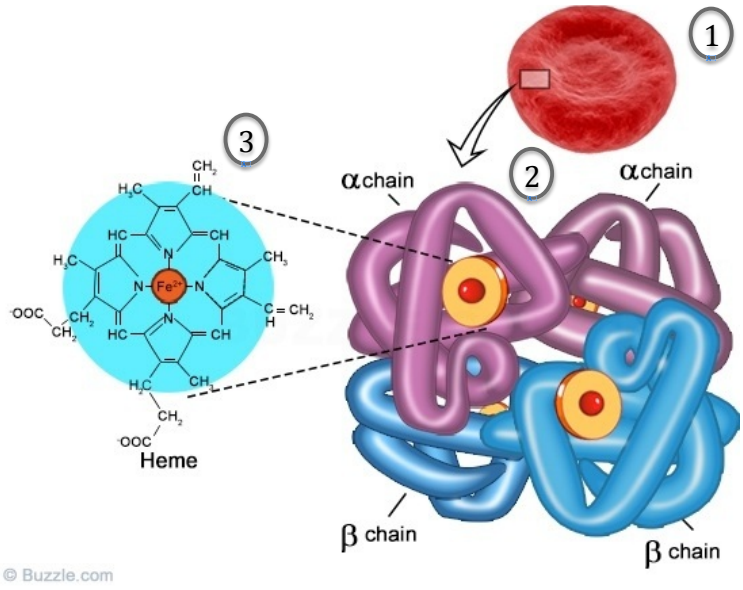

Figure 2.10 – Hemoglobin structure [26]. 1) View of an erythrocyte. 2) The four domains of the hemoglobin. 3) Molecular structure of the heme.

If *Hb* represents one binding domain of hemoglobin, the following complexation reaction of O_2 with hemoglobin can be written [57]:

$$O_2 + \mathrm{Hb} \rightleftharpoons \mathrm{Hb}(O_2)\ . \tag{2.6}$$

However, the complexation reaction is more complex in reality because it can be influenced

by many factors such as temperature, pH and CO_2 partial pressure (PCO_2). In addition, the four domains of the hemoglobin are not independent and the kinetic of reaction 2.6 changes if one or several neighboring domains are already complexed with O_2. Therefore, a more realistic description of the hemoglobin complexation with O_2 is given by the following equations [35, 57]:

$$Hb_4(O_2)_{i-1} + O_2 \underset{k_{-2,i}}{\overset{k_{2,i}}{\rightleftharpoons}} Hb_4(O_2)_i \qquad \forall\ i = 1, 2, 3, 4\ , \tag{2.7}$$

The kinetics of reaction 2.7 are slow when there is little oxygen in blood (there are few oxygen molecules linked to the hemoglobin). The rate of the reaction increases when the O_2 concentration increases and when the hemoglobin is incompletely saturated. However, if the concentration increases again, the hemoglobin gets saturated and the rate of the reaction becomes very slow. In this way, the hemoglobin saturation curve with O_2 in terms of O_2 partial pressure (directly related to the O_2 concentration dissolved in blood plasma) has an "S" shape (sigmoid curve). Figure 2.11 represents the saturation curve of hemoglobin and also shows the influence of pH, PCO_2 and temperature on this saturation. Indeed, CO_2 and H^+ can be linked to the hemoglobin (the binding sites are different from the binding site of O_2) and they thus change the hemoglobin configuration. If the temperature, the PCO_2 or the H^+ concentration increases, the saturation curve is shifted to the right (the influence of pH on the saturation of hemoglobin is commonly named the Bohr effect) [46]. In these conditions, the hemoglobin affinity with O_2 is weaker. Since the tissue cells produce heat and CO_2 (and the CO_2 in blood produces H^+), these hemoglobin properties can be used by the body. Indeed, the cells need O_2 for their metabolism and the affinity of hemoglobin with O_2 decreases when temperature and PCO_2 increase. On the contrary, if the temperature, the PCO_2 or the H^+ concentration decreases, the saturation curve is shifted to the left and the hemoglobin affinity with O_2 is stronger.

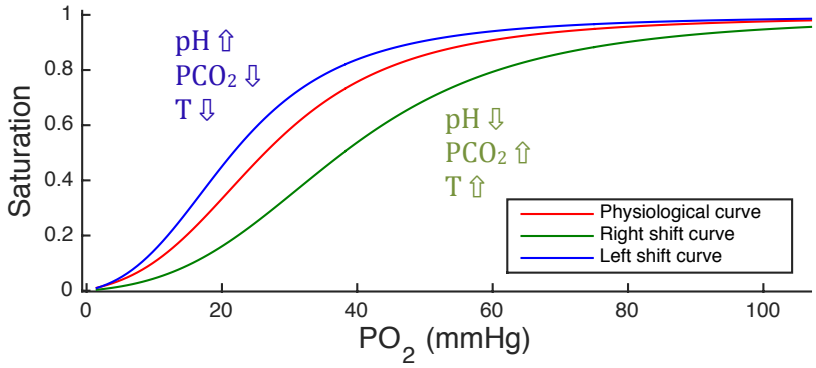

Figure 2.11 – The saturation curve of hemoglobin with O_2 and the influences of pH, PCO_2 and temperature on this curve.

2.2.2 Carbon dioxide

Like O_2, CO_2 is also dissolved in blood plasma ($\approx 10\%$ in venous blood [7]) and complexed to the hemoglobin ($\approx 30\%$ in venous blood [7]). However, CO_2 is also subject to the hydration/dehydration reaction [57]:

$$CO_2 + H_2O \rightleftharpoons HCO_3^- + H^+ \ , \tag{2.8}$$

and the largest proportion of CO_2 in blood is under the form of HCO_3^- ($\approx 60\%$ in venous blood [7]). Since this reaction produces H^+, it influences directly the pH. As mentioned before, PCO_2 and pH influence the saturation of hemoglobin with O_2. In addition, the saturation of hemoglobin with O_2 decreases the saturation of hemoglobin with CO_2 (the Haldane effect) [46]. All the different chemical components in blood are thus related to one another.

2.3 Respiratory system

Coupled with the cardiovascular system, the respiratory system is fundamental for the activity of every part of the body. Indeed, the respiration supplies the tissues with O_2 and rejects in the atmosphere the CO_2 produced by the tissues. The anatomy, the mechanisms and the properties of the respiratory system are described in the next subsections.

2.3.1 The anatomy of the respiratory system

Thanks to the thoracic muscles, the lungs can relax and contract leading to volume variations. When the lung volume changes, the pressure in the lungs changes and the atmospheric air enters the lungs and gets out of the lungs through the respiratory tract.

The lungs

The thorax has 3 main cavities, two for the lungs and one for the heart. The right lung and the left lung are located to the right and to the left of the heart respectively (Figure 2.12). It is mainly the left lung which covers the heart and, consequently, this lung is smaller than the right lung (the right lung has 3 lobes while the left lung has only 2 lobes).

Thoracic muscles

It is mainly the diaphragm, located at the bottom of the lungs, which generates lungs volume variations [46]. The other muscles taking part in the respiration are the external and internal intercostal muscles and the abdominal muscles (Figure 2.13). During inspiration,

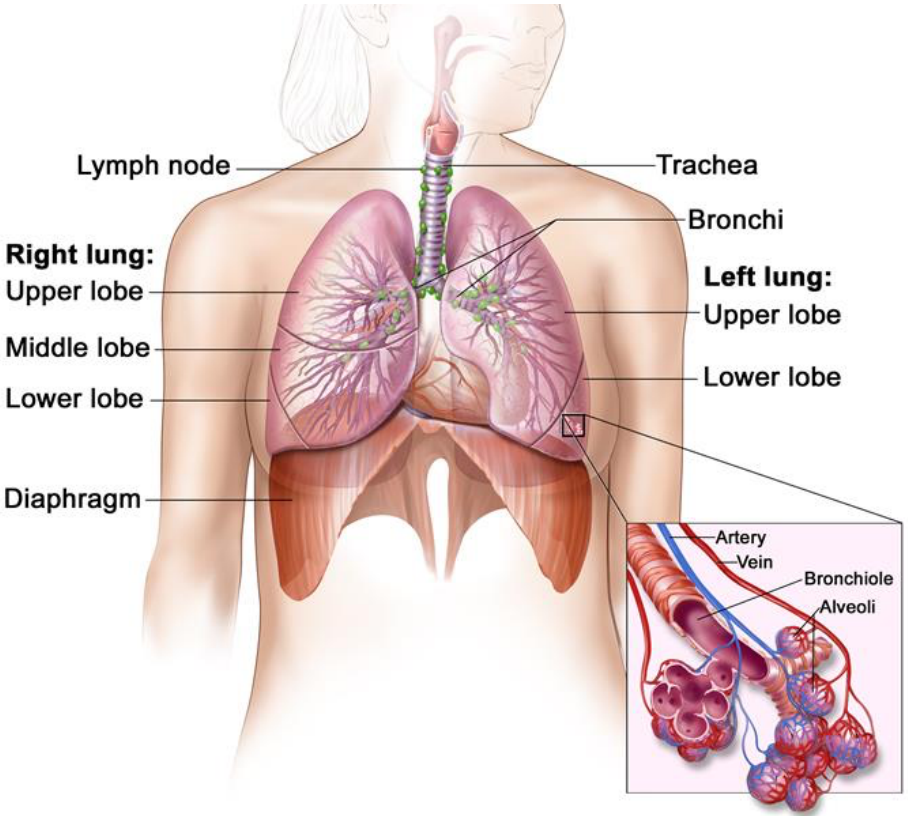

Figure 2.12 – Simplified anatomy of the respiratory system [51].

the diaphragm and the external intercostal muscles contract resulting in an expansion of the chest wall and the lungs. For expiration, there are differences between quiet breathing and active breathing. During quiet breathing, the reduction of the chest wall and the lung volume results from passive recoil of lungs; the diaphragm and the external intercostal muscles relax. During active breathing, in addition to the relaxation of the diaphragm and the external intercostal muscles, the abdominal and the internal intercostal muscles contract.

Respiratory tract

The air goes from the mouth to the alveoli through the respiratory tract. First, the airflow goes in the trachea. Then, the trachea is divided into several bronchi which are divided into bronchioles. Finally, the bronchioles are divided into several alveoli (Figure 2.12). Whereas the bronchi and bronchioles are rigid, the alveoli are elastic and participate in lungs volume variations. The alveoli are in great abundance, their number is approximately equal to 300 million [46], are in very close proximity with the pulmonary capillaries and their membrane is very thin. Consequently, the gas exchanges occur in the alveoli: O_2 goes from the alveoli to the blood in the pulmonary capillaries while CO_2 goes from the

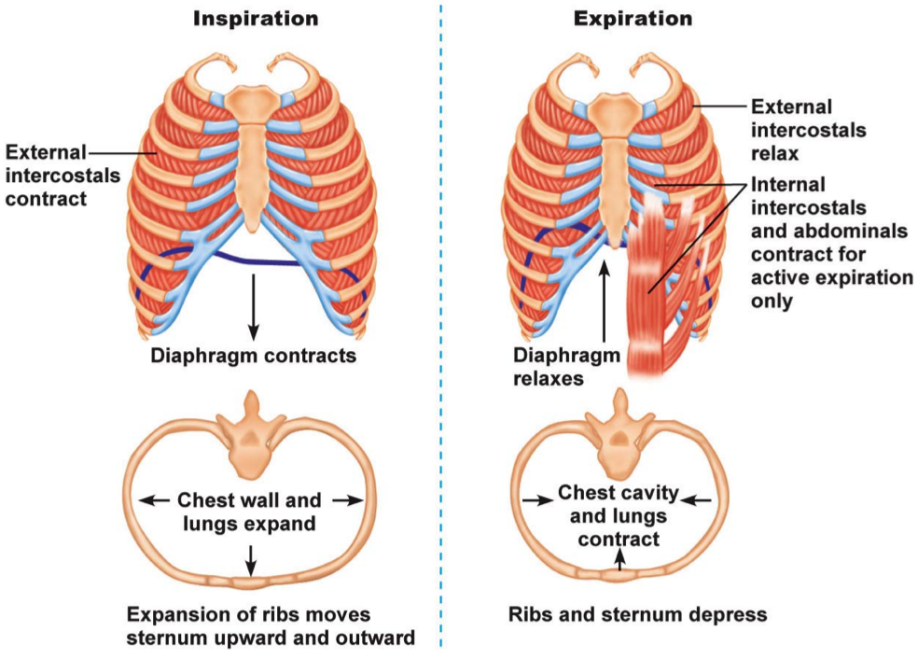

Figure 2.13 – Respiratory muscles [28].

blood contained in the pulmonary capillaries to the alveoli.

2.3.2 The pulmonary ventilation

The pulmonary ventilation consists in cycles of inspiration and expiration [46]. During the inspiration, the air enters the lungs and during the expiration, the air gets out. Thanks to the ventilation, gas exchanges occur between the air in the alveoli and the blood in the pulmonary capillaries. As a result, the blood flow in the pulmonary circulation and the ventilation must be highly correlated and the ratio between the alveolar ventilation and the capillary perfusion ($\dot{V}_A/Q_c$) is an essential parameter [57]. This ratio is not constant for the different parts of the lungs (Figure 2.14); it can be equal to infinity and the corresponding area is named the dead space of the lungs, it can also be equal to 0 and this corresponds to a pulmonary shunt or it can vary between these two extremes because of local perfusion variations (West zones) or local ventilation variations (shunt effect).

Shunt and shunt effect

The pulmonary shunt corresponds to pulmonary capillaries which are not ventilated [13, 2]. The causes could be because the alveolus is obstructed (Chronic Obstructive Pulmonary Disease), collapsed (emphysema) or full with water (pulmonary infection). The pulmonary shunt is illustrated in Figure 2.14 in alveolus C. These specific alveoli can be partially ob-

structed or collapse and the ventilation is thus not always equal to 0. The ventilation is weaker in these alveoli than in normal alveoli and this phenomenon is called the shunt effect.

The pulmonary shunt is also the fraction of blood that does not participate in gas exchanges because blood goes directly from the pulmonary artery to the pulmonary veins without reaching any alveolus. This shunt is called the anatomical shunt.

Dead space and West zones

The dead space refers to the alveoli which are not perfused [2]. The causes could be because of vascular obstructions (pulmonary embolism) or damages of the pulmonary vascular system (pulmonary arteritis or loss of capillary bed). The perfusion can also decrease because of a lack of blood pressure in the pulmonary vessels. For example, if the patient stands up, the blood pressure is weaker in the upper areas and larger in the lower areas because of the gravity [41]. In physiological conditions, 3 zones are distinguished and they are called the West Zones (Figure 2.15):

1. Zone 1 corresponds to the upper area of the lungs. In this region, pulmonary blood pressures in the arteries (P_{pa} in Figure 2.15) and in the veins (P_{pv} in Figure 2.15) are low and both blood pressures are smaller than the alveolar pressure (P_A in Figure 2.15). Since the pressure outside the vessels is larger than the pressures inside, the pulmonary capillaries collapse in this region of the lungs. Therefore, there is no blood flow in these vessels.

2. Further down in the lungs, P_{pa} and P_{pv} become larger and Zone 2 corresponds to the area of the lungs where P_{pa} is greater than P_A but P_{pv} is still smaller than P_A. The vessel diameter is reduced in this zone but the blood can flow in these vessels.

3. Still lower in the lungs, P_{pa} and P_{pv} still increase and Zone 3 corresponds to the area of the lungs where P_{pa} and P_{pv} are larger than P_A. In this last region of the lungs, the capillary system is entirely open and the blood flow is the highest.

The dead space includes also the gas inhaled which does not reach any alveoli and therefore does not contribute to gas exchanges. This dead space is called the anatomical dead space.

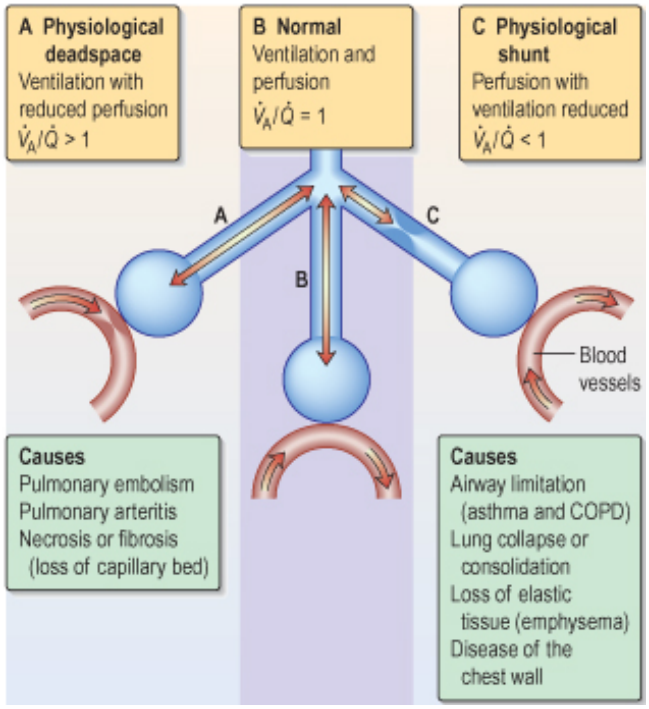

Figure 2.14 – The different ventilation/perfusion ratio [2]. $\dot{V}_A$ is the alveolar ventilation and $\dot{Q}$ is the capillary perfusion. In the text, $\dot{Q}$ is replaced by Q_c.

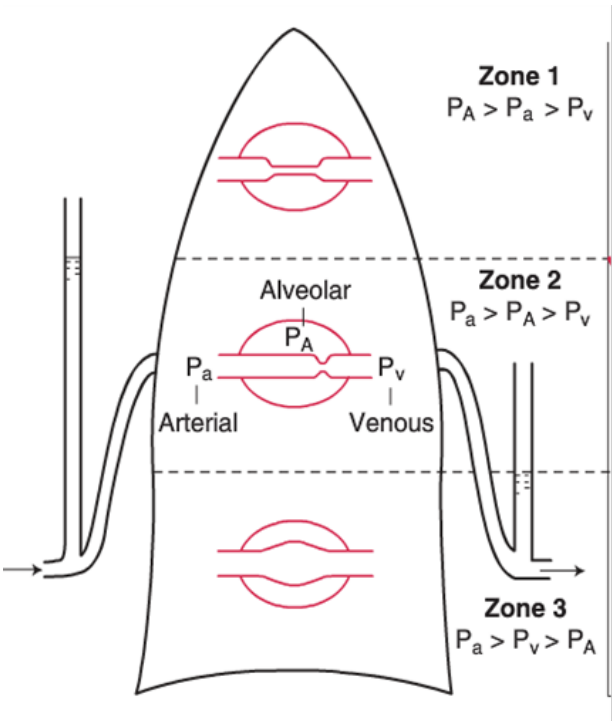

Figure 2.15 – West zones [117]. P_{pa} is the blood pressure in the pulmonary artery, P_{va} is the blood pressure in the pulmonary vein and P_A is the alveolar pressure.

2.3.3 Cellular respiration

Whereas the external respiration or the pulmonary ventilation refers to the gas exchanges in the lungs which reject CO_2 in the atmosphere and deliver O_2 to blood, the internal respiration or the cellular respiration refers to the gas exchanges in the tissues which deliver O_2 to the tissues and reject CO_2 from the tissues into the blood [35]. Therefore, the internal respiration supplies the molecules which are required for the cell activity and a brief description is provided below.

All the body cells need O_2 and carbonate substrates ($C_xH_yO_z$) for their activity [36, 85]. The energy is produced from these substrates and using several reactions called metabolism. These reactions produce CO_2 and H_2O. The ratio of the CO_2 produced to the O_2 consumed, known as the respiratory quotient

$$RQ = \frac{CO_{2,\text{eliminated}}}{O_{2,\text{consumed}}} , \tag{2.9}$$

depends on which substrate is consumed. For carbohydrates ($C_nH_{2n}O_n$) such as glucose ($C_6H_{12}O_6$), the respiratory quotient RQ is equal to 1. However, this quotient is smaller for other substrates such as fats ($RQ \approx 0.7$ [5, 85]) or proteins ($RQ \approx 0.8$ [5, 36]).

2.3.4 Important physiological parameters of the respiratory system

Minute ventilation, lung volumes and respiratory frequency

The minute ventilation $\dot{V}_E$[1] is the quantity of gas entering the lungs during one minute and is equal to [9]:

$$\dot{V}_E = f_r \cdot V_E , \tag{2.10}$$

where f_r is the respiratory frequency and V_E is the respiratory volume. At rest, the respiratory frequency is approximately equal to 16 breathings per minute [102]. When an adult breaths normally, in other words a breath without extra efforts, the respiratory volume is approximately equal to 500 ml and this volume is called the tidal volume (Figure 2.16). The human body can inspire and expire more volume than the tidal volume and these additional volumes are called the inspiratory reserve volume and the expiratory reserve volume respectively. Figure 2.16 shows that the inspiratory reserve volume is approximately equal to 3100 ml and the expiratory reserve volume is approximately equal to 1200

[1]Symbol $\dot{V}_E$ is used in the literature because, historically, this quantity was always measured during expiration [102].

ml for a healthy adult. Therefore, an adult can increase his breathing to 4800 ml. But this volume is not equal to the total lung capacity. Indeed, even with a maximal expiration, the lung volume is never equal to 0 ml. This remaining volume is called the residual volume and is equal to approximately 1200 ml for a healthy adult.

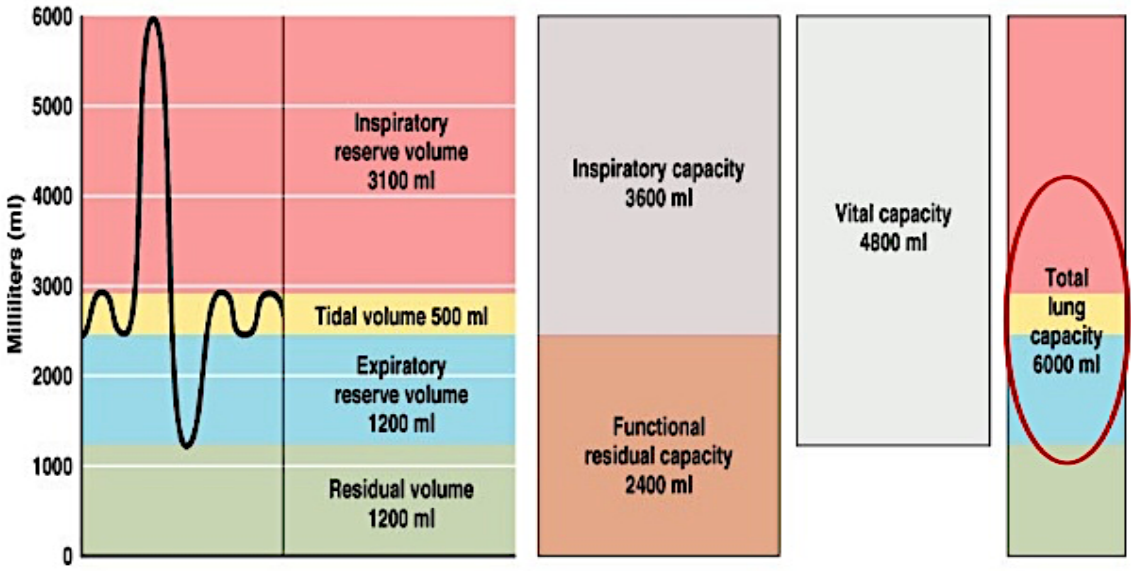

Figure 2.16 – Lung volumes and capacities for an adult [92].

For mechanically ventilated patients admitted to intensive care units, the respiration is often performed without extra volume and the respiratory volume is thus equivalent to the tidal volume V_T. In our study, equation 2.10 is thus replaced by the following equation:

$$\dot{V}_E = f_r \cdot V_T \ . \tag{2.11}$$

Alveolar ventilation and alveolar perfusion

As already mentioned in subsection 2.3.2, all the minute ventilation does not reach the alveoli and therefore does not participate in the gas exchanges. The alveolar ventilation $\dot{V}_A$ is thus smaller than the minute ventilation and is equal to [9, 93, 54]:

$$\dot{V}_A = f_r \cdot (V_T - V_{Dead}) = \dot{V}_E - \dot{V}_{Dead} \ , \tag{2.12}$$

where V_{Dead} is the dead space and $\dot{V}_{Dead}$ is the minute dead space. For a healthy adult, the dead space is approximately equal to 150 ml (and thus $\dot{V}_{Dead} \approx 2.4$ l/min, see Figure 2.17). For perfusion, the same kind of phenomenon is observed; all the pulmonary blood flow Q_p does not participate in gas exchanges and the alveolar perfusion Q_a is equal to [93, 54]:

$$Q_a = (1 - f_s) \cdot Q_p \ , \tag{2.13}$$

where f_s is the pulmonary shunt fraction (the fraction of the pulmonary blood flow which does not participate in gas exchanges).

CO_2 and O_2 partial pressure in the respiratory system

The quantities of O_2 and CO_2 in the different parts of the respiratory system are of paramount importance since the main purpose of this system is to provide enough O_2 and to reject enough CO_2.

If the inhaled gas is atmospheric air, the gas entering the respiratory system is composed of approximately 21% of O_2, approximately 79% of N_2 and nearly 0 % of CO_2 ($\approx$ 0.04 %). In the medical field, these quantities are often measured in partial pressures and the mmHg unit is often used. Since the standard atmospheric pressure is equal to 760 mmHg, the O_2 partial pressure PO_2 is approximately equal to 160 mmHg and the N_2 partial pressure PN_2 is approximately equal to 600 mmHg. When the air is in the trachea and in the bronchi, its composition is almost unchanged except that the air is humidified and warmed up. The total pressure is unchanged (760 mmHg) but the H_2O partial pressure PH_2O must also be considered and it is approximately equal to 47 mmHg [102]. Therefore, in this part of the respiratory system, $PO_2 \approx 0.21 \cdot (760 - 47) = 150$ mmHg and $PN_2 \approx 0.79 \cdot (760 - 47) = 563$ mmHg.

In the alveoli, due to the gas exchanges with the blood in the pulmonary capillaries, PO_2 is weaker, and PCO_2 is larger, than in the bronchi. Figure 2.17 shows that for a healthy human, PO_2 is equal to 100 mmHg and PCO_2 is equal to 39 mmHg in the alveoli [102]. Gas exchanges are very efficient across the alveolar-capillary membrane and PO_2 and PCO_2 in the pulmonary capillaries are equal to PO_2 and PCO_2 in the alveoli [9, 57]. However, PO_2 is weaker (95 mmHg) and PCO_2 is larger (41 mmHg) in the arteries than in the pulmonary capillaries because of the pulmonary shunt [48]. In an analogous manner, PO_2 is larger (115 mmHg) and PCO_2 is weaker (33 mmHg) in the exhaled air than in the alveoli because of the dead space [102].

Finally, PO_2 is weaker in the veins (40 mmHg) than in the arteries because of the O_2 consumption by metabolism and PCO_2 is larger in the veins (45 mmHg) than in the arteries because of the CO_2 production by metabolism.

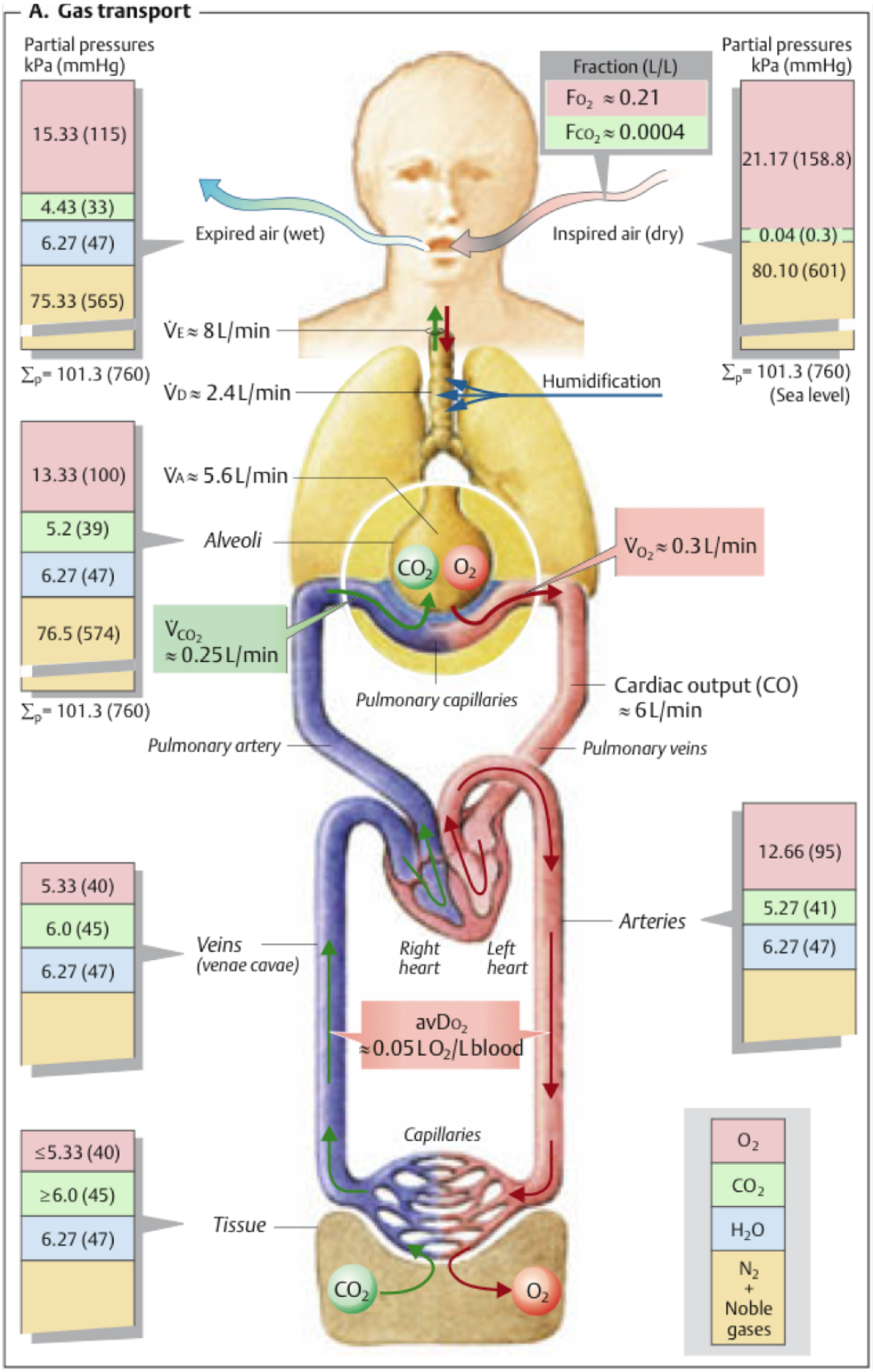

Figure 2.17 – Different physiological values of gas transport for an adult at rest [102]. All the symbols are defined in the text excepted that in the text, the symbols $\dot{V}_{\mathrm{CO}_2}$ and $\dot{V}_{\mathrm{O}_2}$ are replaced by $\dot{V}_{L,\mathrm{CO}_2}$ and $\dot{V}_{L,\mathrm{O}_2}$

In addition, it is important to note that the measures of PO_2 and PCO_2 in blood are only proportional to the concentrations of O_2 and CO_2 dissolved in blood plasma. To estimate the total O_2 and CO_2 blood concentration, the measures of HCO_3^-, of the hemoglobin saturations with O_2 and CO_2 and of the hemoglobin concentration must be estimated in addition to the O_2 and CO_2 partial pressures [94].

CO_2 production and O_2 consumption by metabolism

In the tissues, the important parameters are the quantity of CO_2 produced by metabolism and the quantity of O_2 consumed by metabolism. Our study will be only focused on the global production of CO_2, symbolised by MR_{CO_2}, and the global consumption of O_2, symbolised by MR_{O_2}. These quantities can be estimated by the following formulas [9, 102]:

$$MR_{O_2} = CO \cdot avDO_2 \tag{2.14}$$

$$MR_{CO_2} = CO \cdot (-avDCO_2) \tag{2.15}$$

where $avDO_2$ is the arterial-venous O_2 difference (the difference between O_2 concentrations in the arteries and veins) and $avDCO_2$ is the arterial-venous CO_2 difference. In a stabilized situation, the O_2 consumption by metabolism is equal to the O_2 supply in the lungs ($\dot{V}_{L,O_2}$) and the CO_2 production by metabolism is equal to the CO_2 extraction in the lungs ($\dot{V}_{L,CO_2}$). Note that the concentration unit used in the present study (and in other similar studies [116, 9, 12, 113, 37]) is the partial volume (l_i/l). The relation between molar concentration C_i (mol_i/l) and partial volume V_i is written by using the ideal gas law:

$$V_i = C_i \cdot \frac{R \cdot T}{P} \ , \tag{2.16}$$

where R is the gas constant, T the temperature and P the pressure. For a healthy adult, the $avDO_2$ is approximately equal to 0.05 l_{O_2}/l and the MR_{O_2}, which is equal to $\dot{V}_{L,O_2}$, is thus approximatively equal to 0.3 l_{O_2}/min for a CO of 6 l/min [102] (Figure 2.17). Since the respiratory quotient RQ (see equation 2.9) is equal or smaller than 1, MR_{CO_2} is equal or smaller than MR_{O_2} ($MR_{CO_2} = \dot{V}_{L,CO_2} \approx 0.25\ l_{CO_2}/min$ in Figure 2.17).

2.4 Controls and regulations of the cardio-pulmonary system

Even if the controls and the regulations of the cardio-pulmonary system are not considered in the mathematical models described in the next chapters, it is important to know these

physiological effects to understand the impacts of several simplifications on the models. The controls and the regulations act on different parts of the body to satisfy the human homeostasis which is essential for the proper functioning of the different organs.

2.4.1 Controls and regulations of the cardiovascular system

Two important parameters of the cardiovascular system are strictly controlled to ensure an appropriate hemodynamics in all the cardiovascular vessels. These two parameters are the blood pressure and the blood flow. The control mechanisms on these parameters are very complex and 3 major types can be distinguished: local (intrinsic) control, humoral control and neural (extrinsic) control [57]. These 3 controls are only short-term controls (seconds to hours) but long term controls (days to weeks), such as renal mechanisms, also exist and allow to regulate the partial pressure. However, there is no real interest in discussing here the long-term control since the aim of our study is to stimulate the cardio-pulmonary system during minutes to hours and not days to weeks.

Local (intrinsic) control

The blood flow in the different tissues must correspond to their activity. If the blood flow is too low, not enough O_2 is transported to the tissue and not enough CO_2 is evacuated from the tissues. Hence, local controls are able to adjust the flow through an arteriole according to the activity of the tissue which is supplied by this arteriole. The complete mechanism is not known yet but it is assumed that chemoreceptor estimates the activity of the tissues by measuring the concentrations of O_2, CO_2 and H^+ in the veins [57]. If the activity is not proportional to the blood flow, regulatory substances, called vasodilators, are transported to the arterioles. For instance, when the blood flow is too low for the activity of the tissues (concentration of O_2 is too low and concentration of CO_2 and H^+ are too high), the vasodilators induce an increase in the arteriole diameters.

Neural (extrinsic) control

The nervous system has several nerve fibres controlling the vascular vessels and the heart. Contrary to the previous control, the nervous control has a more global effect. It regulates the cardiac function (heart rate and contractility), the distribution of blood to the different parts of the body and the systemic arterial pressure. The rapid control of the arterial pressure by the neural control is called the baroreflex and it is the most important extrinsic control of the cardiovascular system [57]. This control works thanks to the baroreceptors located in the carotid sinus and the aortic arch. When the nervous system detects a drop in the arterial pressure, it sends several signals which increase the sympathetic stimulation

and decrease the parasympathetic stimulation in order to increase the heart activity (heart rate and contractility) and in order to constrict the small arteries, the arterioles and the veins. The baroreflex mechanism is illustrated in Figure 2.18.

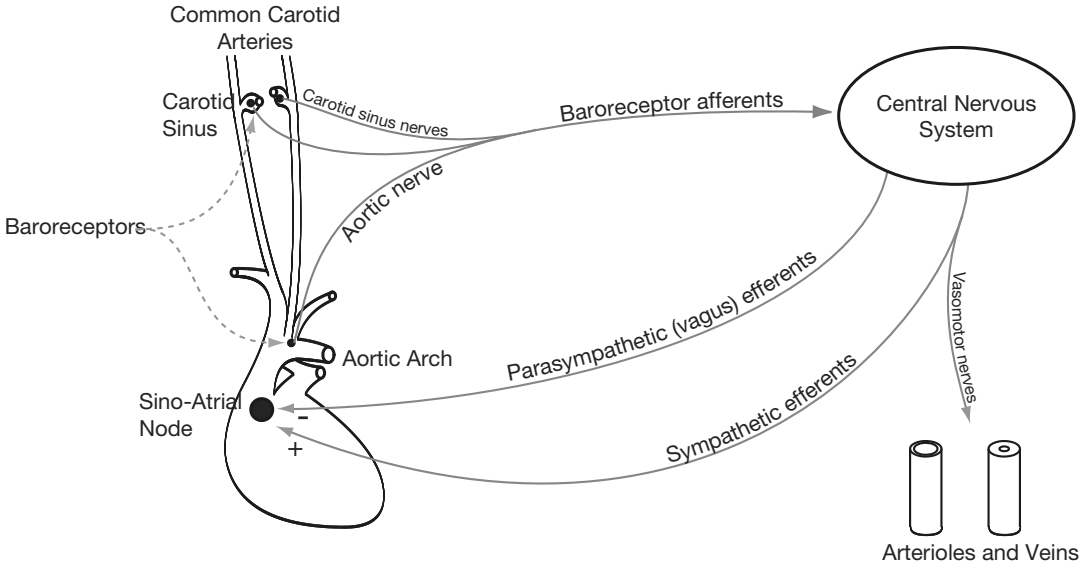

Figure 2.18 – Schematic diagram of the baroreflex pathway [57].

Humoral control

Humoral control is mediated by substances secreted or absorbed in blood such as hormones and ions [46, 57] and these substances can interact with chemoreceptors. Some of these substances have local effects but others are transported throughout different parts of the body and are able to control the entire cardiovascular system [46]. For example, hypercapnic acidosis (CO_2 and H^+ concentrations increase) changes several cardiovascular properties: the pulmonary vascular resistance increases, the systemic vascular resistance decreases and the heart rate increases [108].

2.4.2 Controls and regulations of the respiratory system

Unlike the heart which has its own rhythm thanks to specific cardiac cells (cells of the sinus node), the lungs cannot move without the control of the nervous system. It is mainly the dorsal respiratory group located in the dorsal portion of the medulla which controls the respiration cycle; it is active for inspiration and inactive for expiration. Two other respiratory groups are stimulated for extra breathing; the ventral respiratory group for expiration and the pneumotaxic center for the rate and depth of breathing [46]. The nervous system is able to modulate the amplitude and the frequency of respiratory ventilation. Chemical

factors stimulate or inhibit the respiratory nerves located in the medulla but Figure 2.19 shows that several other factors interact with the respiratory nerves.

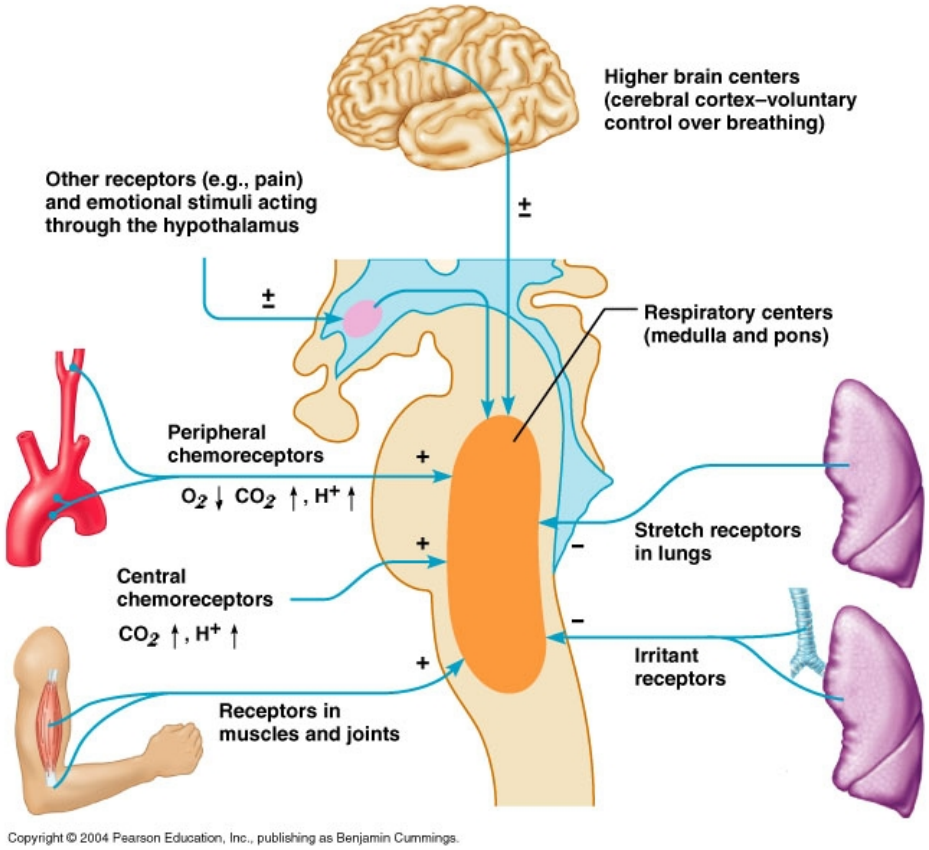

Figure 2.19 – Controls of the respiratory system [25].

Chemical factors

There are two groups of chemoreceptors: the central chemoreceptors located in the central nervous system (in the pons) and the peripheral chemoreceptors located in the carotid and in the aortic arch (Figure 2.19). Since the aim of the respiration is to maintain appropriate CO_2, O_2 and H^+ concentrations, these 3 molecules have a direct effect over the respiratory activity [64, 46].

For the central nervous system, it is mainly PCO_2 in blood which regulates the breathing. Indeed, PO_2 has no direct effect on the respiratory center of the brain and H^+ ions in blood cannot cross the blood-brain barrier. However, PCO_2 has an indirect effect over the central nervous system. The CO_2 molecules in blood cross the blood-brain barrier and the CO_2 molecules react with water in the cerebrospinal fluid and in the interstitial fluid

of the medulla to form H^+ ions (see reaction 2.8, p. 26). The neural sensors in the brain are especially excited by these H^+ ions. Therefore, if PCO_2 increases in blood, the PCO_2 and the H^+ ions in the interstitial fluid of the medulla increase and the H^+ ions stimulate the respiratory groups. The stimulation of the respiratory groups increases the respiratory activity [64, 46].

For the peripheral chemoreceptor system, it detects and controls the PO_2, the PCO_2 and the H^+ concentration in blood. For a small increase in PCO_2 and H^+ concentrations, the respiratory groups are stimulated and the ventilation is increased. For the O_2 molecules, the respiratory groups are stimulated only if PO_2 decreases below 60 mmHg [64, 46].

Other factors

Stretch receptors (proprioceptors) in the lungs are used to inhibit the breathing when the lung walls are too stretched. Some irritant factors, such as smoke, dust or pollen, also trigger the inhibition of the respiration thanks to irritant receptors. Furthermore, human being is of course able to control their breathing voluntary. Other information of the brain can affect the respiration such as emotional or pain stimuli. The last stimulation of the respiratory system is provoked by the proprioceptors located in the muscles and joints. This stimulus is used to anticipate the increased oxygen requirement during exercise [64, 25].

2.5 Summary

This chapter has introduced the major concepts of the cardiovascular and respiratory systems. The anatomy and the physiological performance of both systems have been described and the important parameters characterizing these systems have been developed for each system (the cardiac parameters have been described in subsection 2.1.2, the vascular parameters have been described in subsection 2.1.4 and the respiratory parameters have been described in subsection 2.3.4). In addition, several blood chemistry properties have also been introduced in this chapter (in section 2.2). The last section (section 2.4) has introduced the cardiopulmonary controls and regulations.

Chapter 3

Extracorporeal life support

In the previous chapter, the vital functions of the lungs and of the cardiovascular system have been described. If one or both of these systems are seriously damaged, the whole human body is in real danger. Therefore, scientists, physician and engineer have developed several extracorporeal circulations such as the Extracorporeal Life Support (ECLS) which is able to reproduce the vital functions of the lungs or/and the heart. The acronym ECMO for Extracorporeal Membrane Oxygenation is also used for this device. However, this designation is a bit misleading since this device also extracts the CO_2. Therefore, the acronym ECLS will be used in our study.

In this chapter, the history of extracorporeal circulations, the different components of the ECLS device, its applications in the ICU and the important parameters of the extracorporeal circulation will be discussed. In order to train the medical staff before real interventions on patients, several ECLS simulators have been developed. The different simulators available on the market are also discussed in this chapter.

3.1 History of ECLS

The first extracorporeal circulation was set up by surgeon John Gibbon in 1954 [8]. This device is called a cardio-pulmonary bypass and it is used to accomplish cardiac surgeries. Cardio-pulmonary bypass is rather different from the ECLS device; the latter is used for a longer support (several days or weeks) than cardio-pulmonary bypass and this extracorporeal circulation takes only a fraction of the cardiac blood flow whereas, cardio-pulmonary bypass diverts all the blood flow to the extracorporeal circulation. Therefore, the ECLS device must have an excellent hemocompatibility and the first successful use of this device was performed by physician J. Donald Hill in 1971.

Even if several improvements have been made during the last decades (the size of the different components have been reduced, the efficacy and the hemocompatibility of the different components have been improved), the side effects of setting an ECLS remains high and the use of this technology is thus only intended for patients with acute heart or/and lungs failures.

3.2 The different components of ECLS

The ECLS has three main components: a permeable membrane carrying out the gas exchanges between blood and the injected gas (atmospheric air or O_2 enriched air), a pump carrying out the extracorporeal blood flow and tubing and cannulae transporting blood from the patient to the membrane and back to the patient.

The synthetic membrane attempts to maximize the O_2 and CO_2 gas exchanges like the alveolar capillary membrane. The first membranes were in polyethylene. Then, using the development of new materials, silicone and finally polymethylpentene (PMP) hollow-fiber have been used [101]. Manufacturers try to produce a surface area as small as possible with a high effectiveness. Indeed, a larger surface area involves more hemocompatibility constraints. To increase the hemocompatibility an anticoagulant named heparin is used and the risk of hemorrhage is consequently increased. Furthermore, to avoid a large decrease in the blood volume in the vascular system when the ECLS is initialized, the membrane and the extracorporeal circuit are filled with physiological liquid before the initialization of the extracorporeal therapy. Smaller membranes thus involve smaller priming volumes and the blood dilution is weaker.

For the extracorporeal circulation, a centrifugal pump is often preferred than a roller pump. The tubing is in PVC and the cannulae are in wire-reinforced polyurethane [101].

In addition, surface coatings are applied to the different components to improve biocompatibility. Indeed, these substances are able to bond heparin molecules and thus prevent the coagulation of blood in the synthetic components.

3.3 The different applications of ECLS in the ICU

The ECLS can be set up in different configurations according to the pathology of the patient. If the patient has a heart disorder or a cardiopulmonary disorder, the clinicians

set up the ECLS in the venoarterial configuration, whereas if the patient has only a pulmonary disorder, the ECLS is in the venovenous configuration.

Venoarterial ECLS The main cardiovascular pathologies which are apt to venoarterial ECLS (va-ECLS) are the cardiogenic shock [82] and the septic shock [3]. The cardiogenic shock brings several heart damages together and this general pathology leads to insufficient cardiac output and thus insufficient tissue perfusions [69]. The septic shock is a body infection which leads to a low blood pressure because of a large decrease in the systemic vascular resistance [70]. In addition, a va-ECLS is also used after cardiac surgeries such as replacements of cardiac valves. In Figure 3.1, the left picture illustrates the standard configuration of a va-ECLS for an adult. The cannula extracting the venous blood is inserted into the femoral vein and placed just below the junction of the right atrium and the inferior vena cava. The cannula reinjecting the extracorporeal blood flow is inserted into the femoral artery and placed in the aortic arch (near the aortic valve). The placement of the arterial cannula must be strictly controlled. Indeed, the blood flow in the carotid is of paramount importance since it irrigates the brain and the arterial cannula must be thus appropriately placed.

Venovenous ECLS Acute respiratory distress syndrome (ARDS) is a serious lung pathology and a venovenous ECLS (vv-ECLS) is often used with this pathology [15, 63, 29]. ARDS is characterized by pulmonary inflammations and pulmonary edema which leads to severe hypoxemia [31]. In Figure 3.1, the right picture illustrates the standard configuration of a vv-ECLS for an adult. The cannula extracting the venous blood is inserted in the same way as for the venoarterial configuration. On the other hand, the cannula reinjecting the extracorporeal blood flow is inserted into the right internal jugular vein and placed towards the junction of the right atrium and the superior vena cava. The two cannulae are very closed to each other and their placement must be checked carefully to limit the recirculation of the extracorporeal blood flow. In addition, a new kind of vv-ECLS has been developed recently: the extracorporeal CO_2 removal device ($ECCO_2RD$) which is used for moderate ARDS [75, 11, 30, 110] and for chronic obstructive pulmonary disease (COPD) [1, 104]. COPD is characterized by airflow limitation. This pathology is progressive, treatable but not fully reversible [20]. More details about $ECCO_2RD$ are described in the next paragraph.

$ECCO_2RD$ Despite several technical improvements for the different components of the ECLS, the setting of this device still leads to severe complications such as hemorrhages. Therefore, the ECLS is reserved for patients with serious cardio-pulmonary disorders.

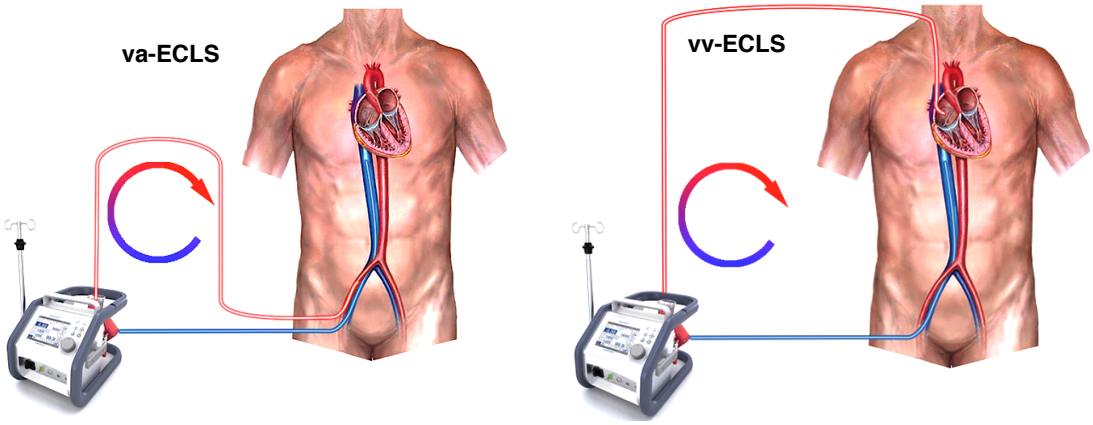

Figure 3.1 – Venoarterial ECLS (left picture) and venovenous ECLS (right picture) [90].

However, recent studies have shown that the setting of an ECLS could be beneficial for patients with moderate pulmonary disorders [75, 11, 30, 110]. The explanation is that it is worse to impose large inspired volume using a ventilator than to proceed to a super-protective ventilation combined with an extracorporeal CO_2 removal therapy ($ECCO_2RT$) [75]. Indeed, when the lungs are injured, large inspired volumes can increase pulmonary disorders. A super protective ventilation, which consists in a ventilation with very small tidal volume ($\approx$ 3ml/kg) and high O_2 concentration in inspired air, is thus recommended for patients with pulmonary insufficiencies. However, with this kind of ventilation, the CO_2 extraction is too small and an additional respiratory support must be included: an $ECCO_2RD$. The difference between an $ECCO_2RD$ and a conventional vv-ECLS is that the $ECCO_2RD$ is specialized in CO_2 extraction. Since it is easier to extract CO_2 than to oxygenate blood, the membrane of the $ECCO_2RD$ and the extracorporeal blood flow are thus smaller than in the vv-ECLS. This device is thus less invasive and has a smaller synthetic membrane. Therefore, it has fewer complications than the vv-ECLS.

3.4 Important parameters of the ECLS

Since the ECLS is able to support the functions of the heart and lungs, the important parameters concern both hemodynamic and gas exchanges properties.

The gas exchanges across the synthetic membrane are based on similar concepts than the gas exchanges in the lungs. The important parameters are thus similar to those of the lungs and are the following:

- PO_2, PCO_2, pH, HCO_3^- concentration and saturation of hemoglobin at the inlet and outlet cannulae.

- O_2 and CO_2 volume fraction in the gas entering the ECLS and in the gas getting out of the ECLS.
- Extracorporeal blood flow.
- Gas flow entering the extracorporeal device.
- O_2 and CO_2 diffusion coefficients across the synthetic membrane.

On the other hand, the extracorporeal pump is quite different from the cardiac pump. The extracorporeal pump delivers a continuous blood flow thanks to a mechanical rotation. For a given rotation speed, the extracorporeal blood flow varies according to the preload and the afterload of the pump. Figure 3.2 illustrates these concepts by clamping the pump inlet or the pump outlet for different rotations.

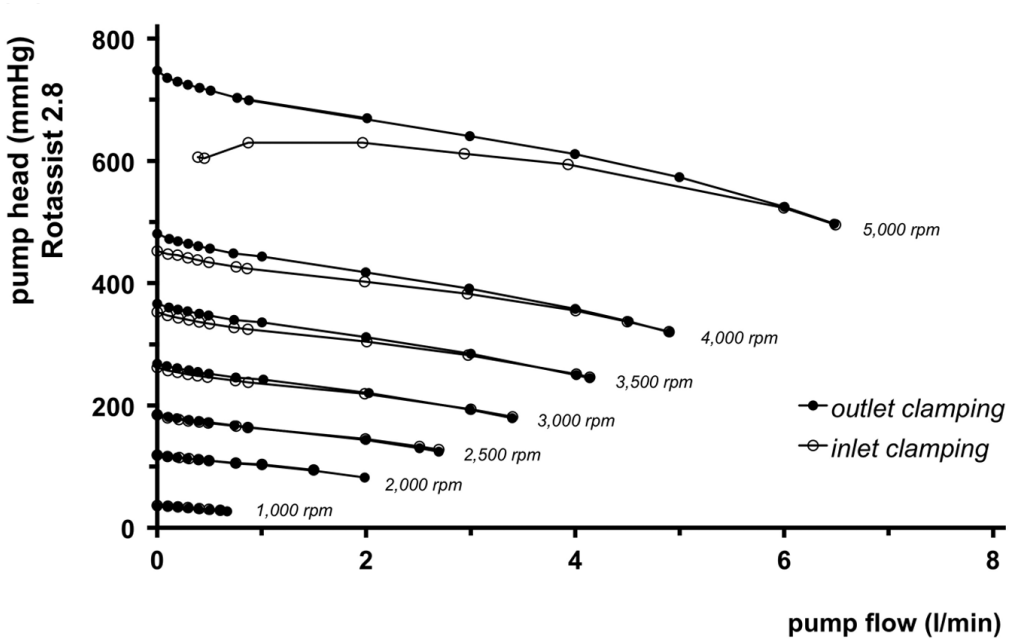

Figure 3.2 – Pump performance of the Rotassist 2.8 centrifugal pump® [103]. The preload of the pump is decreased by clamping the inlet cannula while the afterload of the pump is increased by clamping the outlet cannula.

For the extracorporeal circuit, the blood flow resistances are mainly located at the inlet and outlet cannulae. Figure 3.3 represents the pressure drop in pediatric femoral venous cannulae (left panel) and in adult femoral venous cannulae (right panel). However, the values must be read with cautious since the experimental data are carried out with water

instead of blood. The pressure drop curves are thus underestimated. Blood pressure and pressure drop are important parameters to avoid blood damages. It is mainly the negative pressure which must be limited [79]. The inlet pressure has to be superior than -50 mmHg [84, 24]. The limitation of positive pressure is less severe; the outlet pressure has to be inferior than 300 mmHg [73].

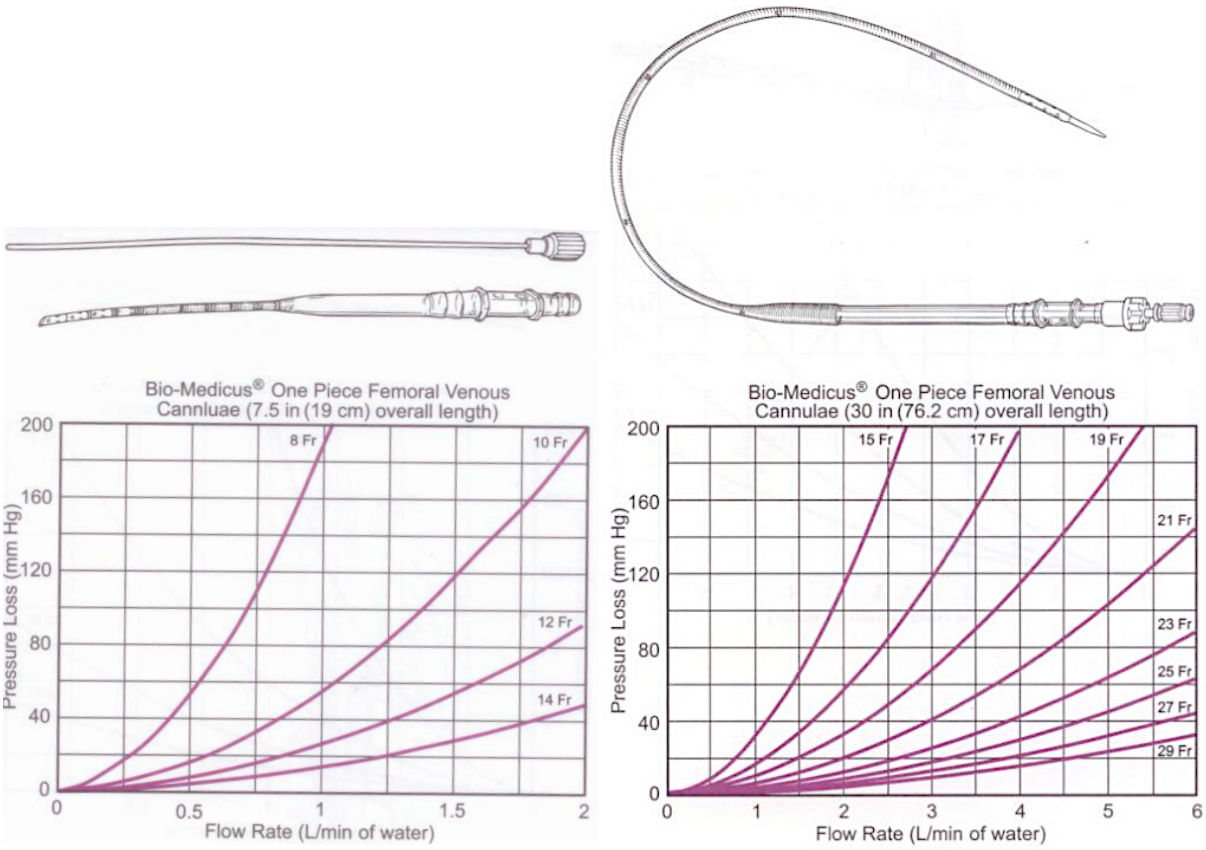

Figure 3.3 – Pressure drops in femoral venous cannulae with different diameter sizes [71]. The left panel corresponds to pediatric cannulae and the right panel corresponds to adult cannulae.

Note that in the cardiovascular model that will be developed in Chapter 4, the blood pressures and the blood volumes of the extracorporeal circuit will not be explicitly included. Indeed, the goal of our study is to characterize the behavior of the patient according to different ECLS functionings. The hemodynamic interactions of the ECLS with the patient are only the extracorporeal blood flow. Since the extracorporeal blood flow is continuously measured and can be controlled by the medical team, this blood flow is simply an input of the cardiovascular model. Nevertheless, we must keep in mind that the extracorporeal blood flow depends on several parameters.

3.5 The ECLS simulators

The setting and the control of an ECLS are complex and some technical errors could lead to the death of a patient. The medical staff thus has to be well trained before using this device. Two types of ECLS simulators designed for training purposes can be distinguished: computer based simulators and simulators with hands-on approach. Computer based simulations are really easy to use since the medical staff only needs a computer and the appropriate program. Several programs already exist on the internet like the *ECMOjo simulator* developed by the Telehealth Research Institute in the University of Hawaii and the *ECMO simulator* developed by the Modular Simulation Environment (MSE) company located in Australia [27]. Simulations with hands-on approach need more equipments but are closer to reality. Indeed, these simulations are carried on real ECLS circuits and the computer programs are often integrated to a material system such as a black box or a mannequin. The price of such simulator is thus higher and fewer hospitals own this type of tools. Several training device with hands-on simulations are available on the market. There are the *Califia* developed by BioMed Simulation from California, *ECMOsim* developed at the Radboud University Medical Center in Nijmegen, *ECMO simulation training* developed in the Hawaiian medical center and *ECMO crisis training* developed in Minnesota's Mayo Clinic [27]. Figure 3.4 illustrates two ECLS simulators: picture A represents the computer based simulation of the Telehealth Research Institute (the *ECMOjo* program) and picture B represents the hands-on simulation of the Radboud University Medical Center (the *ECMOsim* device).

3.6 Summary

Chapter 3 has described the role of extracorporeal life support (ECLS) in the medical field. The different components and the different application of this device have been described. Then, the important parameters characterizing the proper functionning of the extracoporeal device have been briefly discussed. Finally, ECLS simulators have already been developed by several firms and these have been briefly presented in this chapter.

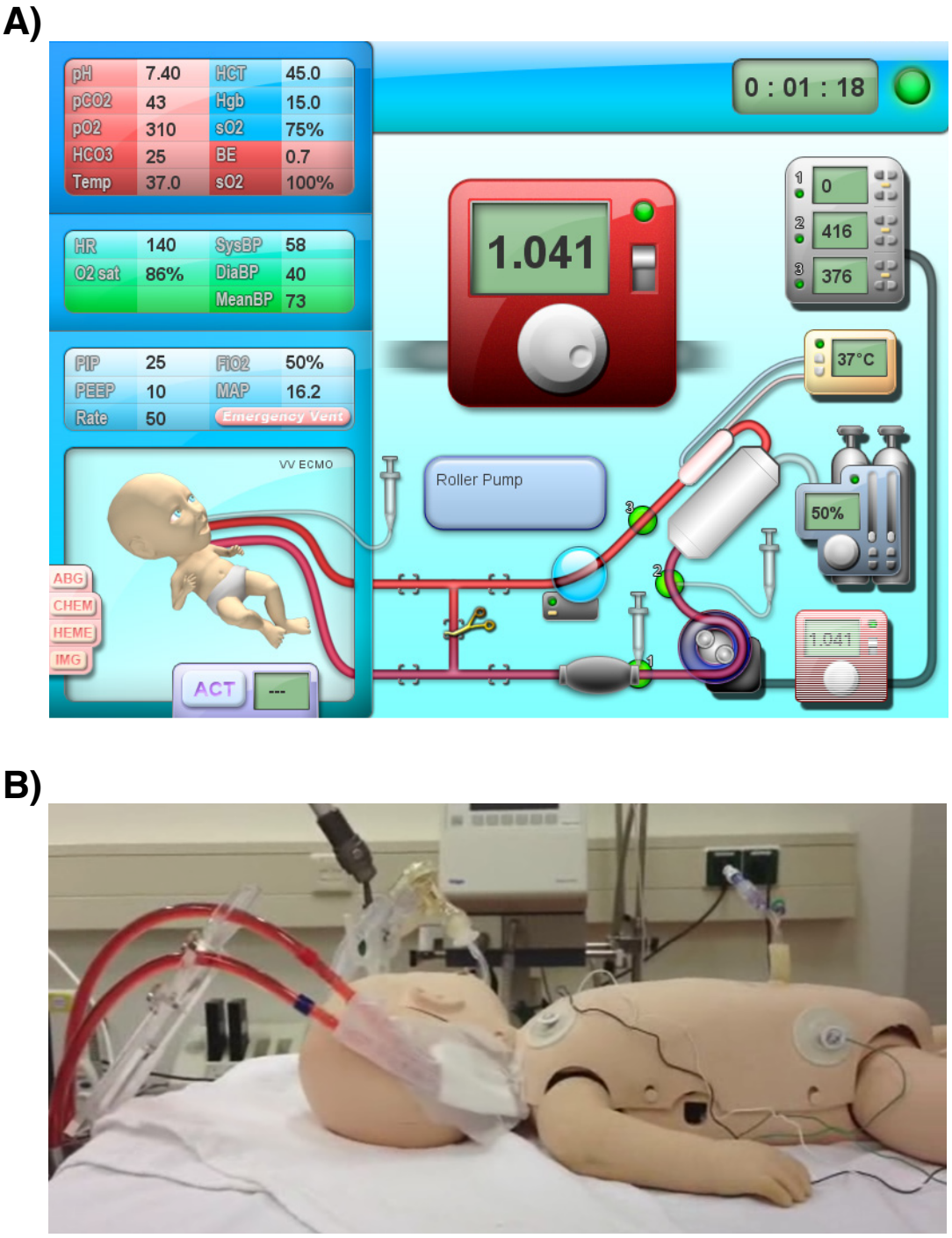

Figure 3.4 – Illustration of two simulators. Picture A represents an online simulator while picture B represents a hands-on simulator [27].

Part II

Mathematical modeling

The second part of the thesis describes the modeling of the cardiovascular system, the respiratory system and the extracorporeal life support. Since these systems are very complex, many simplifications are going to be introduced. The models must be simple enough to be identifiable with the available measurements in the ICU and necessitate a small computation time to satisfy the need of a rapid decision by clinicians at the patient bedside. There is a large number of cardiovascular and respiratory models in the literature with various complexity. The most complex models are the *distributed* models, which are 3-D finite elements models with millions degrees of freedom [50, 58]. These models are used to understand local part of the cardiovascular system or of the respiratory system with an excellent accuracy. On the other extreme of complexity lie *lumped* parameter models, which gather different components of the system together in several boxes [18, 107, 86, 105, 67, 93, 54, 9, 45]. Figure 3.5 illustrates these two extreme methods for the modeling of the heart. In this example, the *distributed* method divides the right ventricle, the right atrium, the left ventricle, the left atrium, the pulmonary artery and the aorta in small pieces whereas the *lumped* method represents the heart with only two boxes; one for the right ventricle and the other one for the left ventricle. To achieve the goal of our study (rapid simulations which are identifiable in the ICU), the *lumped* parameter method is chosen.

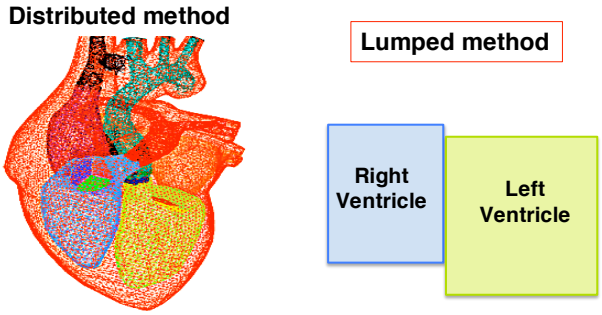

Figure 3.5 – Modeling of the heart with the *distributed* method (picture on the left [120]) and with the *lumped* method (picture on the right).

This second part consists in two chapters. Chapter 4 describes our modeling of the cardiovascular system connected to a va-ECLS. Even if the va-ECLS has gas exchange functions, the mathematical model focuses only on the mechanical side of the system. Chapter 5 describes our modeling of the respiratory system connected to a vv-ECLS. This configuration assists only the lungs and the model thus focuses only on the gas exchanges in the lungs, in the tissues and in the ECLS. Therefore, our cardiovascular model will not be taken into account for the modeling of patients under vv-ECLS and the respiratory model will not be taken into account for the modeling of patients under va-ECLS. In this part, several parameters are introduced and their estimations will be described in Part III.

Chapter 4

Modeling of the cardiovascular system connected to a va-ECLS

Most lumped parameter models of the cardiovascular system are derived from the Windkessel model [18, 107, 86, 105, 67]. A certain amount of them are very complex and take into account numerous compartments [67] while others try to be as simple as possible to be identifiable in the ICU [89, 86]. However, all the models are composed with the same elements: cardiac valves, cardiac chambers, vascular vessels with elastance and resistance properties. Since the goal of our study is to build a tool that could help clinicians in their therapeutic approach, the minimal cardiovascular model of Pironet *et al.* [89] is chosen. Indeed, these authors have presented practical identifiability of the mathematical model from limited clinical data. To obtain the mathematical model of the cardiovascular system connected to a va-ECLS, this cardiovascular model is complemented by an additional compartment describing the va-ECLS.

Several hypothesis are introduced to build this model:

- Blood is considered as incompressible
- The different compartments are elastic chambers linked together thanks to rigid cylinders (the resistance and the compliance of blood vessels are uncoupled)
- Pressure is constant over the transversal section of the rigid cylinders and the pressure gradient is constant along the rigid cylinders.
- Gravity is neglected
- Control systems are neglected
- Inertia of blood flows is neglected

- The pulmonary circulation is not considered in this approach. The model is composed of one ventricle which sucks blood in the vena cavae and rejects it in the aorta.

This chapter is divided into 3 sections; section 4.1 describes the different elements and concepts of the cardiovascular model, section 4.2 presents the ECLS compartment and section 4.3 shows how the different elements are linked together and describes all the differential equations of the cardiovascular model connected to a va-ECLS.

4.1 Cardiovascular model

The cardiovascular system is composed of active elements (the ventricles), passive elements (the vascular system) and cardiac valves. The hemodynamics of this system derived from the Windkessel model and this concept is described in subsection 4.1.1. The pressure volume relationships are described by considering a new variable: the stressed volume, and the concept of stressed and unstressed volumes is introduced in subsection 4.1.2. Finally, the mathematical descriptions of the passive and active elements are explained in subsection 4.1.3 and 4.1.4 respectively, while the mathematical description of the cardiac vales is explained in subsection 4.1.5.

4.1.1 Windkessel model

In the 18^{th} century, researchers realized that the cardiovascular system is similar to the contemporary hydraulic system used by firemen (Figure 4.1). Indeed, the pump activity is analogous to the ventricle contraction, the valves are analogous to the cardiac valves and the accumulation chamber (V_X in Figure 4.1) is analogous to the elastic properties of the vascular system (arteries and veins, see subsection 2.1.3). In addition, the resistance in the fire hose is also observed in the small vessels of the cardiovascular system (the arterioles, see subsection 2.1.3).

This analogy leads to simple equations describing the cardiovascular system. The volume variation in the accumulation chamber $\dot{V}_X$ is equal to:

$$\dot{V}_X = Q_X = Q_{pump} - Q_{OUT} \ , \tag{4.1}$$

where Q_X is the water flow entering the accumulation chamber, Q_{pump} is the water flow ejected from the pump and Q_{OUT} is the water flow moving into the fire hose. The water flow Q_{OUT} crossing the resistance R is equal to:

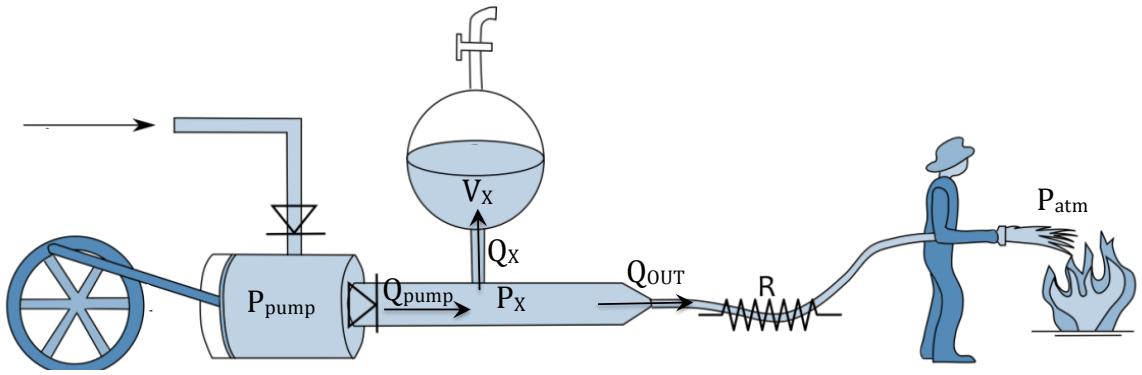

Figure 4.1 – Origins of the Windkessel model (adapted from [83]). All the symbols are defined in the text and in the list of symbols.

$$Q_{OUT} = \frac{P_X - P_{atm}}{R} \ , \tag{4.2}$$

where P_X is the hydraulic pressure measured before the fire hose and P_{atm} is the atmospheric pressure (the pressure measured after the fire hose). The volume V_X is analogous to the volume in the aorta where Q_{pump} is the blood flow going out of the left heart, Q_{OUT} is the blood flow crossing the small vessels (the arterioles and the capillaries) and P_X is the blood pressure in the aorta.

The cardiovascular system is composed of elastic chamber elements. Indeed, the vessel walls are deformable and the vessel volumes follow the variations of blood pressures. The pressure-volume relationship of the cardiac chambers are described in the following subsections 4.1.3 and 4.1.4.

4.1.2 Stressed and unstressed volumes

The different equations written above describe the behavior of blood when it is stressed. However, the whole amount of blood in the vascular system is not stressed; there is also a quantity of blood which is not stressed. These two quantities are named the stressed blood volume and the unstressed blood volume. Since the venous system hoards a large fraction of blood, the unstressed volume is significant in the veins. In addition, the vein volumes can vary according to patient needs and, thus, the unstressed volume is not constant for different physiological conditions.

An hydraulic analogy of the unstressed and stressed volumes is depicted in the left part of Figure 4.2. This drawing represents a large container which is supplied by one

pipe located on the upper right of the picture. The container has also an outflow pipe characterized by a resistance *VenR*. The unstressed volume (named V_u in the left picture of Figure 4.2) is located at the bottom of the container, below the outflow pipe. This volume has thus no influence on the flow crossing the resistance *VenR*. On the contrary, the stressed volume (named V_s in the left picture of Figure 4.2) is located above the outflow pipe and this volume has a direct influence on the outflow. Indeed, if the stressed volume increases, the pressure at the entrance of the outflow piper increases. Hence, this analogy shows that the stressed volume contributes to the hemodynamics of the cardiovascular system while the unstressed volume is responsible for the passive filling of the cardiovascular system.

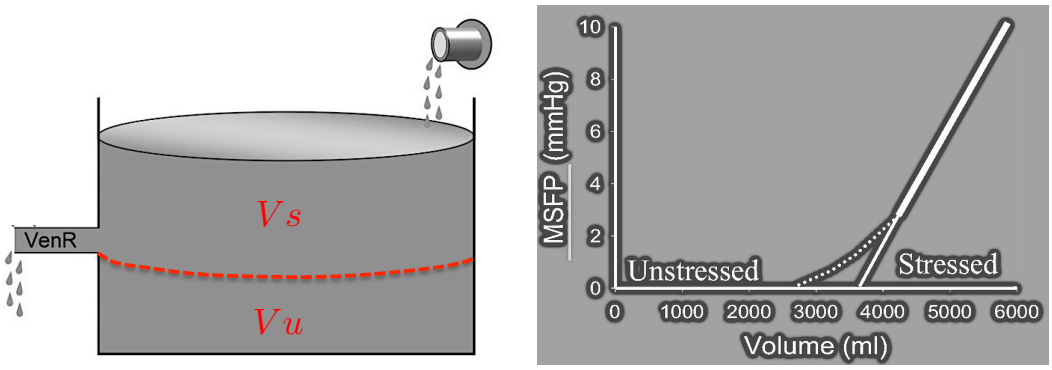

Figure 4.2 – Illustration of stressed and unstressed blood volumes [34, 68].

The right panel of Figure 4.2 represents the evolution of the *Mean Circulatory Filling Pressure* (MSFP) in terms of the total blood volume in the cardiovascular system. The MSFP is the blood pressure in the cardiovascular system when there is no hemodynamics. In these conditions, there is no cardiac beat, no blood flow across the vessels and the blood pressure is the same in all blood vessels. The MSFP is thus equal to zero when the total blood volume is small since the vessels are not fully filled and the vessel walls undergo no pressure. When the total blood volume reaches approximately 3 l for a healthy adult, the MSFP becomes positive. First, the MSFP increases non-linearly with the total blood volume. Then, when the total blood volume exceeds 4 l, the MSFP increases linearly with the total blood volume. The equations written previously (equations 4.3 and 4.7) have assumed this linear relationship.

4.1.3 Pressure-volume relationship for passive elements

As already mentioned in subsection 2.1.4 (see equations 2.4), the cardiac chamber volumes and pressures are linked together with the elastance E or the compliance C of the cor-

responding cardiac chamber. The approximation of constant elastance or compliance is taken for granted for the passive elements and the following pressure-volume relationship is written:

$$P_i(V_i) = E_i \cdot (V_i - V_{u,i}) \tag{4.3a}$$

$$= \frac{1}{C_i} \cdot (V_i - V_{u,i}) \ , \tag{4.3b}$$

where P_i and V_i are the pressure and the volume of the cardiac chamber i, E_i and C_i are the elastance and the compliance of the cardiac chamber i and $V_{u,i}$ is the volume of the cardiac chamber i when the blood pressure P_i is equal to 0 (the cardiac chamber wall is unstressed). This approximation is represented by the straight line in the left panel of Figure 4.3.

For our cardiovascular model, the following change of variable is considered:

$$V_{s,i} = V_i - V_{u,i} \ , \tag{4.4}$$

where $V_{s,i}$ and $V_{u,i}$ are the stressed and unstressed volumes of the cardiac chamber i. This change of variable is illustrated on the right panel of Figure 4.3. If the change of variable defined in equation 4.4 is used in equations 4.3, they become:

$$P_i(V_{s,i}) = E_i \cdot V_{s,i} \tag{4.5a}$$

$$= \frac{1}{C_i} \cdot V_{s,i} \ , \tag{4.5b}$$

4.1.4 Pressure-volume relationship for the active elements

The ventricles are active elements and, therefore, the pressure in these cardiac chambers does not solely depend on the volume. Indeed, the ventricles are subject to contraction and the pressure thus also depend on time. Consequently, the ventricles follow a cycle and the pressure-volume relationship results in a pressure-volume loop (see subsection 2.1.1 and subsection 2.1.2). To describe these active elements with a mathematical model, the time-varying elastance theory is commonly used in the literature [18, 107, 86, 105, 67] and it is the most simple model to describe the ventricle activity. The time-varying elastance

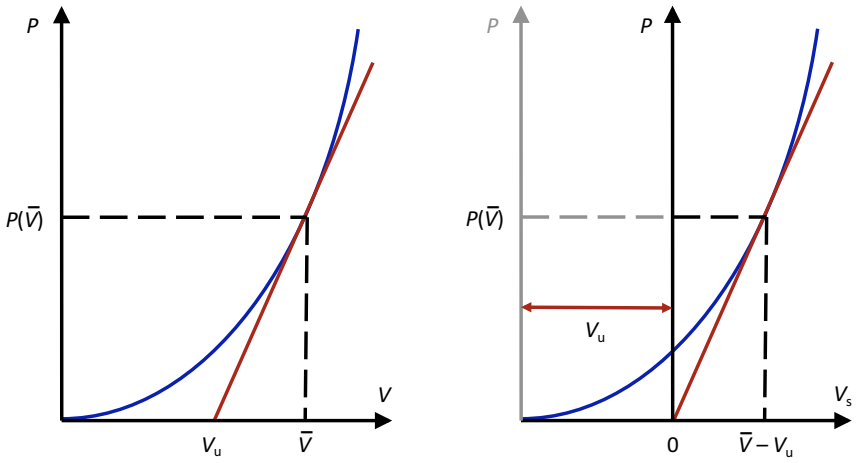

Figure 4.3 – The left panel illustrates the pressure volume relationship in the passive elements and illustrates the linear approximation of this pressure volume relationship. The right panel illustrates the change of variable $V_s = V - V_u$ [86].

theory is based on 3 concepts: the EDPVR, the ESPVR and the cardiac driver function $e(t)$ (the EDPVR and the ESPVR have already been introduced in subsection 2.1.2). The mathematical development of these 3 concepts are described in the following paragraphs.

EDPVR

The EDPVR describes the passive filling of the heart (Figure 4.4) and this curve can be approached by an exponential [106, 18]:

$$P_{ed} = B_h \cdot \left(e^{A_h \cdot (V_h - V_{u,h})} - 1\right) = B_h \cdot \left(e^{A_h \cdot (V_{s,h})} - 1\right) \ , \tag{4.6}$$

where P_{ed} is the end-diastolic pressure in the heart, V_h is the heart volume, $V_{u,h}$ and $V_{s,h}$ are the unstressed and stressed heart volumes. Like the passive elements, the change of variable $V_s = V - V_u$ is used. A_h and B_h are two parameters of the model.

ESPVR

The ESPVR can be determined by considering the PV loop of several physiological states corresponding to different afterloads and different preloads (Figure 2.4 in subsection 2.1.2, p. 16). The ESPVR corresponds to the top-left point of each of these loops and it has been shown [109] that this line can be approximated by a straight line:

$$P_{es} = E_h \cdot (V_h - V_{u,h}) = E_h \cdot (V_{s,h}) \ , \tag{4.7}$$

where P_{es} is the end-systolic pressure in the heart and E_h is the slope of the straight line.

E_h is a parameter of paramount importance since it characterizes the contractility of the heart. Like equation 4.6, the change of variable $V_s = V - V_u$ is considered.

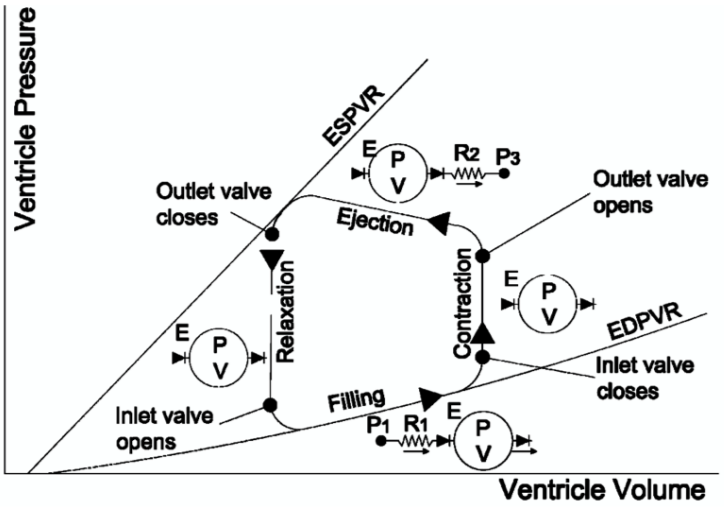

Figure 4.4 – Modeling of a cardiac cycle using the EDPVR and the ESPVR [105].

Cardiac driver function

The ESPVR and the EDPVR describe two extreme behaviors of the heart. To go from one curve to the other one, a cardiac driver function e(t) is defined to have the following pressure-volume relationship (Figure 4.5):

$$\begin{aligned} P_h &= e(t) \cdot P_{es} &&+(1 - e(t)) \cdot P_{ed} \\ &= e(t) E_h \cdot V_{s,h} &&+(1 - e(t)) \cdot B_h \cdot \left(e^{A_h \cdot V_{s,h}} - 1\right) \ , \end{aligned} \tag{4.8}$$

where e(t) is defined to vary between 0 and 1; when e(t) = 1 the pressure volume relationship is defined by the ESPVR and when e(t) = 0 the pressure volume relationship is defined by the EDPVR. Using the cardiac driver function, the entire PV loop can be simulated. Several cardiac driver functions have been developed in literature. A common one defines e(t) as an arithmetic series of exponential:

$$e(t) = \sum_{i=1}^{N} A_i \cdot e^{-B_i \cdot (t - C_i)^2} \ , \tag{4.9}$$

where the different parameters have the following values [107, 105]: $N = 1$, $A_1 = 1$, $B_1 = 80$ s^{-2} and $C_1 = 0.27$ s. However, these parameters do not depend on the heart rate and are thus only valid for a human at rest in physiological conditions (heart rate between 70 and 90 beats per minute). In our study, the model must be subject-specific

and the heart rate can be high since the patient has cardiovascular pathologies. If the parameters B_1 and C_1 are considered constant, the function e(t) defined by equation 4.9 presents non negligible discontinuities for high heart rates (the dashed lines presented in Figure 4.6 illustrates this phenomena). Therefore, in our approach, e(t) is scaled according to the cardiac period T and parameters B_1 and C_1 are replaced by $B_{1,T}$ and $C_{1,T}$, which are defined as follow:

$$\begin{cases} B_{1,T}(T) &= (\beta \cdot T)^{-2} \\ C_{1,T}(T) &= \gamma \cdot T \end{cases} , \tag{4.10}$$

where β and γ are constant parameters. For a heart rate of 80 beats per minute (a cardiac period of 0.75 s), the following assumption can be taken

$$\begin{cases} B_{1,T}(0.75) = B_1 = 80 \text{ s}^{-2} \\ C_{1,T}(0.75) = C_1 = 0.27 \text{ s} \end{cases} ,$$

and the parameters β and γ can thus be estimated:

$$\begin{cases} \beta = 0.149 \\ \gamma = 0.36 \end{cases} .$$

In our cardiovascular model, the driver function e(t) is thus described with the following equation:

$$e(t) = \exp\left[-B_{1,T} \cdot (t - C_{1,T})^2\right] = \exp\left[-\frac{1}{(0.149 \cdot T)^2} \cdot (t - 0.36 \cdot T)^2\right] . \tag{4.11}$$

Figure 4.6 illustrates this function e(t) during two cardiac periods and for different heart rates (80, 100, 120 and 150 beats per minute). The solid lines represent e(t) when the parameters $B_{1,T}(T)$ and $C_{1,T}(T)$ are used while the dashed lines represents e(t) when the parameters B_1 and C_1 are used. When the parameters of the e(t) function are constant, Figure 4.6 shows that the function e(t) is not valid for heart rates larger than 120 beats per minute. Indeed, for a heart rate of 150 beats per minute, the dash line shows a significant discontinuity. Note that in order to represent the e(t) function for several cardiac periods, the time t in equation 4.11 is replaced by $t^\star$ and the relationship between these two times is written as follow:

$$t^\star = \text{mod}(\ t\ ,\ T\ ) \tag{4.12}$$

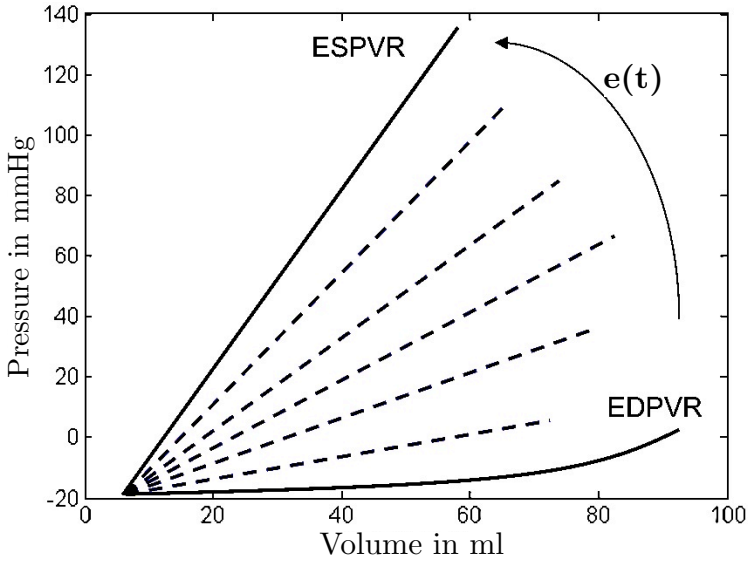

Figure 4.5 – Illustration of the e(t) function which allows to go from the EDPVR to the ESPVR [107].

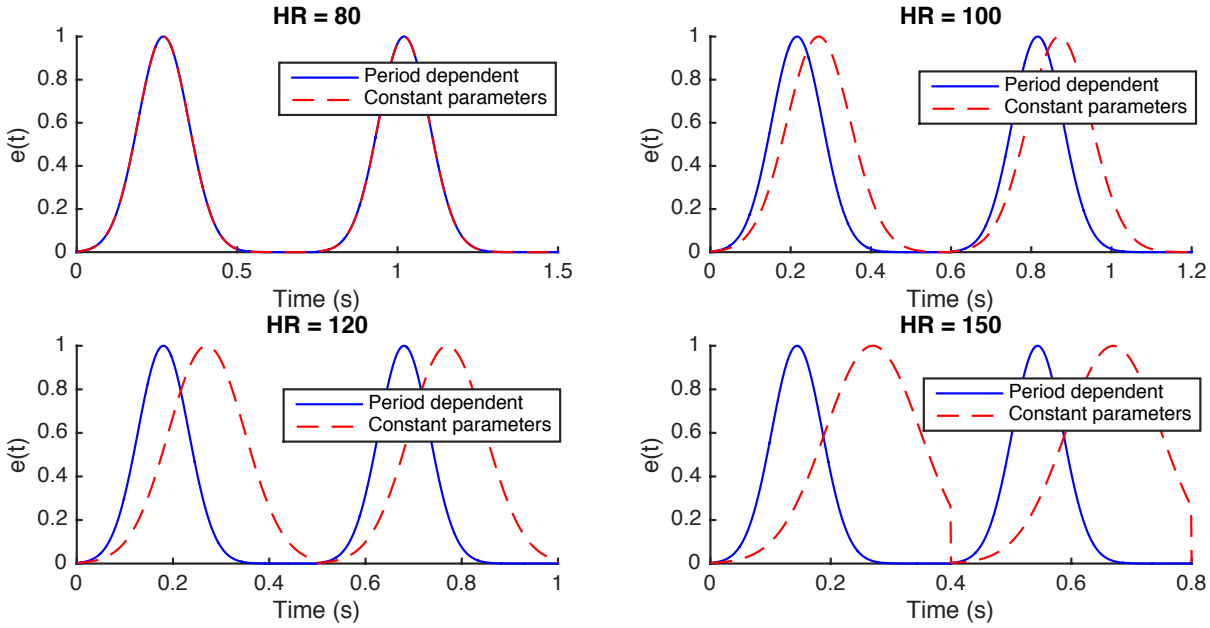

Figure 4.6 – Illustration of the e(t) function during two cardiac cycles. The solid lines represent the e(t) function defined by equation 4.11 while the dashed lines represent the e(t) function when the constant parameter $B_1 = 80$ s^{-2} and $C_1 = 0.27$ s are used.

4.1.5 Valve modeling

In the cardiovascular system, the cardiac valves allow the blood flow to circulate in only one direction. If there is no cardiac valve, the blood flow can be written as equation 2.5 (see section 2.1.4, p. 21). However, when the blood flow crosses a cardiac valve, this equation is not always right. For example, the water flow Q_{pump} presented in Figure 4.1 has the following values:

$$Q_{pump} = \begin{cases} 0 & \text{si} \quad P_{pump} \leq P_X \\ \dfrac{P_{pump} - P_X}{R_{valve}} & \text{si} \quad P_{pump} > P_X \end{cases} , \tag{4.13}$$

where P_{pump} is the pressure in the pump of the hydraulic system presented in Figure 4.1 and R_{valve} is the resistance of the valve located between the pump and the accumulation chamber X. Using the Heaviside function $H(x)$, equation 4.13 can be rewritten:

$$Q_{pump} = H\left[P_{pump} - P_X\right] \cdot \frac{P_{pump} - P_X}{R_{valve}} . \tag{4.14}$$

where:

$$H\left[P_{pump} - P_X\right] = \begin{cases} 0 & \text{si} \quad P_{pump} - P_X \leq 0 \\ 1 & \text{si} \quad P_{pump} - P_X > 0 \end{cases} . \tag{4.15}$$

4.2 va-ECLS

When the ECLS assists the heart, this device takes a fraction of the blood flow in the veins and rejects it in the arteries (see section 3.3 for the details). The contribution of the ECLS in the cardiovascular model is very simplified. The ECLS compartment is modeled as a parameter input. This parameter is the extracorporeal blood flow beginning in the vena cava and ending in the aorta.

4.3 Differential equations for the cardiovascular model connected to a va-ECLS

The cardiovascular model is a minimal model to be identifiable in the ICU. This model has only 3 compartments: one for the heart, one for the arteries and one for the veins. This cardiovascular model is complemented by the ECLS compartment which takes a fraction of blood in the vena cava and rejects it in the aorta.

Figure 4.7 depicts a schematic representation of the 4 compartments model. The arteries compartment is characterized by the two variables P_a and $V_{s,a}$ for the blood pressures and the stress blood volumes in the arteries and by one parameters E_a defining the elastance of the arteries (see subsection 4.1.3). The veins compartment is characterized by the two variables P_v and $V_{s,v}$ for the blood pressure and the stress blood volume in the veins and by one parameter E_v defining the elastance of the veins. The variables and the parameters of the heart compartment have already be presented in subsection 4.1.4. The blood flow ejected by the heart Q_o is characterized by the resistance R_o (the resistance of the output valve), the blood flow going from the arteries to the veins Q_s is characterized by the resistance R_s (systemic resistance) and the blood flow entering the heart Q_i is characterized by the resistance R_i (resistance of the input valve). The ECLS is characterized by the extracorporeal blood flow Q_d which takes blood in the vena cava (just before the input valve) and rejects it in the aorta (just after the output valve).

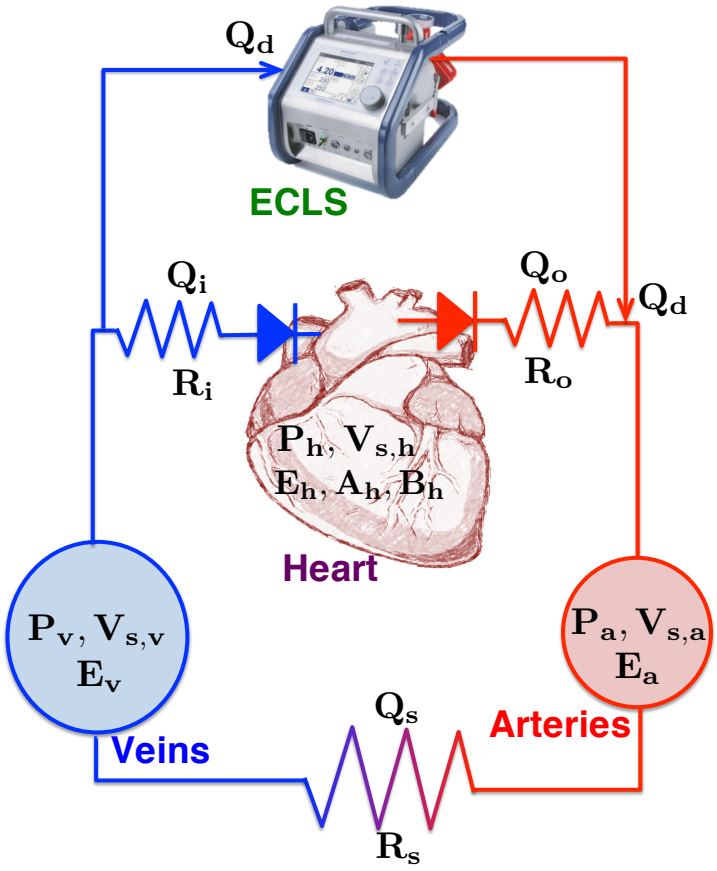

Figure 4.7 – Model of the respiratory system connected to a va-ECLS. All the symbols are defined in the text of this chapter and in the list of symbols page xxiii.

If equations 4.1 and 4.14 are applied to this model, the following differential equations can be written:

$$\begin{cases} \dot{V}_{s,h} = Q_i - Q_o = H(\mathrm{P_v - P_h}) \cdot \dfrac{P_v - P_h}{R_i} - H(\mathrm{P_h - P_a}) \cdot \dfrac{P_h - P_a}{R_o} \\ \dot{V}_{s,a} = Q_o - Q_s + Q_d = H(\mathrm{P_h - P_a}) \cdot \dfrac{P_h - P_a}{R_o} - H(\mathrm{P_a - P_v}) \cdot \dfrac{P_a - P_v}{R_s} + Q_d \\ \dot{V}_{s,v} = Q_s - Q_i - Q_d = H(\mathrm{P_a - P_v}) \cdot \dfrac{P_a - P_v}{R_s} - H(\mathrm{P_v - P_h}) \cdot \dfrac{P_v - P_h}{R_i} - Q_d \end{cases} , \tag{4.16}$$

where the pressures are related to the volumes by equation 4.8 for the heart compartment and by equation 4.3 for the arteries and veins compartments.

If the 3 equations of system 4.16 are summed, the following equation is written:

$$\dot{V}_{s,h} + \dot{V}_{s,a} + \dot{V}_{s,v} = 0 \ . \tag{4.17}$$

The right-hand side of equation 4.17 is equal to 0 and this confirms that the system is a closed loop. The integration of both-hand side of equation 4.17 gives the following relation:

$$V_{s,h} + V_{s,a} + V_{s,v} = SBV \ , \tag{4.18}$$

where SBV is the total stress blood volume and this parameter is constant in time.

4.4 Summary

This chapter has described the different components of the cardiovascular model assisted by a va-ECLS. Like several cardiovascular models, this model is based on the Windkessel model. The different components of the model are one active compartment (the heart), two passive compartments (arteries and veins) and the va-ECLS compartment. For the active and passive compartments, the pressure volume relationship has been described and the blood flows going from one compartment to another have been modeled by taking into account resistive elements and cardiac valves. In addition, the concept of unstressed and stressed blood volume have also been introduced.

Chapter 5

Modeling of the respiratory system connected to a vv-ECLS

Our model of the respiratory system connected to a vv-ECLS is a lumped parameter model with 3 compartments: the lungs, the tissues and the vv-ECLS (the 3 compartments are sketched in Figure 5.1 and this model has also been presented in the paper of Habran *et al.* [45]). Every compartment is discussed in this chapter. In addition, a blood chemistry model is needed and is discussed in section 5.4. Finally, the blood transport between the compartments is also discussed in the last section of this chapter.

Several hypothesis are considered to build this model:

- The lungs are considered as one compartment. Hence, the right and left lungs behave alike.
- Gas equilibrium are assumed between alveoli and pulmonary capillaries and between tissues and systemic capillaries.
- Control systems are neglected.
- Temperature in the body, humidity in the body and ambiant pressure are assumed constant and equal to 37°C, 47 mmHg and 760 mmHg respectively.
- Gravity is neglected.
- The mechanics of ventilation are not described in the model. The gas inflow and the gas outflow are continuous and constant flows.

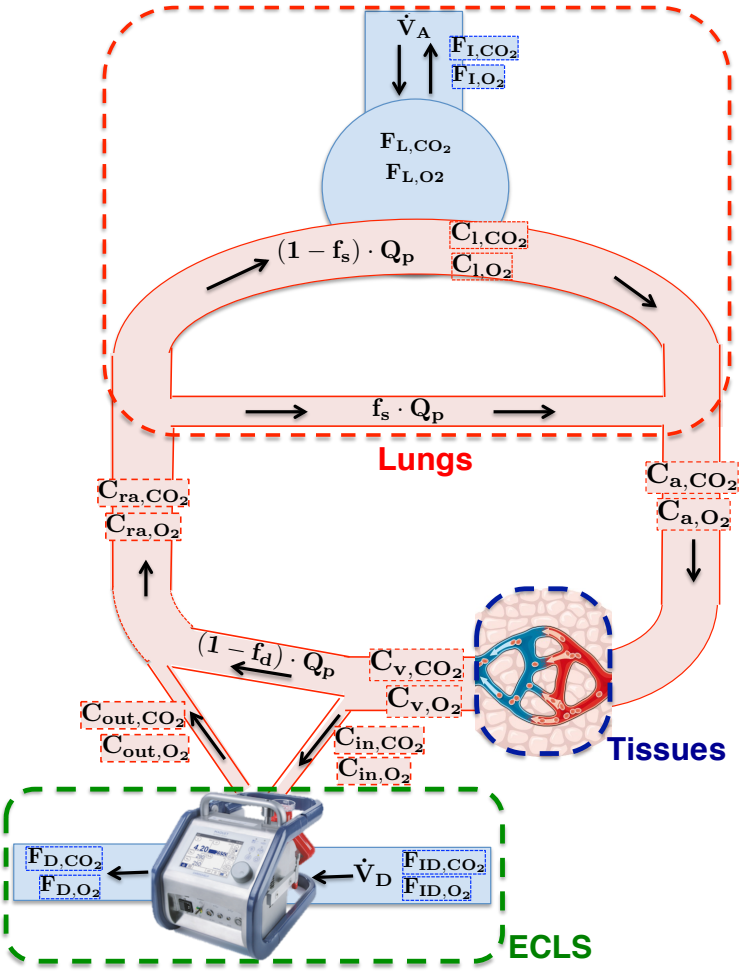

Figure 5.1 – Model of the respiratory system connected to a vv-ECLS. All the symbols are defined in the text of this chapter and in the list of symbols page xxiii.

5.1 Gas exchanges in the lungs

Our mathematical model of pulmonary gas exchanges is based on the work of Batzel *et al.* [9]. This model considers that the diffusions of O_2 and CO_2 through the alveolar-capillary membrane are fast so that equilibrium can be assumed between the alveoli and the capillaries at the end of pulmonary capillaries. To include pulmonary gas exchanges abnormalities, additional parameters and additional equations are required. Lungs failures such as ARDS are complex phenomena and some authors describe this pathology by dividing the lungs into 2 compartments to model ventilation/perfusion mismatch [93, 54]. Since the identification of the parameters of these 2 compartments is not easy (and even impossible in our case with the available data in the ICU), a simpler description will be used. A pulmonary shunt characterized by the fraction f_s of the blood flow not participating in the gas exchanges and an alveolar ventilation $\dot{V}_A$ will be considered. The

value of these 2 parameters will determine the global quality of gas exchanges which will thus allow modeling lung pathologies in a simple way (Figure 5.1 and subsection 2.3.2, p. 28, for more details). In this context, the material balances of O_2 and CO_2 in the lungs can be written as:

$$V_{L,O_2} \cdot \dot{F}_{L,O_2} = (1 - f_s) \cdot Q_p \cdot (C_{ra,O_2} - C_{l,O_2}) + \dot{V}_A \cdot (F_{I,O_2} - F_{L,O_2}) \ , \tag{5.1a}$$

$$V_{L,CO_2} \cdot \dot{F}_{L,CO_2} = (1 - f_s) \cdot Q_p \cdot (C_{ra,CO_2} - C_{l,CO_2}) + \dot{V}_A \cdot (F_{I,CO_2} - F_{L,CO_2}) \ , \tag{5.1b}$$

where:

- V_{L,O_2} (ml) and V_{L,CO_2} (ml) are the effective volumes of O_2 and CO_2 in the lungs (these two quantities are not equal because CO_2 passes easier into solution and an additional storage into lung tissues and fluid is observed for CO_2 [9]),
- F_{L,O_2} and F_{L,CO_2} are the O_2 and the CO_2 volume fractions in the lungs (alveoli),
- f_s is the fraction of the pulmonary blood flow crossing the pulmonary shunt,
- Q_p (ml/s) is the pulmonary blood flow,
- C_{ra,O_2} ($\mathrm{ml}_{\mathrm{O}_2}$/ml) and C_{ra,CO_2} ($\mathrm{ml}_{\mathrm{CO}_2}$/ml) are the O_2 and the CO_2 blood concentrations in the right atrium,
- C_{l,O_2} ($\mathrm{ml}_{\mathrm{O}_2}$/ml) and C_{l,CO_2} ($\mathrm{ml}_{\mathrm{CO}_2}$/ml) are the O_2 and the CO_2 blood concentrations in the lungs (pulmonary capillaries),
- F_{I,O_2} and F_{I,CO_2} are the inspired fractions of O_2 and CO_2,
- $\dot{V}_A$ (ml/s) $= fr \cdot (V_T - V_{Dead})$ is the alveolar ventilation. fr (s^{-1}) is the respiratory frequency, V_T (ml) is the tidal volume and V_{Dead} (ml) is the dead space. Here $\dot{V}_A$ will be identified because the value of V_{Dead} cannot be measured in our experiments. On the other hand, parameters V_T and fr are settings of the ventilator.

The concentrations in blood are measured in STPD whereas the partial pressures in the lungs are measured in BTPS. The acronym STPD stands for Standard Temperature and ambient Pressure, water Dry and has the following features: the temperature is equal to 0°C or 273°K and the pressure is equal to the standard atmospheric pressure without water vapor (= 760 mmHg). The other acronym BTPS stands for Body Temperature and ambient Pressure, water Satured and has the following features: the temperature is

equal to 37°C or 310°K, the total pressure is equal to the atmospheric pressure P_{atm} and water vapor pressure is equal to 47 mmHg. Therefore, the concentration units have to be changed from BTPS to STPD and this conversion is written as follows:

$$\frac{P_{STPD} \cdot V_{STPD}}{P_{BTPS} \cdot V_{BTPS}} = \frac{n \cdot R \cdot T_{STPD}}{n \cdot R \cdot T_{BTPS}} \Leftrightarrow \frac{760 \cdot V_{STPD}}{273} = \frac{(P_{atm} - 47) \cdot V_{BTPS}}{310}$$

$$\Leftrightarrow V_{BTPS} = \frac{863}{(P_{atm} - 47)} \cdot V_{STPD} \ . \tag{5.2}$$

If the concentrations in equations 5.1 are in STPD instead of BTPS, the equations 5.1 become:

$$V_{L,O_2} \cdot \dot{P}_{L,O_2} = 863 \cdot (1 - f_s) \cdot Q_p \cdot (C_{ra,O_2} - C_{l,O_2}) + \dot{V}_A \cdot (P_{I,O_2} - P_{L,O_2}) \ , \tag{5.3a}$$

$$V_{L,CO_2} \cdot \dot{P}_{L,CO_2} = 863 \cdot (1 - f_s) \cdot Q_p \cdot (C_{ra,CO_2} - C_{l,CO_2}) + \dot{V}_A \cdot (P_{I,CO_2} - P_{L,CO_2}) \ , \tag{5.3b}$$

where:

- P_{L,O_2} (mmHg) $= F_{L,\mathrm{O}_2} \cdot (P_{atm} - 47)$ and P_{L,CO_2} (mmHg) $= F_{L,\mathrm{CO}_2} \cdot (P_{atm} - 47)$ are the O_2 and CO_2 partial pressures in the air contained in the lungs (alveoli),
- P_{I,O_2} (mmHg) $= F_{I,\mathrm{O}_2} \cdot (P_{atm} - 47)$ and P_{I,CO_2} (mmHg) $= F_{I,\mathrm{CO}_2} \cdot (P_{atm} - 47)$ are the inspired O_2 and CO_2 partial pressures.

After the oxygenation and the decarboxylation of blood in the lungs, the pulmonary blood is mixed with the venous blood from the shunt and the O_2 and CO_2 concentrations in the arteries, C_{a,O_2} and C_{a,CO_2}, are given by:

$$C_{a,O_2} = f_s \cdot C_{ra,O_2} + (1 - f_s) \cdot C_{l,O_2} \ , \tag{5.4a}$$

$$C_{a,CO_2} = f_s \cdot C_{ra,CO_2} + (1 - f_s) \cdot C_{l,CO_2} \ . \tag{5.4b}$$

5.2 Gas exchanges in the tissues

The tissue compartment includes all the tissues in the body. These tissues produce CO_2 and consume O_2 while the CO_2 removal and the O_2 delivery is performed by the systemic blood flow in the systemic capillaries. The diffusion between capillaries and cells is rapid

and the hypothesis of equilibrium between the tissues and venous blood can be accepted. The material balance equations for O_2 and CO_2 in the tissues are the same as Batzel *et al.* [9] and are given by:

$$V_{T,O_2} \cdot \dot{C}_{v,\mathrm{O}_2} = Q_s \cdot (C_{a,\mathrm{O}_2} - C_{v,\mathrm{O}_2}) - MR_{\mathrm{O}_2} \ , \tag{5.5a}$$

$$V_{T,CO_2} \cdot \dot{C}_{v,\mathrm{CO}_2} = Q_s \cdot (C_{a,\mathrm{CO}_2} - C_{v,\mathrm{CO}_2}) + MR_{\mathrm{CO}_2} \ , \tag{5.5b}$$

where:

- V_{T,O_2} (ml) and V_{T,CO_2} (ml) are the effective volume of O_2 and CO_2 in the tissues,
- C_{v,O_2} ($\mathrm{ml}_{\mathrm{O}_2}$/ml) and C_{v,CO_2} ($\mathrm{ml}_{\mathrm{CO}_2}$/ml) are the O_2 and the CO_2 concentrations in the veins,
- MR_{O_2} ($\mathrm{ml}_{\mathrm{O}_2}$/s) and MR_{CO_2} ($\mathrm{ml}_{\mathrm{CO}_2}$/s) are the quantities of O_2 used and CO_2 produced by metabolism, which will be considered as parameters of our model,
- Q_s (ml/s) is the systemic blood flow.

In our study, the equality $Q_s = Q_p$ is considered and both values are equal to the cardiac output CO. In equations 5.5, the O_2 and CO_2 concentrations and the two parameters MR_{O_2} and MR_{CO_2} are estimated in STPD.

5.3 Gas exchanges in the ECLS

When a vv-ECLS is used to help a patient, the mathematical model of gas exchanges must be complemented by appropriate equations describing the behavior of the respiratory assistance. This device can be considered as a second lung compartment which takes a fraction f_d of the systemic blood flow Q_s in the inferior vena cava and which rejects the corresponding treated blood in the right atrium (Figure 3.1 in section 3.3, p. 42). However, for the extracorporeal device, the diffusion of O_2 and CO_2 across the synthetic membrane is slower than across the lung membrane and the exchange surface is smaller than the alveolar-capillary membrane. The hypothesis of equilibrium between the gas and blood in the device cannot be taken for granted and the diffusion of O_2 and CO_2 across the synthetic membrane should be modeled. Several membranes are available on the market and their features can be very different (geometry, surface area, membrane thickness, ...). In our study, the membranes of Maquet® are used and a sketch of one of their gas exchangers

(the Quadrox PLS®) is shown in Figure 5.2 [91]. The geometry is quite complex (similar to a cross-flow plate heat exchanger) and several assumptions have to be considered to model this device. In the present work, 3 different models of gas exchanges across the ECLS are going to be presented and discussed. These 3 models are illustrated in Figure 5.2.

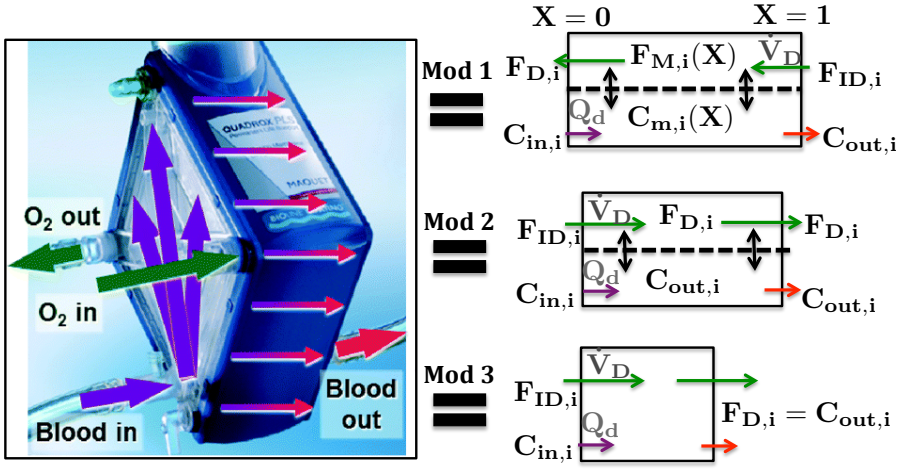

Figure 5.2 – The Maquet®'s gas exchanger on the left and our 3 models of the ECLS on the right. All the symbols are defined in the text of this section (i = O_2 or CO_2) and in the list of symbols page xxiii.

For the first model (named Mod 1 in Figure 5.2), the geometry of the device is reduced to one dimension, and the gas and blood flows are considered in opposite directions (see for instance [14, 66]). The material balance equations for O_2 and CO_2 in the gas and in the blood are thus given by:

Gas

$$V_D \frac{\partial F_{M,\mathrm{O_2}}}{\partial t} - \dot{V}_D \frac{\partial F_{M,\mathrm{O_2}}}{\partial X} = S_m \cdot D_{s,\mathrm{O_2}} (P_{m,\mathrm{O_2}} - P_{M,\mathrm{O_2}}) \ , \tag{5.6a}$$

$$V_D \frac{\partial F_{M,\mathrm{CO_2}}}{\partial t} - \dot{V}_D \frac{\partial F_{M,\mathrm{CO_2}}}{\partial X} = S_m \cdot D_{s,\mathrm{CO_2}} (P_{m,\mathrm{CO_2}} - P_{M,\mathrm{CO_2}}) \ , \tag{5.6b}$$

Blood

$$V_d \frac{\partial C_{m,\mathrm{O_2}}}{\partial t} + Q_d \frac{\partial C_{m,\mathrm{O_2}}}{\partial X} = S_m \cdot D_{s,\mathrm{O_2}} (P_{M,\mathrm{O_2}} - P_{m,\mathrm{O_2}}) \ , \tag{5.6c}$$

$$V_d \frac{\partial C_{m,\mathrm{CO_2}}}{\partial t} + Q_d \frac{\partial C_{m,\mathrm{CO_2}}}{\partial X} = S_m \cdot D_{s,\mathrm{CO_2}} (P_{M,\mathrm{CO_2}} - P_{m,\mathrm{CO_2}}) \ , \tag{5.6d}$$

where:

- F_{M,O_2} and F_{M,CO_2} are the O_2 and CO_2 volume fractions in the gas along the synthetic membrane,
- $C_{m,O_2}(ml_{O_2}/ml)$ and $C_{m,CO_2}(ml_{CO_2}/ml)$ are the O_2 and CO_2 concentrations in blood along the synthetic membrane,
- P_{M,O_2} (mmHg) and P_{M,CO_2} (mmHg) are the O_2 and CO_2 partial pressures in the gas along the synthetic membrane,
- P_{m,O_2} (mmHg) and P_{m,CO_2} (mmHg) are the O_2 and CO_2 partial pressures in blood along the synthetic membrane,
- $\dot{V}_D$ and Q_d (ml/s) are the gas and blood flows crossing the extracorporeal device,
- V_D and V_d (ml) are the gas and blood volumes in the extracorporeal device,
- S_m (cm^2) is the exchange surface of the synthetic membrane between the blood and the gas,
- D_{s,O_2} ($ml_{O_2}/s/mmHg/cm^2$) and D_{s,CO_2} ($ml_{CO_2}/s/mmHg/cm^2$) are the O_2 and the CO_2 diffusion coefficients across the synthetic membrane,
- X = x/L is the nondimensional 1-D coordinate, where x is the distance along the membrane and L is the length of the membrane (for example, X=0 (resp. 1) corresponds to the entrance of blood (resp. air) in the device).

The real exchange surface of the device is provided by the manufacturer but does not correspond to the exchange surface of this one dimension model. Therefore, the global factors $S_m \times D_{s,O_2}$ and $S_m \times D_{s,CO_2}$ need to be estimated and they can be considered as global O_2 and CO_2 diffusion coefficients D_{O_2} ($ml_{O_2}/s/mmHg$) and D_{CO_2} ($ml_{CO_2}/s/mmHg$). These global coefficients are often used in literature [12, 74]. In equations 5.6, the first terms on the left-hand sides describe the accumulation rates of O_2 and CO_2 in volumes V_D and V_d. The 4 boundary conditions give the values of the O_2 and CO_2 concentrations at the gas and blood inlets. Since these two inlets correspond to X=0 and X=1 respectively, the system of differential equations and boundary conditions must be solved iteratively (note that $C_{m,i}(0,t) = C_{in,i}$ and $F_{M,i}(1,t) = F_{ID,i}$; where $i = O_2$ or CO_2, $C_{in,i}$ is the concentration of component i at the inlet cannula and $F_{ID,i}$ is the volume fraction of component i in the gas entering the extracorporeal device).

The second simplified model of gas exchanges in the device (named Mod 2 in Figure 5.2) can be obtained by considering the two compartments in contact perfectly mixed. Hence, there is no spatial dimension and the mass balance equations for O_2 and CO_2 in the 2 compartments are written as follows [116]:

`Gas`

$$V_D \cdot \dot{F}_{D,\mathrm{O_2}} = \dot{V}_D \cdot (F_{ID,\mathrm{O_2}} - F_{D,\mathrm{O_2}}) - D'_{\mathrm{O_2}} \cdot (P_{D,\mathrm{O_2}} - P_{out,\mathrm{O_2}}) \ , \tag{5.7a}$$

$$V_D \cdot \dot{F}_{D,\mathrm{CO_2}} = \dot{V}_D \cdot (F_{ID,\mathrm{CO_2}} - F_{D,\mathrm{CO_2}}) - D'_{\mathrm{CO_2}} \cdot (P_{D,\mathrm{CO_2}} - P_{out,\mathrm{CO_2}}) \ , \tag{5.7b}$$

`Blood`

$$V_d \cdot \dot{C}_{out,\mathrm{O_2}} = Q_d \cdot (C_{in,\mathrm{O_2}} - C_{out,\mathrm{O_2}}) - D'_{\mathrm{O_2}} \cdot (P_{out,\mathrm{O_2}} - P_{D,\mathrm{O_2}}) \ , \tag{5.7c}$$

$$V_d \cdot \dot{C}_{out,\mathrm{CO_2}} = Q_d \cdot (C_{in,\mathrm{CO_2}} - C_{out,\mathrm{CO_2}}) - D'_{\mathrm{CO_2}} \cdot (P_{out,\mathrm{CO_2}} - P_{D,\mathrm{CO_2}}) \ , \tag{5.7d}$$

where:

- $F_{D,\mathrm{O_2}}$ and $F_{D,\mathrm{CO_2}}$ are the O_2 and CO_2 volume fractions in the gas leaving the extracorporeal device,
- $F_{ID,\mathrm{O_2}}$ and $F_{ID,\mathrm{CO_2}}$ are the O_2 and CO_2 volume fractions in the gas entering the extracorporeal device,
- $D'_{\mathrm{O_2}}$ ($\mathrm{ml_{O_2}/s/mmHg}$) and $D'_{\mathrm{CO_2}}$ ($\mathrm{ml_{CO_2}/s/mmHg}$) are the global O_2 and CO_2 diffusion coefficients across the membrane,
- $P_{out,\mathrm{O_2}}$ (mmHg) and $P_{out,\mathrm{CO_2}}$ (mmHg) are the O_2 and CO_2 partial pressures at the outlet cannula,
- $C_{out,\mathrm{O_2}}$ ($\mathrm{ml_{O_2}/ml}$) and $C_{out,\mathrm{CO_2}}$ ($\mathrm{ml_{CO_2}/ml}$) are the O_2 and CO_2 concentrations at the outlet cannula,
- $C_{in,\mathrm{O_2}}$ ($\mathrm{ml_{O_2}/ml}$) and $C_{in,\mathrm{CO_2}}$ ($\mathrm{ml_{CO_2}/ml}$) are the O_2 and CO_2 concentrations at the inlet cannula,
- $P_{D,\mathrm{O_2}}$ (mmHg) and $P_{D,\mathrm{CO_2}}$ (mmHg) are the O_2 and CO_2 partial pressures in the gas leaving the extracorporeal device ($P_{D,\mathrm{CO_2}} = F_{D,\mathrm{CO_2}} \times P_{atm}$ and $P_{D,\mathrm{O_2}} = F_{D,\mathrm{O_2}} \times P_{atm}$).

The left-hand sides of equations 5.7 describe the accumulation rates of O_2 and CO_2 in volumes V_D and V_d.

Finally, in the third model (named Mod 3 in Figure 5.2) the hypothesis of equilibrium between blood and gas ($P_{D,\mathrm{CO_2}} = P_{out,\mathrm{CO_2}}$) is considered and the mass balance equations 5.7 can thus be reduced to a single relation for O_2 and CO_2 material balances:

$$(V_D + V_d) \cdot \dot{F}_{D,\mathrm{O_2}} = Q_d \cdot (C_{in,\mathrm{O_2}} - C_{out,\mathrm{O_2}}) + \dot{V}_D \cdot (F_{ID,\mathrm{O_2}} - F_{D,\mathrm{O_2}}) \ , \tag{5.8a}$$

$$(V_D + V_d) \cdot \dot{F}_{D,\mathrm{CO_2}} = Q_d \cdot (C_{in,\mathrm{CO_2}} - C_{out,\mathrm{CO_2}}) + \dot{V}_D \cdot (F_{ID,\mathrm{CO_2}} - F_{D,\mathrm{CO_2}}) \ . \tag{5.8b}$$

For the 3 mathematical models of the vv-ECLS, the terms describing accumulation rates in the volumes V_D and V_d are small compared to the CO_2 and O_2 gas transfer. Therefore, these terms will be considered as negligible in our simulations.

5.3.1 Mixing of the treated blood and the venous blood without recirculation

The recirculation of blood in the extracorporeal blood flow is the fraction of blood leaving the outlet cannula which enters the inlet cannula (Figure 5.3 illustrates this phenomenon). In this study, if the recirculation is smaller than 10%, the mathematical model neglects this contribution (the recirculation is smaller than 10 % when the extracorporeal blood flow is smaller than 1l/min [16, 72]). With this assumption, after crossing the device, all the treated blood enters the right atrium and is mixed with venous blood. The concentrations of O_2 and CO_2 entering the right atrium is thus given by:

$$C_{ra,\mathrm{O_2}} = f_d \cdot C_{out,\mathrm{O_2}} + (1 - f_d) \cdot C_{v,\mathrm{O_2}} \ , \tag{5.9a}$$

$$C_{ra,\mathrm{CO_2}} = f_d \cdot C_{out,\mathrm{CO_2}} + (1 - f_d) \cdot C_{v,\mathrm{CO_2}} \ , \tag{5.9b}$$

where f_d is the fraction of the systemic blood flow entering the inlet cannula:

$$f_d = \frac{Q_d}{Q_s} \ . \tag{5.10}$$

Furthermore, when the recirculation is neglected, the O_2 and CO_2 concentrations at the inlet cannula ($C_{in,\mathrm{O_2}}$ and $C_{in,\mathrm{CO_2}}$) are equal to the O_2 and CO_2 concentrations in the veins ($C_{v,\mathrm{O_2}}$ and $C_{v,\mathrm{CO_2}}$)

5.3.2 Mixing of the treated blood and the venous blood with recirculation

If the recirculation is larger than 10 %, the recirculation is taken into account in the mathematical model. In these circumstances, all the treated blood does not reach the right atrium; a fraction R_{recir} of this blood returns at the inlet cannula. The extracorporeal blood flow Q_d is thus composed of a fraction of the systemic blood flow entering the inlet cannula (this blood flow is referred as $(1 - R_{recir}) \cdot Q_d$ in Figure 5.3) and of a fraction of the treated blood flow which returns at the inlet cannula (this blood flow is referred as $R_{recir} \cdot Q_d$ in Figure 5.3). Hence, equation 5.10 is not valid with recirculation and this equation becomes:

$$f_d = \frac{(1 - R_{recir}) \cdot Q_d}{Q_s} \ . \tag{5.11}$$

In addition, the O_2 and CO_2 concentrations at the inlet cannula are not equal to the O_2 and CO_2 concentrations in the veins but are the mixing of the venous blood and the treated blood with the following proportions:

$$C_{in,\mathrm{O}_2} = R_{recir} \cdot C_{out,\mathrm{O}_2} + (1 - R_{recir}) \cdot C_{v,\mathrm{O}_2} \ , \tag{5.12a}$$

$$C_{in,\mathrm{CO}_2} = R_{recir} \cdot C_{out,\mathrm{CO}_2} + (1 - R_{recir}) \cdot C_{v,\mathrm{CO}_2} \ . \tag{5.12b}$$

The value of R_{recir} is not easy to estimate and can vary according to the different cannulae available on the market or even according to the surgeon abilities to insert the cannulae. Several authors have suggested that this recirculation depends linearly on the extracorporeal blood flow [72, 16]. The following relation can thus be written:

$$R_{recir} = k_{recir} \cdot Q_d \ , \tag{5.13}$$

where k_{recir} is the coefficient of recirculation. In our study, this parameter is assumed to be unchanged and equal to 0.0833 min/l [72].

5.4 Blood chemistry

In previous equations, concentrations and partial pressures in blood have been introduced. To estimate how these two quantities are connected, a chemical model is needed. In Chapter 2 (section 2.2), the complexity of the blood chemistry has already been discussed. In-

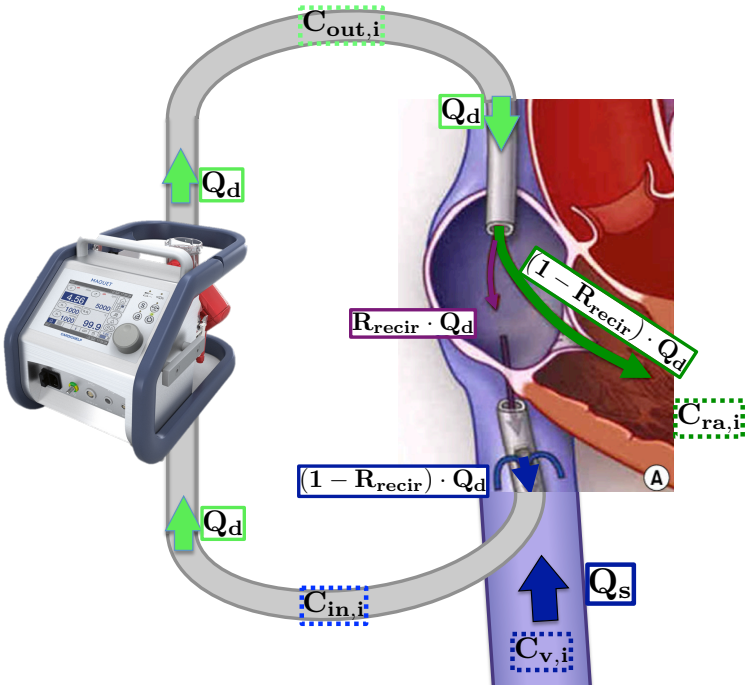

Figure 5.3 – Recirculation of the extracorporeal blood flow during vv-ECLS (adapted from [59]). All the symbols are defined in the text (i = O_2 or CO_2) and in the list of symbols page xxiii.

deed, O_2 and CO_2 are not only dissolved in blood plasma since they can also be complexed with hemoglobin. In addition, CO_2 is also subject to the hydratation/dehydratation reaction (see equation 2.8, p. 26) which influences pH. Therefore, the relations between partial pressures and total concentrations of gases are really complex in blood. In the model, the relation between the total O_2 concentration C_{O_2} and the O_2 partial pressure P_{O_2} follows the equations of Grodins *et al.* [37]:

$$C_{O_2} = 4 \cdot C_{Hb} \cdot Sat_{O_2}(P_{O_2}) + \alpha_{O_2} \cdot P_{O_2} \ , \tag{5.14a}$$

$$Sat_{O_2} = \left(1 - \exp(-S \cdot P_{O_2})\right)^2 \ , \tag{5.14b}$$

$$S = 0.44921 \cdot pH - 0.10098 \cdot pH^2 + 0.0066815 \cdot pH^3 - 0.454 \ , \tag{5.14c}$$

where:

- C_{Hb} (ml_{Hb}/ml) is the hemoglobin concentration,
- Sat_{O_2} is the saturation of hemoglobin with O_2,
- S ($mmHg^{-1}$) is an empiric parameter which accounts for the Bohr effect,
- α_{O_2} ($ml_{O_2}/ml/mmHg$) is the solubility coefficient of O_2 in blood plasma.

The first term on the right-hand side of equation 5.14a describes the concentration of O_2 complexed with hemoglobin whereas the second term describes the concentration of O_2 dissolved in blood plasma. The relations between the total CO_2 concentration C_{CO_2}, the pH in blood plasma and the CO_2 partial pressure P_{CO_2} follow the equations of Trueb *et al.* [113]:

$$C_{CO_2} = (0.149 - 0.014 \cdot Sat_{\mathrm{O}_2}(P_{\mathrm{O}_2})) \cdot {P_{CO_2}}^{0.35} + k_{\mathrm{HCO}_3} \ , \tag{5.15a}$$

$$C_{Pl,\mathrm{CO}_2} = (1.19 + (4 \cdot C_{Hb} - 0.2)) \cdot C_{CO_2} \ , \tag{5.15b}$$

$$pH = -\log_{10}\left(K_{\mathrm{HCO}_3} \cdot \frac{\alpha_{\mathrm{CO}_2} \cdot P_{CO_2}}{C_{Pl,\mathrm{CO}_2} - \alpha_{\mathrm{CO}_2} \cdot P_{CO_2}}\right) \ , \tag{5.15c}$$

where:

- k_{HCO_3} ($\mathrm{ml}_{\mathrm{CO}_2}$/ml) is a correction term which is introduced to compensate for variations between individuals in standard HCO_3 concentration [113],
- C_{Pl,CO_2} ($\mathrm{ml}_{\mathrm{CO}_2}$/ml) is the total CO_2 concentration in blood plasma,
- K_{HCO_3} is the equilibrium constant of chemical reaction 2.8 (see page 26),
- α_{CO_2} ($\mathrm{ml}_{\mathrm{CO}_2}$/ml/mmHg) is the solubility coefficient of CO_2 in blood plasma.

The first term on the right-hand side of equation 5.15a describes the CO_2 concentration for the three species (dissolved in blood plasma, complexed with hemoglobin and under the form of HCO_3). Figure 5.4 illustrates equation 5.15a for different Sat_{O_2} when $k_{\mathrm{HCO}_3} = 0$. Note that the Haldane effect is taken into account by equation 5.15a since Figure 5.4 shows an increase in the CO_2 complexed with hemoglobin when Sat_{O_2} decreases.

This section shows that O_2, CO_2 and pH are linked to each other and have to be estimated simultaneously (see equations 5.14 and 5.15).

5.5 Transport delays

The blood leaving the pulmonary capillaries does not reach the systemic capillaries instantaneously and transport delays must be taken into account. Delays are the durations of the blood transport to reach the different parts of the body compartments. For example, the CO_2 and O_2 concentrations at the entrance of the pulmonary capillaries at time t are equal to the CO_2 and O_2 concentrations in the right atrium (C_{ra,CO_2} and C_{ra,O_2}) at an earlier time $(t-\tau)$. The time that blood needs to cross a part i of the body is proportional

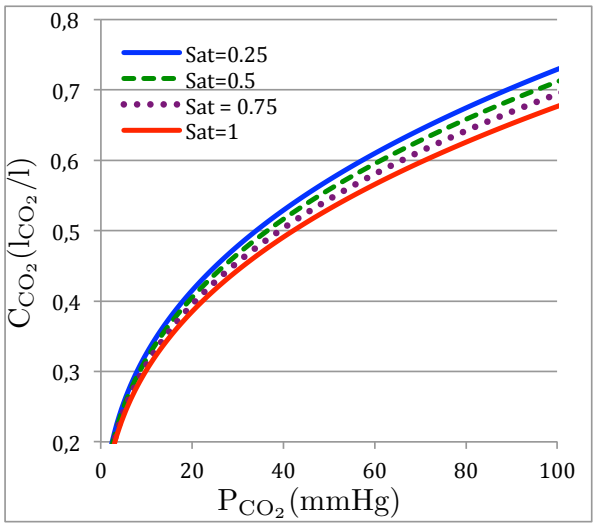

Figure 5.4 – Total CO_2 concentration as a function of CO_2 partial pressure for different hemoglobin saturations with O_2. These curves are obtained using equation 5.15a when $k_{HCO_3} = 0$.

to the volume of blood contained in i and is inversely proportional to the cardiac blood flow Q_i which crosses this part i:

$$\tau_i = \frac{\chi_i \cdot V_{TB}}{Q_i}\,, \tag{5.16}$$

where V_{TB} is the total blood volume and χ_i is the blood volume ratio of part i. In our approach, 3 vascular delays are necessary and the 3 following symbols are used: $i = LT, TH, HL$ (Figure 5.5). Symbol LT refers to the transport of blood from the lungs (pulmonary capillaries) to the tissues symbol, TH refers to venous transport from the tissues to the heart (right atrium) and symbol HL refers to transport from the heart (right atrium) to the lungs (pulmonary capillaries). In this model, the different cardiac blood flows Q_i can be considered as equal to the cardiac output CO (note that the hypothesis of $Q_p = Q_s = CO$ has already been introduced in section 5.2).

The delays τ_{IN} and τ_{OUT} related to the transport to and from the vv-ECLS are determined by the priming volumes V_{IN} and V_{OUT} of the pipes connecting the device to the body. These delays can be estimated as follows:

$$\tau_i = \frac{V_i}{Q_d}\,, \tag{5.17}$$

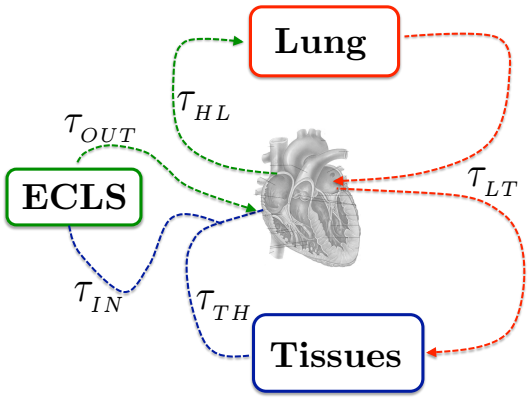

Figure 5.5 – The delays in the respiratory system. All the symbols are defined in the text of this section and in the list of symbols page xxiii.

where i = IN or OUT.

Taking the delays into account, the differential equations presented before become delay differential equations and, for instance, equations 5.3, 5.4 and 5.5 become:

Lungs

$$V_{L,O_2} \cdot \dot{P}_{L,O_2}(t) = 863 \cdot (1 - f_s) \cdot Q_p \cdot (C_{ra,O_2}(t - \tau_{HL}) - C_{l,O_2}(t)) + \dot{V}_A \cdot (P_{I,O_2} - P_{L,O_2}(t)) \ , \tag{5.18a}$$

$$V_{L,CO_2} \cdot \dot{P}_{L,CO_2}(t) = 863 \cdot (1 - f_s) \cdot Q_p \cdot (C_{ra,CO_2}(t - \tau_{HL}) - C_{l,CO_2}(t)) + \dot{V}_A \cdot (P_{I,CO_2} - P_{L,CO_2}(t)) \ , \tag{5.18b}$$

$$C_{a,O_2}(t) = f_s \cdot C_{ra,O_2}(t - \tau_{HL}) + (1 - f_s) \cdot C_{l,O_2}(t) \ , \tag{5.18c}$$

$$C_{a,CO_2}(t) = f_s \cdot C_{ra,CO_2}(t - \tau_{HL}) + (1 - f_s) \cdot C_{l,CO_2}(t) \ , \tag{5.18d}$$

Tissues

$$V_{T,O_2} \cdot \dot{C}_{v,\mathrm{O}_2}(t) = Q_s \cdot (C_{a,\mathrm{O}_2}(t - \tau_{LT}) - C_{v,\mathrm{O}_2}(t)) - MR_{\mathrm{O}_2} \ , \tag{5.18e}$$

$$V_{T,CO_2} \cdot \dot{C}_{v,\mathrm{CO}_2}(t) = Q_s \cdot (C_{a,\mathrm{CO}_2}(t - \tau_{LT}) - C_{v,\mathrm{CO}_2}(t)) + MR_{\mathrm{CO}_2} \ . \tag{5.18f}$$

5.6 Summary

Chapter 5 has described the different compartments of the respiratory model assisted by a vv-ECLS. The different compartments are the lungs, the tissues and the ECLS. For the

ECLS compartment, 3 mathematical models have been built and, when the extracorporeal blood flow is equal or larger than 1 l/min, a recirculation of this blood flow is taken into account. In addition, the blood chemistry model and the transport delays are included in the model and have also been described in this chapter.

Part III

Identification

After developing the differential equations of the mathematical model, several parameters have to be estimated in order to simulate our model. Most parameters are estimated using experimental measurements and are thus subject-specific, but some parameters are also taken from literature and are thus identical for different animals or for different patients. In our study, several retrospective experiments and several retrospective clinical trials are analyzed. For the animal experiments, pigs have been chosen because their cardiovascular and respiratory physiologies are similar to human.

In this third part of this thesis, two chapters are introduced. Chapter 6 describes the parameter estimation for the model of the cardiovascular system connected to a va-ECLS while Chapter 7 describes the parameter estimation for the model of the respiratory system connected to a vv-ECLS.

Chapter 6

Identification of the cardiovascular model connected to a va-ECLS

The identification of the cardiovascular model connected to a va-ECLS consists in estimating the parameters of the equations describing the model dynamics (equations 4.3, 4.8, 4.16 and 4.18). These parameters are estimated using experimental or clinical measurements. Therefore, the first section of this chapter describes the experimental animal trials and the clinical trials carried out in the CHU of Liège (CHU is the French abbreviation of *Centre Hospitalier Universitaire*). However, the number of measurements is limited (mainly for the clinical trials) and all the parameters cannot be identified; some of them are taken from literature and are thus assumed to be identical for all subjects. Section 6.2 discusses which parameters are identified and develops different methods to estimate them.

6.1 Experimental and clinical data

6.1.1 Animal experiments

Animal experiments, approved by the Ethics Committee of the Medical Faculty of the University of Liège, are carried out on 8 Pietrain pigs.

At the beginning of the experiments, the pigs are anesthetized and intubated. The ventilator is set to a tidal volume of 10 ml/kg, an F_{I,O_2} of 0.5, a respiratory frequency of 20 respirations per minute and a PEEP (Positive End-Expiratory Pressure) of 5 mmHg. Three catheters (Transonic®, USA) are placed in the cardiovascular system: an admittance pressure-volume catheter is inserted in the left carotid artery and placed in the left ventricle (the left picture of Figure 6.1), a pressure catheter with two sensors (the distance between the two sensors is equal to 40 cm) is inserted in the right femoral artery and placed

in the aortic arch and a pressure catheter with one sensor is inserted in the femoral venous and placed in the inferior vena cava (the right picture of Figure 6.1). A Forgarty balloon is also placed in the inferior vena cava in order to modify the preload of the ventricle. Using the 3 catheters, the blood pressures in the left ventricle, in the aortic arch, in the vessel located 40 cm below the aortic arch (in the iliac artery) and in the inferior vena cava are continuously measured as well as the left ventricular volume. Using the Forgarty balloon, the left ventricle PV loop can be shifted to the left when the balloon is inflated and the contractility of the left ventricle can be estimated (see subsection 2.1.2 p. 14). In addition, the stroke volume and the cardiac output are also evaluated by echocardiography and can be compared to the stroke volume obtained with the pressure volume catheter. Furthermore, two cannulae to be connected to the va-ECLS are placed in the cardiovascular system: one is inserted in the left femoral artery and placed in the aorta and one is inserted in the left jugular vein and placed in the superior vena cava (near the right atrium).

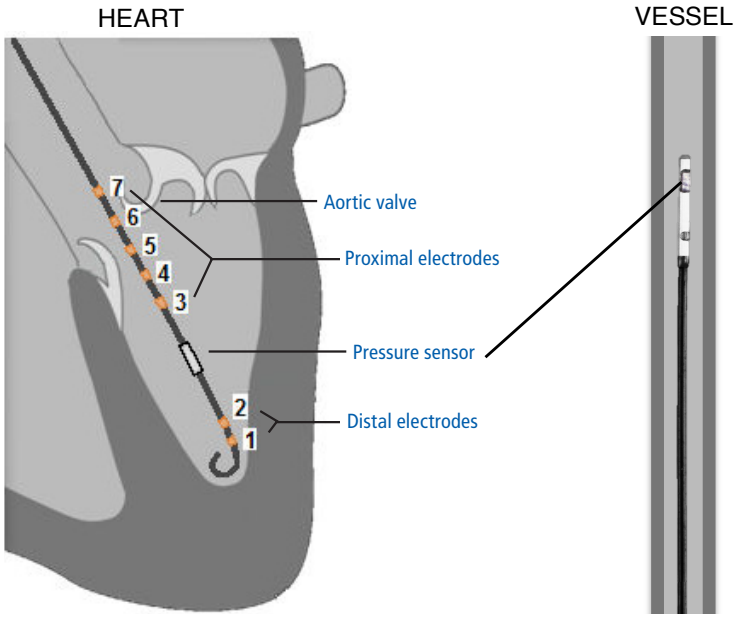

Figure 6.1 – Catheters inserted in the cardiovascular system. The left picture illustrates an admittance pressure-volume catheter inserted in the left ventricle [111] while the right picture illustrates a pressure catheter inserted in a cardiovascular vessel (adapted from [112]).

After the introduction of all the measurement instruments, the balloon and the cannulae, all the data are recorded and this data defines the baseline situation. Then, a cardiac arrest is induced by an electric current leading to a ventricular fibrillation. This current is maintained during 5 min and the ventilation is stopped during this state. Then, the ventilator is restarted with the same settings than before except for the F_{I,O_2} which is increased to 1. In addition, a va-ECLS (CARDIOHELP®, Getinge, Sweden) is connected

to the cannulae and an extracorporeal blood flow is initiated with blood extracted in the vena cava and reinjected in the aorta. The settings of this extracorporeal device are such that the extracorporeal blood flow is as large as possible (the inlet pressure must be larger than -60 mmHg), the gas flow is equal to 8 l/min and the fraction of O_2 in the gas entering the device is equal to 1. Furthermore, a defibrillator is used to restore a normal sinus rythm. If the mean arterial blood pressure is smaller than 60 mmHg, a drug, called noradrenaline, is injected to ensure a mean arterial blood pressure larger than 60 mmHg.

When the cardiovascular system connected to the va-ECLS is stabilized, weaning tests are performed with a procedure relatively similar to the ones carried out on patients in the ICU. To simulate these weaning tests, the extracorporeal blood flow is gradually decreased by approximately 15 % every 5 min. At the end of each of these steps, the ventilator is turned off during 1 min to remove the effects of breathing on the circulatory system. During this phase, the experimental data are recorded. In the present study, the pressure in the aortic arch will not be used and only the distal arterial pressure (the pressure in the iliac artery) will be considered for the identification. Indeed, the sensor in the aorta is close to the arterial cannula and the effect of the re-injected extracorporeal blood flow is better taken into account if the pressure measurements are taken in the iliac artery. In addition, this location is more appropriate to compare animal experiments with ICUs since the arterial measurement taken in the ICU corresponds to the peripheral arterial pressure and not to the aortic blood pressure. The end of the weaning test is defined when the extracorporeal blood flow reaches approximately 0.3 l/min. Like the other steps, the extracorporeal blood flow is maintained for 5 min, the ventilator is turn off during 1 min and the experimental data are recorded. Then, the extracorporeal blood flow is increased and fixed to its initial value (an extracorporeal blood flow as large as possible with the constraint of an inlet pressure larger than -60 mmHg). After at least 30 min of stabilization, this weaning test is restarted again once or twice according to the experimental conditions.

6.1.2 Application in the ICU

Since the final goal of our study is to improve the therapeutic approaches of va-ECLS in the ICU, the validation of the mathematical model with pig experiments is not sufficient and the mathematical model must also be validated with clinical data. These data are taken from several patients suffering from various acute heart diseases and assisted by a va-ECLS.

Data available in the ICU are extracted from measurement instruments that are less invasive than those used in the lab: the stroke volume and the diastolic volume are estimated by echocardiography (pressure-volume catheter is not inserted in the left ventricle

of a patient), the arterial pressure is estimated using the arterial line with a pressure transducer and the venous pressure is estimated using the central venous line with a pressure transducer (Figure 6.2).

The different data are recorded during the weaning test from a va-ECLS with the following protocol. At the beginning of the test, all the hemodynamic data (the diastolic and systolic pressures in the arteries, the mean venous pressure in the veins, the stroke volume and the diastolic volume in the left ventricle) are recorded. Then, the extracorporeal blood flow is gradually decreased by approximately 1 l/min every 5 min until reaching an extracorporeal blood flow of 0.5 l/min. For each extracorporeal blood flow, the hemodynamic data are recorded.

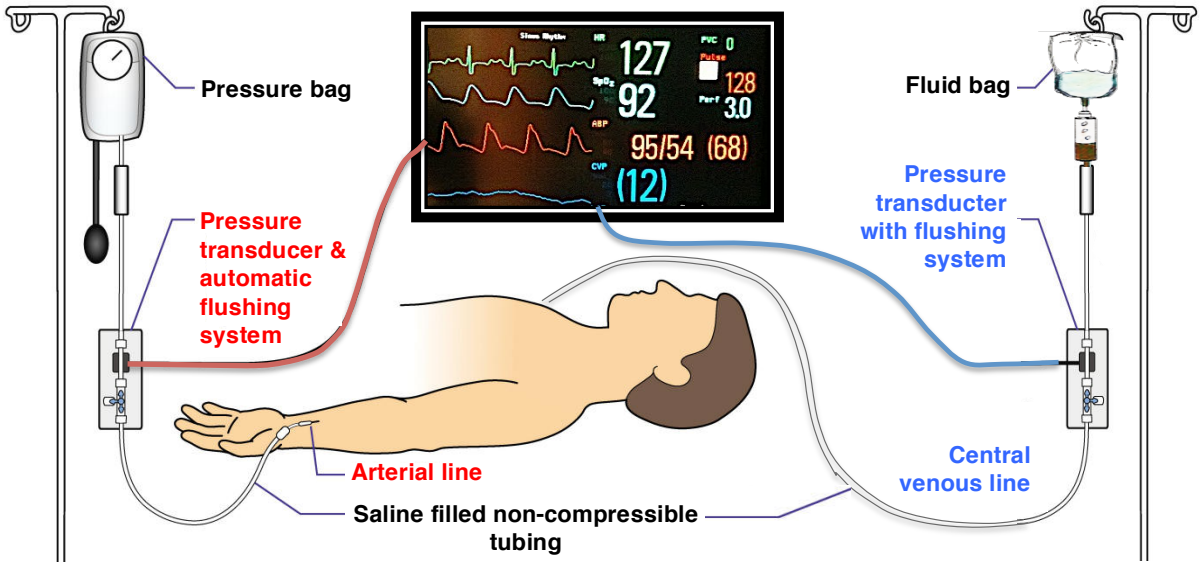

Figure 6.2 – Estimation of arterial and venous blood pressures in the ICU (adapted from [52, 19]).

6.2 Identification of the parameters

6.2.1 Identification of the parameters for one given extracorporeal blood flow

The cardiovascular model connected to a va-ECLS contains 9 parameters (R_i, R_o, R_s, B_h, A_h, E_h, E_a, E_v, SBV, see section 4.3, p. 62) which have to be estimated from the available data. These data are continuous blood pressures in the arteries and veins, the stroke volume in the left ventricle and the diastolic volume in the left ventricle. For the

blood pressure in the arteries, two essential values are extracted: the mean blood pressure and the pulse blood pressure (or the amplitude blood pressure). For the blood pressure in the veins only the value of the mean blood pressure can be extracted. Indeed, this signal is not accurate enough to extract its amplitude. Consequently, the parameter E_v cannot be estimated from clinical data since it depends strongly on this amplitude. In our study, this parameter is thus considered constant and its value is taken from literature (Table 6.1). Three of the 8 remaining parameters must also be extracted from literature and considered constant since only 5 measurements are available (3 blood pressures and 2 blood volumes). These parameters are R_i, R_o and B_h and their values are presented in Table 6.1. Indeed, R_i and R_o are non-identifiable with the available data since the blood pressure in the heart is not estimated in the ICU. In addition, if the subject does not have any valve pathology, the resistance of the valves should not vary much between different subjects or between different hemodynamic situations. Note then, the two parameters of the EDPVR equation, B_h and A_h, cannot be both identified with the available data. In our study, we assume that parameter A_h is more likely to change since, in previous studies [18, 105], B_h is identical for both ventricles while A_h is smaller for the right ventricle than the left ventricle. Therefore, A_h is taken as a patient-specific parameter and B_h is taken from literature (Table 6.1). To summarize, the remaining 5 parameters R_s, A_h, E_h, E_a and SBV are estimated using the vector $\mathbf{y^{data}}$ containing the following 5 elements:

$$\mathbf{y^{data}} = \begin{pmatrix} \overline{P}_a \\ PP_a \\ \overline{P}_v \\ \max_{\mathrm{T}}(V_h) \\ SV \end{pmatrix}, \tag{6.1}$$

where:

- $\overline{P}_a$ is the mean blood pressure in the arteries. For the pig experiments and for the clinical trials, this value is estimated with the following equation: $\overline{P}_a = \frac{1}{3}\max_{\mathrm{T}}(P_a) + \frac{2}{3}\min_{\mathrm{T}}(P_a)$, where $\max_{\mathrm{T}}(P_a)$ and $\min_{\mathrm{T}}(P_a)$ are respectively the maximum and the minimum of the blood pressure in the arteries during one cardiac period [64].

- PP_a is the pulse blood pressure in the arteries. For the pig experiments and for the clinical trials, this value is estimated by subtracting the diastolic blood pressure in the arteries ($\min_{\mathrm{T}}(P_a)$) from the systolic blood pressure in the arteries ($\max_{\mathrm{T}}(P_a)$).

- $\overline{P}_v$ is the mean blood pressure in the veins. For the pig experiments, this value is estimated by calculating the mean venous pressure for one beat. On the other hand, for the clinical trials, $\overline{P}_v$ is directly displayed by the manometer (Figure 6.2).

- $\max_{\mathrm{T}}(V_h)$ is the maximum blood volume in the heart during one cardiac period. For the pig experiments, this quantity is estimated using the pressure-volume catheter in the left ventricle, and, for the clinical trials, it is estimated by echocardiography of the left ventricle during the end-diastolic period.

- SV is the stroke volume. For the pig experiments, SV is estimated using the pressure-volume catheter and by subtracting the minimum blood volume in the left ventricle ($\min_{\mathrm{T}}(V_h)$) from the maximum blood volume in the left ventricle ($\max_{\mathrm{T}}(V_h)$). For the clinical trials, SV is estimated using Doppler echocardiography. With this technique, the clinicians estimate the VTI (velocity time integral) of flow through the left ventricular outflow tract (LVOT) and the diameter of the LVOT ϕ_{LVOT} [32]. With these two values, the stroke volume is estimated as follows:

$$SV = \pi \left(\frac{\phi_{LVOT}}{2} \right)^2 VTI \ . \tag{6.2}$$

Furthermore, the cardiovascular model connected to a va-ECLS contains 2 other parameters, the heart rate HR ($HR = T^{-1}$) and the extracorporeal blood Q_d which are directly measured in our lab and in the ICU. Remark that Table 6.1 summarizes all the parameters of this mathematical model.

Note that for the animal experiments, data are recorded on several cardiac beats. Therefore, the 5 values in vector $\mathbf{y^{data}}$ are the means of the different quantities for the considered beats. For the clinical trials, only one measurement of $\overline{P}_a$, PP_a, $\overline{P}_v$, $\max_{\mathrm{T}}(V_h)$ and SV is recorded in vector $\mathbf{y^{data}}$.

If $\mathbf{p}$ is the vector containing the 5 parameters, the parameter identification is performed by finding $\mathbf{p} = \mathbf{p}^*$ which minimizes the error function Ψ, defined as follows [89]:

$$\Psi(\mathbf{p}) = \sum_{k=1}^{m} \left(\frac{y_k^{data} - y_k^{model}(\mathbf{p})}{\sigma_k} \right)^2 \ , \tag{6.3}$$

where:

- $m = 5$ is the size of vector $\mathbf{y^{data}}$,

- $\mathbf{y^{model}}(\mathbf{p})$ is the same vector than $\mathbf{y^{data}}$ but the different hemodynamic values are estimated with the mathematical model when the parameter values are defined by the vector $\mathbf{p}$ and

- σ_k are standard errors related to the different elements of vector $\mathbf{y}^{\mathbf{data}}$. These quantities are defined more precisely below.

With the experimental data, the means of the different elements of vector $\mathbf{y}^{\mathbf{data}}$ are estimated for each extracorporeal blood flow of the different weaning tests carried out on the 8 pigs. For each extracorporeal blood flow, a standard error σ_k is associated to each elements. In the present study, the mean of these errors will be used for taking into account the experimental errors in our lab and the different values of σ_k are given in Table 6.2. Since these standard errors cannot be estimated with clinical data (only one measurement is recorded), the standard errors of the clinical trials will be assumed the same as the pig experiments. The quantitative values of these errors is certainly erroneous for the clinical trials since the clinical environment is different than the lab environment but the qualitative values should be relatively similar. Indeed, the volume measurements such as the stroke volume are always less accurate than the blood pressure measurements [87]. It is thus preferable to put more importance on the errors between simulated and measured blood pressures than on the errors between simulated and measured ventricular volumes. This important consideration is taken into account by minimizing $\Psi(\mathbf{p})$ defined in equation 6.3.

Table 6.1 – Parameters of the cardiovascular model connected to a va-ECLS

Parameters	Descriptions	Values
	Identified parameters	
A_h	Exponential parameter of the EDPVR equation	Subject-specific
E_a	Elastance of the arteries	Subject-specific
E_h	Slope of the ESPVR equation	Subject-specific
R_s	Systemic resistance	Subject-specific
SBV	Stress blood volume	Subject-specific
	Measured parameters	
HR	Heart rate	Subject-specific
	Parameters taken from the literature	
B_h	Pre-exponential parameter of the EDPVR equation	0.35 mmHg [18]
E_v	Elastance of the veins	0.014 mmHg/ml [18]
R_i	Resistance of the input valve	0.015 mmHg $\cdot$ s/ml [18]
R_o	Resistance of the output valve	0.03 mmHg $\cdot$ s/ml [18]
	ECLS settings	
Q_d	Extracorporeal blood flow	Chosen by the clinicians

Table 6.2 – The different measurement standard errors

Measurement	σ
$\max_{\mathrm{T}}(V_h)$	2 ml
PP_a	0.4 mmHg
$\overline{P}_a$	0.2 mmHg
$\overline{P}_v$	0.1 mmHg
SV	3 ml

6.2.2 Identification of the parameters corresponding to several extracorporeal blood flows

One should remember that the goal of our mathematical model is to predict the behavior of the cardiovascular system when the extracorporeal blood flow is decreased. However, if the extracorporeal blood flow decreases, the cardiovascular system changes significantly since the preload is decreased and the afterload is increased. It thus seems reasonable to assume that all the parameters of the cardiovascular system are not constant if the extracorporeal blood flow varies. The simplest way for taking into account the variation of the parameters with Q_d is to assumed a linear relationship. If this assumption is taken for the 5 subject-specific parameters, the following equations can be written:

$$\begin{cases} A_h &= A_{Sl,h} \cdot Q_d + A_{0,h} \\ E_h &= E_{Sl,h} \cdot Q_d + E_{0,h} \\ E_a &= E_{Sl,a} \cdot Q_d + E_{0,a} \\ R_s &= R_{Sl,s} \cdot Q_d + R_{0,s} \\ SBV &= SBV_{Sl} \cdot Q_d + SBV_0 \end{cases} , \tag{6.4}$$

where: $A_{Sl,h}$, $A_{0,h}$, $E_{Sl,h}$, $E_{0,h}$, $E_{Sl,a}$, $E_{0,a}$, $R_{Sl,s}$, $R_{0,s}$, SBV_{Sl} and SBV_0 are the 10 parameters whose values must be determined from the available data. To estimate these parameters, the identification procedure introduced before must be modified as follows.

The extracorporeal blood flow is an input of the cardiovascular system connected to a va-ECLS and the medical team can control this quantity. The identification of the parameters can thus be carried out with the same measurements as in the previous section but the measurements related to different extracorporeal blood flows will be taken into account and a new error function Ψ is introduced:

$$\Psi(\mathbf{p}) = \sum_{j=1}^{n} \sum_{k=1}^{m} \left(\frac{y_{k,j}^{data} - y_{k,j}^{model}(\mathbf{p})}{\sigma_k} \right)^2 , \tag{6.5}$$

where n is the number of the different extracorporeal blood flows, $\mathbf{p}$ is the vector of the 10 sought coefficients and $m = 5$ is the number of measurements for one extracorporeal blood flow. With this method, the number of measurements is multiplied by the number of extracorporeal blood flows used for the identification. Since 10 values must be identified, m must be larger than or equal to 2.

6.3 Summary

This chapter has presented how the different parameters of the cardiovascular system connected to a va-ECLS can be estimated. Section 6.1 has described the experimental protocol and the clinical protocol that provide the experimental and clinical data and section 6.2 has explained 2 different methods to estimate the parameters of the model with experimental or clinical data. The first method identifies 5 parameters of the cardiovascular model using the experimental or clinical data corresponding to one extracorporeal blood flow while the second method identifies the 10 coefficients describing the same parameters using the experimental or clinical data corresponding to at least 2 different extracorporeal blood flows.

Chapter 7

Identification of the respiratory model connected to a vv-ECLS

The identification of the respiratory model connected to a vv-ECLS consists in estimating the parameters of the equations describing the model dynamics described previously in Chapter 5 (equations 5.18 for the lungs and tissues, equations 5.6 to 5.13 for vv-ECLS, equations 5.14 and 5.15 for blood chemistry and equations 5.16 and 5.17 for transport delays). Most parameters are subject-specific and are thus evaluated using experimental or clinical measurements. Therefore, the first section of this chapter describes the experimental animal trials and the clinical trials carried out in the CHU of Liège. Afterwards, the second section discusses how the different parameters are estimated from the measurements and which parameters are taken from literature (these parameters are assumed to be identical for the different subjects).

7.1 Experimental and clinical data

7.1.1 Animal experiments

A new technology of vv-ECLS is used in our animal trials: the extracorporeal CO_2 removal device ($ECCO_2RD$, see section 3.3, p. 43). Two sets of retrospective experiments (approved by the Ethics Committee of the Medical Faculty of the University of Liège) including an $ECCO_2RD$ are used for testing the mathematical model. The first set of experiments, that are referred to as *experiments H* in the text below, are carried out on 4 healthy pigs, named H1 to H4, subject to protective ventilation (ventilation with small tidal volume, this concept has already been described in section 3.3, p. 42). For the second set of experiments, that are referred to as *experiments A*, 6 animals (labelled A1 to A6) are analyzed and ARDS is induced in addition to protective ventilation (for the detailed

protocol of the induction of ARDS, see Morimont *et al.* [76]).

At the beginning of both sets of experiments, the pigs are anesthetized and intubated. After a 30 min stabilization period, whose end defines the baseline situation, several experimental data (blood flow, CO_2 and O_2 concentrations in venous and arterial blood samples) are measured and the settings of the ventilator are also recorded. Then, protective ventilation is started. In *experiments A*, ARDS is induced during this phase of the protocol by the normal saline lavage method [76]. After approximately 45 minutes of protective ventilation, the $ECCO_2RD$ (PALP®, Getinge, Sweden) is switched on to remove the excess CO_2. In all experiments, the gas flow through the device is set to 10 liters of atmospheric air per minute. The blood flow in the $ECCO_2RD$ is fixed to several values between 0.2 and 0.8 l/min (the values of the extracorporeal blood flow are specified in Chapter 9).

The cardiac output is measured with the thermodilution technique (PiCCO®, Pulsion, Germany) and also with an admittance pressure-volume catheter (Transonic®, USA) in the right ventricle. Tidal volume, F_{I,O_2}, respiratory frequency and driving pressure are fixed by the ventilator (Engström Carestation®, General Electric, USA) and note that F_{I,CO_2} is always equal to 0. Arterial and venous blood samples are analyzed during the experimentation with a RapidPoint500® device (Siemens, Germany). In *experiments H*, additional blood samples are analyzed at the inlet and outlet cannulae and the gas exiting the $ECCO_2RD$ is also analyzed with a CARBOCAP® device (Vaisala, Finland).

Note that the two sets of experiments are important for the purpose of our work since they complement one another. *Experiments H* are needed because more data are available and the estimation of all the parameters of the model is feasible. However, the model must also be validated in case of gas exchange abnormalities. Therefore, *experiments A* are also needed since an ARDS is induced.

7.1.2 Application in the ICU

Clinical data are also used for the parameter estimations and the protocol should be similar to the pig experiments. Actually, a European study has been launched recently to prove the beneficial effects for the lungs of protective ventilation coupled with an extracorporeal CO_2 removal therapy ($ECCO_2RT$) for patients suffering from moderate ARDS; this study is called *Supernova* [81] and is referred to as *clinical trial S* in the text below. However, only one patient (S1) was recruited in this study at the CHU of Liège and we did not get access to the other patients' data. Therefore, an additional retrospective clinical trial,

that is referred to as *clinical trial R*, is analyzed even if the extracorporeal device used is not an $ECCO_2RD$ but a traditional vv-ECLS (this device is also used to oxygenate blood).

For both sets of clinical trials, the baseline situation is defined as the situation just before the initialization of the extracorporeal device. The baseline is thus different from that of the animal trials since the patients have lung failures at that time. Then, the extracorporeal device is switched on and the protective ventilation is induced after a few minutes. The ventilator and the extracorporeal device settings are recorded at least every hour and several blood samples are taken in the veins, in the arteries, at the inlet and outlet cannulae. The cardiac output is estimated with an electrocardiograph manipulated by an experienced physician.

Whereas *clinical trial R* have no rigorous protocol (the protective ventilation and the extracorporeal device settings are chosen according to the patient and are specified in Chapter 11), *clinical trial S* follow a strict protocol and the most important features are following. The inclusion criteria of *clinical trial S* are a mechanical ventilation with expected duration longer than 24 hours and a patient with moderate ARDS ($P_{a,O_2}/F_{I,O_2}$: 200-100 mmHg [31]). For the baseline situation, the tidal volume is set to 6 ml/kg and is maintained constant during two hours. Then, the $ECCO_2RD$ is switched on and the protective ventilation is progressively induced by decreasing the tidal volume from 6 ml/kg to 5 ml/kg when the $ECCO_2RD$ is switched on, from 5 ml/kg to 4.5 ml/kg after 45 min of $ECCO_2RT$ and from 4.5 ml/kg to 4 ml/kg after 90 min of $ECCO_2RT$. The gas flow through the device is set to 6 liters of atmospheric air per minute and the blood flow in the $ECCO_2RD$ is set to 1 l/min. The membrane of the $ECCO_2RD$ used in the CHU of Liège is an HLS Set Advanced 5.0® (Maquet, Getinge, Sweden). For each step (baseline situation, $V_T = 5$ ml/kg, $V_T = 4.5$ ml/kg and $V_T = 4$ ml/kg), blood samples are taken in the veins, in the arteries, at the inlet and outlet cannulae. The ventilator and extracorporeal device settings are also recorded for each step.

7.2 Identification of the parameters

As already mentioned, several parameters describe the patient's status and must be estimated with several measurements. These parameters are thus subject-specific and their estimation, which is described below, is of paramount importance. Other parameters are simply the settings of the devices or are considered constant and identical for all subjects. All the parameters of the respiratory system connected to a vv-ECLS are summarized in Table 7.1.

The parameters related to the blood chemistry and transport delays are described in subsections 7.2.1 and 7.2.2 respectively while those related to the tissues and the lungs are discussed in subsections 7.2.3 and 7.2.4 respectively. In addition, the value of the diffusion coefficients characterizing the membrane of the vv-ECLS is not provided by the manufacturer and this quantity must also be considered as a parameter. Its value is determined by a procedure which is explained in the last subsection below.

7.2.1 Blood chemistry

Quantity k_{HCO_3} in equations 5.15 (see section 5.4, p. 74) is a subject-specific parameter and it must be evaluated for each pig or each patient. Its value is assumed constant in time and can be estimated using equations 5.15 and the values of pH, P_{CO_2} and the hemoglobin saturation with O_2 in the arteries during baseline situation. Parameter C_{Hb} is directly estimated from blood sample analysis. The other parameters, α_{O_2}, α_{CO_2} and K_{HCO_3}, are considered constant and their values are taken from the literature (Table 7.1). Even if these chemical constants are derived from human studies, the same values are used for pig experiments. This assumption is reasonable since the human blood is very similar to the pig blood.

7.2.2 Transport delays

To estimate the delays in the respiratory system, the values of the blood volume ratio (χ_i) are adapted from the work of Willem van Meurs [114] (Table 7.1) where the unstressed volumes in the different compartments are proposed. The total blood volume V_{TB} is assumed proportional to the body weight and its value is adapted from [18] (where this value is given for a man of 75 kg) and gives $V_{TB} = 73 \cdot \text{Weight (kg) ml}$. For example, the transport delay of the whole cardiovascular system ($\tau_{LT} + \tau_{TH} + \tau_{HL}$) for a man of 75 kg with a cardiac output of 5.5 l/min is equal to approximately 1 minute ($1 \times 73 \times 75/5500$). These values of χ_i and V_{TB} are used for both the pig experiments and the clinical trials even if the human morphology is quite different from that of pigs. However, the delays only impact the unstationary behavior of the system and a rough approximation for these parameters is thus enough for the goal of our analysis.

For the delays τ_{IN} and τ_{OUT}, which are the times to go from the inlet cannula to the ECLS and to go from the ECLS to the outlet cannula, they depend on the ECLS used. For the Maquet products, the PALP membrane has a priming volume of 250 ml [38] and the other membranes (PLS, HLS advanced 5.0 and 7.0) have a priming volume of

Table 7.1 – Parameters of the respiratory model connected to a vv-ECLS

Parameters	Descriptions	Values
	Identified parameters	
D_{CO_2}	CO_2 diffusion coefficient across the synthetic membrane	Membrane-specific
D_{O_2}	O_2 diffusion coefficient across the synthetic membrane	Membrane-specific
f_s	Pulmonary shunt	Subject-specific
k_{HCO_3}	Correction term for variations between individuals in standard HCO_3 concentration	Subject-specific
MR_{CO_2}	Quantities of CO_2 produced by metabolism	Subject-specific
MR_{O_2}	Quantities of O_2 used by metabolism	Subject-specific
$\dot{V}_A$	Alveolar ventilation	Subject-specific
	Measured parameters	
C_{Hb}	Hemoglobin concentration	Subject-specific
CO	Cardiac output (in this model $CO = Q_s = Q_p$)	Subject-specific
	Parameters taken from the literature	
α_{CO_2}	Solubility coefficient of CO_2 in blood plasma	$6.9 \cdot 10^{-4}$ l_{CO_2}/l/mmHg [94]
α_{O_2}	Solubility coefficient of O_2 in blood plasma	$2.837 \cdot 10^{-5}$ l_{O_2}/l/mmHg [94]
K_{HCO_3}	Equilibrium constant of chemical equation 2.8	$10^{-6.1}$ [94]
V_{L,CO_2}	Effective volume of CO_2 in the lungs	43 · Poids (kg) ml [9]
V_{L,O_2}	Effective volume of O_2 in the lungs	33 · Poids (kg) ml [9]
V_{IN}	Volume that blood crosses to go from the inlet cannula to the ECLS	125 ml for PALP, 300 ml for others [38, 40, 39]
V_{OUT}	Volume that blood crosses to go from the ECLS to the outlet cannula	125 ml for PALP, 300 ml for others [38, 40, 39]
V_{T,CO_2}	Effective volume of CO_2 in the tissues	200 · Poids (kg) ml [9]
V_{T,O_2}	Effective volume of O_2 in the tissues	80 · Poids (kg) ml [9]
V_{TB}	Total blood volume	73 · Poids (kg) ml [18]
χ_{LT}	Blood volume ratio of pulmonary veins, left heart and systemic arteries	30.2 % [114]
χ_{TH}	Blood volume ratio of systemic veins	66.3 % [114]
χ_{HL}	Blood volume ratio of right heart and pulmonary arteries	3.5 % [114]
	Ventilator settings	
F_{I,CO_2}	Inspired fraction of CO_2	0
F_{I,O_2}	Inspired fraction of O_2	Chosen by the clinicians
	ECLS settings	
F_{ID,CO_2}	Fraction of CO_2 at the gas inlet	0
F_{ID,O_2}	Fraction of O_2 at the gas inlet	Chosen by the clinicians
Q_d	Extracorporeal blood flow	Chosen by the clinicians
$\dot{V}_D$	Ventilation of the ECLS	Chosen by the clinicians

approximately 600 ml [40, 39]. The priming volume is the quantity of saline water one has to fill in the extracorporeal circuit before switching on the ECLS. In our study, we consider that half of this volume corresponds to the inlet circuit and the other half corresponds to the outlet circuit. Therefore, $V_{IN} = V_{OUT} = 125$ml when the PALP membrane is used and $V_{IN} = V_{OUT} = 300$ ml when other membranes are used.

7.2.3 Gas exchanges in the tissues

MR_{CO_2} and MR_{O_2} describe the CO_2 production and O_2 consumption by the tissue. These parameters are assumed not to be affected by the ventilator settings or by the induction of ARDS. These quantities are thus estimated only at baseline situation for each individual. Parameter MR_{O_2} can be determined using the values of cardiac output and O_2 concentrations in arterial and venous blood samples in a time independent situation. For the CO_2 production in the tissues, the equality $MR_{\mathrm{CO}_2} = MR_{\mathrm{O}_2}$ is assumed. In clinical trials, cardiac output and O_2 concentrations in arterial and venous blood samples are rarely estimated together in the ICU during baseline situation. Therefore, MR_{CO_2} and MR_{O_2} cannot be identified before the ECLST and these two parameters could be assumed proportional to the body weight. If this approximation is used, their values could be adapted from [9] (where these parameters are given for a man weighting 75 kg) and give the following relation: $MR_{\mathrm{CO}_2} = MR_{\mathrm{O}_2} = 3.6 \cdot \text{Weight (kg) ml/min}$. Another solution is to estimate these two parameters with arterial and venous blood samples in a time independent situation and with a weight based approximation of the cardiac output. An approximation of the cardiac output can be obtained by using the cardiac index which is the cardiac output divided by the body surface area (BSA, see for instance the Mosteller formula [115]). A standard value of the cardiac index is 3 l/min/m^2 when the patient is at rest [80, 96]. Note also that the body temperature of the animals is not perfectly controlled in our pig experiments and a significant decrease in the temperature is observed as soon as the ECCO$_2$RT is started (blood loses heat in the pipes and in the device). This temperature decrease induces a change in metabolism and the values of MR_{CO_2} and MR_{O_2} have to be modified accordingly (see Appendix A for the details). However, since the temperature of the body is controlled in the ICU, this decrease is not observed in clinic. MR_{CO_2} and MR_{O_2} are thus kept constant in our clinical trials.

The other two parameters in the tissues are V_{T,CO_2} and V_{T,O_2}. These effective volumes are assumed proportional to the body weight and their values are adapted from [9] where these parameters are given for a man weighting 75 kg (the values are given in Table 7.1). These values are used for the pig experiments and for the clinical trials. The morphology of humans and pigs is of course different and taking the values adapted from Batzel *et*

al. for the pig experiments is thus a rather rough approximation. However, the effective volumes influence just the unstationary terms of the system, which is not of paramount importance for the goal of this paper.

7.2.4 Gas exchanges in the lungs

Parameters f_s and $\dot{V}_A$ are used to describe the global efficiency of gas exchanges in the lungs and their estimation is crucial. To our knowledge, this approach is unique in the literature since it is the first time that the pulmonary gas exchange abnormalities are described with these two parameters when an ECLS is connected to the respiratory system. The settings of the ventilator (tidal volume and respiratory frequency) and ARDS notably influence the gas exchange. Parameters f_s and $\dot{V}_A$ must thus be re-evaluated each time these settings are modified and after the induction of ARDS for *experiments A*. For example, these quantities must be identified twice in pig experiments (once during baseline situation and once during protective ventilation, combined with ARDS induction in *experiments A*) and 4 times in the clinical trial Supernova (baseline situation, $V_T = 5$ ml/kg, $V_T = 4.5$ ml/kg and $V_T = 4$ ml/kg). The identification of these parameters is obtained by fitting the measurements of arterial PCO_2 and PO_2 (the venous counterparts being linked to the arterial values by the previously determined MR_{CO_2} and MR_{O_2}) with the corresponding simulated values. During baseline, the system is stabilized and the variables are thus time independent. The identification of these parameters is more difficult for the other situations. Indeed, for the pig experiments, the protective ventilation is usually too short (less than 45 min) to reach a real steady state in the respiratory system. Therefore, the fitting of f_s and $\dot{V}_A$ is based on the comparison of the measurements and the time evolution obtained from the solution of the differential equations. Since the unstationary evolution of PCO_2 and PO_2 obtained with the mathematical model is based on several rather rough assumptions, only the last measurements are used to estimate f_s and $\dot{V}_A$ during this period. For the clinical trials, the protective ventilation is induced during the extracorporeal therapy. Since the final goal of the study is to predict the O_2 and CO_2 time evolutions when the ECLS is switched on, f_s and $\dot{V}_A$ must be estimated before the ECLST. Therefore, the only method to estimate these parameters is to predict their variations for a given decrease in tidal volume. This method will be presented in Chapter 11.

The other 2 parameters in the lungs are V_{L,CO_2}, V_{L,O_2}. These effective volumes are assumed proportional to the body weight and their values are adapted from [9] like in the tissues (the values are given in Table 7.1 and they are used for pig experiments and clinical trials).

7.2.5 ECLS

The CO_2 and O_2 exchanges in the ECLS are characterized by the CO_2 and O_2 diffusion coefficients across the synthetic membrane. Their values are independent of the patient's status and ventilator settings. For the first model (Mod 1, see Figure 5.2, p. 70), D_{CO_2} and D_{O_2} can be obtained by fitting the predictions of equations 5.6 (with $V_D = V_d = 0$) with the measures of PCO_2 and PO_2 at the inlet and outlet canulae and, for the pig experiments, with the measures of PCO_2 in the gas flowing out of the device. For the second model (Mod 2, see Figure 5.2, p. 70), D'_{CO_2} and D'_{O_2} can be obtained by fitting the predictions of equations 5.7 (with $V_D = V_d = 0$) with the measures of PCO_2 and PO_2 at the inlet and outlet canulae and, for the pig experiments, with the measures of PCO_2 in the gas flowing out of the device.

For the O_2 diffusion coefficients across the synthetic membrane D_{O_2} and D'_{O_2}, the measurements of the O_2 fraction in the gas flowing out of the ECLS was not available. In addition, the accuracy of O_2 concentration measurements in blood is not high enough to estimate D_{O_2} and D'_{O_2} in our pig experiments. For these reasons, D_{O_2} and D'_{O_2} are assumed to be 40 times smaller than D_{CO_2} and D'_{CO_2} respectively for the pig experiments as is the case of the heart-lung machine described in [74]. This estimation of D_{O_2} and D'_{O_2} is a bit rough but it is still sufficient for the main purpose of this work. Indeed, this quantity has only a minute influence on the time evolution of PCO_2, which is the main quantity of interest for the pig experiments.

7.3 Summary

This chapter has described the methods to estimate the parameters of the respiratory model connected to a vv-ECLS with experimental data. The identification of the parameters is carried out in each compartment (tissues, lungs and ECLS) independently (see subsection 7.2.3, 7.2.4 and 7.2.5) and several differences between pig experiments and clinical trials have also been underlined in this chapter. In addition, some parameters cannot be estimated with our animal experiments and clinical trials and their values are taken from literature, especially for the parameters related to the blood chemistry (see subsection 7.2.1) and related to the transport delays (see subsection 7.2.1).

Part IV

Animal experiments

After building the mathematical model, we used several experiments in order to validate it. With these experiments, all the subject-specific parameters can be estimated (see part III) and the mathematical model can then be used to start simulations. This part of the thesis shows the results of the pig experiments and discusses the values of the different parameters. It also analyzes the validity of the mathematical model by comparing the experimental data with the simulations.

This fourth part includes two chapters. Chapter 8 describes, discusses and analyzes the results of the pig experiments under va-ECLS while Chapter 9 describes, discusses and analyzes the results of the pig experiments under vv-ECLS.

Chapter 8

Experiments with a va-ECLS

The protocol of the animal experiments has already been described in subsection 6.1.1, p. 85. With the experimental data, all the subject-specific parameters can be estimated and their values are presented in section 8.1. To identify all the parameters, the measurements corresponding to the first 3 extracorporeal blood flows of a weaning test are considered. After estimating all the parameters, the mathematical model of the cardiovascular system connected to a va-ECLS can be used to predict the evolution of the system for other extracorporeal blood flows. In order to validate the predictions of the mathematical model describing the weaning of a va-ECLS, the simulations are compared to experimental data and the results are presented in section 8.2. Afterwards, another approach, consisting in identifying the parameters with the measurements related to all the extracorporeal blood flows, is introduced in section 8.3. Then, all the results are discussed and analyzed in section 8.4 and the limitations of our model are outlined in section 8.5. Finally, section 8.6 summarizes the results of this chapter.

8.1 Values of the parameters

8.1.1 During baseline situation

The values of the parameters are estimated during baseline situation (this phase correspond to the data recorded before the cardiac arrest, see subsection 6.1.1). During this phase, the parameter HR is directly measured and the 5 parameters of the mathematical model are estimated using the methods described in subsection 6.2.1 (minimize the function $\Psi(\mathbf{p})$ defined by equation 6.3) for $Q_d = 0$ l/min. With this method and our experimental data, the errors between the simulated values and the measurements are very small ($\Psi(\mathbf{p}^*) \approx 0$) and the values of the 5 parameters and HR for each pig are given in Table 8.1. All the parameters are of the same order of magnitude for the different pigs

and these baseline values will be used to compare the baseline situation with the ECLST situation.

Table 8.1 – Values of the 5 parameters and of the heart rate during baseline situation.

Data	Pig1	Pig2	Pig3	Pig4	Pig5	Pig6	Pig7	Pig8	**Mean** $\pm$ σ
Parameter identification									
E_h (mmHg/ml)	1.17	1.15	1.24	1.74	1.75	1.25	2.37	1.58	**1.53** $\pm$ 0.42
SBV (ml)	846	1046	1064	1764	691	1093	1085	961	**1069** $\pm$ 314
A_h (ml^{-1})	0.025	0.052	0.046	0.035	0.035	0.032	0.054	0.031	**0.039** $\pm$ 0.011
E_a (mmHg/ml)	0.82	1.47	1.72	0.83	1.70	1.40	2.03	1.59	**1.44** $\pm$ 0.43
R_s (mmHg·s/ml)	0.93	1.58	1.62	0.91	2.05	1.63	2.21	1.83	**1.59** $\pm$ 0.47
Heart rate measurement									
HR (s^{-1})	1.26	1.18	1.35	1.69	1.17	1.23	1.31	1.33	**1.32** $\pm$ 0.17

8.1.2 During ECLST

For the parameter identification during ECLST, HR and Q_d are directly measured and the values of HR in terms of Q_d for each weaning test are presented in Figure 8.1. Except for Pig1 and Pig3, two weaning tests (labeled T1 and T2) are carried out for each pig. Whereas the first 4 panels in Figure 8.1, which refer to the weaning tests Pig1 T1 to Pig3 T1, depict only 3 crosses, the other panels, which refer to the weaning tests Pig4 T1 to Pig8 T2, depict 3 crosses and several diamonds. The experimental data related to the 3 highest Q_d (the crosses) are distinguished from the other Q_d (the diamond) because the measurements related to these two sets of Q_d do not have the same function. Indeed, the measurements related to the 3 highest Q_d are used for the parameter identification while the measurements corresponding to the others Q_d are used for testing the predictions of the mathematical model. When testing the prediction of the model, the values of HR represented by the diamonds cannot thus be used as input data and an estimation of these quantities must be evaluated. In the present study, a linear relationship between HR and Q_d will be assumed:

$$HR = HR_{Sl} \cdot Q_d + HR_0 \ , \tag{8.1}$$

where HR_{Sl} and HR_0 can be estimated for each weaning test, using only the HR values described by the crosses in Figure 8.1.

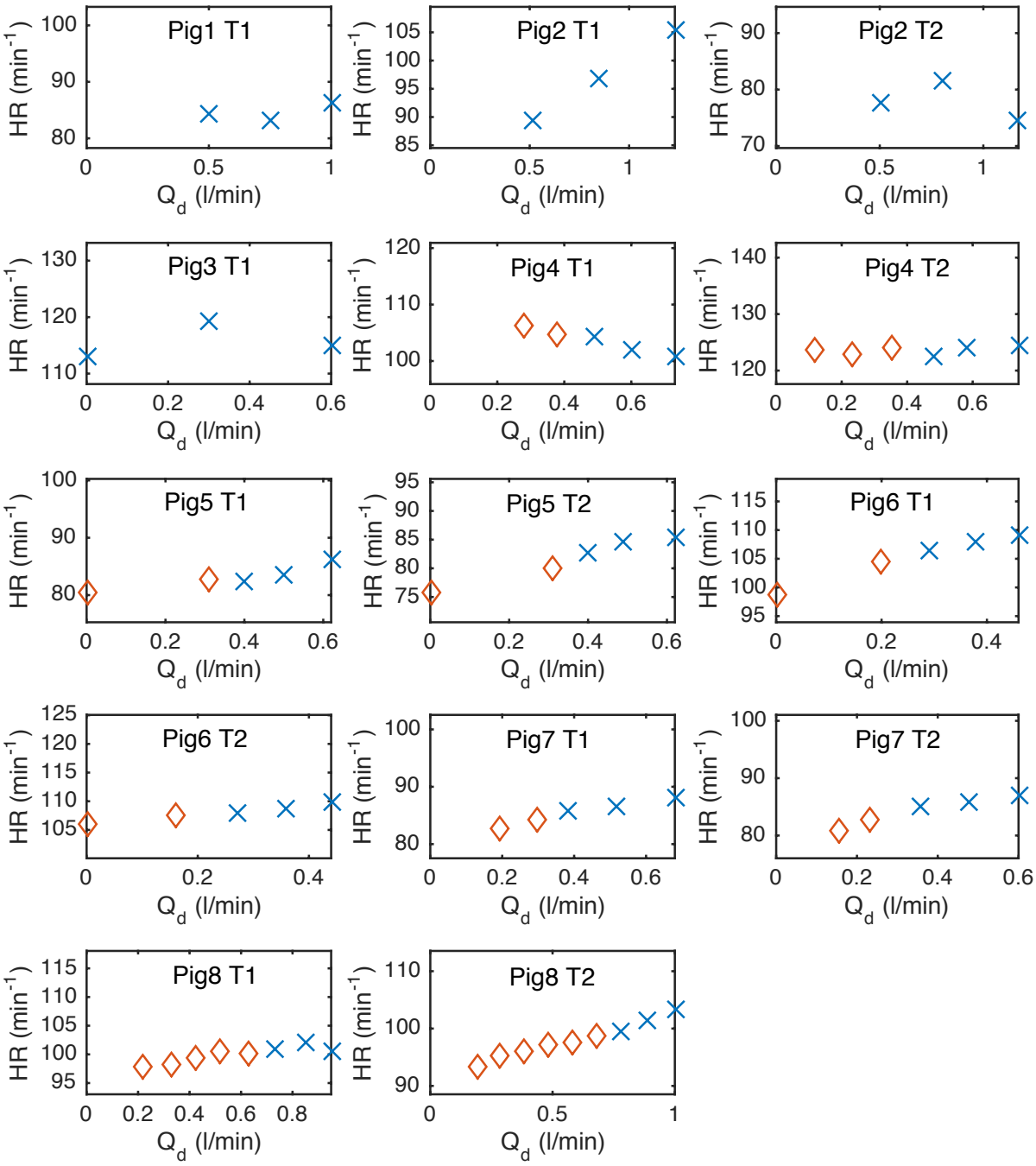

Figure 8.1 – Heart rate in terms of Q_d for the different weaning tests. The crosses correspond to the experimental data used for the parameter identification and the diamonds correspond to the experimental data used for testing the predictions of the mathematical model.

The values of HR_{Sl} and HR_0 for each weaning test are given in Table 8.2. Except for the weaning tests Pig2 T2 and Pig4 T1, Figure 8.1 shows that HR decreases with the decrease in Q_d. The values of HR_{Sl}, given in Table 8.2, show similar results (except for 2 weaning tests, HR_{Sl} is positive) except for the weaning test Pig8 T1 (for this weaning test, the 3 first data do not have the same trend than all the 8 data).

The values of the 10 coefficients, $E_{Sl,a}$, $E_{0,a}$, SBV_{Sl}, SBV_0, $A_{Sl,h}$, $A_{0,h}$, $E_{Sl,a}$, $E_{0,a}$, $R_{Sl,s}$ and $R_{0,s}$ are determined by the method presented in section 6.2 using $n = 3$. Their values are provided in Table 8.2 for each weaning test. Note that the values of the independent terms in equation 6.4 are of the same order for the different weaning tests. However, the values of the slopes in equation 6.4 are quite different for the different pigs and even for different weaning tests of a given pig.

In the minimization process allowing the identification of the 10 coefficients, the minimum value of $\Psi(\mathbf{p})$, $\Psi(\mathbf{p}^*)$, is not equal to 0 (Table 8.3) and there is thus an error between the experimental data and the corresponding values estimated by the mathematical model. It is interesting to analyze separately the errors corresponding to the different components of the vector defined in equation 6.1 and it is worth introducing the following quantities:

$$\overline{|\Delta PP_a/PP_a|} = \frac{1}{n}\sum_{j=1}^{n}\frac{1}{n}\frac{|PP_{a,j}^{\ sim} - PP_{a,j}^{\ exp}|}{PP_{a,j}^{\ exp}} \ , \tag{8.2}$$

$$\overline{|\Delta \overline{P}_a/\overline{P}_a|} = \frac{1}{n}\sum_{j=1}^{n}\frac{|\overline{P}_{a,j}^{\ sim} - \overline{P}_{a,j}^{\ exp}|}{\overline{P}_{a,j}^{\ exp}} \ , \tag{8.3}$$

$$\overline{|\Delta \overline{P}_v/\overline{P}_v|} = \frac{1}{n}\sum_{j=1}^{n}\frac{1}{n}\frac{|\overline{P}_{v,j}^{\ sim} - \overline{P}_{v,j}^{\ exp}|}{\overline{P}_{v,j}^{\ exp}} \ , \tag{8.4}$$

$$\overline{|\Delta \max_{\mathrm{T}}(V_h)/\max_{\mathrm{T}}(V_h)|} = \frac{1}{n}\sum_{j=1}^{n}\frac{|\max_{\mathrm{T}}(V_{h,j})^{sim} - \max_{\mathrm{T}}(V_{h,j})^{\ exp}|}{\max_{\mathrm{T}}(V_{h,j})^{exp}} \ , \tag{8.5}$$

$$\overline{|\Delta SV/SV|} = \frac{1}{n}\sum_{j=1}^{n}\frac{|SV_j^{\ sim} - SV_j^{\ exp}|}{SV_j^{\ exp}} \ , \tag{8.6}$$

Table 8.2 – Values of the 2 coefficients of the linear expressions for each parameter (E_h, SBV, A_h, E_a and R_s) and the 2 coefficients of the linear expressions of HR.

	Pig1	Pig2		Pig3	Pig4		Pig5		Pig6		Pig7		Pig8		
Data	T1	T1	T2	T1	T1	T2	T1	T2	T1	T2	T1	T2	T1	T2	**Mean** $\pm \sigma$
Parameter identification															
$E_{0,h}$ (mmHg/ml)	0.51	0.92	1.20	0.98	1.03	1.43	0.88	1.01	1.26	1.45	0.86	0.79	0.93	0.90	**1.01** $\pm$ 0.25
SBV_0 (ml)	783	723	613	1173	2187	1813	1160	1268	962	943	844	812	1159	1181	**1116** $\pm$ 430
$A_{0,h}$ (ml^{-1})	0.026	0.059	0.047	0.041	0.035	0.033	0.040	0.041	0.036	0.036	0.030	0.029	0.028	0.029	**0.037** $\pm$ 0.009
$E_{0,a}$ (mmHg/ml)	0.63	1.34	1.22	1.22	2.39	2.26	1.94	1.31	1.65	1.26	1.71	1.70	2.03	1.79	**1.60** $\pm$ 0.47
$R_{0,s}$ (mmHg·s/ml)	0.96	1.74	1.44	1.00	1.16	1.28	1.30	1.24	1.09	0.86	1.50	1.56	1.74	1.61	**1.32** $\pm$ 0.29
$E_{Sl,h}$ ($mmHg \cdot s/ml^2$)	0.004	0.013	0.014	0.029	-0.001	-0.005	0.049	0.033	0.030	-0.010	0.009	0.012	0.006	0.005	**0.013** $\pm$ 0.016
SBV_{Sl} (s)	-0.44	-6.09	-1.06	8.24	-10.35	-2.49	21.21	-4.78	14.41	14.32	3.32	0.80	-5.73	-12.29	**1.363** $\pm$ 9.90
$A_{Sl,h}$ (s/ml^2)	-2·e-4	-6·e-5	3·e-4	-2·e-4	-3·e-4	-1·e-4	8·e-5	-1·e-4	2·e-4	-3·e-5	-1·e-4	-8·e-5	-3·e-5	-2·e-4	**-7·e-5** $\pm$ 2·e-4
$E_{Sl,a}$ ($mmHg \cdot s/ml^2$)	0.002	0.014	0.016	0.014	-0.061	-0.018	-0.011	0.025	0.019	0.059	-0.022	-0.011	-0.041	-0.023	**-0.003** $\pm$ 0.030
$R_{Sl,s}$ ($mmHg \cdot s^2/ml^2$)	-0.003	-0.034	-0.013	-0.009	-0.025	-0.025	-0.003	0.011	-0.006	0.016	-0.025	-0.028	-0.038	-0.029	**-0.015** $\pm$ 0.017
Heart rate estimation															
HR_0 (s^{-1})	1.36	1.30	1.37	1.92	1.84	1.99	1.24	1.30	1.69	1.74	1.38	1.36	1.71	1.45	**1.55** $\pm$ 1.64
HR_{Sl} (ml^{-1})	0.004	0.022	-0.005	0.003	-0.013	0.007	0.018	0.012	0.017	0.012	0.007	0.009	-0.002	0.016	**0.008** $\pm$ 0.025

Table 8.3 – Errors between the simulations and the measurements of $\overline{P}_a$, PP_a, $\overline{P}_v$, $\max_{\mathrm{T}}(V_h)$ and SV during the parameter identification phase.

	Pig1	Pig2		Pig3	Pig4		Pig5		Pig6		Pig7		Pig8		
Data	T1	T1	T2	T1	T1	T2	T1	T2	T1	T2	T1	T2	T1	T2	**Mean** $\pm\ \sigma$
$\Psi(\mathbf{p}^*)$	47.5	31.4	507.9	231.9	13.5	30.2	22.8	13.7	1.5	7.6	1.9	2.9	44.1	16.5	**69.5** $\pm$ 139.1
$\overline{\lvert\Delta PP_a/PP_a\rvert}$	0.019	0.018	0.092	0.068	0.003	0.003	0.013	0.012	0.001	0.009	0.004	0.003	0.006	0.008	**0.018** $\pm$ 0.027
$\overline{\lvert\Delta\overline{P}_a/\overline{P}_a\rvert}$	0.023	0.019	0.066	0.030	0.003	0.008	0.004	0.006	0.002	0.001	0.001	0.003	0.011	0.003	**0.013** $\pm$ 0.018
$\overline{\lvert\Delta\overline{P}_v/\overline{P}_v\rvert}$	0.016	0.020	0.010	0.014	0.007	0.014	0.014	0.007	0.003	0.002	0.011	0.010	0.015	0.033	**0.013** $\pm$ 0.008
$\overline{\left\lvert\frac{\Delta\max_{\mathrm{T}}(V_h)}{\max_{\mathrm{T}}(V_h)}\right\rvert}$	0.006	0.009	0.010	0.014	0.011	0.004	0.004	0.004	0.004	0.005	0.001	0.002	0.004	0.003	**0.006** $\pm$ 0.004
$\overline{\lvert\Delta SV/SV\rvert}$	0.009	0.055	0.097	0.081	0.005	0.007	0.023	0.007	0.012	0.023	0.005	0.017	0.013	0.014	**0.026** $\pm$ 0.030
$\overline{\Delta PP_a/PP_a}$	0.005	0.003	-0.092	0.003	-0.002	0.003	0.004	-0.001	-0.001	0.006	-0.001	-0.002	0.005	-0.003	**-0.005** $\pm$ 0.025
$\overline{\Delta\overline{P}_a/\overline{P}_a}$	0.006	0.006	0.066	0.008	0.003	0.004	0.004	0.000	-0.001	0.000	0.000	0.001	0.004	0.000	**0.007** $\pm$ 0.017
$\overline{\Delta\overline{P}_v/\overline{P}_v}$	0.016	0.015	0.010	0.014	0.005	0.014	0.014	0.007	0.001	0.000	0.011	0.010	0.015	0.002	**0.010** $\pm$ 0.006
$\overline{\frac{\Delta\max_{\mathrm{T}}(V_h)}{\max_{\mathrm{T}}(V_h)}}$	0.006	0.004	0.002	0.004	0.002	0.003	0.004	-0.001	-0.001	0.005	0.000	0.002	0.004	-0.003	**0.002** $\pm$ 0.003
$\overline{\Delta SV/SV}$	0.005	0.009	-0.097	0.008	0.000	-0.001	0.005	0.001	0.000	0.008	-0.005	0.001	0.006	-0.010	**-0.005** $\pm$ 0.027

where $\overline{|\Delta PP_a/PP_a|}$ is the mean relative error between simulated and experimental PP_a, while index j corresponds to the different values of Q_d. The other symbols defined in equation 8.3 to 8.6 have similar meanings. In order to estimate if the model tends to overestimate or to underestimate the experimental data, the mean relative errors are also computed without the absolute values (and the corresponding symbols are written as $\overline{\Delta\overline{P}_a/\overline{P}_a}$, $\overline{\Delta PP_a/PP_a}$, $\overline{\Delta\overline{P}_v/\overline{P}_v}$, $\overline{\Delta\max_{\mathrm{T}}(V_h)/\max_{\mathrm{T}}(V_h)}$ and $\overline{\Delta SV/SV}$). Remember that for the parameter identification, $n = 3$ in equations 8.2 to 8.6.

The different errors are given in Table 8.3. This table shows that the errors between the measurements and the corresponding simulated value are in fact quite small: for all the weaning tests, the means $\overline{|\Delta PP_a/PP_a|}$, $\overline{|\Delta\overline{P}_a/\overline{P}_a|}$, $\overline{|\Delta\overline{P}_v/\overline{P}_v|}$ and $\overline{|\Delta\max_{\mathrm{T}}(V_h)/\max_{\mathrm{T}}(V_h)|}$ are all smaller than 2 % and the mean $\overline{|\Delta SV/SV|}$ is smaller than 3 %. Table 8.3 also shows that the simulated venous pressure overestimates the measured venous pressure ($\overline{\Delta\overline{P}_v/\overline{P}_v} = 1\%$) while there is no global overestimation or global underestimation for the other quantities.

8.2 Predictions of the mathematical model

Once all the parameters of the mathematical model are estimated, the model can be used to predict the evolution of the cardiovascular system during a weaning test. To estimate the quality of these predictions, the simulated values are compared with the experimental data. Figure 8.2 illustrates the evolution of simulated and experimental hemodynamic variables of Pig8 for the two weaning tests T1 and T2. The simulated values are depicted by solid lines while experimental data are depicted by crosses and diamonds. As already mentioned, the experimental data depicted by crosses are used for the parameter identification while the experimental data depicted by diamonds are used to validate the mathematical model. In this figure, the agreement between the simulations and the crosses is very good and this fact has already been discussed for all the weaning tests in the previous section. On the other hand, Figure 8.2 shows a rather small difference between the simulations and the diamonds. The results for the weaning tests Pig4 T1 to Pig7 T2 have similar features and are given in Figure B.1 and Figure B.2 of Appendix B.1.

To quantify the differences between the simulations and the experimental data (the diamonds), the different values of $\overline{\Delta PP_a/PP_a}$, $\overline{\Delta\overline{P}_a/\overline{P}_a}$, $\overline{\Delta\overline{P}_v/\overline{P}_v}$, $\overline{\Delta\max_{\mathrm{T}}(V_h)/\max_{\mathrm{T}}(V_h)}$ and $\overline{\Delta SV/SV}$ are calculated with and without the absolute values for each weaning test (these symbols have already been defined by equations 8.2 to 8.6). Table 8.4 gives all these values for the weaning tests Pig4 T1 to Pig8 T2. For the weaning tests Pig1 T1 to Pig3 T1,

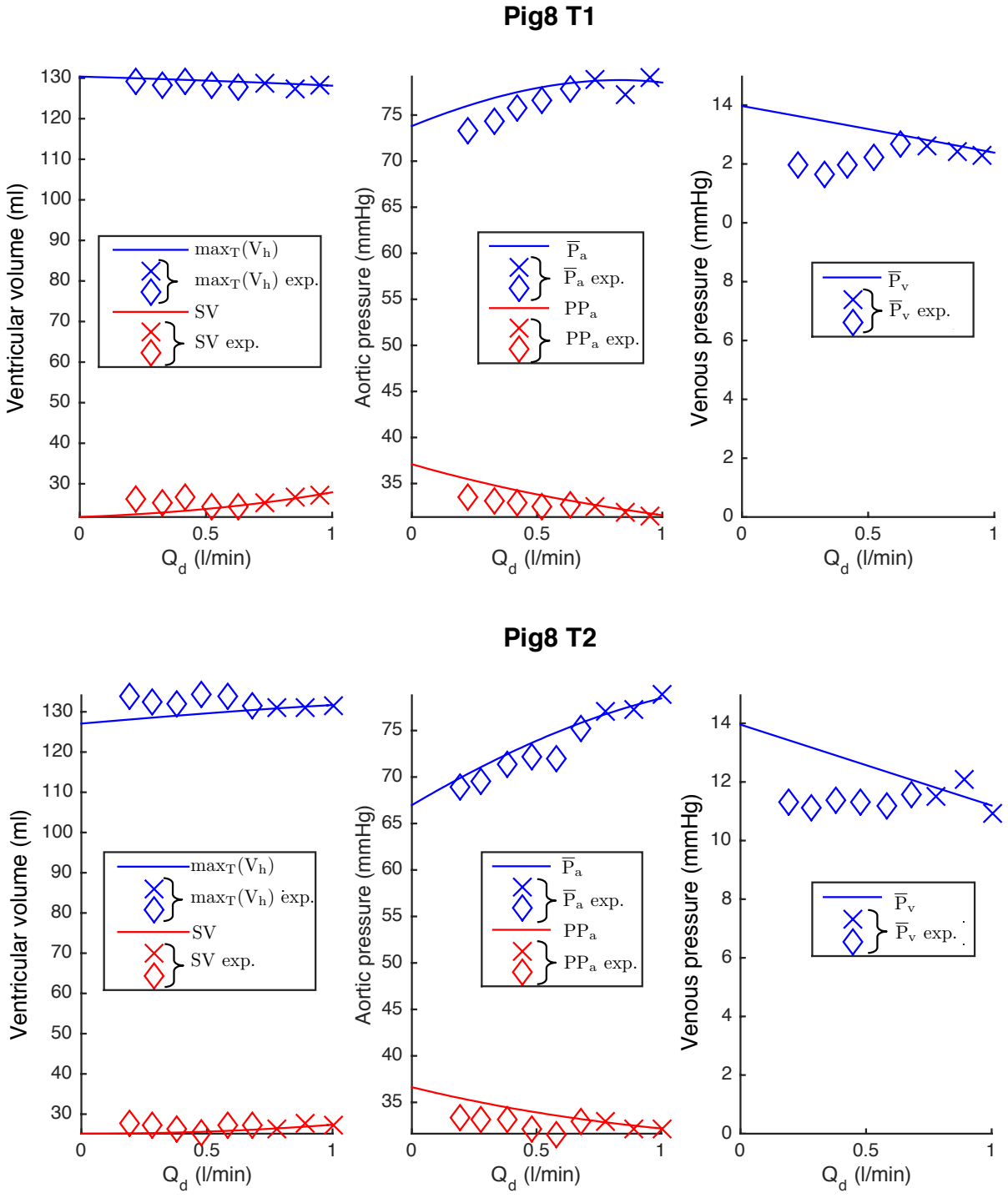

Figure 8.2 – Evolution of $\overline{P}_a$, PP_a, $\overline{P}_v$, $\max_T(V_h)$ and SV in terms of different Q_d for the two weaning tests Pig8 T1 and Pig8 T2. The solid lines are the simulations and the crosses and diamonds are the experimental data (the difference between diamonds and crosses has already been explained in Figure 8.1).

these values cannot be estimated since the hemodynamic data related to only 3 Q_d were recorded during the weaning tests. Table 8.4 provides also the number n of the different Q_d used to compare the predictions with the experimental data. This table shows that the errors are small for PP_a, $\overline{P}_a$, $\overline{P}_v$ and $\max_{\mathrm{T}}(V_h)$ (the mean of $\overline{|\Delta\overline{P}_a/\overline{P}_a|}$, $\overline{|\Delta PP_a/PP_a|}$, $\overline{|\Delta\overline{P}_v/\overline{P}_v|}$, $\overline{|\Delta\max_{\mathrm{T}}(V_h)/\max_{\mathrm{T}}(V_h)|}$ for all the tests are all smaller or equal to 5 %) but it shows a more significant, but still acceptable, error for SV ($\overline{|\Delta SV/SV|} = 9.2\%$). This table also shows that there is no global overestimation or global underestimation of the different hemodynamic data simulated with the mathematical model.

8.3 Improving the parameter identification by using all the Q_d

Another approach to analyze the validity of the model is to identify the parameters using measurements related to all the Q_d. In this context, the predictions of the mathematical model cannot, of course, be tested, but one can check that the mathematical model can reproduce the general behavior of the cardiovascular system during a weaning test. The parameter identification used here is similar to the previous one except that the measurements related to all the Q_d are used in equation 6.5 (with this method, the diamonds depicted in Figure 8.1 and Figure 8.2 are replaced by crosses). The 10 values of the linear coefficients estimated with this method are given in Table 8.5 and the relative differences between the simulated and experimental values for $\overline{\Delta PP_a/PP_a}$, $\overline{\Delta\overline{P}_a/\overline{P}_a}$, $\overline{\Delta\overline{P}_v/\overline{P}_v}$, $\overline{\Delta\max_{\mathrm{T}}(V_h)/\max_{\mathrm{T}}(V_h)}$ are given in Table 8.6 (the values for Pig1 to Pig3 are not given since they are the same as those in Table 8.2 and Table 8.3). Note that the corresponding evolution of simulated and experimental hemodynamic variables for the weaning tests Pig4 T1 to Pig8 T2 are given in Figure B.3, Figure B.4 and Figure B.5 of Appendix B.1.

Except the values of $E_{sl,a}$ and $A_{sl,h}$, the values provided in Table 8.5 are quite similar to those given in Table 8.2. On the other hand, Table 8.6 shows larger errors with the parameter identification using the measurements related to all the Q_d than with the previous parameter identification (Table 8.3). Nevertheless, these errors are still acceptable since the means $\overline{|\Delta PP_a/PP_a|}$, $\overline{|\Delta\overline{P}_a/\overline{P}_a|}$, $\overline{|\Delta\overline{P}_v/\overline{P}_v|}$ and $\overline{|\Delta\max_{\mathrm{T}}(V_h)/\max_{\mathrm{T}}(V_h)|}$ are all smaller than 2.5 % and the mean $\overline{|\Delta SV/SV|}$ is smaller than 5 %. Finally, as expected, Table 8.5 shows smaller errors with the parameter identification using the measurements related to all the Q_d than those obtained with the predictions (Table 8.4).

Table 8.4 – Errors between the predictions of the mathematical model and the measurements of $\overline{P}_a$, PP_a, $\overline{P}_v$, $\max_{\mathrm{T}}(V_h)$ and SV.

	Pig4		Pig5		Pig6		Pig7		Pig8		
Data	T1	T2	T1	T2	T1	T2	T1	T2	T1	T2	**Mean** $\pm$ σ
$\overline{\lvert\Delta PP_a/PP_a\rvert}$	0.017	0.021	0.083	0.193	0.016	0.042	0.044	0.059	0.036	0.039	**0.055** $\pm$ 0.053
$\overline{\lvert\Delta\overline{P}_a/\overline{P}_a\rvert}$	0.006	0.026	0.105	0.024	0.010	0.014	0.021	0.039	0.020	0.013	**0.028** $\pm$ 0.029
$\overline{\lvert\Delta\overline{P}_v/\overline{P}_v\rvert}$	0.047	0.014	0.055	0.006	0.018	0.030	0.006	0.014	0.087	0.096	**0.037** $\pm$ 0.033
$\overline{\left\lvert\frac{\Delta\max_{\mathrm{T}}(V_h)}{\max_{\mathrm{T}}(V_h)}\right\rvert}$	0.057	0.067	0.023	0.010	0.002	0.015	0.001	0.013	0.005	0.036	**0.023** $\pm$ 0.023
$\overline{\lvert\Delta SV/SV\rvert}$	0.195	0.149	0.185	0.022	0.052	0.113	0.015	0.059	0.081	0.053	**0.092** $\pm$ 0.065
$\overline{\Delta PP_a/PP_a}$	0.017	0.021	-0.083	0.193	-0.016	-0.042	0.044	0.059	0.036	0.039	**0.027** $\pm$ 0.073
$\overline{\Delta\overline{P}_a/\overline{P}_a}$	0.006	0.026	-0.105	0.013	-0.010	-0.014	0.021	0.039	0.020	0.010	**0.001** $\pm$ 0.040
$\overline{\Delta\overline{P}_v/\overline{P}_v}$	0.047	0.014	-0.055	0.001	-0.012	-0.030	0.002	0.007	0.087	0.096	**0.016** $\pm$ 0.048
$\overline{\frac{\Delta\max_{\mathrm{T}}(V_h)}{\max_{\mathrm{T}}(V_h)}}$	-0.057	-0.040	-0.007	0.010	0.002	-0.015	-0.001	0.013	0.005	-0.036	**-0.013** $\pm$ 0.024
$\overline{\Delta SV/SV}$	-0.195	-0.066	-0.185	0.021	0.052	0.113	0.014	0.021	-0.073	-0.052	**-0.035** $\pm$ 0.099
n	2	3	2	2	2	2	2	2	5	6	

Table 8.5 – Values of the 2 coefficients of the linear expressions for each parameter (E_h, SBV, A_h, E_a and R_s) obtained with the parameter identification using the measurements related to all the Q_d.

	Pig4		Pig5		Pig6		Pig7		Pig8		
Data	T1	T2	T1	T2	T1	T2	T1	T2	T1	T2	**Mean ± σ (Pig1 T1 to Pig8 T2)**
$E_{0,h}$ (mmHg/ml)	1.00	1.33	1.10	0.97	1.24	1.35	0.81	0.73	0.93	0.85	**0.99** ± 0.24
SBV_0 (ml)	2105	1820	1279	1280	991	978	845	805	1016	970	**1099** ± 419
$A_{0,h}$ (ml^{-1})	0.031	0.032	0.040	0.040	0.037	0.036	0.030	0.030	0.027	0.026	**0.036** ± 0.009
$E_{0,a}$ (mmHg/ml)	1.72	2.11	1.73	1.03	1.80	1.53	1.70	1.67	1.62	1.48	**1.49** ± 0.37
$R_{0,s}$ (mmHg·s/ml)	0.90	1.15	1.21	1.26	1.21	0.98	1.57	1.58	1.55	1.41	**1.28** ± 0.27
$E_{Sl,h}$ ($mmHg \cdot s/ml^2$)	0.002	0.004	0.023	0.033	0.033	0.006	0.015	0.020	0.005	0.008	**0.015** ± 0.011
SBV_{Sl} (s)	-0.852	-2.832	7.322	-6.923	11.748	8.577	3.180	1.954	4.609	1.696	**2.081** ± 5.587
$A_{Sl,h}$ (s/ml^2)	5·e-5	3·e-5	9·e-5	1·e-6	1·e-4	1·e-5	-1·e-4	-1·e-4	6·e-5	4·e-5	**-9·e-6** ± 1·e-4
$E_{Sl,a}$ ($mmHg \cdot s/ml^2$)	0.001	-0.008	0.011	0.065	-0.006	0.015	-0.023	-0.007	-0.011	0.000	**0.006** ± 0.021
$R_{Sl,s}$ ($mmHg \cdot s^2/ml^2$)	-0.001	-0.016	0.005	0.016	-0.025	-0.001	-0.033	-0.030	-0.023	-0.014	**-0.013** ± 0.015

Table 8.6 – Errors between the simulations and the measurements of $\overline{P}_a$, PP_a, $\overline{P}_v$, $\max_{\mathrm{T}}(V_h)$ and SV for the parameter identification using the measurements related to all the Q_d.

	Pig4		Pig5		Pig6		Pig7		Pig8			
Data	T1	T2	T1	T2	T1	T2	T1	T2	T1	T2	**Mean $\pm$ σ (Pig4 T1 to Pig8 T2)**	**Mean $\pm$ σ (Pig1 T1 to Pig8 T2)**
$\Psi(\mathbf{p}^*)$	82.2	501.7	219.0	104.3	24.2	10.0	22.9	125.6	91.8	97.5	**127.9** $\pm$ 144.8	**149.9** $\pm$ 164.7
$\overline{\lvert\Delta PP_a/PP_a\rvert}$	0.007	0.008	0.021	0.030	0.008	0.006	0.016	0.031	0.009	0.011	**0.015** $\pm$ 0.010	**0.025** $\pm$ 0.025
$\overline{\lvert\Delta\overline{P}_a/\overline{P}_a\rvert}$	0.005	0.010	0.024	0.012	0.005	0.002	0.004	0.017	0.007	0.006	**0.009** $\pm$ 0.007	**0.016** $\pm$ 0.017
$\overline{\lvert\Delta\overline{P}_v/\overline{P}_v\rvert}$	0.014	0.015	0.018	0.004	0.015	0.009	0.011	0.014	0.021	0.019	**0.014** $\pm$ 0.005	**0.014** $\pm$ 0.005
$\overline{\left\lvert\frac{\Delta\max_{\mathrm{T}}(V_h)}{\max_{\mathrm{T}}(V_h)}\right\rvert}$	0.014	0.040	0.008	0.006	0.005	0.003	0.001	0.005	0.004	0.006	**0.009** $\pm$ 0.011	**0.009** $\pm$ 0.009
$\overline{\lvert\Delta SV/SV\rvert}$	0.062	0.084	0.042	0.054	0.016	0.021	0.020	0.037	0.033	0.032	**0.040** $\pm$ 0.021	**0.046** $\pm$ 0.027
$\overline{\Delta PP_a/PP_a}$	0.007	0.008	0.001	0.003	0.008	0.001	0.002	0.002	0.006	0.001	**0.004** $\pm$ 0.003	**-0.003** $\pm$ 0.026
$\overline{\Delta\overline{P}_a/\overline{P}_a}$	0.005	0.005	0.002	0.002	0.004	0.001	0.000	0.000	0.005	0.000	**0.002** $\pm$ 0.002	**0.008** $\pm$ 0.017
$\overline{\Delta\overline{P}_v/\overline{P}_v}$	0.014	0.015	0.014	0.002	0.015	0.004	0.011	0.013	0.016	0.001	**0.010** $\pm$ 0.006	**0.011** $\pm$ 0.005
$\overline{\frac{\Delta\max_{\mathrm{T}}(V_h)}{\max_{\mathrm{T}}(V_h)}}$	0.003	0.004	0.003	0.001	0.004	0.001	0.000	-0.001	0.004	0.000	**0.002** $\pm$ 0.002	**0.002** $\pm$ 0.002
$\overline{\Delta SV/SV}$	0.000	0.000	-0.002	-0.031	0.002	-0.002	-0.007	-0.006	0.002	-0.021	**-0.006** $\pm$ 0.011	**-0.010** $\pm$ 0.027
n	5	6	5	5	5	5	5	5	8	9		

8.4 Discussion

8.4.1 Values of the parameters for $Q_d = 0$

Table 8.1 has shown the values of the 5 parameters during baseline situation and Table 8.2 has shown the coefficients of the linear development of the parameters in terms of Q_d. These developments can be used to calculate the values of the parameters corresponding to $Q_d = 0$ and these values can be compared with the corresponding quantities in Table 8.1. Note however that, during ECLST, noradrenaline is injected to maintain a mean arterial pressure larger than 60 mmHg. This drug influences the parameters of the cardiovascular system since it is known to increase the contractility of the heart and to constrict the blood vessels. To carefully compare these 2 sets of parameters values, Table 8.7 provides all these quantities and also mentions the injection of noradrenaline. The mean SBV, A_h and E_a for all the pigs during baseline situation are relatively similar to, respectively, the mean SBV_0, $A_{0,h}$ and $E_{0,a}$ during ECLST. On the other hand, the mean E_h during baseline situation is larger than the mean $E_{0,h}$ and the mean R_s during baseline situation is a little bit larger than the mean $R_{s,0}$. A decrease in E_h after the baseline situation corresponds to a reduction of the contractility of the heart. These results make sense since the cardiovascular system has been perturbed and traumatized after the baseline situation. Moreover, a septic shock was observed after the induction of the ventricular fibrillation and this pathology reduces the systemic resistance R_s. Table 8.7 also shows that the decrease in $E_{h,0}$ is even more significant when there is no noradrenaline injection during the weaning test (see Pig1 T1, Pig5 T1, Pig7 T1, Pig7 T2, Pig8 T1 and Pig 8 T2). This result confirms the influence of noradrenaline, which increases the heart contractility. Therefore, the evolution of parameters $E_{0,h}$ and $R_{0,s}$ seems to be of paramount importance to check the evolution of the cardiovascular system.

8.4.2 Variations of the parameters with Q_d

Table 8.2 has also provided the slopes of the parameters with respect to Q_d. These quantities are of paramount importance since they describe the variation of the parameters with the extracorporeal blood flow. With these values, the response of the cardiovascular system to the decrease in Q_d can be investigated. In order to analyze these variations easier, one can calculate the following relative variations of the 5 parameters for a change of Q_d equal to 1l/min:

Table 8.7 – Values of the 5 parameters and of the noradrenaline injection during baseline situation and values of the 5 coefficients of the independent term of the 5 parameters and of noradrenaline injection during ECLST.

	Pig1	Pig2		Pig3	Pig4		Pig5		Pig6		Pig7		Pig8		**Mean ± σ**
Baseline situation															
Noradrenaline (μg/min)	0.0	0.0		0.0	0.0		0.0		0.0		0.0		0.0		**0.0** ± 0.0
E_h (mmHg/ml)	1.17	1.15		1.24	1.74		1.75		1.25		2.37		1.58		**1.53** ± 0.42
SBV (ml)	846	1046		1064	1764		691		1093		1085		961		**1069** ± 314
A_h (ml^{-1})	0.025	0.052		0.046	0.035		0.035		0.032		0.054		0.031		**0.039** ± 0.011
E_a (mmHg/ml)	0.82	1.47		1.72	0.83		1.70		1.40		2.03		1.59		**1.44** ± 0.43
R_s (mmHg·s/ml)	0.93	1.58		1.62	0.91		2.05		1.63		2.21		1.83		**1.59** ± 0.47
ECLST															
Weaning test	T1	T1	T2	T1	T1	T2	T1	T2	T1	T2	T1	T2	T1	T2	**All tests**
Noradrenaline (μg/min)	0.0	5.33	5.33	2.67	5.33	5.33	0.0	2.67	2.67	2.67	0.0	0.0	0.0	0.0	**2.29** ± 0.2.29
$E_{0,h}$ (mmHg/ml)	0.51	0.92	1.20	0.98	1.03	1.43	0.88	1.01	1.26	1.45	0.86	0.79	0.93	0.90	**1.01** ± 0.25
SBV_0 (ml)	783	723	613	1173	2187	1813	1160	1268	962	943	844	812	1159	1181	**1116** ± 430
$A_{0,h}$ (ml^{-1})	0.026	0.059	0.047	0.041	0.035	0.033	0.040	0.041	0.036	0.036	0.030	0.029	0.028	0.029	**0.037** ± 0.009
$E_{0,a}$ (mmHg/ml)	0.63	1.34	1.22	1.22	2.39	2.26	1.94	1.31	1.65	1.26	1.71	1.70	2.03	1.79	**1.60** ± 0.47
$R_{0,s}$ (mmHg·s/ml)	0.96	1.74	1.44	1.00	1.16	1.28	1.30	1.24	1.09	0.86	1.50	1.56	1.74	1.61	**1.32** ± 0.29

$$\Delta_1 E_h/E_h = \frac{E_h(\mathrm{Q_d} = 1\ \mathrm{l/min}) - E_h(\mathrm{Q_d} = 0\ \mathrm{l/min})}{E_h(\mathrm{Q_d} = 0\ \mathrm{l/min})}\ , \tag{8.7a}$$

$$\Delta_1 SBV/SBV = \frac{SBV(\mathrm{Q_d} = 1\ \mathrm{l/min}) - SBV(\mathrm{Q_d} = 0\ \mathrm{l/min})}{SBV(\mathrm{Q_d} = 0\ \mathrm{l/min})}\ , \tag{8.7b}$$

$$\Delta_1 A_h/A_h = \frac{A_h(\mathrm{Q_d} = 1\ \mathrm{l/min}) - A_h(\mathrm{Q_d} = 0\ \mathrm{l/min})}{A_h(\mathrm{Q_d} = 0\ \mathrm{l/min})}\ , \tag{8.7c}$$

$$\Delta_1 E_a/E_a = \frac{E_a(\mathrm{Q_d} = 1\ \mathrm{l/min}) - E_a(\mathrm{Q_d} = 0\ \mathrm{l/min})}{E_a(\mathrm{Q_d} = 0\ \mathrm{l/min})}\ , \tag{8.7d}$$

$$\Delta_1 R_s/R_s = \frac{R_s(\mathrm{Q_d} = 1\ \mathrm{l/min}) - R_s(\mathrm{Q_d} = 0\ \mathrm{l/min})}{R_s(\mathrm{Q_d} = 0\ \mathrm{l/min})}\ . \tag{8.7e}$$

It is worth remembering that the 5 slopes have been identified with the measurements related to 3 different Q_d. With the aim of analyzing the variations of the 5 parameters with more reliability, the 10 coefficients of the linear expression of the 5 parameters can also be identified using the measurements related to all the Q_d (see section 8.3) and the corresponding values of $\Delta_1 E_h/E_h$, $\Delta_1 SBV/SBV$, $\Delta_1 A_h/A_h$, $\Delta_1 E_a/E_a$ and $\Delta_1 R_s/R_s$ can also be estimated.

Figure 8.3 represents $\Delta_1 E_h/E_h$ for each weaning test for the 2 parameter identifications (the parameter identification using only 3 Q_d is represented by the full bars while the parameter identification using all the Q_d is represented by the empty bars). This figure demonstrates that $\Delta_1 E_h/E_h$ is always positive for the parameter identification using all the Q_d. This implies that E_h always decreases when Q_d decreases. Such a change of the contractility with Q_d is not surprising since the preload and the afterload change with Q_d. Indeed, the load independence of the ventricle contractility is only true for an instantaneous variation of the PV loop [77, 65, 56]. In the situation analyzed in our work, the preload and afterload are changed for a relative long time (approximately 5 min between 2 different Q_d) and the heart has time to adjust its activity. The results for the parameter identification using 3 Q_d is similar except for Pig5 T1 which has a much larger value of $\Delta_1 E_h/E_h$ and for Pig4 T2 and Pig6 T2 for which a small negative value is found. Note that the 2 parameter identifications are identical for Pig1 T1, Pig2 T1, Pig2 T2 and Pig3 T1 since there is only 3 Q_d available for these weaning tests.

Figure 8.4 describes $\Delta_1 SBV/SBV$. For both parameter identification, the values are small in comparison with $\Delta_1 E_h/E_h$ and the signs vary between the different weaning tests. Except for Pig8 T1 and Pig8 T2, the parameter identification using 3 Q_d has the same trend as the other parameter identification.

Figure 8.5 represents $\Delta_1 A_h/A_h$. The signs vary between the different weaning tests

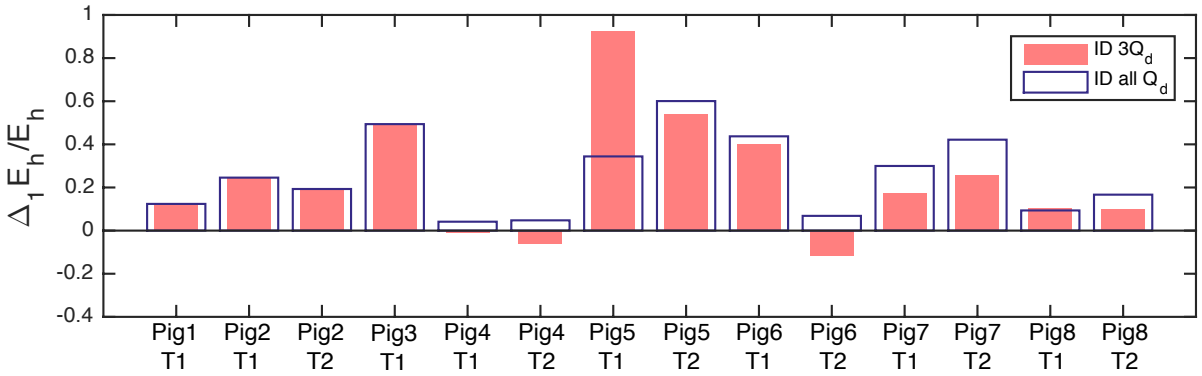

Figure 8.3 – Values of $\Delta_1 E_h/E_h$ for each weaning test when only 3 Q_d are used for the parameter identification (full bars) and when all the Q_d are used for the parameter identification (empty bars).

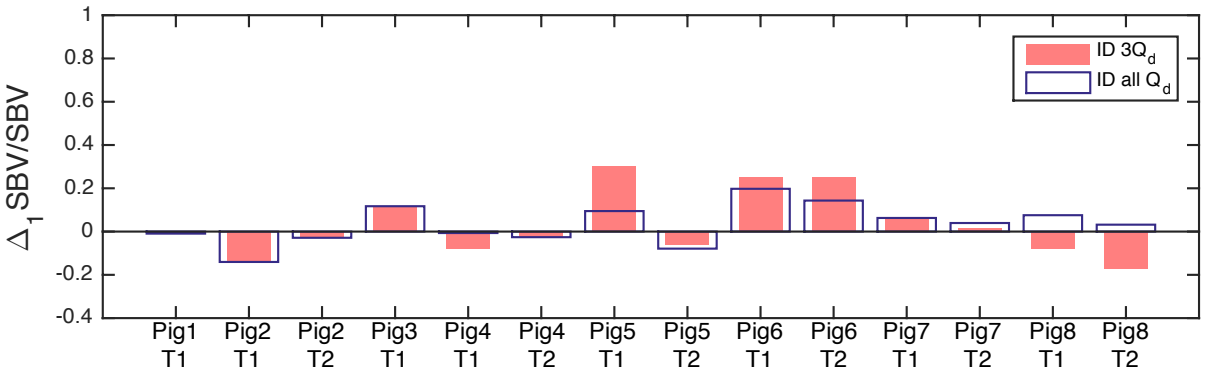

Figure 8.4 – Values of $\Delta_1 SBV/SBV$ for each weaning test when only 3 Q_d are used for the parameter identification (full bars) and when all the Q_d are used for the parameter identification (empty bars).

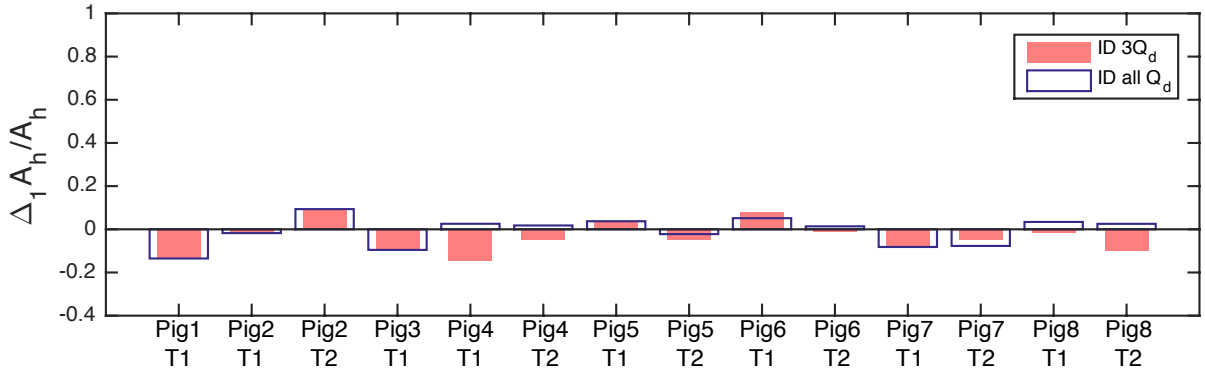

Figure 8.5 – Values of $\Delta_1 A_h/A_h$ for each weaning test when only 3 Q_d are used for the parameter identification (full bars) and when all the Q_d are used for the parameter identification (empty bars).

and the parameter identification using 3 Q_d does not have the same trend as the other parameter identification but, for both parameter identifications, the values are much smaller than the values of $\Delta_1 E_h/E_h$.

Figure 8.6 represents $\Delta_1 E_a/E_a$. This figure demonstrates that parameter E_a varies significantly and the sign of $\Delta_1 E_a/E_a$ changes between the different weaning tests. The variations of E_a thus do not have a clear trend. In addition, there is a significant difference between the values of $\Delta_1 E_a/E_a$ obtained with the 2 parameter identifications. A possible explanation of this result is that coefficient $E_{sl,a}$ is very sensitive to experimental errors and physiological interpretations of the variation of E_a are quite delicate.

Finally, Figure 8.7 describes $\Delta_1 R_s/R_s$. This figure demonstrates that $\Delta_1 R_s/R_s$ is almost always negative. Parameter R_s thus increases when Q_d decreases. This result could possibly be related to the baroreflex (see section 2.4, p. 35). Indeed, when Q_d decreases, the aortic pressure decreases and, in order to restore a higher blood pressure in the arteries, the nervous system constricts small vessels, which increases R_s.

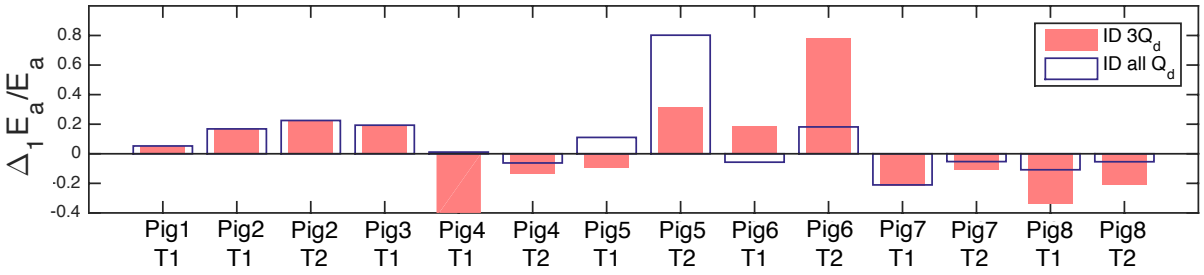

Figure 8.6 – Values of $\Delta_1 E_a/E_a$ for each weaning test when only 3 Q_d are used for the parameter identification (full bars) and when all the Q_d are used for the parameter identification (empty bars).

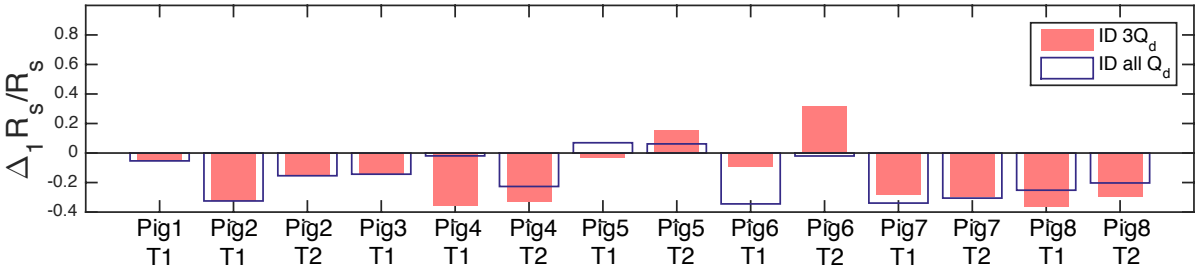

Figure 8.7 – Values of $\Delta_1 R_s/R_s$ for each weaning test when only 3 Q_d are used for the parameter identification (full bars) and when all the Q_d are used for the parameter identification (empty bars).

8.4.3 Prediction of the mathematical model

Table 8.4 has shown small prediction errors for PP_a, $\overline{P}_a$, $\overline{P}_v$ and $\max_{\mathrm{T}}(V_h)$ (relatives errors smaller or equal to 5 %) and a relative error of approximately 9 % for SV. These errors are acceptable and the larger error for SV makes sense since the measurements of SV are not very accurate.

Another important information is to check that the model allows a better prediction of the physiologically relevant quantities than a simple interpolation from previous measurements. Indeed, the model, after the parameter identification using PP_a, $\overline{P}_a$, $\overline{P}_v$, $\max_{\mathrm{T}}(V_h)$ and SV measurements related to 3 different Q_d, allows to predict the evolution of these quantities for lower values of Q_d. Another approach could consist in linearly interpolating the quantities corresponding to the 3 Q_d. Figure 8.8 compares these two methods for determining the evolutions of SV and $\overline{P}_a$ during the weaning test Pig8 T1. This figure illustrates that better predictions of SV and $\overline{P}_a$ are obtained by using our mathematical model. The quantitative errors for the predictions obtained with the interpolations can also be estimated and compared with the previous errors obtained with the mathematical model. Table 8.8 shows that the predicted values of $\overline{P}_a$, $\overline{P}_v$ and SV are slighty better with the model than with the interpolation but the predicted values of PP_a is little worse with the model than with the interpolation. However, the values of PP_a are notably less important for the patient monitoring than the other hemodynamic quantities.

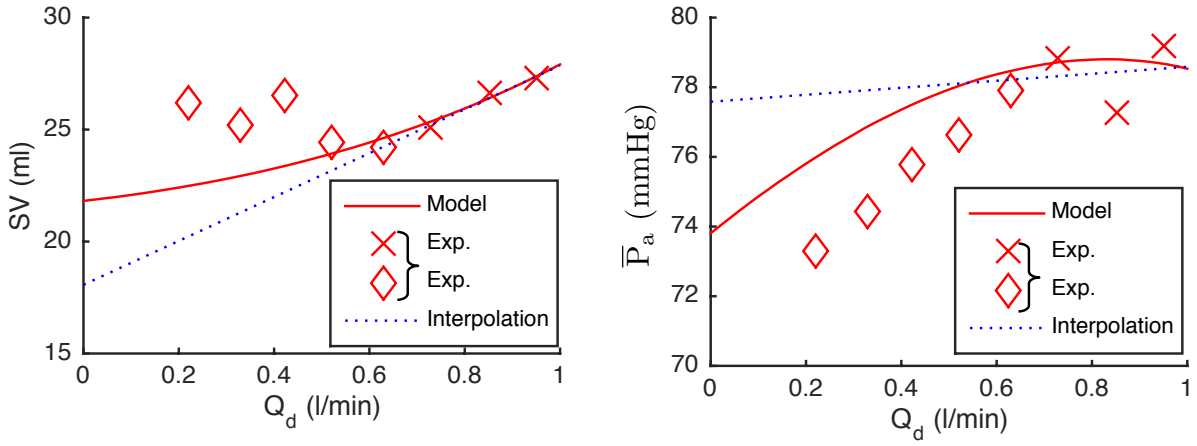

Figure 8.8 – Comparison of SV and $\overline{P}_a$ evolutions obtained using the model (solid lines) with the linear interpolations of SV and $\overline{P}_a$ obtained with the first 3 Q_d (dotted lines) for the weaning test Pig8 T1. The crosses and diamonds are the experimental data (the difference between diamonds and crosses has already been explained in Figure 8.1).

Table 8.8 – Comparison between the prediction errors obtained with the mathematical model and the prediction errors obtained with the interpolations of the measurements.

Global errors	Mathematical model	Interpolation
$\overline{\lvert\Delta PP_a/PP_a\rvert}$	0.055 ± 0.053	0.049 ± 0.050
$\overline{\lvert\Delta\overline{P}_a/\overline{P}_a\rvert}$	0.028 ± 0.029	0.034 ± 0.029
$\overline{\lvert\Delta\overline{P}_v/\overline{P}_v\rvert}$	0.037 ± 0.033	0.043 ± 0.049
$\overline{\left\lvert\frac{\Delta\max_{\mathrm{T}}(V_h)}{\max_{\mathrm{T}}(V_h)}\right\rvert}$	0.023 ± 0.023	0.020 ± 0.025
$\overline{\lvert\Delta SV/SV\rvert}$	0.092 ± 0.065	0.102 ± 0.059
$\overline{\Delta PP_a/PP_a}$	0.027 ± 0.073	0.024 ± 0.066
$\overline{\Delta\overline{P}_a/\overline{P}_a}$	0.001 ± 0.040	0.008 ± 0.044
$\overline{\Delta\overline{P}_v/\overline{P}_v}$	0.016 ± 0.048	0.015 ± 0.065
$\overline{\frac{\Delta\max_{\mathrm{T}}(V_h)}{\max_{\mathrm{T}}(V_h)}}$	-0.013 ± 0.024	-0.012 ± 0.024
$\overline{\Delta SV/SV}$	-0.035 ± 0.099	-0.042 ± 0.106

To refine the comparison between the model and the linear interpolation, it is interesting to consider the parameter identification using all the Q_d (see section 8.3). Table 8.9 gives the global errors (averaged values for Pig4 T1 to Pig8 T2) for the values of PP_a, $\overline{P}_a$, $\overline{P}_v$, $\max_{\mathrm{T}}(V_h)$ and SV simulated with the model and obtained with the interpolations of the measurements related to all the Q_d. This approach leads to similar results than the previous one; the predicted values of $\overline{P}_a$ and SV is slighty better with the model than with the interpolation but the predicted values of $\overline{P}_v$ is little worse with the model than with the interpolation.

In conclusion, the errors between the simulated values obtained with the mathematical model and the experimental data are small and these errors are a little bit smaller than those obtained with linear interpolations. SV and $\overline{P}_a$ are two quantities of paramount importance to check the vital functions of the cardiovascular system and the mathematical model improves by 10 % the prediction of SV and by 15 % the prediction of $\overline{P}_a$. Our mathematical model thus provides a promising first step to predict the evolution of the cardiovascular system for a decrease in Q_d.

Table 8.9 – Comparison between the identification errors obtained with the mathematical model and the interpolation errors when the measurements related to all Q_d are used.

Global errors	Mathematical model	Interpolation
$\overline{\lvert\Delta PP_a/PP_a\rvert}$	0.015 ± 0.010	0.015 ± 0.019
$\overline{\lvert\Delta \overline{P}_a/\overline{P}_a\rvert}$	0.009 ± 0.007	0.012 ± 0.015
$\overline{\lvert\Delta \overline{P}_v/\overline{P}_v\rvert}$	0.014 ± 0.005	0.010 ± 0.006
$\overline{\left\lvert\frac{\Delta \max_{\mathrm{T}}(V_h)}{\max_{\mathrm{T}}(V_h)}\right\rvert}$	0.009 ± 0.011	0.009 ± 0.012
$\overline{\lvert\Delta SV/SV\rvert}$	0.040 ± 0.021	0.045 ± 0.042
$\overline{\Delta PP_a/PP_a}$	0.004 ± 0.003	0.0004 ± 0.0008
$\overline{\Delta \overline{P}_a/\overline{P}_a}$	0.002 ± 0.002	0.0003 ± 0.004
$\overline{\Delta \overline{P}_v/\overline{P}_v}$	0.010 ± 0.006	0.0002 ± 0.0002
$\overline{\frac{\Delta \max_{\mathrm{T}}(V_h)}{\max_{\mathrm{T}}(V_h)}}$	0.002 ± 0.002	0.0004 ± 0.0011
$\overline{\Delta SV/SV}$	-0.006 ± 0.011	0.0027 ± 0.0037

8.5 Limitations

Several assumptions were introduced to build the mathematical model of the cardiovascular system connected to a va-ECLS. Probably the most limiting hypothesis is the absence of a description of the cardio-pulmonary controls since this model is used for different values of Q_d. However, our model takes into account the variations of the parameters E_h, A_h, E_a, SBV and R_s with Q_d. Therefore, the controls and the regulations of the cardio-pulmonary system are implicitly described using the 5 slopes $E_{Sl,h}$, $A_{Sl,h}$, $E_{Sl,a}$, SBV_{Sl} and $R_{Sl,s}$.

Volume measurements of the left ventricle are used for the parameter identification of the mathematical model and these measurements are not quite accurate. The reliability of the estimated parameters is thus impacted. A potential solution could be to take an additional continuous measurement of the left ventricle volume, such as the estimation of the cardiac output with an ultrasound flow probe surrounding the aorta [87].

The weaning tests performed on the 8 pigs are undertaken in different conditions than those performed on humans. Indeed, for the pigs, the weaning tests began approximately one hour after the cardiac arrest, while for ICU patients, weaning tests can be considered

after at least 24 hours of stable hemodynamic status. Therefore, the pigs analyzed in this chapter are less stable and still have heart failure symptoms during the weaning tests. In addition, the vessels of the studied pigs are smaller than those of adult humans and the range of extracorporeal blood flows is thus rather limited in the pig experiments. In order to overcome this limitation, the experiments could be carried out on larger pigs and these experiments could last longer than several hours. Of course, the optimal solution is to validate the mathematical model with clinical data during weaning tests and this approach will be developed in Chapter 10.

8.6 Summary

In this chapter, the model of the cardiovascular system connected to a va-ECLS has been used to simulate weaning tests of a va-ECLS using experimental data.

First, the values of the different parameters have been estimated using the measurements related to 3 different extracorporeal blood flows (Q_d). These parameters are thus subject-specific and their values have been discussed in subsection 8.4.1 and subsection 8.4.2. In addition, the parameters have also been estimated using the measurements related to all Q_d.

After the parameter identification using the measurements related to 3 Q_d, the model was tested by comparing the values simulated by the mathematical model with the experimental data related to different Q_d (smaller than the Q_d used for the parameter identification). Except for the stroke volume, the errors between the simulated values and the experimental data are rather small (less or equal to 5 %). The slightly larger error on the stroke volume ($\approx 9\%$) remains acceptable and can also be related to the rather poor quality of the corresponding measurement precision. In addition, subsection 8.4.3 provides the errors between the predictions obtained with the linear interpolations using the same measurements as the parameter identification and the clinical data. The prediction errors of the mean arterial pressure and of the stroke volume obtained with the mathematical model are smaller than those obtained with the linear interpolations.

The comparison between the mathematical model and the linear interpolations is also analyzed when the estimated values are obtained with the parameter identification using the measurements related to all Q_d (and when the linear interpolations are obtained using the measurements related to all Q_d). Of course, this approach gives much smaller errors between the simulated values and the experimental data. On the other hand, the errors

obtained with the mathematical model are a little bit smaller than the errors obtained with the linear interpolations.

Chapter 9

Experiments with a vv-ECLS

The protocol of the two set of experiments has already been described in subsection 7.1.1, p. 95. With the experimental data, the parameters of the model are estimated and their values are presented in section 9.1. Afterwards, the mathematical model of the respiratory system connected to a vv-ECLS can be used to start simulations and the results are shown in section 9.2. The main results consist in the time evolution of PCO_2 estimated by the mathematical model at several places in the body during the first hours of ECLST. Then, the results are discussed and analyzed in section 9.3 and the limitations of our model are drawn in section 9.4. Finally, the section 9.5 summarizes the results of this chapter.

9.1 Values of the parameters

To determine the diffusion coefficients across the membrane of the $ECCO_2RD$, the data of *experiments H* are used. Using the method presented in subsection 7.2.5, one finds D_{CO_2}= 6.33 $\times 10^{-5}$ $l_{CO_2}/s/mmHg$, D'_{CO_2}= 3.97 $\times 10^{-4}$ $l_{CO_2}/s/mmHg$, $D_{O_2} = 1.58 \times 10^{-6}$ $l_{O_2}/s/mmHg$ and $D'_{O_2} = 9.93 \times 10^{-6}$ $l_{O_2}/s/mmHg$. As already mentioned, the settings of the $ECCO_2RD$ are such that the atmospheric air flow is always equal to 10 liters per minute, while parameter Q_d is changed several times (200 ml/min, 400 ml/min and 600 ml/min) for *experiments H* and, except for pig *A*1, set to one value (around 700 ml/min) for *experiments A*. For pig *A*1, parameter Q_d is changed several times (200 ml/min, 400 ml/min, 600 ml/min and 800 ml/min). Since Q_d is always smaller than 1 l/min, the recirculation of the extracorporeal blood flow is not taken into account for the pig experiments (see subsection 5.3.1, p. 73).

The other parameters of the model are given in Table 9.1 for all animals. Parameter F_{I,O_2}, V_T and fr are the ventilator settings. On the other hand, the values of MR_{CO_2}, MR_{O_2}, k_{HCO_3}, f_s and $\dot{V}_A$ are determined by the procedures described in subsections 7.2.1,

7.2.3 and 7.2.4. Note that in Table 9.1, parameter f_s increases when protective ventilation is induced and it increases even more when protective ventilation is coupled with ARDS. On the other hand, the alveolar ventilation $\dot{V}_A$ decreases when protective ventilation is induced.

Cardiac blood flow values for the different animals during the experiments are also parameters of the model and Figure 9.1 provides these values for all pigs. The hemoglobin concentration C_{Hb} is estimated in arterial and venous blood samples for every pig and the mean of all these values is used and is equal to 0.15 l_{Hb}/l. This value is smaller than other values found in literature (0.2 l_{Hb}/l [9, 94]) since blood is diluted in our experiments.

Finally, parameters V_{L,CO_2}, V_{L,O_2}, V_{T,CO_2}, V_{T,O_2} and V_{TB} are proportional to the body weight (Table 7.1, p. 99) and are directly estimated from the weight specified in Table 9.1.

Table 9.1 – Measurements, settings of the ventilator and identified parameters for *experiments H* (H1 – H4) and *experiments A* (A1 – A6)

	Experiments H ("healthy" pigs)				*Experiments A* (pigs with ARDS)					
Data	H1	H2	H3	H4	A1	A2	A3	A4	A5	A6
Baseline situation										
Measurements										
Weight (kg)	22	29	28	31	28	35	22	22.7	30	30
Ventilator settings										
F_{I,O_2}	0.5	0.5	0.5	0.5	0.5	0.5	0.5	0.5	1	0.5
V_T (l)	0.290	0.375	0.360	0.400	0.280	0.300	0.222	0.230	0.300	0.250
fr (min^{-1})	25	25	25	25	20	20	20	20	20	20
Identified parameters										
MR_{O_2} (l_{O_2}/min)	0.147	0.202	0.183	0.226	0.173	0.182	0.142	0.108	0.133	0.195
MR_{CO_2} (l_{CO_2}/min)	0.147	0.202	0.183	0.226	0.173	0.182	0.142	0.108	0.133	0.195
k_{HCO_3} (l_{CO_2}/l)	0.06	0.028	0.068	-0.001	0.042	0.05	-0.053	0.018	0.055	0.06
f_s	0.044	0.066	0.047	0.029	0.037	0.08	0.133	0.08	0.059	0.050
$\dot{V}_A$ (l/min)	3	5.85	4.325	6.875	3.24	3.9	2.76	2.2	3.92	4.58
	Protective ventilation				**Protective ventilation and ARDS**					
Ventilator settings										
F_{I,O_2}	1	1	1	1	0.5	0.5	1	1	1	1
V_T (l)	0.135	0.170	0.175	0.185	0.200	0.200	0.132	0.120	0.180	0.180
fr (min^{-1})	15	15	15	15	20	20	20	20	20	20
Identified parameters										
f_s	0.105	0.092	0.069	0.128	0.304	0.436	0.49	0.57	0.409	0.532
$\dot{V}_A$ (l/min)	0.93	1.73	1.38	2.1	1.42	1.92	1.44	1.2	2	2.7

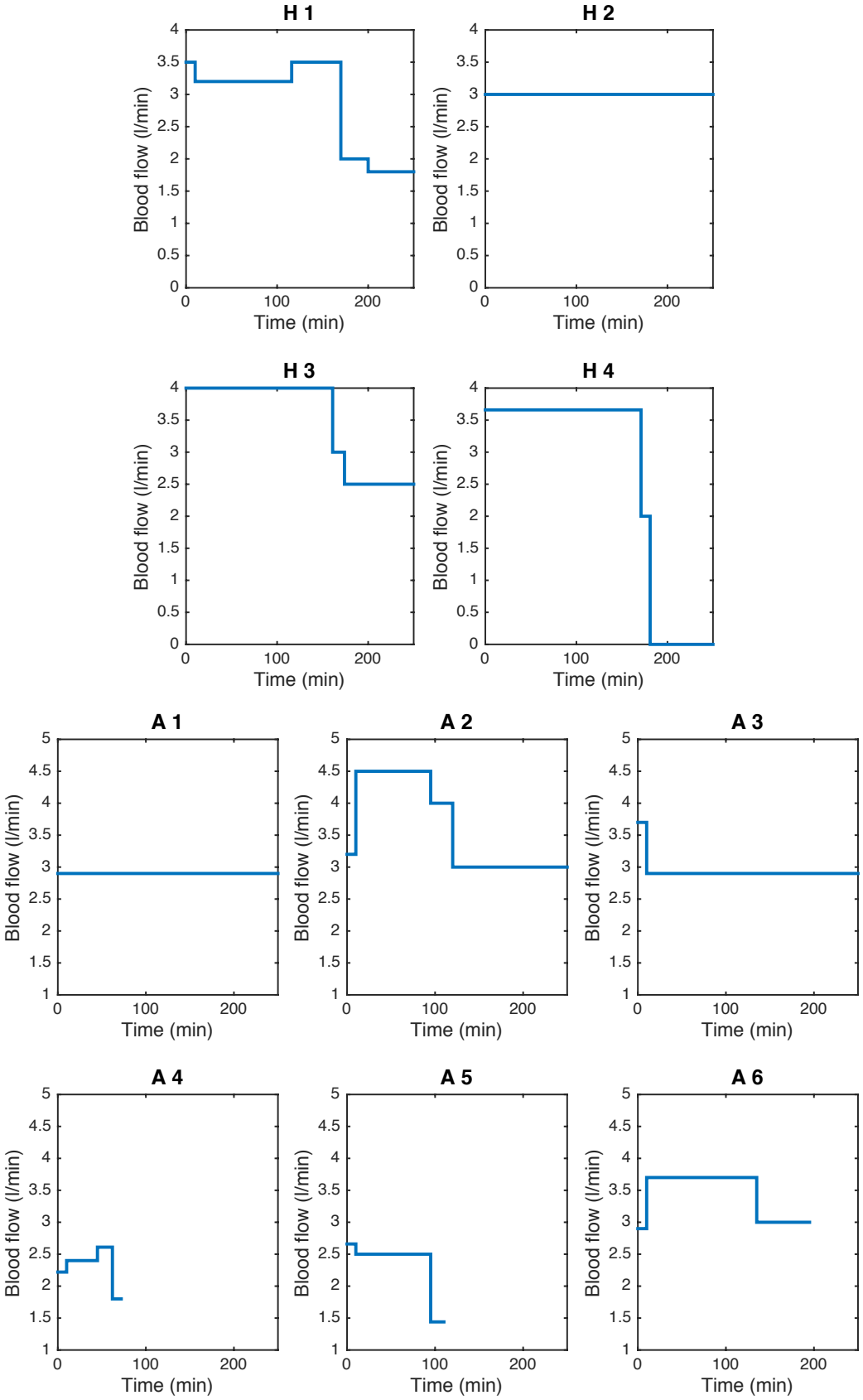

Figure 9.1 – Time evolution of the cardiac blood flows for *experiments H* (H1 – H4) and *experiments A* (A1 – A6).

9.2 Comparaison between simulations and experimental data

To validate the model, the simulations must be compared with experimental data. To test the predictions of the model, the mean difference ($\overline{|\Delta P_i|}$ where i = CO_2 or O_2) between the simulations and the experimental data is estimated with the following formula:

$$\overline{|\Delta P_i|} = \frac{1}{m}\sum_{j=1}^{m} |P_{i,j}^{sim} - P_{i,j}^{exp}| \ , \tag{9.1}$$

where m is the number of PCO_2 or PO_2 measurements, $P_{i,j}^{exp}$ is the PCO_2 or PO_2 measurement j and $P_{i,j}^{sim}$ is the corresponding PCO_2 or PO_2 simulated with the model. The mean relative difference ($\overline{|\Delta P_i/P_i|}$ where i = CO_2 or O_2) provides another way to estimate the error :

$$\overline{|\Delta P_i/P_i|} = \frac{1}{m}\sum_{j=1}^{m} \frac{|P_{i,j}^{sim} - P_{i,j}^{exp}|}{P_{i,j}^{exp}}. \tag{9.2}$$

In addition, to estimate whether the model tends to overestimate or to underestimate the partial pressures, the mean differences and the mean relative differences are also computed without the absolute value (and the corresponding symbols are written as $\overline{\Delta P_i}$ and $\overline{\Delta P_i/P_i}$). Since the purpose of the $ECCO_2RD$ is to remove CO_2, in this chapter, only the simulated CO_2 partial pressure are compared with the experimental data (i = CO_2).

The ECLS compartment is of paramount importance and the 3 ECLS models presented previously (see section 5.3) are tested independently of the other compartments in subsection 9.2.1. On the other hand, subsection 9.2.2 describes the results of the whole model of the respiratory system connected to an ECLS.

9.2.1 Results for the ECLS models alone

To compare the 3 ECLS models presented in section 5.3 (Figure 5.2), the composition of blood (PCO_2, PO_2, pH and HCO_3^-) entering the device is assumed given and the predictions of the 3 models concerning the change of PCO_2 across the device are compared. The results are presented in Figure 9.2 and Figure 9.3, which show PCO_2 of the blood exiting the machine and PCO_2 of the gas exiting the machine respectively. The experimental data presented in these figures correspond to the data available for pigs H1-H4. Note that the error on the measurements in blood is equal to $0.03 \times \{value\ of\ the\ measurement\} + 0.17$ mmHg according to the manufacturer of the RapidPoint500® device and the error on

the measurements in gas is equal to $0.02 \times \{value\ of\ the\ measurement\} + 0.342$ mmHg according to the manufacturer of the CARBOCAP® device. As expected, the 3 models agree rather well for small blood flow, but Mod 1 gets better and better as the blood flow is increased in the $ECCO_2RD$. Table 9.2 provides the mean errors $\overline{|\Delta P_{CO_2}|}$ and the mean relative errors $\overline{|\Delta P_{CO_2}/P_{CO_2}|}$ for each ECLS model. $\overline{|\Delta P_{CO_2}|}$ and $\overline{|\Delta P_{CO_2}/P_{CO_2}|}$ for Mod 1 are smaller than $\overline{|\Delta P_{CO_2}|}$ and $\overline{|\Delta P_{CO_2}/P_{CO_2}|}$ for Mod 2 and much smaller than $\overline{|\Delta P_{CO_2}|}$ and $\overline{|\Delta P_{CO_2}/P_{CO_2}|}$ for Mod 3. For this reason, Mod 1 is preferred and it will be used in the next simulations.

Table 9.2 – Errors between the simulations and the measurements of the CO_2 partial pressure exiting the $ECCO_2RD$. m is the number of PCO_2 or PO_2 measurements

Models	Mod 1	Mod 2	Mod 3
$\overline{\lvert\Delta P_{CO_2}\rvert}$ (mmHg)	0.78 ± 0.50	1.23 ± 1.32	2.70 ± 2.09
$\overline{\lvert\Delta P_{CO_2}/P_{CO_2}\rvert}$	0.09 ± 0.01	0.13 ± 0.04	0.29 ± 0.06
m	26	26	27

9.2.2 Result of the respiratory model connected to a vv-ECLS

Using the values of the parameters given in section 9.1, the mathematical model is able to describe the gas exchanges for *experiments H* and *experiments A* during the $ECCO_2RT$. The main results consist in the time evolution of PCO_2 at several places in the body. The right panel of Figure 9.4 illustrates the time evolution of PCO_2 in the veins, in the arteries and in the right ventricle for pig H2 and the left panel of Figure 9.4 illustrates the time evolution of PCO_2 in the veins and arteries for pig A6. The results for the other pigs have similar features and are given in Figure B.6 and Figure B.7 of Appendix B.2. In the two panels, the vertical lines indicate the beginning of the different phases of the experiments. As expected, PCO_2 in the body increases when protective ventilation and ARDS are induced and decreases when the $ECCO_2RD$ is initialized.

Figure 9.4 shows a good agreement between the numerical simulations and the corresponding experimental data. During baseline situation (the first 10 minutes in Figure 9.4), the agreement is perfect for PCO_2 in the arteries since parameters f_s and $\dot{V}_A$ are identified to fit PCO_2 in the arteries. On the other hand, the agreement is not perfect for the venous PCO_2 because MR_{CO_2} is not estimated with the measurements but with the approximation $MR_{CO_2} = MR_{O_2}$. After baseline situation, protective ventilation is induced

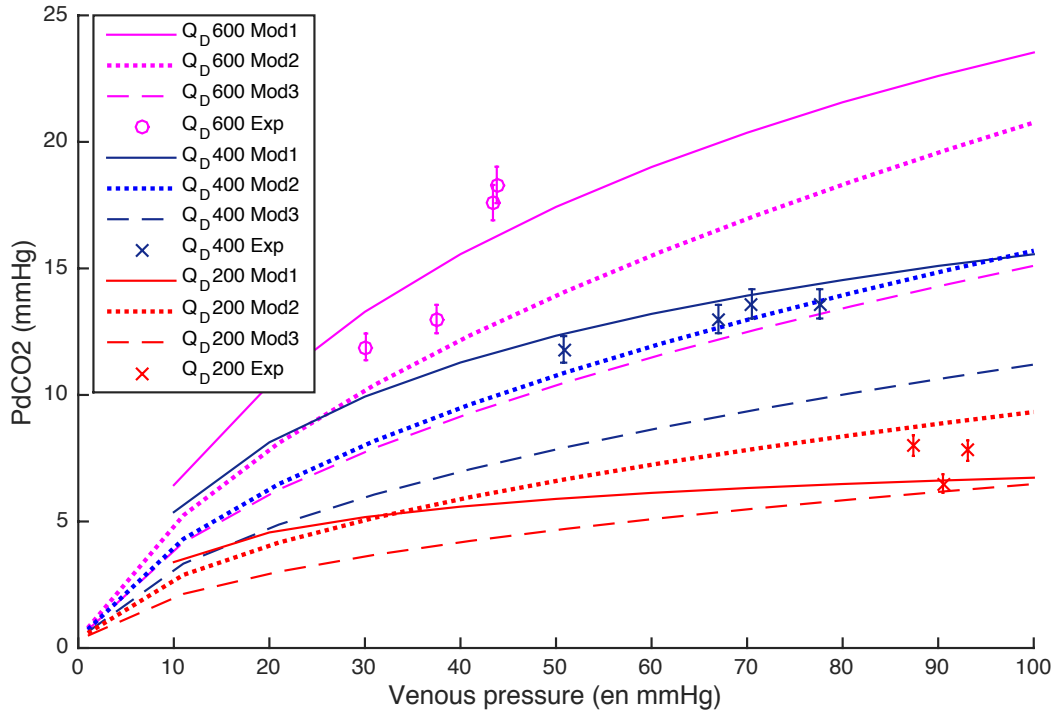

Figure 9.2 – PCO_2 in the blood exiting the $ECCO_2RD$ (P_{out,CO_2}) as a function of PCO_2 in venous blood and for different blood flows entering the $ECCO_2RD$.

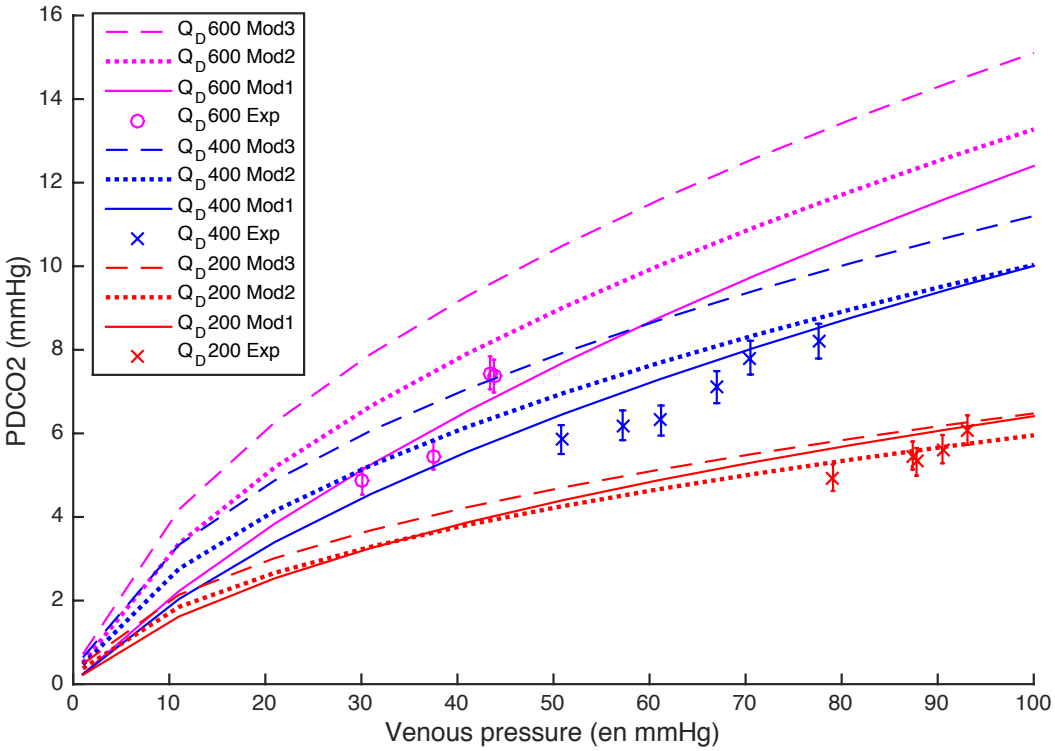

Figure 9.3 – PCO_2 in the gas exiting the $ECCO_2RD$ (P_{D,CO_2}) as a function of PCO_2 in venous blood and for different blood flows entering the $ECCO_2RD$.

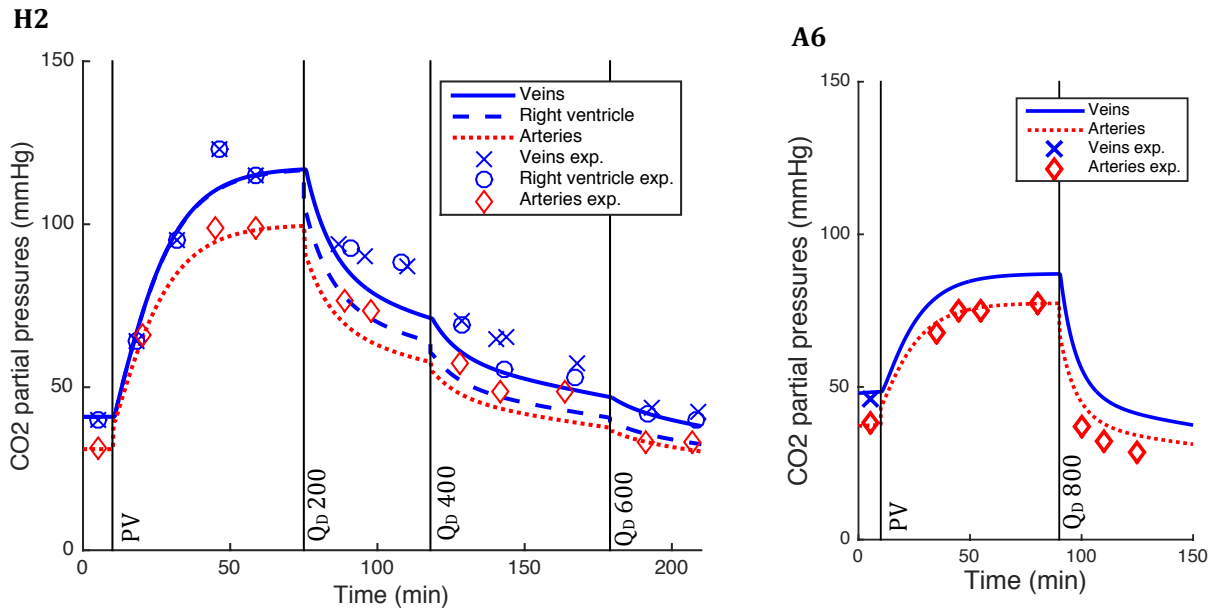

Figure 9.4 – Time evolution of calculated (lines) and measured (crosses, circles and diamonds) CO_2 partial pressures in the veins, in the right ventricle and in the arteries for pig H2 (the left panel) and in the veins and arteries for pig A6 (the right panel). The labels PV, Q_D 200, Q_D 400, Q_D 600 and Q_D 800 mean respectively the start of protective ventilation and the blood flow through the $ECCO_2RD$ set to 200, 400, 600 and 800 ml/min.

(combined with ARDS in *experiments A*) and the agreement is still good since parameters f_s and $\dot{V}_A$ are re-evaluated. Now, the comparison between experimental and numerical results during the $ECCO_2RT$ will be analyzed in detail. During this period, all parameters are kept constant and the agreement between simulations and experimental data remains quite good, for a relatively long period of time. Table 9.3 provides the mean errors $\overline{\Delta P_{CO_2}}$ and the mean relative errors $\overline{\Delta P_{CO_2}/P_{CO_2}}$ with and without absolute value for each pig of the two sets of experiments. The number of PCO_2 measurements (m) is also given. Note that the standard deviation of the errors is not given for *experiments A* since the number of measurements is small (less than 5 measurements). One can observe that the errors for *experiments H* are larger than for *experiments A*. However, *experiments H* have more experimental data in different parts of the body (*experiments A* have only arterial measurements during the $ECCO_2RT$). For *experiments H*, the model always underestimates the PCO_2 measurements (the value of $\overline{\Delta P_{CO_2}}$ and $\overline{\Delta P_{CO_2}/P_{CO_2}}$ is always negative) whereas overestimations are almost always observed for *experiments A* (every pigs except A1). Therefore, the mean error $\overline{\Delta P_{CO_2}}$ and the mean relative error $\overline{\Delta P_{CO_2}/P_{CO_2}}$ without the absolute value for all pigs are close to 0. On the other hand, the mean relative error $\overline{|\Delta P_{CO_2}/P_{CO_2}|}$ is equal to 11%.

Table 9.3 – Errors between the simulations and the measurements during the $ECCO_2RT$ for *experiments H* and *experiments A*. The line m indicates the number of PCO_2 measurements available during the $ECCO_2RT$.

	Experiments H				*Experiments A*						
Data	H1	H2	H3	H4	A1	A2	A3	A4	A5	A6	**Mean** $\pm$ σ
$\overline{\lvert\Delta P_{CO_2}\rvert}$ (mmHg)	9.82 $\pm$ 7.40	7.47 $\pm$ 6.60	4.24 $\pm$ 6.02	7.00 $\pm$ 5.76	2.93	9.04	4.51	5.77	0.08	4.96	**5.58** $\pm$ **2.91**
$\overline{\lvert\Delta P_{CO_2}/P_{CO_2}\rvert}$	0.14 $\pm$ 0.10	0.12 $\pm$ 0.06	0.06 $\pm$ 0.07	0.11 $\pm$ 0.05	0.06	0.21	0.12	0.14	0.00	0.15	**0.11** $\pm$ **0.06**
$\overline{\Delta P_{CO_2}}$ (mmHg)	-9.48 $\pm$ 9.97	-7.37 $\pm$ 4.88	0.91 $\pm$ 7.33	-5.28 $\pm$ 6.08	-2.49	9.04	4.51	0.39	0.08	4.96	**-0.47** $\pm$ **5.81**
$\overline{\Delta P_{CO_2}/P_{CO_2}}$	-0.13 $\pm$ 0.12	-0.11 $\pm$ 0.06	-0.00 $\pm$ 0.09	-0.09 $\pm$ 0.08	-0.06	0.21	0.12	0.00	0.00	0.15	**0.01** $\pm$ **0.12**
m	23	23	24	16	4	2	1	2	1	3	

9.3 Discussion

This section discusses the physiological meaning of important parameters and discusses the ability of our model to predict the decrease in PCO_2 during the $ECCO_2RT$. The application of the mathematical model in the ICU is also discussed in this section.

9.3.1 Modeling of lung gas exchanges

Since the aim of our work is to find subject-specific parameters before $ECCO_2RT$ is initiated, the description of the possible lung pathologies is quite crucial. For this reason, our model uses two parameters with clear physiological meaning to describe the impairments of gas exchange: f_s which describes the importance of the pulmonary shunt and $\dot{V}_A$ which is the mean alveolar ventilation. In the literature, the mean alveolar ventilation $\dot{V}_A$ is often not identified as in our approach, but directly estimated [93, 55]. $\dot{V}_A$ depends on the tidal volume and the respiratory frequency, which are easily known since these are settings of the ventilator. But $\dot{V}_A$ also depends on the dead space V_{Dead}, which is much more difficult to obtain. Some authors assume that this space is equal to 150 ml for an adult patient [93], while others measure the dead space with a stand-alone respiratory monitor [55]. In our experiments on pigs, the assumption of a human value equal to 150 ml can of course not be made. It is not either possible to estimate V_{Dead} with a gas analyzer at the outlet of the ventilator. Indeed, the experimental data related to the CO_2 expired out of the ventilator are not enough accurate to estimate the dead space with the small ventilation used in our experiments. Consequently, $\dot{V}_A$ is identified together with the pulmonary shunt f_s and these two parameters describe the global efficiency of gas exchanges in the lungs. Note that, in physiology, the quality of gas exchanges in the lungs depends on several factors, such as ventilation-perfusion mismatch or the quality of diffusion across the alveolar-capillary membrane. In the present work, these effects are not explicitly modeled and parameters f_s and $\dot{V}_A$ must thus be considered as lumped parameters that allow a global description of all gas exchange abnormalities in the mathematical model.

During the animal experiments, the tidal volume is decreased drastically when the protective ventilation starts. Of course, the alveolar ventilation changes with the tidal volume but the pulmonary shunt can also change since the lung dynamics are modified. The induction of ARDS has also an impact on the pulmonary shunt. Therefore, it is necessary that the two parameters are estimated twice: first during the baseline situation and then during protective ventilation (combined with ARDS induction in *experiments A*). The changes of these two parameters between the two phases are discussed in the next subsection.

9.3.2 Values of the parameters

Table 9.1 shows that the two lumped parameters f_s and $\dot{V}_A$ behave as physiologically expected. Indeed, during ARDS, a significant fraction of alveoli does not work properly and an increase in the pulmonary shunt is expected in physiology [6, 100]. The value of f_s during ARDS (45.7±9.6%) is larger than in previous studies on human suffering from ARDS (31±10% [54]) but note that the experiments are carried out on pigs and that the ARDS is simulated by injecting water into the lungs. This ARDS model is thus different from the respiratory pathology and could lead to different values of f_s. The value of f_s at baseline (6.3±3%) is also larger than expected for a healthy human (2% [46]) but the pigs are intubated and anesthetized and thus not in a truly physiologically healthy state. The small increase in f_s during protective ventilation for *experiments H* can be interpreted by the collapse of some alveoli when the pressure in the lungs is lower. With regards to parameter $\dot{V}_A$, its decrease during protective ventilation is clearly related to the drastic decrease in the tidal volume.

MR_{CO_2} and MR_{O_2} values are in the same range as in previous studies. All pigs of *experiment H* and pigs A1, A3 and A6 have MR_{O_2} (and MR_{CO_2}) values very close to the standard empirical relation used by Karagiannidis *et al.* [53]: MR_{O_2} $(= MR_{\mathrm{CO}_2})$ $= 7 \cdot 10^{-3} \cdot \mathrm{Weight(kg)}$ $\mathrm{l}_{\mathrm{O}_2}/\mathrm{min/kg}$.

9.3.3 Quality of the PCO_2 predictions

Even if the CO_2 removal therapies considered are rather complex for *experiments H*, since the settings of the device are changed several times during the period of interest, the model is able to describe the general behavior of the system throughout the whole experiment. The global relative error $\overline{|\Delta P_{\mathrm{CO}_2}/P_{\mathrm{CO}_2}|}$ for all pigs of *experiments H* and *experiments A* is larger than the accuracy of the blood analyser RapidPoint500 (11% compared to 3%) but the simulation of the PCO_2 prediction depends on several other measurements such as the cardiac output, the inspired fraction of O_2 and the PO_2. In addition, for the simulations, the extracorporeal blood flow is assumed perfectly controlled whereas in reality, it is difficult to achieve that goal. Recall also that the parameters f_s and $\dot{V}_A$ are kept constant throughout the $\mathrm{ECCO}_2\mathrm{RT}$ and are estimated before the $\mathrm{ECCO}_2\mathrm{RT}$. If this global relative error (11%) is compared to the global relative error of the ECLS model alone (9%, see subsection 9.2.1), the global relative error of the respiratory model connected to a vv-ECLS is slightly larger than the global relative error of the ECLS model alone. This result confirms that the error of 11% is mainly due to experimental uncertainties and not due to an error of the mathematical prediction. For these reasons, we can consider that our mathematical

model of the respiratory system connected to an $ECCO_2RD$ can predict rather nicely the decrease in PCO_2 during the $ECCO_2RT$, and our model can be considered as validated by the pig experiments.

One main purpose of the mathematical model is to determine an appropriate extracorporeal blood flow for a specific patient. Therefore, it is interesting to know how the 11% relative error on PCO_2 impacts the prediction of the blood flow. To test the sensitivity of the extracorporeal blood flow with respect to the PCO_2 error, we have considered the "mean pig" of all the experiments. This "mean pig" is obtained by considering the mean of all the parameters given in Table 9.1 ($MR_{CO_2} = MR_{O_2} = 0.17$ l/min, $\dot{V}_A = 1.7$ l/min, $f_s = 0.25\%$ and $k_{HCO_3} = 0.03$ l_{CO_2}/l, $F_{I,O_2} = 0.9$ and a weight of 28 kg) and we have used our mathematical model to determine the blood flow that allows to achieve a PCO_2 equal to 50 mmHg in the arteries after 1 hour of the $ECCO_2RT$. Then, the blood flows corresponding to $50+11\%$ mmHg and $50-11\%$ mmHg are also determined. The situation is illustrated in Figure 9.5 and the values of the three blood flows are 268 ml/min, 199 ml/min and 377 ml/min respectively. The positive and negative errors in PCO_2 thus give rise to 26% and 40% of imprecision in the calculated blood flows respectively, which is not negligible but nevertheless acceptable in comparison with the global error of all our experiments. In addition, in a clinical environment, the patients' status is often quite unstable like in our pig experiments and an uncertainty over the appropriated blood flow is unavoidable.

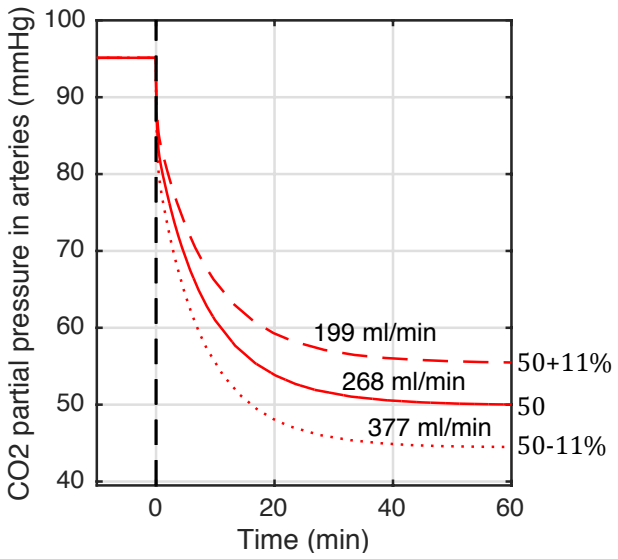

Figure 9.5 – Decrease in PCO_2 in the arteries during the $ECCO_2RT$ for different extracorporeal blood flows.

9.3.4 Application of the model in the ICU

Results show that the mathematical model is able to predict the decrease in PCO_2 during the $ECCO_2RT$ performed on pigs. This is a very encouraging step to extend the use of this model to the ICU. It could improve patient-specific care under $ECCO_2RT$. In the context of this possible extension of the use of the model, 3 additional points need to be made.

Fast computation time

Delay differential equations need much more time to be solved than classical differential equations. The time needed for a numerical simulation of PCO_2 decrease during a one hour of $ECCO_2RT$ is around 32 min (on a standard laptop computer and using *MATLAB®*) for the mathematical model with delay differential equations while it takes only 3 min for the mathematical model with classical differential equations. If the transport delays are neglected, the values of the two parameters $\dot{V}_A$ and f_s are slightly different during protective ventilation since they are identified in an unstationary state (their values are given in Table B.1 of Appendix B.2). Figure 9.6 compares our simulations when delays in blood circulation are or are not taken into account and one can observe that the two simulations are slightly different when the system is in an unsteady state. However, the long-term evolution does not require taking the delays into account, which is a consequence of the smallness of the delays with respect to the duration of the $ECCO_2RT$. The delays of blood circulation can thus safely be disregarded in the description. In addition, the mean relative errors $\overline{\Delta P_{CO_2}/P_{CO_2}}$ for all pigs is still equal to 11 % when the delays are not taken into account (the values of the mean errors $\overline{\Delta P_{CO_2}}$ and the mean relative errors $\overline{\Delta P_{CO_2}/P_{CO_2}}$ with and without absolute value for each pig are given in Table B.2 of Appendix B.2). The mathematical model with classical differential equations is thus preferred since the computation time is sufficiently small to allow the model to participate in the rapid decision-making that is required by clinicians at the patients bedside in the ICU. Therefore, the differential equations without transport delays will be used in the next simulations (end of this chapter and in Chapter 11).

Weight-based estimation of cardiac output

The cardiac blood flow, which is continuously measured in our experiments, is introduced as a given function of time in the calculations. However, if the model is used in the ICU before starting the $ECCO_2RT$ to determine the best settings of the device, the change of cardiac output is of course unknown when the calculations are carried out. In addition, cardiac blood flow is not often measured before the $ECCO_2RT$. For these reasons, it is important to check the validity of our model when approximate values of cardiac output

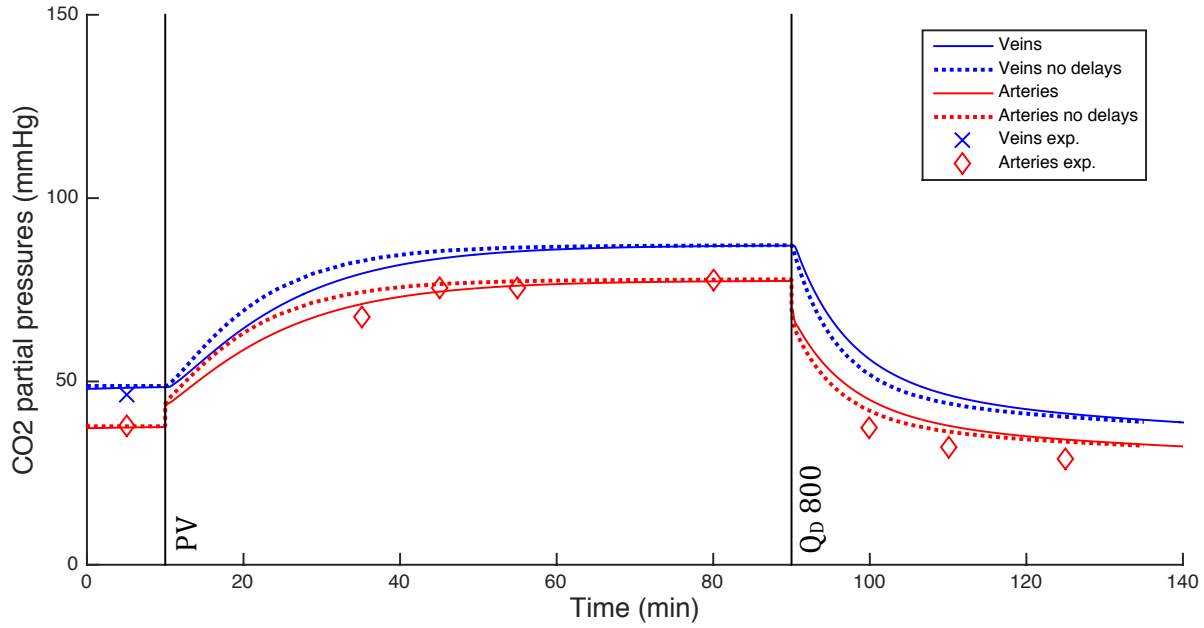

Figure 9.6 – Time evolution of calculated (lines) and measured (crosses and diamonds) CO_2 partial pressures in the veins and arteries for pig A6 when transport delays are considered (continuous lines) and when they are not (dotted lines).

are introduced in the calculations.

An approximation of the cardiac blood flow can be obtained by using the cardiac index, which is the cardiac output divided by the BSA (subsection 7.2.3, p. 100). Various formulae have been published to estimate the BSA and a commonly used expression is the Mosteller formula [115]. This approximation is based on human morphology and can be used in the ICU. However, it cannot be used in our experiments that were carried out on pigs. To test the validity of our model when a precise value of cardiac output is not known, the mean value obtained by considering all our available measurements (all pigs, baseline situation and protective ventilation) will be used, which is equal to 3.21 l/min. This value will be kept constant during all the simulations considered in the present section. Table 9.4 gives the corresponding new estimations of parameters f_s and $\dot{V}_A$ (with all the other parameters and measurements remaining the same as in Table 9.1). Let us mention that as expected, the re-identified alveolar ventilation keeps the same value as before. On the other hand, parameters f_s describing the pulmonary shunt decreases (resp. increases) when the approximate cardiac output is larger (resp. smaller) than the measured value. To test the validity of our approach with approximate cardiac output, we consider the mean errors $\overline{\Delta P_{CO_2}}$ and the mean relative errors $\overline{\Delta P_{CO_2}/P_{CO_2}}$ with and without absolute value like in subsection 9.2.2. The results are similar than those with precise values of the

cardiac output and the mean relative errors $\overline{\Delta P_{CO_2}/P_{CO_2}}$ for all pigs is still equal to 11 % (the values of the mean errors $\overline{\Delta P_{CO_2}}$ and the mean relative errors $\overline{\Delta P_{CO_2}/P_{CO_2}}$ with and without absolute value for each pig are given in Appendix B.2 in Table B.3). We can thus conclude that the quality of the predictions of our model is almost not affected when only approximate cardiac output is known. This is an important result for the use of our model in the ICU.

Table 9.4 – Parameters for *experiments H* and *experiments A* when the cardiac output is equal to 3.21 l/min and when transport delays are neglected.

	Experiments H				*Experiments A*					
Data	H1	H2	H3	H4	A1	A2	A3	A4	A5	A6
Baseline situation										
f_s	0.041	0.07	0.038	0.025	0.041	0.077	0.117	0.11	0.07	0.055
$\dot{V}_A$ (l/min)	3	5.85	4.325	6.875	3.24	3.9	2.76	2.2	3.92	4.58
Protective ventilation					**Protective ventilation and ARDS**					
f_s	0.105	0.098	0.069	0.114	0.326	0.425	0.516	0.62	0.47	0.495
$\dot{V}_A$ (l/min)	0.93	1.8	1.695	2.1	1.58	1.92	1.44	1.2	2	2.66

Weight-based estimation of MR_{CO_2} and MR_{O_2}

In ICU, venous blood samples are not always taken before starting the extracorporeal circulation and, as previously mentioned, cardiac output is not often measured. In such circumstances, the estimation of metabolism production and consumption cannot be done as explained in subsection 7.2.3. For this reason, our model is also tested when these production and consumption are simply estimated by using a weight-based estimation MR_{O_2} ($= MR_{CO_2}$) $= 7\times10^{-3}\mathrm{l}_{O_2}/\mathrm{min/kg}$ [53]. Table 9.5 provides the corresponding values of metabolism production and consumption for the pigs of our two sets of experiments. The associated values of parameter f_s and $\dot{V}_A$ are also given. For most pigs (7 out of 10), the values given in Table 9.5 are quite similar to the values of Table 9.1. However, for pigs A2, A4 and A5, the two estimations give significantly different values for the parameters. In particular, in the baseline situation, parameter $\dot{V}_A$ has a larger value than the tidal minute ventilation ($fr \times V_T$) for pig A5, which is physiologically unacceptable and thus makes the weight-based estimation unusable for pig A5. For the other pigs, the mean errors $\overline{\Delta P_{CO_2}}$ and the mean relative errors $\overline{\Delta P_{CO_2}/P_{CO_2}}$ with and without absolute value are estimated (all the values are given in Table B.4 of Appendix B.2) and the mean relative error for all pigs is equal to 14 %. This error is larger than the previous one (Table 9.3) because pig A4 shows much larger errors when the weight-base approximation is used to estimate metabolism (the mean relative error is equal to 27%). We can thus

conclude that estimating the metabolism production and consumption from measured data always provides good results and this method must thus be preferred. However, when experimental data are not available, the weight-based estimation of MR_{CO_2} and MR_{O_2} can also provide acceptable results in most cases.

Table 9.5 – Parameters for *experiments H* and *experiments A* when metabolism is estimated with the weight-based approximation and when transport delays are neglected.

	Experiments H				*Experiments A*					
Data	H1	H2	H3	H4	A1	A2	A3	A4	A5	A6
Baseline situation										
MR_{O_2} (l_{O_2}/min)	0.154	0.203	0.196	0.217	0.196	0.245	0.154	0.159	0.210	0.210
MR_{CO_2} (l_{CO_2}/min)	0.154	0.203	0.196	0.217	0.196	0.245	0.154	0.159	0.210	0.210
f_s	0.043	0.065	0.040	0.030	0.033	0.060	0.124	0.056	0.038	0.047
$\dot{V}_A$ (l/min)	3.15	5.875	4.65	6.6	3.68	5.24	3	3.24	6.18	4.9
Protective ventilation					**Protective ventilation and ARDS**					
f_s	0.085	0.085	0.080	0.090	0.278	0.383	0.470	0.401	0.304	0.512
$\dot{V}_A$ (l/min)	0.975	1.65	1.5	1.875	1.7	2.6	1.56	1.2	3.3	2.88

9.4 Limitations

CO_2 production MR_{CO_2} and O_2 consumption MR_{O_2} are two important quantities in the functioning of the respiratory system. These two quantities are equal for the carbohydrate metabolism but if the patient's metabolism uses different sources such as fats or proteins, MR_{CO_2} is smaller than MR_{O_2} (subsection 2.3.3). Unfortunately, because the total concentration of CO_2 in blood depends on 3 chemical species (CO_2 dissolved in blood, HCO_3^- and CO_2 complexed with hemoglobin), the identification of the value of MR_{CO_2} from blood sample analyses has proved to be quite delicate and even impossible in our experiments. For this reason, we have introduced the approximation of equal MR_{CO_2} and MR_{O_2}.

If the long-term purpose of our work is to provide an additional therapeutic tool to clinicians, other limitations must also be emphasized. First, the status of the pigs used in experiments does not exactly correspond to that of humans in the ICU. In the experiments, hypercapnia was induced by protective ventilation and injection of water in the lungs, but no real ARDS or chronic obstructive pulmonary disease was considered. In addition, even if the pig cardiopulmonary system is close to that of human, ICU patients could have different responses to the $ECCO_2RT$. Therefore, the model has been only validated for pig

experiments and clinical studies have to be carried out in order to validate the model in the ICU. This aspect will be developed in Chapter 11.

Finally, this mathematical model is validated only for a specific ECLS, which is the Maquet ECCO$_2$RD (PALP®, Germany). Other and larger ECLS, such as venovenous extracorporeal membrane oxygenation (vv-ECMO), should also be considered. In particular, it is worth mentioning that larger ECLS are also used to oxygenate blood and this chapter does not consider this possibility.

9.5 Summary

The mathematical model of the respiratory system connected to a vv-ECLS has several subject-specific parameters. These parameters have been estimated with experimental data and their values are close to the values that can be observed in real patients. When all the parameters are identified before the ECCO$_2$RT, the mathematical model can correctly simulate the decrease in PCO_2 during the ECCO$_2$RT.

To validate the mathematical model, the PCO_2 predictions are compared with experimental results obtained in pigs. First the ECLS model has been tested alone and the model Mod1 (the most complexed one) have shown the best results. Consequently, this model was used for all the simulations of the respiratory system connected to a vv-ECLS. The results show that these simulations are able to reproduce experimental data for quite long periods of time (up to about 150 minutes for *experiments H* and up to about 60 minutes for *experiments A*) and until the stabilization of the respiratory system is reached. The quite good agreement between the theoretical approach and animal data can thus be considered as a strong argument proving the validity of our model.

Furthermore, the adaptations of the mathematical model to be used in the ICU are also discussed and analyzed. The results show that the mathematical model without the transport delays should be preferred since the computation time is smaller and the errors between the measurements and the simulations are approximatively the same. In the ICU, various measurements are not always taken and different parameters cannot be estimated. For the cardiac output, this chapter demonstrates that a weight-based approximation could be used. On the other hand, a weight approximation for the parameters MR_{CO_2} and MR_{O_2} should be avoided.

Part V

Application in the intensive care unit

To prepare the use of the mathematical model in the ICU, the validation with pig experiments is not sufficient and the model must also be tested and validated in the ICU. Even if the animal experiments were performed with the aim to be similar to clinical applications, the measuring instruments available in the ICU and the clinical environment are quite different from the experiments: less data are estimated and all the surgical operations are safer (less invasive and strict sterility conditions). Moreover, the cardiopulmonary pathologies simulated for the animals experiments try to simulate the pathologies that are really observed on patients but these simulations can significantly differ from those really observed in clinic. Finally, the results can also diverge because the behavior and response of the human cardio-pulmonary system can be different from that of the pig.

In this last part of the thesis, two chapters are introduced. Chapters 10 and 11 respectively describe, discuss and analyze the results related to the clinical uses of va-ECLS and vv-ECLS.

Chapter 10

Application for patients assisted by a va-ECLS

This chapter describes the validation and potential applications of our mathematical model in the ICU. First, the current clinical protocol used to decide if a patient assisted by a va-ECLS can be weaned is presented in section 10.1. The final aim of the study is to couple our mathematical model with this weaning protocol in order to improve the therapeutic approach in the ICU. Therefore, this chapter analyzes clinical data from several patients to validate the mathematical model for ICU applications. The main features of each studied patient are described in section 10.2. With the clinical data of these patients, the values of the parameters of the model can be estimated and are given in section 10.3. After the parameter identification, the model can simulate different hemodynamic states of the cardiovascular system for different extracorporeal blood flows. The comparison between the simulated values and the clinical data is described in section 10.4. Afterwards, the discussion of the different results is developed in section 10.5 and the limitations of the mathematical model are described in section 10.6. Finally, the last section summarizes the results of this chapter.

10.1 Clinical weaning criteria from va-ECLS

If a patient under a va-ECLS recovers from its major metabolic disturbance (such as septic shocks), has a pulsatile arterial waveform for at least 24 hours and has a mean arterial pressure larger than 60 mmHg with low doses of catecholamine (noradrenaline $< 5\mu$g/min and dobutamine $< 10\mu$g/min [77]), clinicians can proceed to a weaning test [4]. The weaning test consists in gradually decreasing the extracorporeal blood flow and checking the following parameters when the extracorporeal blood flow is decreased to approximately $0.5-1$ l/min [4]:

- VTI $>$ 12 cm (this symbol has been defined in section 6.2, p. 88),
- left ventricular ejection fraction (described in our model by $SV/\max_{\mathrm{T}}(V_h)) > 20{-}25$ %,
- mean arterial blood pressure ($\overline{P}_a$) $>$ 60 mmHg.

In addition to these weaning criteria, the pulmonary function should not be severely impaired: if PaO2/FiO2 <100 mmHg when F_{I,O_2} of the ECLS gas flow is set at 21 %, bridging the patient from va- to vv-ECLS should be considered [4].

If all these criteria are respected, the medical team can consider removing the ECLS.

10.2 Clinical trial

With the aim to validate the model in the ICU, clinical data are taken from 6 patients (labeled Patient1 to Patient6) assisted by a va-ECLS. These patients suffer from distinct heart pathologies and a patient-specific care is administered to each of them. For each patient, one or two weaning tests were carried out and their main characteristics are described in Table 10.1. Each weaning test was performed by decreasing progressively the extracorporeal blood flow (Q_d) to different values. For each extracorporeal blood flow, the essential hemodynamic parameters were recorded (diastolic and systolic blood pressure in the arteries, mean central venous pressure, VTI, ϕ_{LVOT} and the diastolic volume, see section 6.2, p. 88). Except for the second weaning test performed on Patient2, each weaning test will be analyzed in this chapter. For the second weaning test performed on Patient2, the parameter identification is impossible with our method since Q_d was directly decreased to 0.5 l/min.

Table 10.1 shows that, except for Patient6, the last weaning test for each patient was conclusive and the va-ECLS was switched off. Unfortunately, 3 of these patients died after the ECLS removal. For Patient6, a high dose of catecholamine was administered in order to increase the arterial pressure ($\overline{P}_a > 60$ mmHg) and this injection should have prevented the weaning of va-ECLS. However, the arterial hypotention of the patient was due to an hepatic dysfunction and not to a cardiovascular dysfunction.

Table 10.1 – Main characteristics of the 6 patients assisted by a va-ECLS. The abbreviations *Nb. of days* and *Noradre.* respectively mean the number of days after the va-ECLS was switched on and the quantity of injected noradrenaline.

	Reason for admission	**First weaning test**			**Second weaning test**			**Clinical outcomes**
		Nb. of days	Noradre. (μg/min)	Q_d (l/min)	Nb. of days	Noradre. (μg/min)	Q_d (l/min)	
Patient1	After the replacement of the aortic and mitral valves, the patient developed an infective endocarditis	13	9.3	5 → 3 → 2 → 1	/			The weaning test was conclusive (except for the noradrenaline injection, which was a little bit higher than the maximum dose: > 5 μg/min) → va-ECLS was switched off. But the patient died 3 days later.
Patient2	Cardiorespiratory arrest probably due to an unknown ischemic heart disease.	11	0	3.1 → 2 → 1 → 0.5	16	0	5→ 0.5	1st weaning test was not conclusive (VTI < 12) but 2nd weaning test was conclusive → va-ECLS was switched off and the patient survived.
Patient3	Cardiogenic shock due to atrial tachycardia.	7	0	3.3 → 2 → 1.5 → 1	/			The weaning test was conclusive → va-ECLS was switched off and the patient survived.
Patient4	Cardiogenic shock due to a myocardial infarction	10	0	2.4 → 2 → 1 → 0.5 → 0	11	0	2.3 → 1.5 → 1 → 0.5	Both weaning tests were conclusive → va-ECLS was switched off. But the patient died one day later, probably due to a septic shock that happened during the removal of the cannulae.
Patient5	After the replacement of the aortic valve, the patient developed an acute dysfunction of the left ventricle.	5	0	2.85 → 2.05 → 1 → 0.5	9	2.7	3.3 → 2 → 1 → 0.5	Both weaning tests were conclusive → va-ECLS was switched off 2 days later. But, the patient died 4 days after the removal of the ECLS.
Patient6	After the replacement of the tricuspid valve, the patient developed an acute dysfunction of the right ventricle.	1	133!	4.67 → 3.67 → 2.7 → 1.5 → 1.2 → 0.3	/			The high dose of noradrenaline should have prevented the weaning of va-ECLS but the arterial hypotension of the patient was due to an hepatic dysfunction and not to a cardiovascular dysfunction. The weaning test showed a recovery of the right ventricle function and the va-ECLS was switched off 2 days later. The patient survived and followed a dialysis treatment.

10.3 Value of the parameters

The parameters of the model are estimated with the procedure described in subsection 8.1.2 of Chapter 8. The heart rate (HR) and the extracorporeal blood flow (Q_d) are directly measured and the values of HR in terms of Q_d are presented in Figure 10.1 for each weaning test. For Patient4 and Patient5, 2 weaning tests (labeled T1 and T2 respectively) were carried out. Other patients had only one weaning test which is labeled T1. Remember that the experimental data depicted by crosses are used for the identification while the experimental data depicted by diamonds are used for testing the predictions of the mathematical model (see section 8.1). The values of HR represented by diamonds are thus not used as input data and, in evaluating the prediction of the mathematical model, HR is estimated using equation 8.1 from section 8.1. The 2 coefficients of the linear development of HR in terms of Q_d are given, for each weaning test, in Table 10.2. Except for the weaning test Patient1 T1, Figure 10.1 and Table 10.2 demonstrate that HR increases with the decrease in Q_d.

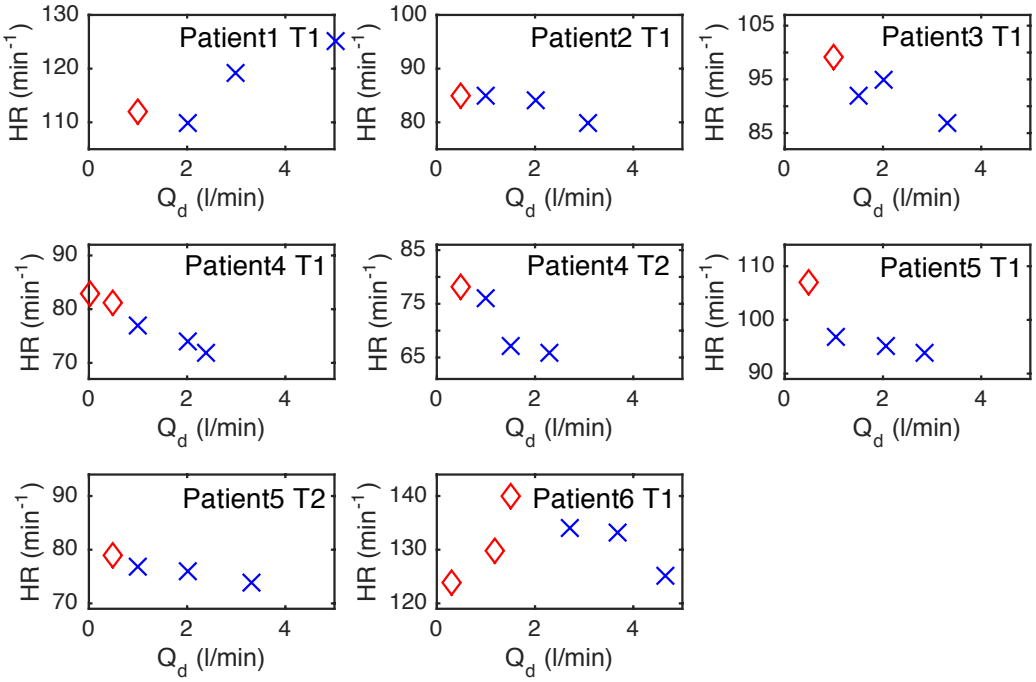

Figure 10.1 – Heart rate in terms of Q_d for the different weaning tests. The crosses correspond to the experimental data used for the parameter identification and the diamonds correspond to the experimental data used for testing the predictions of the mathematical model.

As in Chapter 8, the values of the 10 coefficients, defining the linear dependence of the 5 parameters with respect to Q_d, are determined by the method presented in section 6.2 and using $n = 3$. Their values are provided in Table 10.2 for each weaning test. Note

Table 10.2 – Values of the 2 coefficients of the linear expressions for each parameter (E_h, SBV, A_h, E_a and R_s) and the two coefficients of the linear expression of HR.

	Patient1	Patient2	Patient3	Patient4		Patient5		Patient6	
Data	T1	T1	T1	T1	T2	T1	T2	T1	**Mean** $\pm \sigma$
Parameter identification									
$E_{0,h}$ (mmHg/ml)	2.81	1.74	1.01	0.90	0.97	1.93	1.93	3.58	**1.86** $\pm$ 0.95
SBV_0 (ml)	1159	410	789	1026	820	1108	1276	1305	**987** $\pm$ 300
$A_{0,h}$ (ml^{-1})	0.050	0.022	0.016	0.025	0.022	0.036	0.034	0.051	**0.032** $\pm$ 0.013
$E_{0,a}$ (mmHg/ml)	2.03	0.93	1.30	1.12	1.44	1.49	1.96	1.20	**1.43** $\pm$ 0.39
$R_{0,s}$ (mmHg $\cdot$ s/ml)	1.20	1.29	0.63	0.82	0.83	0.76	0.79	0.35	**0.84** $\pm$ 0.30
$E_{Sl,h}$ (mmHg $\cdot$ s/ml^2)	-0.011	0.002	0.002	0.000	-0.005	-0.003	-0.003	-0.014	**-0.004** $\pm$ 0.006
SBV_{Sl} (s)	-3.97	3.50	-2.61	-2.25	0.92	-7.09	-3.62	-6.78	**-2.74** $\pm$ 3.59
$A_{Sl,h}$ (s/ml^2)	-7·e-5	2·e-4	-4·e-5	-7·e-5	-8·e-5	-1·e-4	-6·e-5	-1·e-4	**-5·e-5** $\pm$ 1·e-4
$E_{Sl,a}$ (mmHg $\cdot$ s/ml^2)	-0.003	0.044	0.007	0.004	-0.003	0.019	0.004	0.014	**0.011** $\pm$ 0.015
$R_{Sl,s}$ (mmHg $\cdot$ s^2/ml^2)	-0.007	-0.008	-0.001	-0.004	-0.004	0.004	-0.003	0.000	**-0.003** $\pm$ 0.004
Heart rate estimation									
HR_0 (s^{-1})	1.70	1.46	1.65	1.34	1.35	1.64	1.31	2.46	**1.62** $\pm$ 0.37
HR_{Sl} (ml^{-1})	0.005	-0.002	-0.003	-0.003	-0.007	-0.002	-0.001	-0.005	**-0.002** $\pm$ 0.003

that, like in the pig experiments, the values of the independent terms in equation 6.4 are of the same order of magnitude for the different weaning tests but the values of the slopes in equation 6.4 are different for the different patients.

For the identification of the 10 coefficients, the differences between experimental data (crosses in the different figures) and the simulated values of $\overline{P}_a$, PP_a, $\overline{P}_v$, $\max_{\mathrm{T}}(V_h)$ and SV are minimized. The corresponding relative errors, $\overline{\Delta\overline{P}_a/\overline{P}_a}$, $\overline{\Delta PP_a/PP_a}$, $\overline{\Delta\overline{P}_v/\overline{P}_v}$, $\overline{\Delta\max_{\mathrm{T}}(V_h)/\max_{\mathrm{T}}(V_h)}$ and $\overline{\Delta SV/SV}$, with and without the absolute values (these symbols have already been introduced in section 8.1), are given in Table 10.3. In addition, the relative errors of the ejection fraction (EF) and VTI are also given in this table. Indeed, these quantities are of paramount importance in the ICU since their values determine the decision of weaning a va-ECLS. VTI is directly proportional to SV and the proportional factor is the area of the left ventricular outflow tract (equation 6.2). Since

Table 10.3 – Errors between the simulations and the measurements of $\overline{P}_a$, PP_a, $\overline{P}_v$, $\max_{\mathrm{T}}(V_h)$, SV, VTI and EF during the parameter identification phase.

	Patient1	Patient2	Patient3	Patient4		Patient5		Patient6	
Data	T1	T1	T1	T1	T2	T1	T2	T1	**Mean** $\pm\ \sigma$
$\Psi(\mathbf{p}^*)$	548	117	262	106	25	371	112	374	**239** $\pm$ 180
$\overline{\lvert\Delta PP_a/PP_a\rvert}$	0.034	0.020	0.017	0.002	0.009	0.028	0.007	0.037	**0.019** $\pm$ 0.013
$\overline{\lvert\Delta\overline{P}_a/\overline{P}_a\rvert}$	0.040	0.007	0.030	0.023	0.005	0.017	0.005	0.025	**0.019** $\pm$ 0.013
$\overline{\lvert\Delta\overline{P}_v/\overline{P}_v\rvert}$	0.032	0.076	0.024	0.034	0.012	0.054	0.015	0.065	**0.039** $\pm$ 0.024
$\overline{\left\lvert\frac{\Delta\max_{\mathrm{T}}(V_h)}{\max_{\mathrm{T}}(V_h)}\right\rvert}$	0.004	0.009	0.003	0.001	0.009	0.069	0.045	0.006	**0.018** $\pm$ 0.025
$\overline{\lvert\Delta SV/SV\rvert}$ or $\overline{\lvert\Delta VTI/VTI\rvert}$	0.018	0.018	0.010	0.022	0.021	0.052	0.004	0.010	**0.019** $\pm$ 0.015
$\overline{\lvert\Delta EF/EF\rvert}$	0.019	0.017	0.007	0.023	0.029	0.127	0.044	0.009	**0.034** $\pm$ 0.039
$\overline{\Delta PP_a/PP_a}$	0.010	0.020	0.001	0.000	0.002	0.016	0.007	0.014	**0.009** $\pm$ 0.008
$\overline{\Delta\overline{P}_a/\overline{P}_a}$	0.005	-0.002	0.001	0.000	0.001	0.005	0.005	0.005	**0.002** $\pm$ 0.003
$\overline{\Delta\overline{P}_v/\overline{P}_v}$	0.016	0.023	0.019	0.017	0.012	0.019	0.015	0.019	**0.018** $\pm$ 0.003
$\overline{\frac{\Delta\max_{\mathrm{T}}(V_h)}{\max_{\mathrm{T}}(V_h)}}$	0.004	0.009	0.001	0.000	0.002	-0.004	0.004	0.006	**0.003** $\pm$ 0.004
$\overline{\Delta SV/SV}$ or $\overline{\Delta VTI/VTI}$	0.000	0.018	-0.003	-0.006	-0.003	0.008	0.004	0.006	**0.003** $\pm$ 0.008
$\overline{\Delta EF/EF}$	-0.004	0.000	-0.004	-0.007	-0.005	0.023	0.002	0.000	**0.001** $\pm$ 0.009

the experimental value of ϕ_{LVOT} is used as an input data for the parameter identification, $\overline{\Delta SV/SV} = \overline{\Delta VTI/VTI}$. Table 10.3 shows that the errors between the measurements and the corresponding values are small: for all the weaning tests, the means $\overline{|\Delta \overline{P}_a/\overline{P}_a|}$, $\overline{|\Delta PP_a/PP_a|}$, $\overline{|\Delta \max_{\mathrm{T}}(V_h)/\max_{\mathrm{T}}(V_h)|}$ and $\overline{|\Delta SV/SV|}$ ($= \overline{|\Delta VTI/VTI|}$) are all smaller than 2 % and the means $\overline{|\Delta \overline{P}_v/\overline{P}_v|}$ and $\overline{|\Delta EF/EF|}$ are both smaller than 4 %. Table 10.3 also shows that the simulated $\overline{P}_v$ and PP_a overestimate the corresponding clinical data ($\overline{\Delta \overline{P}_v/\overline{P}_v} = 1.8$ % and $\overline{\Delta PP_a/PP_a} = 0.9$ %) while there is no global overestimation or underestimation for the other quantities.

10.4 Predicted and clinical values during weaning tests

After estimating all the parameters of the mathematical model, this model can be used to simulate the cardiovascular system during weaning tests and these simulations can be compared to available clinical data taken during these tests.

Figure 10.2, Figure 10.3 and Figure 10.4 represent the evolution of simulated and clinical hemodynamic variables for all the weaning tests. The simulated values are depicted by solid lines while experimental data are depicted by crosses and diamonds (as already mentioned, the experimental data depicted by crosses are used for the parameter identification while the experimental data depicted by diamonds are used to validate the mathematical model). The simulations and the clinical data demonstrate that all the hemodynamic criteria to wean a va-ECLS are respected for the weaning test Patient1 T1, Patient 3 T1, Patient 4 T2, Patient5 T1 and Patient5 T2. After these weaning tests, the ECLS was actually switched off. For the weaning test Patient2 T1 (Figure 10.2), VTI obtained with the mathematical model and measured in the ICU are both smaller than 12 cm. The ECLS was thus not switched off after this weaning test. For the weaning test Patient4 T1 (Figure 10.3), the clinical value of VTI is close to 12 cm for $Q_d = 0.5$ l/min. In addition, it is worth mentioning that VTI decreases with the decrease in Q_d while the other weaning tests show an apposite trend. This weaning test was thus not totally conclusive and a second weaning test was carried out the next day. Finally, for the weaning test Patient6 T1 (Figure 10.4), $\overline{P}_a$ obtained with the mathematical model and measured in the ICU are both smaller than 60 mmHg even if a high dose of noradrenaline was administered. However, the ECLS was switched off because the arterial hypotention was due to a hepatic dysfunction and not a cardiovascular dysfunction.

These figures also show that the agreement between the simulations and crosses is good and this fact has already been discussed in section 10.3. The difference between the diamonds and the simulations are a bit larger and the quantitative values of these errors

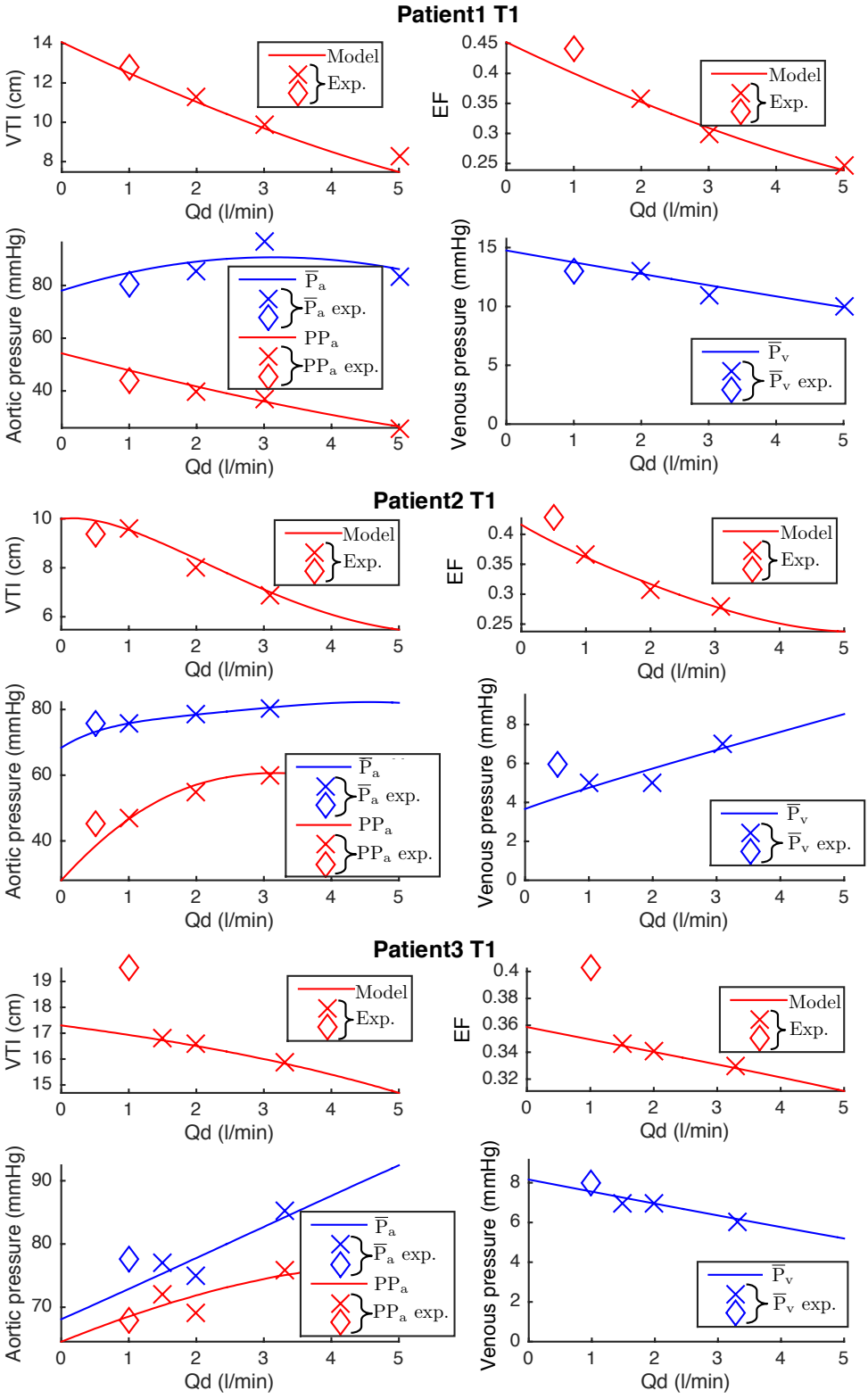

Figure 10.2 – Evolution of $\overline{P}_a$, PP_a, $\overline{P}_v$, $\max_T(V_h)$ and SV in terms of different Q_d for the 3 weaning tests Patient1 T1, Patient2 T1 and Patient3 T1. The solid lines are the simulations and the crosses and diamonds are the experimental data (the difference between diamonds and crosses has already been explained in Figure 10.1).

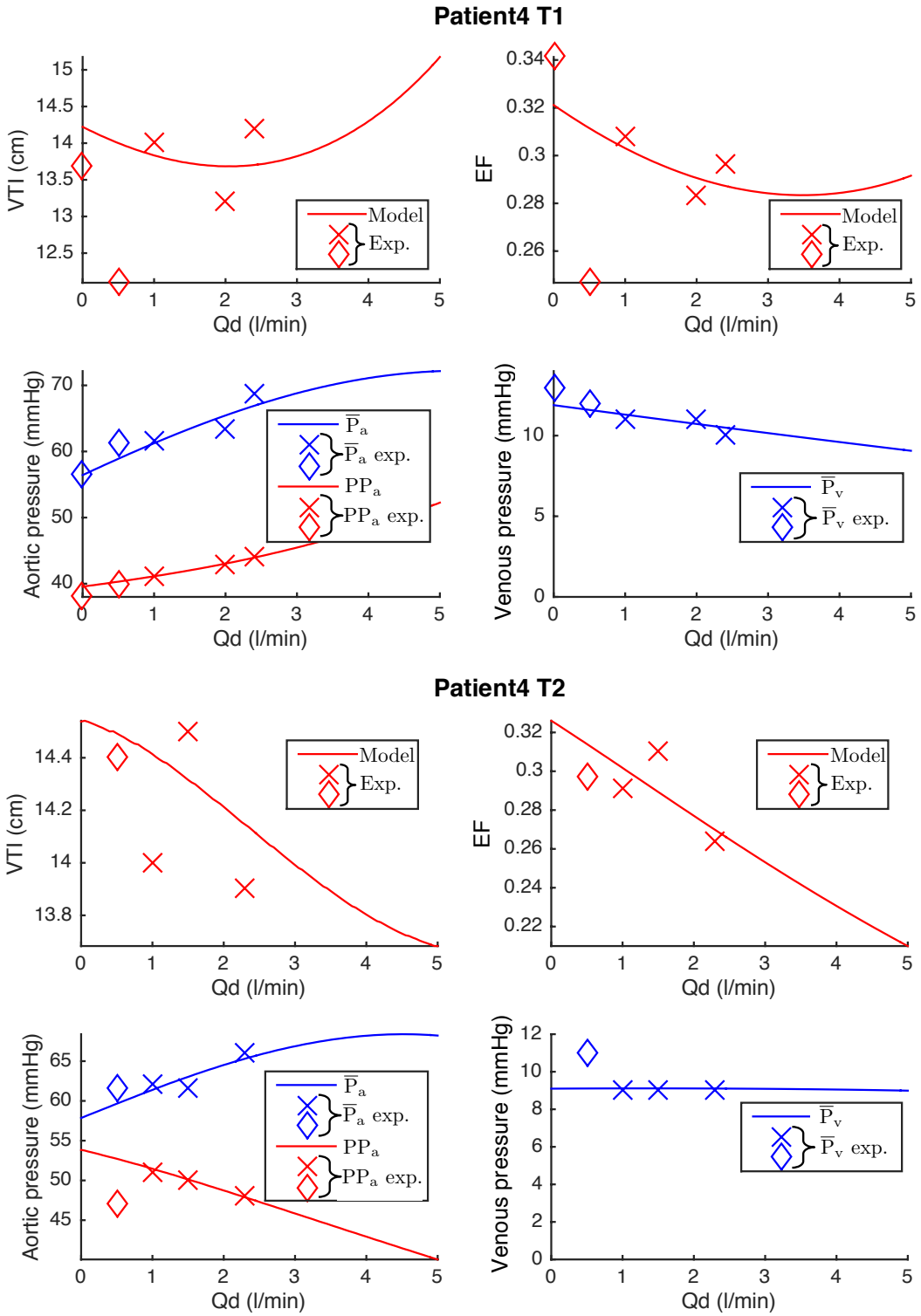

Figure 10.3 – Evolution of $\overline{P}_a$, PP_a, $\overline{P}_v$, $\max_T(V_h)$ and SV in terms of different Q_d for the 2 weaning tests Patient4 T1 and Patient4 T2. The solid lines are the simulations and the crosses and diamonds are the experimental data (the difference between diamonds and crosses has already been explained in Figure 10.1).

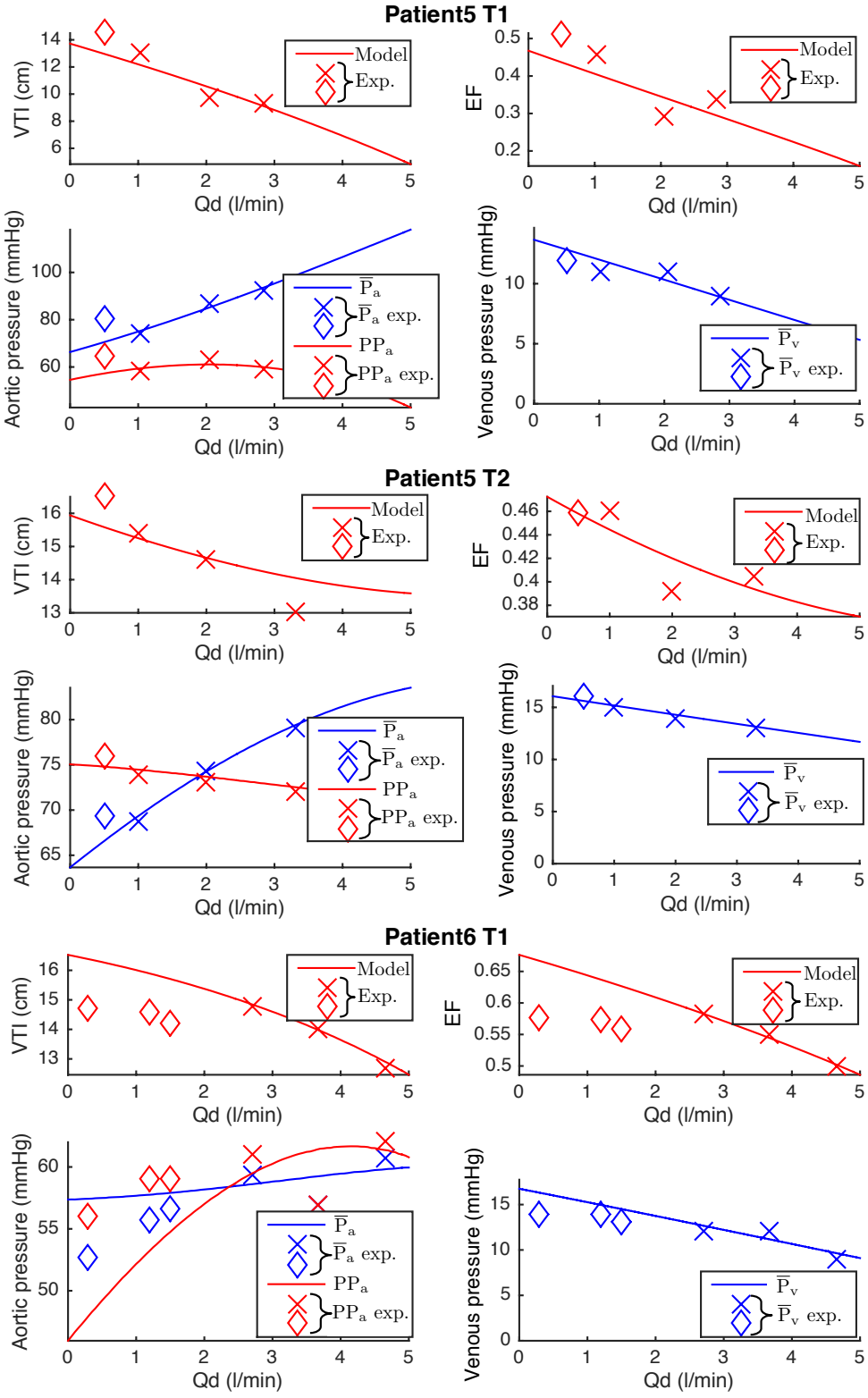

Figure 10.4 – Evolution of $\overline{P}_a$, PP_a, $\overline{P}_v$, $\max_T(V_h)$ and SV in terms of different Q_d for the 3 weaning tests Patient5 T1, Patient5 T2 and Patient6 T1. The solid lines are the simulations and the crosses and diamonds are the experimental data (the difference between diamonds and crosses has already been explained in Figure 10.1).

are given in Table 10.4. The relative errors $\Delta\max_{\mathrm{T}}(V_h)/\max_{\mathrm{T}}(V_h)$ and $\Delta SV/SV$ are also provided in this table. Note that in this case, $\Delta SV/SV \neq \Delta VTI/VTI$ since, in testing the prediction of the model, the values of experimental ϕ_{LVOT} are not used as input data. To estimate the values of ϕ_{LVOT}, the assumption of a constant value for the different Q_d is taken and the estimated value is equal to the mean of the 3 experimental values used during the parameter identification phase (crosses)[1]. Table 10.4 shows that the errors are small (the mean errors of $\overline{P}_a$, $\max_{\mathrm{T}}(V_h)$, SV and VTI are all smaller than 7 % and the mean errors of PP_a, $\overline{P}_v$ and EF are all smaller than 10 %).

10.5 Discussion

This section discusses the values of the different coefficients estimated in the previous section and compares these values with the values obtained in the pig experiments (see Chapter 8). Indeed, this comparison can be considered since the pig's cardiovascular system is rather similar than the human's cardiovascular system and the literature has provided similar parameter values ([86, 105, 18]). In addition, this section discusses the ability of our model to predict the essential hemodynamic quantities during weaning tests.

10.5.1 Values of the parameters for $Q_d = 0$

Table 10.2 has shown that the coefficient $E_{0,h}$, which correspond to the value of parameter E_h for $Q_d = 0$, has larger values than those obtained with the pig experiments during ECLST (Table 8.7). This result makes sense since the weaning tests are carried on patients only when they have almost recovered a healthy cardiac activity while the weaning tests are carried out only a few minutes after the cardiac arrest for the pig experiments. However, the values shown in Table 10.2 are smaller than those presented in the literature for a healthy adult ($E_h = 3$ mmHg/ml [18]). This difference can be explained by the fact that the studied patients have not yet fully recovered a normal cardio-vascular activity. Another important parameter is the systemic resistance R_s and Table 10.2 shows that the values of $R_{0,s}$, which correspond to the values of parameter R_s for $Q_d = 0$, are smaller than those obtained with the pig experiments during ECLST (Table 8.7). However, these values are of the same order of magnitude than those found in literature for a healthy adult ($R_s = 0.95$ mmHg $\cdot$ s/ml [18]). The values of the other coefficients indexed with "0" are similar to those obtained with the pig experiments (during baseline situation and ECLST, see Table 8.7).

[1]The accuracy of ϕ_{LVOT} and the variation of ϕ_{LVOT} with Q_d are too small to be estimated

Table 10.4 – Errors between the predictions of the mathematical model and the measurements of $\overline{P}_a$, PP_a, $\overline{P}_v$, $\max_{\mathrm{T}}(V_h)$, SV, EF and VTI.

	Patient1	Patient2	Patient3	Patient4		Patient5		Patient6	
Data	T1	T1	T1	T1	T2	T1	T2	T1	**Mean** $\pm\ \sigma$
$\overline{\lvert\Delta PP_a/PP_a\rvert}$	0.085	0.148	0.007	0.023	0.121	0.098	0.016	0.105	**0.075** $\pm$ 0.053
$\overline{\lvert\Delta\overline{P}_a/\overline{P}_a\rvert}$	0.052	0.037	0.061	0.022	0.032	0.118	0.039	0.050	**0.051** $\pm$ 0.030
$\overline{\lvert\Delta\overline{P}_v/\overline{P}_v\rvert}$	0.058	0.295	0.056	0.060	0.172	0.003	0.024	0.116	**0.098** $\pm$ 0.096
$\overline{\left\lvert\frac{\Delta\max_{\mathrm{T}}(V_h)}{\max_{\mathrm{T}}(V_h)}\right\rvert}$	0.002	0.137	0.001	0.094	0.036	0.152	0.022	0.024	**0.058** $\pm$ 0.060
$\overline{\lvert\Delta SV/SV\rvert}$	0.089	0.045	0.130	0.098	0.018	0.044	0.023	0.103	**0.069** $\pm$ 0.042
$\overline{\lvert\Delta EF/EF\rvert}$	0.091	0.081	0.131	0.161	0.056	0.093	0.001	0.130	**0.093** $\pm$ 0.050
$\overline{\Delta VTI/VTI}$	0.024	0.060	0.131	0.098	0.006	0.048	0.056	0.103	**0.066** $\pm$ 0.042
$\overline{\Delta PP_a/PP_a}$	0.085	-0.148	0.007	0.023	0.121	-0.098	-0.016	-0.105	**-0.016** $\pm$ 0.095
$\overline{\Delta\overline{P}_a/\overline{P}_a}$	0.052	-0.037	-0.061	-0.022	-0.032	-0.118	-0.039	0.050	**-0.026** $\pm$ 0.056
$\overline{\Delta\overline{P}_v/\overline{P}_v}$	0.058	-0.295	-0.056	-0.060	-0.172	0.003	-0.024	0.116	**-0.054** $\pm$ 0.130
$\overline{\frac{\Delta\max_{\mathrm{T}}(V_h)}{\max_{\mathrm{T}}(V_h)}}$	0.002	0.137	0.001	0.011	-0.036	0.152	-0.022	-0.024	**0.028** $\pm$ 0.074
$\overline{\Delta SV/SV}$	-0.089	0.045	-0.130	0.098	0.018	0.044	-0.023	0.103	**0.008** $\pm$ 0.084
$\overline{\Delta EF/EF}$	-0.091	-0.081	-0.131	0.102	0.056	-0.093	-0.001	0.130	**-0.014** $\pm$ 0.100
$\overline{\Delta VTI/VTI}$	-0.024	0.060	-0.131	0.098	0.006	-0.048	-0.056	0.103	**0.001** $\pm$ 0.082
n	1	1	1	2	1	1	1	3	

10.5.2 Variation of the parameters with Q_d

Table 10.2 has provided the slopes of the parameters in terms of Q_d and these values allow us to analyze the variation of the different parameters with respect to Q_d. For parameter HR, this table and Figure 10.1 have shown that HR increases with the decrease in Q_d while the pig experiments have shown an opposite trend (Table 8.2). This difference can be explained by the fact that the heart of the patients partially recovered its normal activity. Their heart thus responds differently than the heart of the pigs, which were still in a pathological condition (see also discussion in subsection 8.4.2). For the other parameters, one calculates the relative variations of the 5 parameters for a change of Q_d equal to 3 l/min (similar relative variations have been calculated in subsection 8.4.2 but for a change of Q_d equal to 1 l/min, see equations 8.7). The symbols $\Delta_3 E_h/E_h$, $\Delta_3 SBV/SBV$, $\Delta_3 A_h/A_h$, $\Delta_3 E_a/E_a$ and $\Delta_3 R_s/R_s$ are introduced to respectively describe the relative variations of E_h, SBV, A_h, E_a and R_s. Remember that the 5 slopes have been identified with the measurements related to 3 different Q_d. These variations can be estimated with more experimental data (see section 8.3). Indeed, the 10 coefficients of the linear expression of the 5 parameters can also be identified using the measurements related to all the Q_d and the corresponding values of $\Delta_3 E_h/E_h$, $\Delta_3 SBV/SBV$, $\Delta_3 A_h/A_h$, $\Delta_3 E_a/E_a$ and $\Delta_3 R_s/R_s$ can also be estimated (the values of the 10 coefficients estimated with this approach are given in Table B.5 of Appendix B.3 and the errors obtained for this parameter identification are given in Table B.6 of Appendix B.3).

Figure 10.5 represents the values of $\Delta_3 E_h/E_h$, $\Delta_3 SBV/SBV$, $\Delta_3 A_h/A_h$, $\Delta_3 E_a/E_a$ and $\Delta_3 R_s/R_s$ for the different weaning tests obtained with the two parameter identifications (the parameter identification using only 3 Q_d is represented by the full bars while the parameter identification using all the Q_d is represented by the empty bars).

This figure demonstrates that the values of $\Delta_3 E_h/E_h$ are always negative for the parameter identification using all the Q_d. The patients thus show an opposite trend in comparison with the pig experiments. Indeed, for the clinical trials, the heart partially recovered its normal activity and thus responds differently than the heart of the pigs, which were still in a pathological condition. In addition, the increase in the heart contractility with the decrease in Q_d is in agreement with the literature. Indeed, several articles claim that the heart contractility increases with the increase in preload [65] (remember that the preload increase with the decrease in Q_d). Finally, note that the results for the parameter identification using 3 Q_d show a similar general trend but the values of $\Delta_3 E_h/E_h$ obtained with this method are rather different from those obtained with the parameter identification using all Q_d.

Except for the weaning test Patient2 T1, the values of $\Delta_3 SBV/SBV$ are always nega-

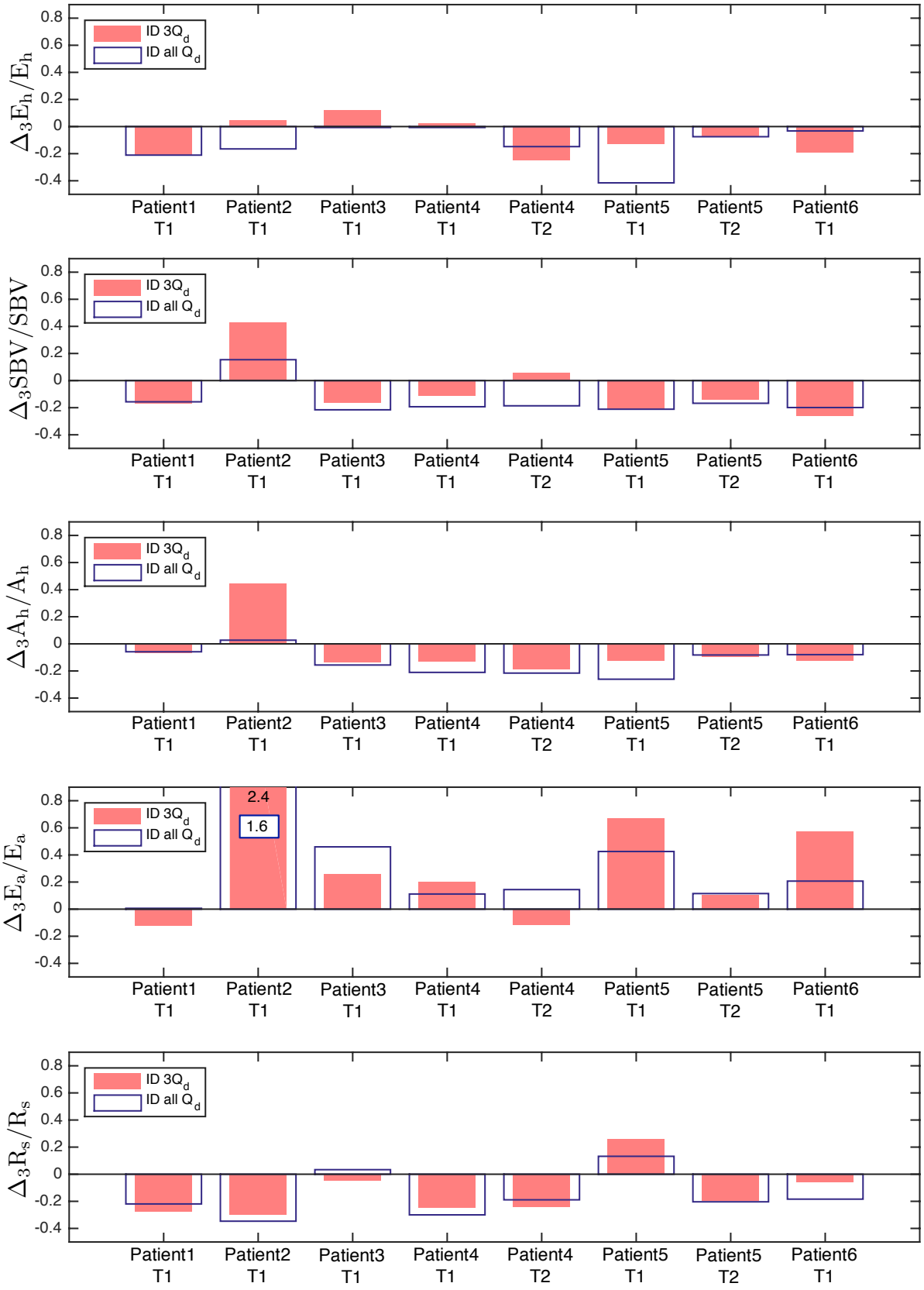

Figure 10.5 – Values of $\Delta_3 E_h/E_h$, $\Delta_3 SBV/SBV$, $\Delta_3 A_h/A_h$, $\Delta_3 E_a/E_a$ and $\Delta_3 R_s/R_s$ obtained with the parameter identification using the measurements related to 3 Q_d and with the parameter identification using the measurements related to all Q_d for each weaning test.

tive for the parameter identification using all Q_d (remember that for the pig experiments, $\Delta_1 SBV/SBV$ has not shown clear trend but their values were small). Except for Patient4 T2, the results for the parameter identification using 3 Q_d present similar values. The increase in SBV with the decrease in Q_d could result from the vasoconstriction of the small vessels and the increase in heart contractility when Q_d decreases.

Figure 10.5 also shows that, except for the weaning test Patient2 T1, the values of $\Delta_3 A_h/A_h$ are always negative for both parameter identifications (remember that for the pig experiments, $\Delta_1 A_h/A_h$ has not shown clear trend but their values were small). The increase in A_h with the decrease in Q_d could result from an inadequate description of EDPVR by equation 4.6 (see subsection 4.1.4, p. 57). Indeed, if Q_d decreases, the preload and afterload of the heart change (the preload increases and the afterload decreases) and the values of pressure and volume in the heart also vary.

While the values of $\Delta_1 E_a/E_a$ have not shown clear trend for the pig experiments, Figure 10.5 shows that the values of $\Delta_3 E_a/E_a$ are always positive for the parameter identification using all Q_d. Except for the weaning tests Patient1 T1 and Patient4 T2, the results for the parameter identification using 3 Q_d present similar trends. The decrease in E_a with the decrease in Q_d can be explained as follows. The assumption of a linear relationship between the pressure and the volume was taken for the passive element of the cardiovascular system whereas, in reality, the pressure volume relationship has a convex shape. Figure 10.6 illustrates this pressure volume relationship and this figure shows that the slope of the curve decreases when the pressure decreases. If Q_d decreases from $Q_{d,1}$ to $Q_{d,2}$, the hemodynamic in the arteries changes; the pressures and the volumes in the arteries decreases and the slope of the curve decreases from $E_a(Q_{d,1})$ to $E_a(Q_{d,2})$.

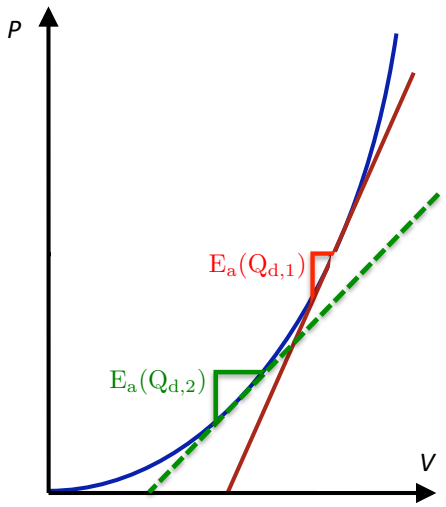

Figure 10.6 – Pressure volume relationship in the cardiovascular system for the passive elements.

Finally, Figure 10.5 shows that, as it was the case for the pig experiments, the values of $\Delta_3 R_s/R_s$ are always negative for the parameter identification using 3 Q_d (the values obtained with parameter identification using all the Q_d are rather similar). As previously mentioned in subsection 8.4.2, a possible physiological interpretation could be explained by the baroreflex.

10.5.3 Prediction of the mathematical model

Table 10.4 has shown small prediction errors (all the relative errors are smaller than 10 %) but the estimated values of $\overline{|\Delta\overline{P}_a/\overline{P}_a|}$, $\overline{|\Delta\overline{P}_v/\overline{P}_v|}$ and $\overline{|\Delta\mathrm{max_T}(V_h)/\mathrm{max_T}(V_h)|}$ are larger than those obtained with the pig experiments. The larger error on $\mathrm{max_T}(V_h)$ could be due to a worse accuracy with the estimation of this volume by echocardiography. Indeed, with this method, the clinician has to measure a specific 2D dimension with the electrocardiograph and the volume is calculated by assuming that the heart is spherical [98]. The larger error on $\overline{P}_a$ and $\overline{P}_v$ could be explained by the fact that the breathing of the patient interferes with the blood pressure signals. Indeed, for the pig experiments, the ventilator was disconnected to remove the effects of breathing on the cardiovascular system while this disconnection is, of course, not imposed to the ICU patients. Figure 10.7 illustrates the time evolution of left ventricle volume, arterial pressure and venous pressure before and after switching off the ventilator for Pig8. This figure shows that the systolic and diastolic blood pressures in the arteries are affected by breathing and that the venous pressure is actually greatly impacted by breathing. This effect could explain the large error on $\overline{P}_v$ ($\overline{|\Delta\overline{P}_v/\overline{P}_v|} = 9.8$ %) for the clinical trial.

As already mentioned in subsection 8.4.3 of Chapter 8, another important information is to check that the model allows a better prediction of the physiologically relevant quantities than a simple interpolation from previous measurements. The quantitative errors for the predictions obtained with the interpolations can be estimated with the same method as the prediction errors obtained with the mathematical model. Table 10.5 compares the mean relative errors obtained using the mathematical model with the corresponding errors obtained with the interpolations. This table shows the same general results as the pig experiments: the predicted values of $\overline{P}_a$, $\overline{P}_v$ and SV are a little better with the model than with the interpolations but the predicted values of PP_a is a little worse with the model than with the interpolations. As far as the values of SV and $\overline{P}_a$, which are of paramount importance to check the patient recovery, are concerned, the values obtained with the mathematical model present relative errors 15 % smaller than those obtained with the interpolation. This result shows the interest of our modeling approach.

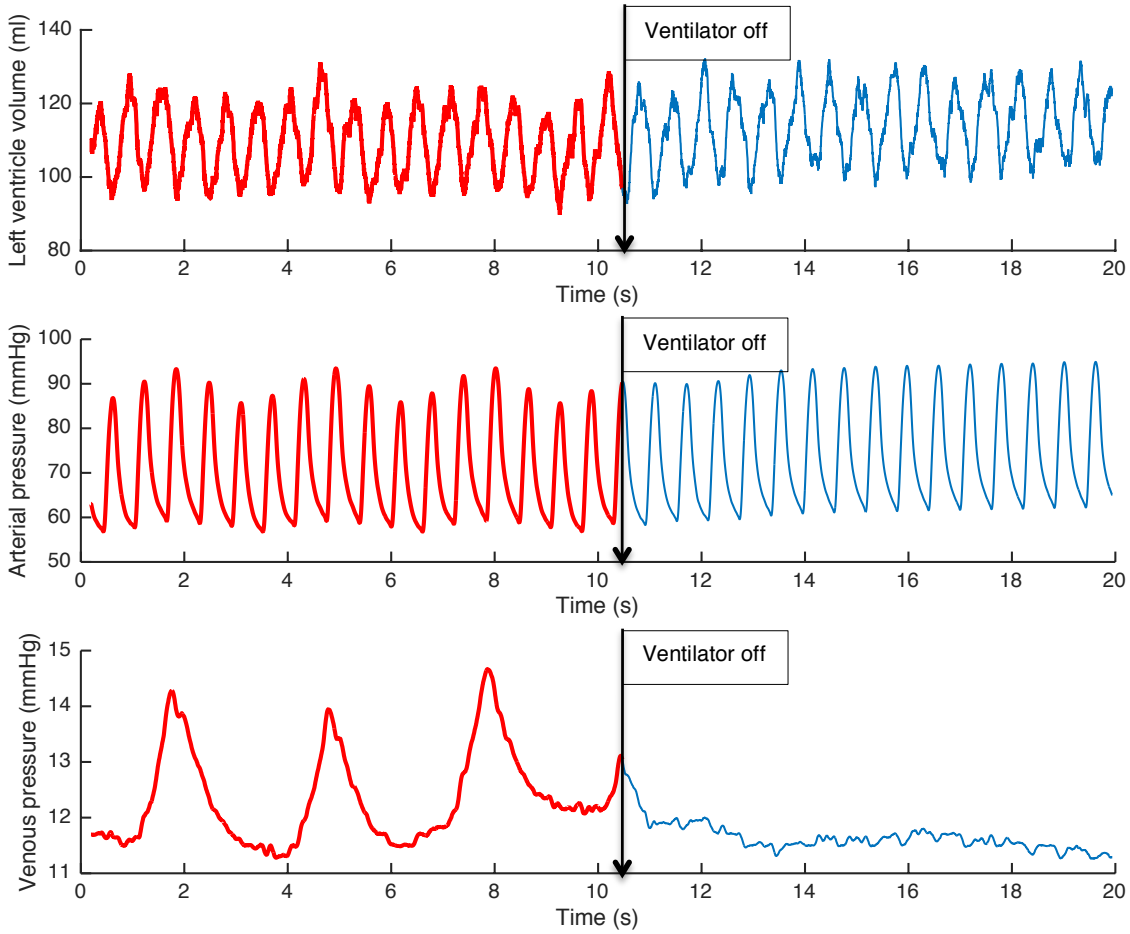

Figure 10.7 – Time evolution of left ventricle volume, arterial pressure and venous pressure before and after switching off the ventilator (these experimental data are taken from Pig8).

10.6 Limitations

As already mentioned in Chapter 8, several assumptions were introduced to build the mathematical model of the cardiovascular system connected to a va-ECLS. A limiting hypothesis is the absence of a description of the cardio-pulmonary controls. For the clinical trials, another rough hypothesis is that the values of R_i and R_o, describing the resistance of the input and output valves, are not patient-specific and are taken from literature. Indeed, some of our patients (Patient1, Patient5 and Patient6) had a replacement of one or two cardiac valves and the mechanical features of these synthetic valves are certainly different from real cardiac valves.

Even if the arterial and venous blood pressures are measured continuously in the ICU, it is impossible, with the current technology used in the CHU of Liège, to extract and record the complete time evolution of the data. The medical team thus records the hemo-

Table 10.5 – Comparison between the prediction errors obtained with the mathematical model and the prediction errors obtained with the interpolations of the measurements.

Global errors	Mathematical model	Interpolation
$\overline{\lvert\Delta PP_a/PP_a\rvert}$	0.075 ± 0.053	0.039 ± 0.040
$\overline{\lvert\Delta \overline{P}_a/\overline{P}_a\rvert}$	0.051 ± 0.030	0.060 ± 0.049
$\overline{\lvert\Delta \overline{P}_v/\overline{P}_v\rvert}$	0.098 ± 0.096	0.103 ± 0.096
$\overline{\left\lvert\frac{\Delta \max_{\mathrm{T}}(V_h)}{\max_{\mathrm{T}}(V_h)}\right\rvert}$	0.058 ± 0.060	0.064 ± 0.075
$\overline{\lvert\Delta SV/SV\rvert}$	0.069 ± 0.042	0.081 ± 0.050
$\overline{\lvert\Delta EF/EF\rvert}$	0.093 ± 0.050	0.102 ± 0.052
$\overline{\lvert\Delta VTI/VTI\rvert}$	0.066 ± 0.042	0.073 ± 0.047
$\overline{\Delta PP_a/PP_a}$	-0.016 ± 0.095	0.006 ± 0.057
$\overline{\Delta \overline{P}_a/\overline{P}_a}$	-0.026 ± 0.056	-0.016 ± 0.079
$\overline{\Delta \overline{P}_v/\overline{P}_v}$	-0.054 ± 0.130	-0.067 ± 0.127
$\overline{\frac{\Delta \max_{\mathrm{T}}(V_h)}{\max_{\mathrm{T}}(V_h)}}$	0.028 ± 0.074	0.035 ± 0.088
$\overline{\Delta SV/SV}$	0.008 ± 0.084	0.010 ± 0.099
$\overline{\Delta EF/EF}$	-0.014 ± 0.100	-0.018 ± 0.108
$\overline{\Delta VTI/VTI}$	0.001 ± 0.082	0.006 ± 0.091

dynamic data by hand and only one value of $\overline{P}_a$, PP_a and $\overline{P}_v$ are taken for each Q_d. It would be useful to investigate a solution in order to extract and record the complete blood pressure signal since the current method looses a large number of information.

Finally, the number of patients that were considered in our study is rather small and additional clinical trials should be carried out. Furthermore, the number of different Q_d for each weaning test is also small. The decrease in Q_d could be performed with more intermediate steps and more clinical data would be available with the aim of testing the predictions of the mathematical model.

10.7 Summary

In this chapter, the clinical application of the cardiovascular model connected to a va-ECLS has been presented. The current strategy to decide if a patient can be weaned from

va-ECLS has been described in section 10.1. It consists in estimating several hemodynamic parameters for a low value of extracorporeal blood flow ($Q_d \approx 0.5 - 1$ l/min). Our cardiovascular model could be helpful in predicting the hemodynamic parameters for this low value of Q_d. Indeed, with this approach, the clinicians would not need to decrease Q_d until this low value is reached.

To validate the prediction of weaning tests simulated by the mathematical model, the different parameters of the model have been estimated using clinical data corresponding to 3 different Q_d. These estimated parameters are thus patient-specific and their values have been discussed in subsection 10.5.1 and subsection 10.5.2. After the parameter identification, the mathematical model is used to simulate the weaning tests performed on patients and the simulated values are compared to the clinical data. The relative errors between the predictions obtained with mathematical model and the clinical data are rather small (all the relative errors are smaller than 10 %). Like in the pig experiments, the prediction errors of the mean arterial pressure and of the stroke volume obtained with the mathematical model are smaller than those obtained with the linear interpolations using the same measurements as the parameter identification.

Chapter 11

Application for patients assisted by a vv-ECLS

This chapter describes the methodology to validate our model of the respiratory system connected to a vv-ECLS with clinical data obtained in the CHU of Liège. The protocol of the studied clinical trials is described in section 11.1. Using the clinical data, the parameters corresponding to the baseline situation can be estimated with the procedure described in section 7.2. For the protective ventilation, the method is different and the procedure is described in section 11.2. The values of the identified parameters are given in section 11.3. Afterwards, the mathematical model of the respiratory model connected to a vv-ECLS can be used to simulate the system and the results are presented in section 11.4. Since the results of the experiments presented in Chapter 9 have shown that the ECLS model Mod1 is the best ECLS model and that transport delays do not improve the prediction of the respiratory model connected to a vv-ECLS, the ECLS model used in this chapter is Mod1 and the transport delays are neglected. As for the pig experiments, the main results consist in the time evolution of PCO_2 estimated by the mathematical model at several places in the body. Then, the results are discussed and analyzed in section 11.5 and the limitations of our model are drawn in section 11.6. Finally, section 11.7 summarizes the results of this chapter.

11.1 Clinical trials

As already mentioned in subsection 7.1.2, two sets of clinical trials are distinguished: *clinical trial S*, which refers to the European study *Supernova* [81], and *clinical trial R*, which refers to a retrospective study performed on patients assisted by a vv-ECLS in the CHU of Liège. *Clinical trials S* should be preferred to test our mathematical model since they follow a stringent protocol (the protocol has already been described in subsection 7.1.2) and

more clinical data are available. Unfortunately, only one patient (S1) has been recruited in *clinical trial S* at the CHU of Liège. Four patients in *clinical trial R* (R1-R4) are also analyzed in this chapter. These 4 patients do not follow a unique rigorous protocol: the main characteristics of each patient are provided in Table 11.1 and the different ventilator and ECLS settings are summarized in Table 11.2 of section 11.3. Table 11.1 shows that all patients suffer from severe ARDS ($P_{a,\mathrm{O}_2}/F_{I,\mathrm{O}_2} < 100$ mmHg [31]) and, except for patient R3, the patients also have severe hypercapnia ($P_{a,\mathrm{CO}_2} > 70$ mmHg). For each patient, the protective ventilation (or the change of ventilator settings for patient R1) is induced a few minutes after the ECLS is launched and Table 11.2 provides the values of the ventilator settings before and after they are changed.

For *clinical trial R*, the membrane used for the extracorporeal therapy is a Quadrox-iD Adult® (Maquet, Getinge Group). Blood samples at the inlet and outlet cannulae are taken several hours after the ECLS initialization.

Table 11.1 – Main characteristics of *clinical trial R*.

Patient		R1	R2	R3	R4
		Baseline situation			
Severity of ARDS: $P_{a,\mathrm{O}_2}/F_{I,\mathrm{O}_2}$ (mmHg)		45	41	50	52
Hypercapnia: P_{a,CO_2} (mmHg)		108	88	41	88
		ECLST			
Time when blood samples are drawn (number of minutes after the ECLS is switched on)*	Arterial blood sample	45, 210, 260	30	25, 90	2, 50
	Venous blood sample	267	60	1, 2, 25	65

11.2 Estimation of parameters f_s and $\dot{V}_A$ during the protective ventilation

Whereas the method to estimate the parameters during baseline situation is the same as in the pig experiments, the estimation of the parameters f_s and $\dot{V}_A$ during protective ventilation (or after the change of the ventilator settings for patient R1) is different (see

*The number of minutes is approximate

section 7.2). Indeed, for the patient safety, the protective ventilation is never induced before the ECLST. In the ICU, the change of the ventilator settings is thus always started a few minutes after the beginning of the ECLST. Therefore, the goals of the study is not to predict only the ECLST but it is to predict the ECLST combined with the protective ventilation. The value of the two parameters f_s and $\dot{V}_A$ after the change of the ventilator settings must thus be estimated without any measurements. In such a situation, a first approximation for these parameters will be obtained from the animal experiments previously analyzed. In these experiments, one can determined the relative variation of f_s and $\dot{V}_A$ in terms of the relative variation of $\dot{V}_E$ ($\dot{V}_E = f_r \cdot V_T$) and these relations will also be simply assumed valid for human.

Figure 11.1 shows the relative variation of $\dot{V}_A$ with respect to the relative variation of $\dot{V}_E$ for the animal experiments. Since ARDS is also induced in *experiments A* during protective ventilation, only experimental data from *experiments H* are shown in Figure 11.1 and will be used here (ARDS increases the pulmonary shunt and ARDS could decrease the alveolar ventilation). In this figure, the diamonds are the experimental data and the dashed line is the linear interpolation of these data with the natural constraint of passing through the trivial point ($\Delta\dot{V}_E/\dot{V}_E = 0$, $\Delta\dot{V}_A/\dot{V}_A = 0$). The interpolation shows that $\Delta\dot{V}_A/\dot{V}_A$ is almost equal to $\Delta\dot{V}_E/\dot{V}_E$ and the equality $\Delta\dot{V}_A/\dot{V}_A = \Delta\dot{V}_E/\dot{V}_E$ is thus considered valid for human. Therefore, the estimate $\left(\dot{V}_A\right)_{PV}$, defining $\dot{V}_A$ during protective ventilation (or after the change of ventilator settings for patient R1), can be obtained as follows:

$$\Delta\dot{V}_A/\dot{V}_A = \Delta\dot{V}_E/\dot{V}_E$$

$$\Leftrightarrow \frac{\left(\dot{V}_A\right)_{PV} - \left(\dot{V}_A\right)_{Baseline}}{\left(\dot{V}_A\right)_{Baseline}} = \frac{\left(\dot{V}_E\right)_{PV} - \left(\dot{V}_E\right)_{Baseline}}{\left(\dot{V}_E\right)_{Baseline}}$$

$$\Leftrightarrow \left(\dot{V}_A\right)_{PV} = \left(\dot{V}_A\right)_{Baseline} \cdot \frac{\left(\dot{V}_E\right)_{PV}}{\left(\dot{V}_E\right)_{Baseline}}, \tag{11.1}$$

where $\left(\dot{V}_E\right)_{PV}$ is known since this parameter is directly related to the settings fr and V_T of the ventilator that are chosen by the clinicians.

The estimation of parameter f_s after a variation of $\dot{V}_E$ is more delicate. Indeed, the left panel of Figure 11.2 shows the relative variation of f_s with respect to the relative

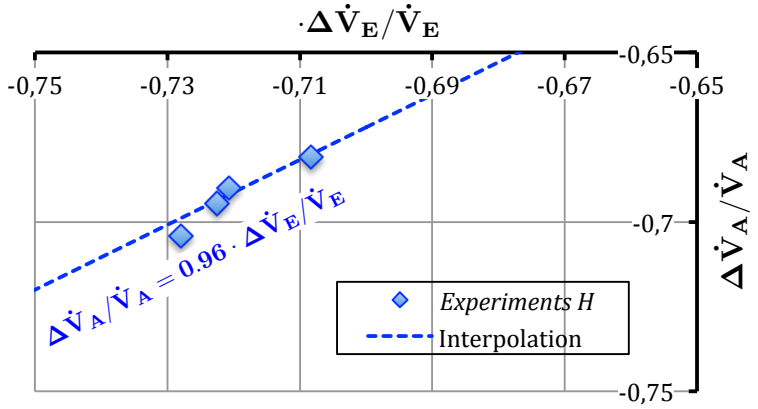

Figure 11.1 – Relative variation of alveolar ventilation $\Delta\dot{V}_A/\dot{V}_A$ in terms of relative variation of minute ventilation $\Delta\dot{V}_E/\dot{V}_E$ for *experiments H*.

variation of $\dot{V}_E$ for *experiments H* and no clear relationship between these two quantities can be established. However, the pig experiments have shown that the ARDS significantly increases f_s (see subsection 9.3.2). These experiments also show that the increase in f_s with the decrease in $\dot{V}_E$ is much smaller than the increase in f_s related to ARDS induction. The right panel of Figure 11.2 confirms this statement by comparing the value of $\overline{\frac{\Delta f_s/f_s}{|\Delta\dot{V}_E/\dot{V}_E|}}$ for *experiments H* with the value of $\overline{\frac{\Delta f_s/f_s}{|\Delta\dot{V}_E/\dot{V}_E|}}$ for *experiments A* and by showing that the values for *experiments A* is almost 10 times larger than that of *experiments H*. Therefore, the variation of f_s with the variation of $\dot{V}_E$ is small in comparison with the large changes of f_s for a subject suffering from ARDS. As a first approximation, the variation of f_s with the variation of $\dot{V}_E$ will thus be neglected in our mathematical model. This assumption gives the following estimation of f_s during protective ventilation:

$$(f_s)_{PV} = (f_s)_{Baseline} \ . \tag{11.2}$$

Note that these estimations of the 2 parameters $\dot{V}_A$ and f_s after the change of the ventilator settings are first approximations. The estimations of these parameters will be discussed in subsection 11.5.2 and, using clinical data, a new and better estimation of $(f_s)_{PV}$ will be suggested.

11.3 Values of the parameters

The diffusion coefficients across the membrane of the ECLS are not supposed to be the same in *clinical trial S* than in *clinical trial R* since the membranes are different. Using

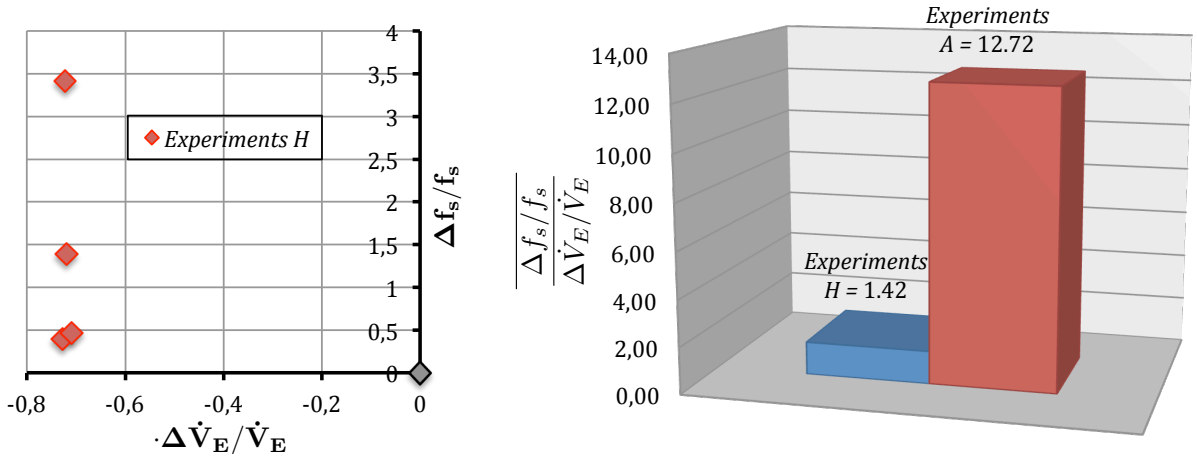

Figure 11.2 – Relative variation of pulmonary shunt $\Delta f_s/f_s$ in terms of relative variation of minute ventilation $\Delta \dot{V}_E/\dot{V}_E$ (left panel) and mean of the fraction of the relative variation of pulmonary shunt $\Delta f_s/f_s$ over the absolute value of the relative variation of minute ventilation $\Delta \dot{V}_E/\dot{V}_E$ for *experiments H* and *experiments A* (right panel).

the method presented in subsection 7.2.5, the coefficients D_{CO_2} and D_{O_2} can be estimated for each membrane and the values are given in Table 11.2. The setting of the ECLS are different for each clinical trials and are also given in Table 11.2. For the extracorporeal blood flow Q_d, it is always larger or equal to 1 l/min and the recirculation is thus taken into account for the clinical trials (see subsection 5.3.2, p. 74).

The other parameters of the model are also provided in Table 11.2 for all the patients. Parameter F_{I,O_2}, V_T and fr are the ventilator settings. On the other hand, the values of MR_{CO_2}, MR_{O_2} and k_{HCO_3} are determined by the procedures described in subsections 7.2.1 and 7.2.3. However, for *clinical trial R*, no venous measurements are taken before the ECLST and MR_{CO_2}, MR_{O_2} have to be estimated during ECLST. Indeed, some venous and arterial blood samples are taken during ECLST when the patient reaches a stabilized state (PO_2 and PCO_2 are in a time independent situation). Since the mathematical model assumes constant metabolism for ICU patients, these estimated values are also valid during baseline situation.

The values of the parameters describing the pulmonary insufficiencies, f_s and $\dot{V}_A$, are determined by the procedures described in subsections 7.2.4 for the baseline situation and in section 11.2 for the protective ventilation. The values of these parameters for each patient are also given in Table 11.2.

Table 11.2 – Measurements, settings of the ventilator and ECLS, identified parameters and estimated parameters for *clinical trial S* (S1) and for *Clinical trial R* (R1-R4).

	Clinical trial S	*Clinical trial R*			
Data	S1	R1	R2	R3	R4
Baseline situation					
Measurements					
Weight (kg)	77	80	113	132	71.3
Height (cm)	177	181	186	175	160
Weight base parameters					
CO (l/min)	5.84	6	7.25	7.60	5.34
V_{L,CO_2} (l)	3.29	2.99	4.81	5.63	3.04
V_{L,O_2} (l)	2.54	2.31	3.72	4.36	2.35
V_{T,CO_2} (l)	15.5	14.0	22.5	26.4	14.3
V_{T,O_2} (l)	6.2	5.6	9.0	10.6	5.7
Ventilator settings					
F_{I,O_2}	0.6	1	1	1	1
V_T (l)	0.475	0.317	0.329	0.422	0.362
fr (min^{-1})	25	40	35	22	26
Identified parameters					
MR_{O_2} ($\mathrm{l}_{\mathrm{O}_2}$/min)	0.204	0.300	0.276	0.258	0.258
MR_{CO_2} ($\mathrm{l}_{\mathrm{CO}_2}$/min)	0.204	0.300	0.276	0.258	0.258
k_{HCO_3} ($\mathrm{l}_{\mathrm{CO}_2}$/l)	$2.6 \cdot 10^{-5}$	-0.098	0.300	0.064	0.053
f_s	0.319	0.558	0.588	0.573	0.515
$\dot{V}_A$ (l/min)	4.04	2.77	3.19	6.97	2.97
Measured parameters					
C_{Hb} (l_{Hb}/l)	0.163	0.125	0.133	0.191	0.147
ECLST combined with protective ventilation (except R1)					
Ventilator settings					
F_{I,O_2}	0.6	1	1	0.8	1
V_T (l)	$0.375 \rightarrow 0.330 \rightarrow 0.300$	0.554	0.135	0.270	170
fr (min^{-1})	25	27	10	12	10
ECLS setting					
Q_d (l/min)	1	4	4	5	4.1
$\dot{V}_D$ (l/min)	6	4	9	$9 \rightarrow 6$ *	9
F_{ID,O_2}	0.21	0.7	1	1	1
Estimated parameters					
f_s	0.319	0.558	0.588	0.573	0.515
$\dot{V}_A$ (l/min)	$3.19 \rightarrow 2.80 \rightarrow 2.55$	3.27	0.37	2.43	0.54
Identified parameters					
D_{CO_2} ($l_{\mathrm{CO}_2}/s/mmHg$)	$8.5 \cdot 10^{-5}$	$1.6 \cdot 10^{-4}$			
D_{O_2} ($l_{\mathrm{O}_2}/s/mmHg$)	$6.4 \cdot 10^{-6}$	$5.8 \cdot 10^{-6}$			

*The decrease in $\dot{V}_D$ from 9 to 6 l/min was set approximately 45 minutes after the ECLS was launched

Finally, parameters V_{L,CO_2}, V_{L,O_2}, V_{T,CO_2}, V_{T,O_2} and V_{TB} are proportional to the body weight (Table 7.1, p. 99). Cardiac blood flow is not always measured in the ICU before or after the first hours of ECLST. In our study, CO is assumed to be proportional to the BSA (see subsection 9.3.4, p. 140). To estimate the BSA, the Mosteller formula [115] is used and the approximation of CO is thus given by:

$$CO\ (\mathrm{l/min}) = 3 \cdot \mathrm{BSA} = 3 \cdot \sqrt{\frac{Weight \cdot Height}{3600}}\ , \tag{11.3}$$

where the weight is in kg and the height is in cm. The values of V_{L,CO_2}, V_{L,O_2}, V_{T,CO_2}, V_{T,O_2}, V_{TB} and CO for each patient are given in Table 11.2.

11.4 Comparaison between simulations and clinical data

Like in section 9.2 for the pig experiments, the simulations must be compared with clinical data in order to validate the model in the ICU. In *clinical trial R*, a traditional ECLS is used (not a $\mathrm{ECCO_2RD}$) and the oxygenation of blood is as essential as the $\mathrm{CO_2}$ removal. Therefore, for this chapter, both the $\mathrm{O_2}$ and the $\mathrm{CO_2}$ partial pressure simulations are compared with the experimental data. For both molecules, the mean errors $\overline{\Delta P}$ and the mean relative errors $\overline{\Delta P/P}$ (see section 11.4), with and without the absolute value, are used to test the predictions of the model. Since the first minutes of $\mathrm{PO_2}$ and $\mathrm{PCO_2}$ predictions are not useful for the goal of this study and since the unstationary description of the mathematical model is based on rough approximations, the clinical data taken during the first 10 min of ECLST will not be taken into account to test the prediction of the simulations.

Remember also that the protocols of *clinical trial S* and *clinical trial R* are quite different and the corresponding results will be thus presented separately, with *clinical trial S* considered in subsection 11.4.1 and *clinical trial R* considered in subsection 11.4.2.

11.4.1 *Clinical trial S*

Figure 11.3 presents the time evolutions of $\mathrm{PCO_2}$ (upper panel) and $\mathrm{PO_2}$ (bottom panel) in the arteries and veins during the different phases of observation (before the ECLST, when the ECLS is switched on and the tidal volume is reduced to 0.375 l, when the tidal volume is reduced to 0.330 l and when the tidal volume is reduced to 0.300 l). In this figure, the full lines describe the numerical simulations while diamonds and crosses describe the experimental data in the arteries and veins respectively. Before the ECLST, the agreement is perfect for $\mathrm{PCO_2}$ in the arteries since parameters f_s and $\dot{V}_A$ are iden-

tified to fit PCO_2 in the arteries. On the other hand, as already observed in Figure 9.4 of subsection 9.2.2, the agreement is not perfect for the venous PCO_2 because MR_{CO_2} is not estimated with the measurements but with the approximation $MR_{CO_2} = MR_{O_2}$. During the ECLST, the simulations correspond quite well with the experimental data and they both show a significant decrease in PCO_2 in the arteries and veins when the ECLS is switched on, a small increase in PCO_2 when the tidal volume is reduced to 0.330 l and when the tidal volume is reduced to 0.300 l, a small decrease in PO_2 when the ECLS is switched on and almost no change of PO_2 when the tidal volume is reduced to 0.330 l and to 0.300 l.

Table 11.3 provides the mean errors $\overline{\Delta P}$ and the mean relative errors $\overline{\Delta P/P}$, with and without absolute value, for PCO_2 and PO_2. The number of PCO_2 or PO_2 measurements (m) is also given. It can be seen from this table that the PCO_2 errors are small ($\overline{|\Delta P_{CO_2|}/P_{CO_2}|} = 0.06 \pm 0.04$) and we can consider that the simulations do not overestimate or underestimate the experimental data ($\overline{\Delta P_{CO_2}/P_{CO_2}}$ =0.01 ± 0.05). The PO_2 errors are larger than the PCO_2 errors ($\overline{|\Delta P_{O_2}/P_{O_2}|}$ =0.14 ± 0.08 compared to $\overline{|\Delta P_{CO_2}/P_{CO_2}|}$ = 0.04 ± 0.03) and overestimations are always observed for the PO_2 errors ($\overline{\Delta P_{O_2}/P_{O_2}}$ = 0.14 ± 0.08).

11.4.2 *Clinical trial R*

Figure 11.4 presents the time evolutions of PCO_2 (left panel) and PO_2 (right panel) in the arteries and veins during the different phases of observation (before the ECLST and when the ECLS is switched on) for patient R2. The results for the other patients have similar features and are given in Figure B.8 of Appendix B.4. As in Figure 11.3, the full lines describe the numerical simulations while diamonds and crosses describe the experimental data in the arteries and veins respectively. The agreement is also perfect for PCO_2 in the arteries before the ECLST. During the ECLST, the PCO_2 simulations correspond quite well with the experimental data but, on the other hand, there is a significant error between the PO_2 simulations and the experimental data. The simulations show a large decrease in PCO_2 in the arteries and veins even after the induction of the protective ventilation. They also show a large increase in PO_2 in the arteries and veins when the ECLS is switched on and a significant decrease in PO_2 when the protective ventilation is induced. The increase is larger than the decrease and PO_2 is thus larger during the ECLST combined with the protective ventilation than before the ECLST. The experimental data also show an increase in PO_2 in the arteries during the ECST combined with the protective ventilation.

Table 11.4 provides the mean errors $\overline{\Delta P_{CO_2}}$ and $\overline{\Delta P_{O_2}}$ and the mean relative errors $\overline{\Delta P_{CO_2}/P_{CO_2}}$ and $\overline{\Delta P_{O_2}/P_{O_2}}$, with and without absolute value, for the 4 patients (R1, R2,

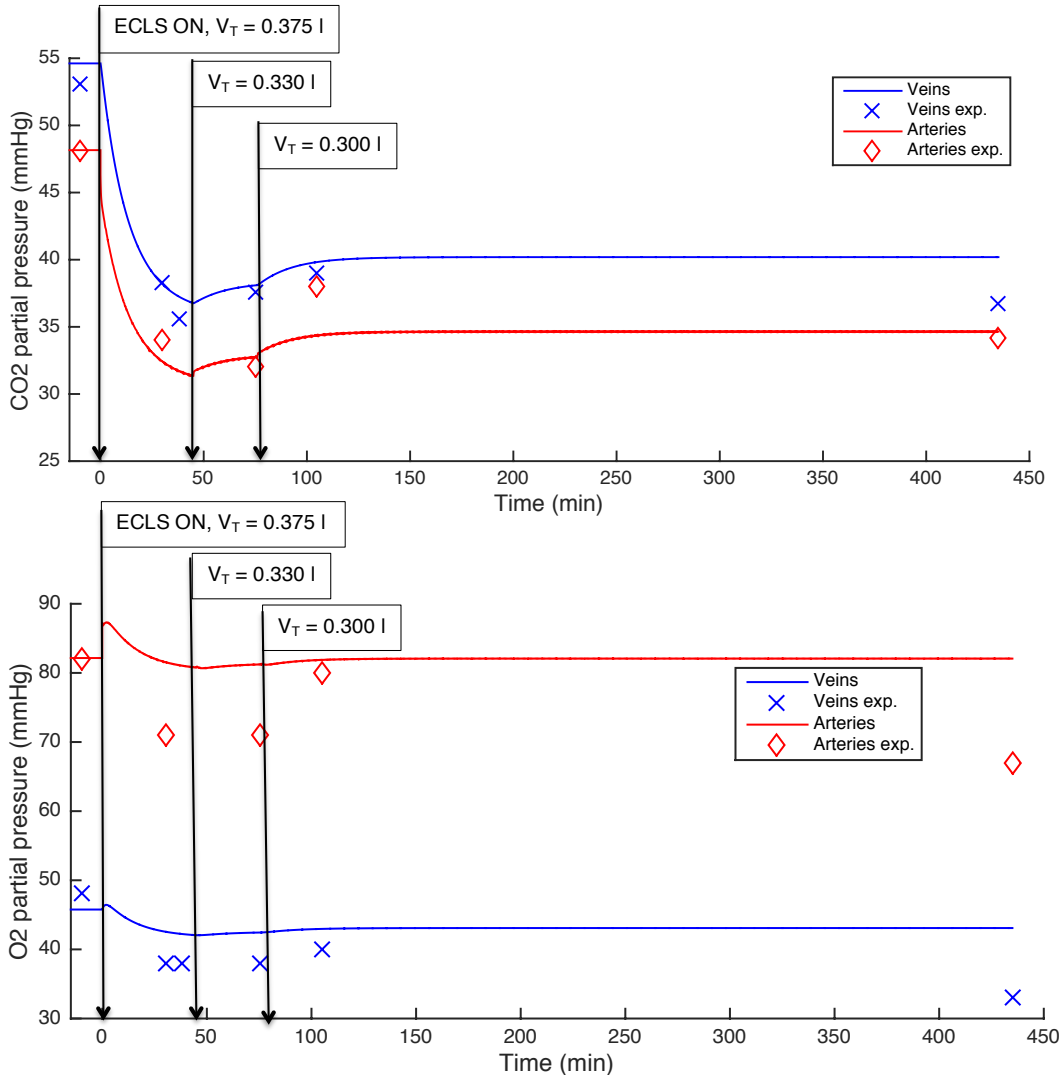

Figure 11.3 – Time evolution of calculated (lines) and measured (crosses and diamonds) CO_2 partial pressures in the veins and arteries (upper panel) and O_2 partial pressures in the veins and arteries (bottom panel) for the patient $S1$. The different phases of observation are delimited by vertical arrows, with self explaining-labels.

Table 11.3 – PCO_2 and PO_2 errors between the simulations and the measurements during ECLST for patient S1. The line m indicates the number of PCO_2 or ¶O_2 measurements available during ECLST .

Data	CO_2	O_2
$\overline{\lvert\Delta P\rvert}$ (mmHg)	1.43 ± 1.28	7.12 ± 4.48
$\overline{\lvert\Delta P/P\rvert}$	0.04 ± 0.03	0.14 ± 0.08
$\overline{\Delta P}$ (mmHg)	-1.00 ± 1.97	7.12 ± 4.48
$\overline{\Delta P/P}$	0.01 ± 0.05	0.14 ± 0.08
m	9	9

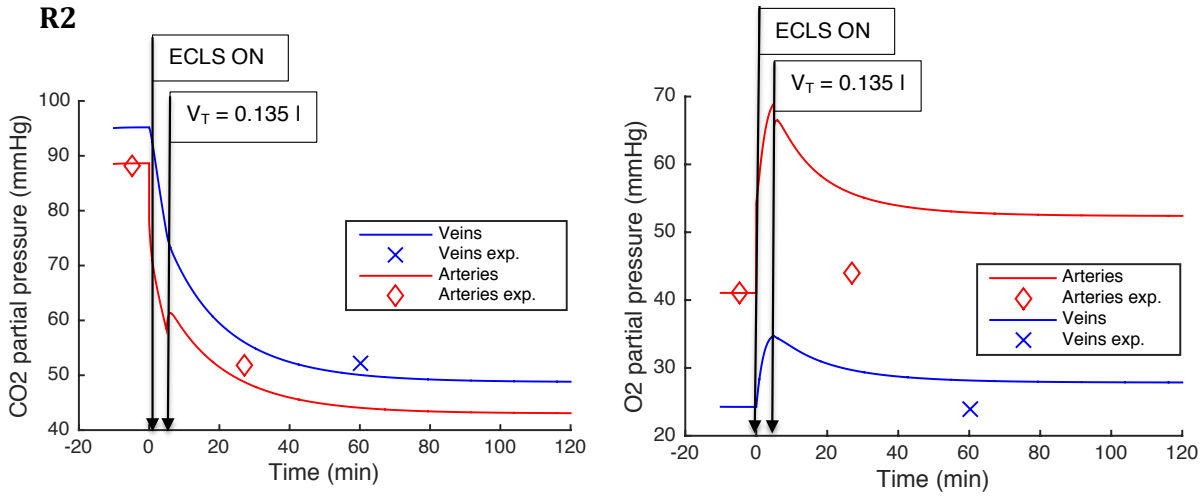

Figure 11.4 – Time evolutions of calculated (lines) and measured (crosses and diamonds) CO_2 partial pressures in the veins and arteries (left panel) and O_2 partial pressures in the veins and arteries (right panel) for the patient R2. The different phases of observation are delimited by vertical arrows, with self-explaining labels.

R3 and R4). The number of PCO_2 or PO_2 measurements (m) is also given. This table demonstrates that the error is small for PCO_2 and the value of $\overline{|\Delta P_{CO_2}/P_{CO_2}|}$ for all the patients is of the same order as the one obtained with pig experiments ($\overline{|\Delta P_{CO_2}/P_{CO_2}|}$ = 11%, see Table 9.3 p. 136). $\overline{\Delta P_{CO_2}/P_{CO_2}}$ for all the patients is positive ($\overline{\Delta P_{CO_2}/P_{CO_2}}$ = 5%) and this result indicates that the PCO_2 simulations frequently overestimate the experimental data. On the other hand, the error is rather large for PO_2 ($\overline{|\Delta P_{O_2}/P_{O_2}|}$ for all patients is equal to 28%) and the simulations overestimate the experimental data ($\overline{\Delta P_{O_2}/P_{O_2}}$ for all patients is equal to 20% and only the patient R1 underestimate the experimental data).

Table 11.4 – PCO_2 and PO_2 errors between the simulations and the measurements during ECLST for *clinical trial R*. The line m indicates the number of PCO_2 or PO_2 measurements available during ECLST (after the change of ventilator settings).

	CO_2					O_2				
Data	R1	R2	R3	R4	**Mean**	R1	R2	R3	R4	**Mean**
$\overline{\lvert\Delta P\rvert}$ (mmHg)	5.47	4.56	4.52	1.68	**4.05**	17.24	8.69	11.32	22.34	**14.90**
$\overline{\lvert\Delta P/P\rvert}$	0.16	0.09	0.16	0.04	**0.11**	0.19	0.25	0.20	0.50	**0.28**
$\overline{\Delta P}$ (mmHg)	5.47	-4.56	3.64	0.17	**1.18**	-16.36	8.69	11.32	22.34	**6.50**
$\overline{\Delta P/P}$	0.16	-0.09	0.13	0.00	**0.05**	-0.16	0.25	0.20	0.50	**0.20**
m	4	2	2	2		4	2	2	2	

11.5 Discussion

This section discusses the physiological meaning of important parameters estimated in this chapter and compares these values with the values obtained with pig experiments (see Chapter 9). In addition, this section also discusses the ability of our model to predict the decrease in PCO_2 and PO_2 during the ECLST.

11.5.1 Values of the parameters

The diffusion coefficients across the membrane of the ECLS, D_{CO_2} and D_{O_2}, are similar for *clinical trial S* and *clinical trial R* (Table 11.2) and, as expected, D_{CO_2} is larger than D_{O_2}. D_{CO_2} and D_{O_2} for the ECLS used in the ICU are larger than those estimated for the pig experiments. This difference can be explained by the exchange surface of the ECLS membrane which is smaller for the pig experiments (the ECLS used in the experiments is a PALP® (Getinge, Sweden) while the ECLS used in the clinical trials is an HLS Set Advanced 5.0® (Getinge, Sweden) or a Quadrox-iD Adult® (Getinge, Sweden)).

Table 11.2 shows that the values of the lumped parameter $\dot{V}_A$ are in the same range than the pig experiments (Table 9.1 p. 130). The values of $\dot{V}_A$ for humans are a bit larger since parameter V_T is larger because of a larger weight for the patients than that of the pigs. In this table, the values of f_s are in the same range as in *experiments A* during the protective ventilation combined with ARDS (Table 9.1 p. 130). f_s is larger for *clinical trial R* than *clinical trial S* and this result is in agreement with clinic since patients R suffer from ARDS while patient *S1* suffers from moderate lung pathology. The value of f_s for patients R is larger than in previous studies on humans suffering from ARDS (31±10% [54]) but in these studies the patients were not assisted with an ECLS and their respiratory pathologies were certainly less severe than in our study. The values of MR_{O_2} and MR_{CO_2} (0.259±0.035 l_{O_2}/min/kg and l_{CO_2}/min/kg) are in the same range than previous studies ($MR_{O_2} = 0.26 - 0.31$ l_{O_2}/min/kg and $MR_{CO_2} = 0.21 - 0.26$ l_{CO_2}/min/kg [9, 10]).

11.5.2 Quality of the PCO_2 and the PO_2 predictions

For the *clinical trial S*, the agreement between the PCO_2 simulations and experimental data is excellent and the agreement between the PO_2 simulations and experimental data is rather good for but only one case $S1$ was recorded in our hospital. However, for this patient *S1*, a significant number of experimental data was recorded during the first hours of ECLST (9 blood samples were taken for this patient). On the other hand, for *clinical trial R*, the agreement between the PCO_2 simulations and experimental data is good but

the difference between the PO_2 simulations and experimental data is significant.

In order to improve the prediction of PO_2, the parameters influencing PO_2 and which were based on rough approximation, are analyzed in more detail in the following paragraphs. The estimation of $\dot{V}_A$ after the change of the ventilator settings is based on the approximation 11.1. However, Figure 11.3 shows that PO_2 undergoes nearly no variation with the decrease in V_T from 0.375 l to 0.300 l while PCO_2 increases appreciably. This phenomena can be explained by the fact that hemoglobin is fully saturated after the pulmonary capillaries even during protective ventilations. Therefore, the decrease in V_T to achieve a protective ventilation will have a minute influence on PO_2 in arteries. Since V_T is directly proportional to $\dot{V}_A$, $\dot{V}_A$ influences mainly PCO_2. With this information and the small errors obtained for the simulated PCO_2 (Table 11.3 and Table 11.4), the value of parameter $\dot{V}_A$ after the change of the ventilator settings, which is estimated using equation 11.1, can be considered as a good approximation. On the contrary, f_s influences PO_2 and the value of this parameter after the change of the ventilator settings, which is estimated using the approximation 11.2, could be erroneous. Table 11.3 and Table 11.4 show that the PO_2 simulations overestimate the experimental data and the difference between these simulations and the experimental data could be decreased by increasing f_s.
Other parameters also greatly influence PO_2. The value of extracorporeal recirculation R_{recir} is based on rough approximation (equation 5.13, p. 74) and an increase in this parameter will decrease PO_2 since the efficacy of the ECLS will be reduced. Finally, the hemoglobin concentration is changed when ECLS is started since extracorporeal circulation is filled with water before the ECLST. As a consequence, a dilution of hemoglobin occurs when the ECLS is switched on and this effect could decrease PO_2 since less hemoglobin molecules will reach the tissues.

The influence of the 2 parameters, f_s and R_{recir}, and of the dilution of hemoglobin on PO_2 and PCO_2 is analyzed below.

Influence of R_{recir}

The value of R_{recir}, defined by equation 5.13, depends on the parameter k_{recir} which has been fixed to an empirical value of 0.083 min/l. If k_{recir} is arbitrary increased from 0.083 to 0.15, the recirculation R_{recir} for patient R2 is increased from 0.332 to 0.6 and Figure 11.5 compares the PCO_2 and the PO_2 simulations in the veins and arteries for patient R2 when $R_{recir} = 0.6$ with the previous PCO_2 and PO_2 simulations in the veins and arteries (R_{recir}= 0.332). This figure shows that the increase in R_{recir} improves the agreement between the PO_2 simulations and experimental data. However, the increase

in R_{recir} has also a significant influence on PCO_2 since the calculated PCO_2 considerably increases when R_{recir} increases. Therefore, the increase in R_{recir} cannot improve the PO_2 description without reducing the quality of the PCO_2 predictions.

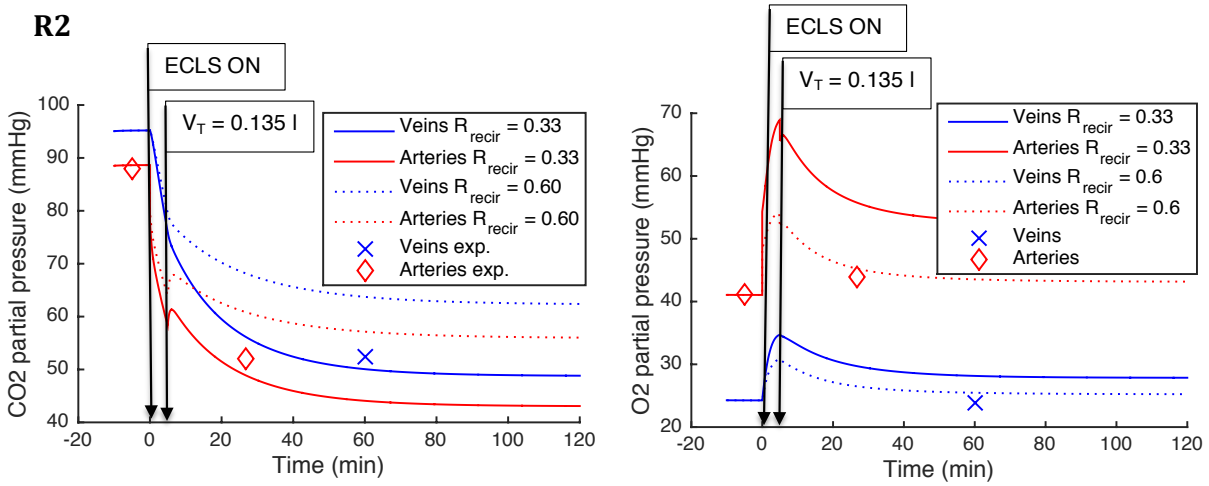

Figure 11.5 – Comparison of the PCO_2 (left panel) and the PO_2 (right panel) simulations in the veins and arteries when $R_{recir} = 0.6$ (dotted lines) with the previous PCO_2 and PO_2 simulations ($R_{recir} = 0.33$, these simulations are described by solid lines). The different phases of observation are delimited by vertical arrows, with self explaining-labels.

Influence of the dilution

For taking into account the dilution of hemoglobin, a dilution ratio D_{Hb} is estimated with the following formula:

$$D_{\mathrm{Hb}} = \frac{V_{TB}}{V_{TB} + V_{IN} + V_{OUT}} \ . \tag{11.4}$$

where the numerator is the total volume of the cardiovascular system and the denominator is the total volume of the cardiovascular system complemented by the extracorporeal circulation (all the symbols have already been defined in subsection 5.5, p. 76). Therefore, the mathematical model can estimate the hemoglobin concentration when the ECLS is switched on by the following equation:

$$(C_{Hb})_{ECLST} = D_{\mathrm{Hb}} \cdot (C_{Hb})_{Baseline} \ , \tag{11.5}$$

and the relative variation of C_{Hb} can be deduced from equation 11.5:

$$\Delta C_{Hb}/C_{Hb} = \frac{(C_{Hb})_{ECLST} - (C_{Hb})_{Baseline}}{(C_{Hb})_{Baseline}} = D_{\mathrm{Hb}} - 1 \ . \tag{11.6}$$

Table 11.5 gives the measurements of hemoglobin concentrations during baseline situation and ECLST situation. This table also provides the relative variation of these measurements and the value of $D_{Hb}-1$ for each patient. The measurements indicates that $\Delta C_{\mathrm{Hb}} \approx -13\%$ while the corresponding estimations $(D_{Hb}-1)$ is approximately equal to -8 %. Therefore, parameter D_{Hb} predicts rather nicely the dilution of blood when the ECLS is switched on. Figure 11.6 compares the PCO_2 and the PO_2 simulations when dilution is taken into account (dotted lines) and when dilution is not taken into account (solid lines). There is almost no difference between the two simulations for PCO_2 in the arteries and veins, there is a tiny difference between the two simulations for PO_2 in the arteries and there is a small difference between the simulations for PO_2 in the veins. Consequently, taking into account the dilution of blood slightly improves the PO_2 description without reducing the quality of the PCO_2 predictions (Table B.7 and Table B.8 of Appendix B.4 that show $\overline{\Delta P_{\mathrm{CO}_2}}$, $\overline{\Delta P_{\mathrm{O}_2}}$, $\overline{\Delta P_{\mathrm{CO}_2}/P_{\mathrm{CO}_2}}$ and $\overline{\Delta P_{\mathrm{O}_2}/P_{\mathrm{O}_2}}$ with and without absolute value for all the patients). Therefore, the dilution of hemoglobin should be taken into account in the mathematical model and this effect will be considered in all the subsequent simulations.

Table 11.5 – Hemoglobin concentrations during baseline situation and ECLST situation, relative variation of these concentrations and the estimation of $1-D_{Hb}$ for *clinical trial S* (S1) and for *clinical trial R* (R1-R4).

	Clinical trial S	*Clinical trial R*			
Data	S1	R1	R2	R3	R4
Baseline situation					
Measured parameters					
C_{Hb} ($\mathrm{l_{Hb}/l}$)	0.163	0.125	0.133	0.191	0.147
ECLST combined with protective ventilation (except R1)					
Measurements					
C_{Hb} ($\mathrm{l_{Hb}/l}$)	0.141	0.108	0.109	0.170	0.132
$\Delta C_{\mathrm{Hb}}/C_{\mathrm{Hb}}$	-0.137	-0.137	-0.178	-0.110	-0.107
Estimated parameters					
$D_{\mathrm{Hb}}-1$	-0.10	-0.09	-0.07	-0.06	-0.10

Influence of f_s

Since $\dot{V}_A$ does not influence PO_2, the estimation of parameter f_s is of paramount importance to fit the experimental PO_2. As in the two previous analysis, it would be useful to estimate if this parameter influences PCO_2. If f_s is estimated to fit the experimental PO_2

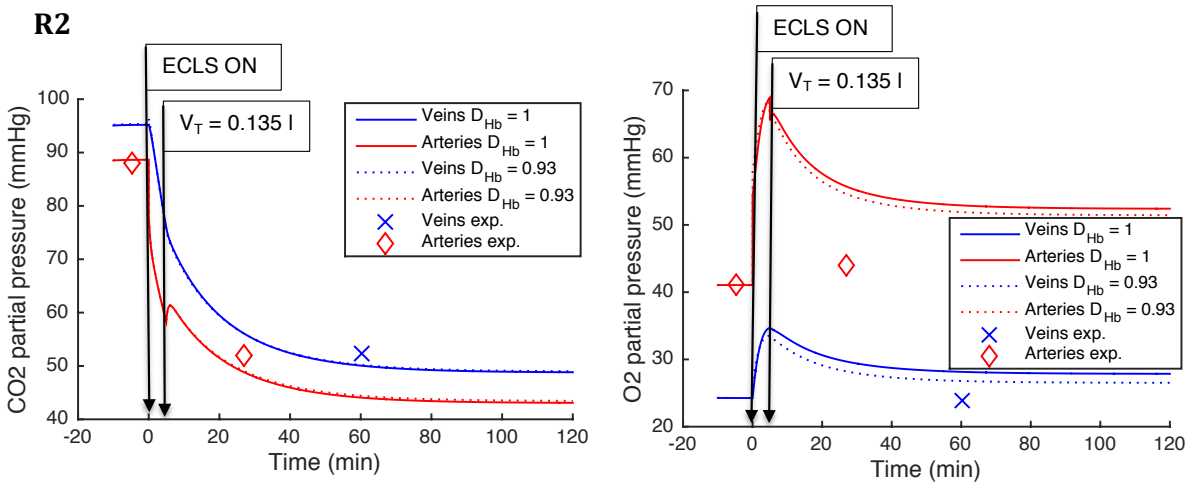

Figure 11.6 – Effect of dilution on the prediction of PCO_2 and PO_2. The solid lines represent the PCO_2 (left panel) and the PO_2 (right panel) simulations in the veins and arteries when $D_{Hb} = 1$ while the dotted lines represent the PCO_2 (left panel) and the PO_2 (right panel) simulations in the veins and arteries when $D_{Hb} = 0.93$). The different phases of observation are delimited by vertical arrows, with self-explaining labels.

after the change of the ventilator settings for patient R2, the identified value of f_s is equal to 0.76. Figure 11.7 compares the PCO_2 and the PO_2 simulations in the veins and arteries for patient R2 when parameter $(f_s)_{PV}$ is increased from 0.588 (previously used value) to 0.76. Note that for these simulations, the dilution of hemoglobin is taken into account. With the new value of f_s, the agreement between simulations and experimental data is perfect for PO_2. The comparison between the PCO_2 simulations obtained with the new value of f_s with the previous PCO_2 simulations shows that the new predicted values are almost identical to the previous simulations.

Since Table 11.3 and Table 11.4 have shown that the PO_2 simulations overestimate the experimental data for each patient except patient R1, the increase in parameter f_s during the protective ventilation for patient S1, R2, R3 and R4 and the decrease in f_s after the change of the ventilator settings for patient $R1$ (for this patient the tidal volume is increased) would improve the PO_2 prediction of our mathematical model. In addition, since f_s has a little influence on PCO_2, this variation of f_s will not affect the good predictions of the simulated PCO_2. Furthermore, the physiological meaning of the increase in f_s with the decrease in $\dot{V}_E$ has already been described in subsection 9.3.2, p. 138 (the lung dynamics are changed and some alveoli could collapse with the reduction of $\dot{V}_E$). Therefore, the assumption of no variation of f_s with $\dot{V}_E$, which has been established in section 11.2, should be reconsidered. To build a relationship between Δf_s and $\Delta\dot{V}_E$, the values of f_s after the change of ventilator setting is estimated by fitting PO_2 in the arteries during this phase and the variation of f_s in terms of $\Delta\dot{V}_E$ could be established.

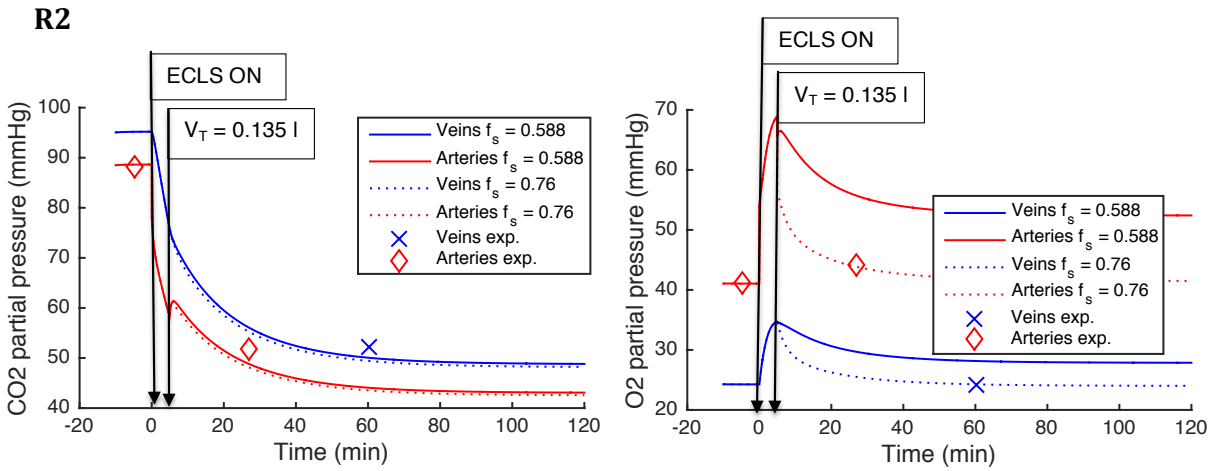

Figure 11.7 – Comparison of the PCO_2 (left panel) and the PO_2 (right panel) simulations in the veins and arteries when $(f_s)_{PV} = 0.75$ (dotted lines) with the previous PCO_2 and PO_2 simulations ($(f_s)_{PV} = 0.558$, these simulations are illustrated by solid lines). The different phases of observation are delimited by vertical arrows, with self-explaining labels.

Table 11.6 shows the values of f_s identified after the change of the ventilator settings and Figure 11.8 shows $\Delta f_s/f_s$ in terms of $\Delta\dot{V}_E/\dot{V}_E$ for all the patients. In Figure 11.8, the diamonds represent the clinical data and the dashed line is the linear interpolation of these data with the natural constraint of passing trough the trivial point ($\Delta\dot{V}_E/\dot{V}_E = 0$, $\Delta f_s/f_s = 0$). This figure shows that the errors between the clinical data and the interpolation are small and well distributed (3 clinical data underestimate $\Delta f_s/f_s$ and 4 clinical data overestimate $\Delta f_s/f_s$). Therefore, the interpolation gives a good approximation of the relative variation of f_s in terms of the relative variation of $\dot{V}_E$ and equation 11.2, which has provided the first approximation of $(f_s)_{PV}$, is thus replaced by the following equation:

$$\begin{aligned} &\Delta f_s/f_s = -0.45 \cdot \Delta\dot{V}_E/\dot{V}_E \\ \Leftrightarrow\ &(f_s)_{PV} = (f_s)_{Baseline} \cdot (-0.45) \cdot \Delta\dot{V}_E/\dot{V}_E + (f_s)_{Baseline} \ . \end{aligned} \tag{11.7}$$

With this new estimation of f_s after the variation of the ventilator settings, the mathematical model is simulated for each patient and $\overline{\Delta P_{CO_2}}$, $\overline{\Delta P_{O_2}}$, $\overline{\Delta P_{CO_2}/P_{CO_2}}$ and $\overline{\Delta P_{O_2}/P_{O_2}}$, with and without absolute value, are provided in Table 11.7 and Table 11.8. These tables demonstrate that the PO_2 errors is greatly decreased with the new values of $(f_s)_{PV}$: $\overline{|\Delta P_{O_2}/P_{O_2}|} = 0.11$ instead of 0.26 for patients R (Table B.7 of Appendix B.4) and $\overline{|\Delta P_{O_2}/P_{O_2}|} = 0.05$ instead of 0.10 for patient S1 (Table B.8 of Appendix B.4). The PCO_2 errors have still the same values ($\overline{|\Delta P_{CO_2}/P_{CO_2}|} = 0.11$ for patients R and $\overline{|\Delta P_{CO_2}/P_{CO_2}|} = 0.04$ for patient S1). Therefore, the agreement between the simulations and the experimental data is much better with the new estimations of $(f_s)_{PV}$.

Table 11.6 – Identified f_s during baseline and after the change of ventilator settings for *clinical trial S* (S1) and for *clinical trial R* (R1-R4).

	Clinical trial S	*Clinical trial R*			
Data	S1	R1	R2	R3	R4
Baseline situation					
f_s	0.319	0.558	0.588	0.573	0.515
$ECCO_2RT$ combined with protective ventilation (except R1)					
f_s	$0.388 \rightarrow 0.389 \rightarrow 0.397$	0.502	0.759	0.705	0.744

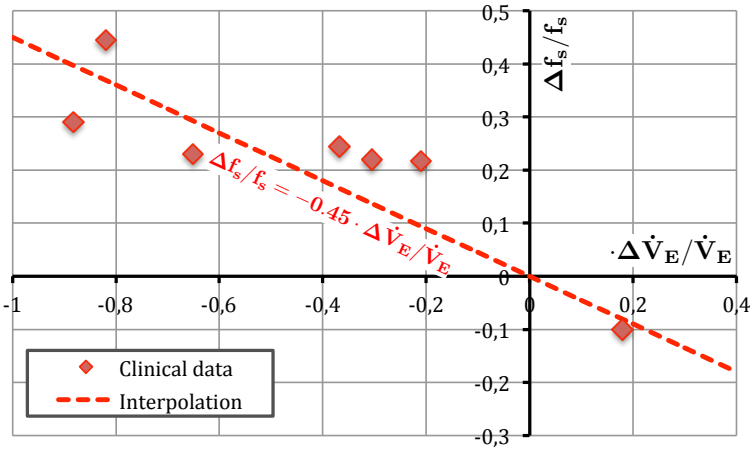

Figure 11.8 – Relative variation of pulmonary shunt $\Delta f_s/f_s$ in terms of relative variation of minute ventilation $\Delta\dot{V}_E/\dot{V}_E$.

Table 11.7 – PCO_2 and PO_2 errors between the simulations and the measurements during ECLS for *clinical trial S* when the dilution is taken into account and when the estimation of parameter f_s is given by equation 11.7. The line m indicates the number of PCO_2 or PO_2 measurements available during ECLST.

Data	CO_2	O_2
$\overline{\lvert\Delta P\rvert}$ (mmHg)	1.37 ± 1.23	3.07 ± 2.84
$\overline{\lvert\Delta P/P\rvert}$	0.04 ± 0.03	0.06 ± 0.05
$\overline{\Delta P}$ (mmHg)	0.15 ± 1.89	0.85 ± 4.23
$\overline{\Delta P/P}$	0.00 ± 0.05	0.03 ± 0.08
m	9	9

Table 11.8 – PCO_2 and PO_2 errors between the simulations and the measurements during ECLS for *clinical trial R* when the dilution is taken into account and when the estimation of parameter f_s is given by equation 11.7. The line m indicates the number of PCO_2 or PO_2 measurements available during ECLST (after the change of ventilator settings).

	CO_2					O_2				
Data	R1	R2	R3	R4	**Mean**	R1	R2	R3	R4	**Mean**
$\overline{\lvert\Delta P\rvert}$ (mmHg)	5.16	5.74	4.50	1.37	**4.19**	12.44	5.80	2.07	2.80	**5.78**
$\overline{\lvert\Delta P/P\rvert}$	0.15	0.11	0.16	0.03	**0.11**	0.13	0.17	0.05	0.08	**0.11**
$\overline{\Delta P}$ (mmHg)	5.16	-5.74	4.50	-0.36	**0.89**	-10.34	-5.80	-2.07	2.80	**-3.85**
$\overline{\Delta P/P}$	0.15	-0.11	0.16	-0.01	**0.05**	-0.09	-0.17	-0.05	0.08	**-0.06**
m	4	2	2	2		4	2	2	2	

11.6 Limitations

Table 11.7 and Table 11.8 show that the errors between the simulations and the experimental data are as small as the errors for pig experiments. Nevertheless, one must keep in mind that several limitations must be emphasized.

Like in the pig experiments, the approximation of equal MR_{CO2} and MR_{O2} is taken (see section 9.4 p. 143). In addition, there is no venous blood sample taken before the ECLST for *clinical trial R* and the value of MR_{CO2} and MR_{O2} are thus estimated during ECLST for these patients. Since the goal of this study is to predict the time evolutions of PCO_2 and PO_2 when the ECLS is switched on, no measurement should be taken during ECLST. Therefore, additional clinical trial should be carried out with venous blood samples taken before the ECLST. These additional data do not requires extra effort from the medical team since a central venous line is often available for patients with these pathological conditions.

The recirculation cannot be neglected for *clinical trial R* since the extracorporeal blood flow is much larger than 1 l/min. However, the value of R_{recir} cannot be estimated with the available clinical data and an empirical relationship is used (see equation 5.13 of subsection 5.3.2 p. 74).

For the clinical trials, the protective ventilation is induced just after the ECLST. Therefore, the goal of the mathematical model is to predict the ECLST but also the protective ventilation. To achieve that goal, one has tried to find the relationship between the relative variation of f_s ($\Delta f_s/f_s$) in terms of the relative variation of $\dot{V}_E$ ($\Delta\dot{V}_E/\dot{V}_E$) and the rela-

tionship between the relative variation of $\dot{V}_A$ ($\Delta\dot{V}_A/\dot{V}_A$) in terms of $\Delta\dot{V}_E/\dot{V}_E$. While the relationship between $\Delta\dot{V}_A/\dot{V}_A$ and $\Delta\dot{V}_E/\dot{V}_E$ seems reasonable ($\Delta\dot{V}_A/\dot{V}_A = \Delta\dot{V}_E/\dot{V}_E$) and this relationship is also valid for the pig experiments, the relationship between $\Delta f_s/f_s$ and $\Delta\dot{V}_E/\dot{V}_E$ is only based on an empirical formula and has been estimated using the clinical data during ECLST. With the aim to increase the validity of the empirical relationship between $\Delta f_s/f_s$ and $\Delta\dot{V}_E/\dot{V}_E$, more clinical data is needed and the additional clinical data could check the linear interpolation which has been presented in Figure 11.8.

The cardiac output was not estimated before the ECLST and an empirical formula have been used to provide an approximation of CO. Even if the accuracy of the CO estimation by echocardiography is weak, this estimation will be irrefutably better than the approximation given by equation 11.3. In addition, taking this value will not change the protocol used in the ICU since an echocardiography is already used to check the localisation of the cannulae in the cardiovasular system.

Finally, the number of measurements is small for *clinical trial R* and, in addition to perform more clinical trials, more blood samples should be drawn during the first hours of ECLST in order to validate the model.

11.7 Summary

The mathematical model of the respiratory system connected to a vv-ECLS has several patient-specific parameters and these parameters have been estimated with clinical data. However, for the clinical trials, the protective ventilation is induced during the ECLST and the new values of f_s and $\dot{V}_A$ cannot be estimated before ECLST. The mathematical model thus estimates these parameters after the change of the ventilator settings without using clinical data during this situation. When all the parameters are identified, the mathematical model can correctly simulate the decrease in PCO_2 and PO_2 during the ECLST.

To validate the mathematical model, the PCO_2 and the PO_2 predictions are compared with clinical data. For the final simulations, the following features are considered:

- the ECLS model is the model Mod 1,
- transport delays are neglected,
- dilution of hemoglobin when the ECLS is switched on is taken into account,

- the value of $\dot{V}_A$ after the change of the ventilator settings is estimated with equation 11.1 and
- the value of f_s after the change of the ventilator settings is estimated with equation 11.7.

The final results show that the agreement between the mathematical simulation and the clinical data is encouraging: the mean relative error $|\overline{\Delta P_{O_2}/P_{O_2}}|$ and $|\overline{\Delta P_{O_2}/P_{O_2}}|$ of all the patients of *clinical trial R* are both equal to 0.11, and $|\overline{\Delta P_{CO_2}/P_{CO_2}}|$ of patient S1 is equal to 0.04 and $|\overline{\Delta P_{O_2}/P_{O_2}}|$ of patient S1 is equal to 0.05. These results could even be better if all the clinical trials followed a stringent protocol such as *clinical trial S*. However, the number of patients and the number of measurements are small and more clinical trials should be carried out to confirm the validation of our mathematical model.

Chapter 12

Conclusion and future work

Extracorporeal life support (ECLS) is already largely used for helping patients suffering from acute heart and/or lung pathologies. When this technology is used in venovenous configuration (vv-ECLS), it ensures vital functions of the lung and, when this device is set up in venoarterial configuration (va-ECLS), it ensures both vital functions of the heart and the lungs. However, clinicians still face several issues with the use of ECLS and new therapeutic approaches could improve the medical care given in the intensive care unit (ICU).

Mathematical models of human physiology become increasingly used to develop unique tools to personalise care in the ICU [22]. These models are elaborated to be subject-specific since the parameters of the model are estimated using clinical data. After a proper validation, the models can be solved in silico to test different clinical approaches or can be used in real-time to provide therapeutic solutions at the patient's bedside [22]. In the present study, such mathematical models have been developed to provide tools which could help clinicians to improve the use of ECLS.

In this final chapter, the content of this thesis is summarized in section 12.1 and the main findings are recalled in section 12.2. The methodology for developing and validating the mathematical models contains of course some limitations, which are summarized in section 12.3. Finally, the long-term prospect of this study, which consists in developing medical tools to improve the therapeutic strategy of patient assisted by ECLS, is presented in section 12.4.

12.1 Summary

This thesis aims to find a solution to overcome two of the main issues related to the use of ECLS. The first one concerns the weaning of va-ECLS. Indeed, the clinicians cannot easily estimate the heart activity when the device is working since, with the venoarterial configuration, the extracorporeal blood flow Q_d decreases the preload and increases the afterload of the heart. Therefore, the medical team decreases progressively Q_d until a value of approximately 0.5 l/min is reached. For this small value, the interaction of the ECLS on the cardiovascular system is minimized and clinicians can estimate the hemodynamics of this system. This approach is called a weaning test. In the present study, a mathematical model has been developed to allow the prediction of the hemodynamics of the cardiovascular system for lower values of Q_d. With this method, an estimation of the essential hemodynamic variables for $Q_d = 0$ l/min can be calculated and the weaning test can thus be performed without reducing Q_d until a value of approximately 0.5 l/min is reached. The second issue concerns the settings of vv-ECLS. Indeed, for a given patient, the clinicians do not know the optimal ventilator and ECLS settings before switching on the vv-ECLS. Therefore, a mathematical model of the respiratory system connected to a vv-ECLS has been developed to allow the predictions of PCO_2 and PO_2 time evolutions. These predictions can be estimated for different ventilator and ECLS settings and, with these results, the optimal ventilator and ECLS settings could be chosen. To provide a potential solution of these two issues, this thesis has been elaborated into 5 main parts and each are summarized below.

Chapter 2 of Part I has introduced a basic description of the cardiovascular and respiratory systems. This chapter has highlighted the important parameters of these systems such as the elastance and the resistance of the cardiovascular system and the alveolar ventilation and the capillary perfusion. The next chapter has introduced the different components and the applications of ECLS. As the previous chapter, Chapter 3 has also highlighted the important parameters of this extracorporeal device such as O_2 and CO_2 diffusion coefficients across the synthetic membrane and the extracorporeal blood flow.

Part II has presented a simple way of modeling the respiratory and cardiovascular systems and ECLS. Chapter 4 has described the relations between pressures and volumes for the passive elements (veins and arteries) and the active element (the heart) of the cardiovascular system. The modeling of va-ECLS hemodynamics has been extremely simplified. The interaction between ECLS and the cardiovascular model is simply modeled as a parameter input. This parameter is the extracorporeal blood flow. Chapter 5 has presented

the equations defining the gas exchanges in the lungs, in the tissues and in the vv-ECLS.

Part III has described the parameter identifications of the cardiovascular and respiratory models and of the ECLS model. Chapter 6 has presented which parameters of the cardiovascular model connected to va-ECLS can be identified with the available measurements in our lab and in the ICU. These parameters are the elastance in the arteries, the stress blood volume, the systemic cardiovascular resistance and two parameters describing the relation between pressures and volumes in the heart (one for the end-diastolic pressure volume relationship and one for the end-systolic pressure volume relationship). These 5 parameters are assumed to vary linearly with Q_d and 10 coefficients describing these linear relationships are estimated with the measurements. The measurements are the mean blood pressure and the pulse blood pressure in the arteries, the mean blood pressure in the veins, the maximum blood volume in the heart and the stroke volume for 3 different Q_d. The 10 coefficients are thus subject-specific. The heart rate is also a parameter of the cardiovascular model and it is directly measured in our lab and in the ICU. The other parameters of the model are considered constant and are taken in the literature. Chapter 7 has presented a simple way to estimate the parameters for the lungs, tissues and vv-ECLS. For the lung, the parameters are the pulmonary shunt and the alveolar ventilation. They are estimated using PO_2 and PCO_2 in arteries. For the tissues, the parameters are MR_{O_2} and MR_{CO_2} defining the consumption of O_2 and the production of CO_2 by the metabolism. The assumption that $MR_{O_2} = MR_{CO_2}$ is taken and MR_{O_2} is estimated using the measurements of O_2 concentrations in arteries and in veins and of cardiac output. For the vv-ECLS, the parameters are the O_2 and CO_2 diffusion coefficients across the synthetic membrane. These coefficients are estimated using the measurements of PO_2 and PCO_2 at the inlet and outlet cannulae. Some parameters do not need to be estimated since they are directly measured. These parameters are the hemoglobin concentration and the cardiac output. Except for the parameter k_{HCO_3} describing the variations between individuals in standard HCO_3 concentration, the parameters related to blood chemistry are considered constant and taken in the literature. The other parameters of the respiratory model are assumed to be proportional to the body weight.

Using the mathematical models with the corresponding parameter identification, the simulations of the cardiovascular system connected to a va-ECLS and of the respiratory system connected to a vv-ECLS can be carried out. Chapter 8 of Part IV discusses the validation of the cardiovascular model during weaning tests from a va-ECLS. This chapter compares the values simulated by the mathematical model with the experimental data related to different Q_d (smaller than the Q_d used for the parameter identification). The

result of this comparison demonstrates that the model is able to reproduce the experimental data. Chapter 9 of Part IV discusses the validation of the respiratory model during the first hours of vv-ECLS therapy. This chapter shows that the PCO_2 values simulated by the mathematical model correspond nicely with the experimental data.

Part V is similar to Part IV except that the simulations are compared to clinical data taken in the ICU. Chapter 10 demonstrates that the model is able to reproduced the clinical data during weaning tests from a va-ECLS. Chapter 11 shows that the PCO_2 and PO_2 values simulated by the mathematical model correspond nicely to the clinical data.

12.2 Main findings

This thesis has presented two new minimal models that can be identifiable using clinical data. Previous models of the cardiovascular system [18, 107, 86, 105, 67, 21, 47, 95, 97, 17] and of the respiratory system [37, 113, 9, 54, 93, 14, 116, 74, 72] have already been published, but this study presents the first subject-specific models describing extracorporeal life support therapies [42, 45, 44]. The two models developed in this thesis are simple enough to be solved with a small computation time and to be used at the patient's bedside. One model describes the cardiovascular system connected to a va-ECLS and the other one describes the respiratory system connected to a vv-ECLS.

The cardiovascular model has been used to predict hemodynamic quantities during the weaning tests from a va-ECLS. The present study has shown that these simulated values are in agreement with experimental data carried out in our lab. In addition, similar analyses have been carried out with clinical data and a similar good agreement was obtained.

The respiratory model has been used to predict PO_2 and PCO_2 values during the first hours of vv-ECLS therapy. For the animal experiments, a new kind of vv-ECLS was used: the extracorporeal CO_2 removal device ($ECCO_2RD$). This device is characterized by a small extracorporeal blood flow and the blood oxygenation is very low with this technology. This thesis has shown that the simulated values of PCO_2 are in agreement with experimental data. In addition, clinical data taken from patients assisted by traditional vv-ECLS and assisted by $ECCO_2RD$ have also been analyzed. The results have demonstrated that the simulated values of PO_2 and PCO_2 are in agreement with the clinical data.

12.3 Limitations

A first validation of both models has been performed and has shown encouraging results. However, experimental and mainly clinical data present several limitations and additional trials should be performed to improve the model validation. These limitations are described in subsection 12.3.1. In addition, with the aim to be simple and identifiable with the available clinical data, the mathematical models are based on several assumptions and some parameters cannot be identified and are taken from literature. These approximations, described in subsection 12.3.2, are also part of the limitations of our work.

12.3.1 Experimental and clinical data

The access to the different measurements is rather delicate in the ICU and even in our lab. Indeed, several experimental and clinical data have weak accuracy and some measurements are not taken continuously such as PCO_2 and PO_2 in arteries and veins. In addition, for the clinical cases, the blood pressures and the left ventricle volumes are not estimated continuously.

The number of pig experiments that were carried out is small: 8 pigs suffering from cardiogenic shock assisted by a va-ECLS, 4 "healthy" pigs assisted by an $ECCO_2R$ therapy and 6 pigs suffering from ARDS assisted by an $ECCO_2R$ therapy. For the experiments using va-ECLS, the weaning tests were performed with only 3 different Q_d for the 3 first pigs. Since the parameter identification needs 3 different Q_d, the prediction of the mathematical model cannot have been analyzed for those pigs. Only the weaning tests carried out on the last pig were performed with more than 8 different Q_d. Additional pig experiments should be considered using a protocol defining weaning tests with as many Q_d as for this pig. In addition, with our experiments, Q_d could not exceed 1.2 l/min. Additional experiments should thus be performed with larger cannulae, which implies larger pigs, in order to increase the highest limit of Q_d (similar experiments have already been presented in the article of Ostadal *et al.* [82]). Concerning the experiments using $ECCO_2RD$, only the first pig suffering from ARDS was subject to different Q_d. For the 5 other pigs of this set of experiments, the ECLS was fixed to only one Q_d during the CO_2 removal therapy. Additional experiments should be carried out with different ECLS and ventilator settings in order to improve the validation of the mathematical model. In addition, only $ECCO_2RD$ was used for the pig experiments and it would be beneficial to carry out also experiments with a traditional vv-ECLS.

Finally, the clinical data that we have considered are taken from retrospective data and additional limitations have been observed. Except for patient $S1$ (see subsection 7.1.2), the clinical trials did not follow a stringent protocol. Therefore, the exact time of the variations of ECLS and ventilator settings were not available. In addition, the values of these settings were not directly fixed. These values are changed several times and only the final fixed values are recorded. As a result, few clinical trials are analyzed in this study. Additional clinical trials with a stringent protocol should thus be carried out.

12.3.2 Model

One of the most limiting hypotheses of our approach is the absence of a description of the cardio-pulmonary controls and regulations. Indeed, for the cardiovascular model, Q_d sharply decreases during weaning tests and the hemodynamics is greatly changed. For the respiratory model, PO_2 increases and PCO_2 steeply decreases when the vv-ECLS is switched on. The variations of PO_2 and PCO_2 have an influence on the cardiovascular system. For instance, hypercapnia and hypoxia induce a reduction of the vascular diameters in the pulmonary circulation [108, 78]. The pulmonary vascular resistance is thus increased and the cardiac output and the pulmonary perfusion can be modified. The variations of PO_2 and PCO_2 can also provoke pulmonary responses by decreasing or increasing the diameters of bronchioles [46] and by decreasing or increasing the tidal volume (if the patient breaths spontaneously, see Section 2.4).

Several parameters are considered constant and are taken from literature. However, some of these parameters could vary between individuals but their estimations are impossible with the available clinical data. For instance, the input and output cardiac valves resistances are considered constant in our model whereas some patients had a replacement of one or two cardiac valves. This could represent a rough approximation since these synthetic valves probably present different hemodynamic properties.

Equally, the models developed in this study could be too simplified. Indeed, lumped models significantly simplify the studied systems and the model elaborated in this study could neglect essential information. For example, the cardiovascular model omits the description of the pulmonary circulation. Our model considers that the heart is only one pump extracting the blood in the vena cava and ejecting the blood in the aorta. This description of the cardiovascular system is a rough approximation since the pulmonary circulation can have a significant influence over the whole circulation. An other example is that the respiratory model omits the mechanics of ventilation. The ventilation is described in our model by only one lumped parameter: the alveolar ventilation $\dot{V}_A$. This

simplification reduces the possible applications of our model in order to improve the therapeutic strategies in the ICU. For instance, the positive end-expiratory pressure (PEEP) is an important ventilator setting and it can increase or decrease $\dot{V}_A$. However, PEEP is not explicitly described in our model but is included in the lumped parameter $\dot{V}_A$. The influence of PEEP on the respiratory system cannot thus be analyzed and optimized using our model.

Finally, the respiratory and cardiovascular systems are modeled separately and no coupling between them is taken into account. Yet, in certain cases, it would be helpful to have a cardio-pulmonary model. For instance, a patient assisted with a va-ECLS can recover a normal cardiac activity without recovering a normal respiratory activity. Therefore, the respiratory model should be added to the cardiovascular model in order to predict the evolution of PO_2 and PCO_2 during weaning tests from va-ECLS. This information could help the clinician with the decision of bridging the patient from va- to vv-ECLS.

12.4 Future work

As already mentioned in the previous section, a first interesting extension of our work would be to perform additional clinical trials with patients assisted with vv- and va-ECLST.

Regarding va-ECLS, the weaning tests should be performed by decreasing Q_d with more intermediate steps. In particular, Q_d used for the parameter identification are not much larger than those used for testing the prediction of the mathematical model. The validation of the cardiovascular model during weaning tests would be stronger if the difference between the 2 sets of Q_d was larger. Another interesting approach would be to perform more than 2 weaning tests for a given patient. With these additional trials, the evolution of the patient's cardiovascular system could be studied and the evolution of the estimated parameters of the model could be analyzed.

After performing additional clinical trials to validate the cardiovascular model connected to a va-ECLS in the ICU, a medical tool could be developed in order to improve the therapeutic strategy used in the ICU. This final goal of the present study is illustrated in Figure 12.1. This figure shows the first version of our computer software estimating different hemodynamic quantities for $Q_d = 0$ l/min. In order to start this va-ECLS simulator, clinicians have to enter the diastolic and systolic blood pressures in the arteries, the

central venous pressure (CVP), the heart rate (HR), the VTI, the diastolic volume in the left ventricle and the diameter of the left ventricular outflow tract (LVOT) related to 3 different Q_d. The upper panel shows the graphic interface before starting the simulation while the bottom panel shows the solution.

Regarding vv-ECLS, the ventilator and ECLS settings are recorded continuously and these data should be saved during the first hours of ECLS therapy. A stringent protocol, like the one already used for the clinical trial $S1$ (see subsection 7.1.2), should be performed to ensure that all the clinical conditions would be respected.

After performing additional clinical trials to validate the respiratory model in the ICU, a medical tool could be developed in order to estimate the adequate ECLS and ventilator settings for a given patient. Figure 12.2 illustrates this final goal with the clinical data of patient $S1$ (see section 11.3). This figure shows the first version of our computer software estimating the stabilized PO_2 and PCO_2 in arteries for different ECLS and ventilator settings. In order to start this va-ECLS simulator, clinicians have to enter the ventilator settings before switching on the ECLS, the features of the gas flow entering the ECLS (F_{ID,O_2} and $\dot{V}_D$), the synthetic membrane used (HLS Set Advanced 5.0 or Quadrox-iD Adult) and several patient parameters (weight, height, cardiac output, PO_2, PCO_2, pH, hemoglobin concentration and hemoglobin saturation in arteries and PO_2 and hemoglobin saturation in veins). The upper panel of Figure 12.2 shows the results for the patient S1. These results demonstrate that an extracorporeal blood flow smaller or equal to 1 l/min is enough for the CO_2 removal of this patient, even for an hyper protective ventilation defined by a tidal volume of 3 ml/kg. This panel also shows that there is no oxygenation of blood when the extracorporeal blood flow increases (note that the irregularity for the isoline PO_2 = 82 mmHg is due to the fact that only 5 different values of tidal volumes and 40 values of extracorporeal blood flow are used to plot the graph). This result is due to the fact that the arterial blood of the patient was already oxygenated and the gas entering the ECLS is atmospheric air. This graph also shows that PO_2 slightly decreases with the increase in tidal volume. This observation is due to the Bohr effect. Indeed, the large decrease in PCO_2 when tidal volume increases induces an alkalosis which modifies the hemoglobin saturation curve. The bottom panel of Figure 12.2 also provides the stabilized PO_2 and PCO_2 in arteries for different ECLS and ventilator settings administered to patient S1 but the gas entering the ECLS is enriched with O_2 (F_{ID,O_2} = 0.9). The PCO_2 in arteries is almost identical to the previous simulation. For the PO_2 in arteries, the estimated values are larger and the PO_2 increases with the increase in the extracorporeal blood flow.

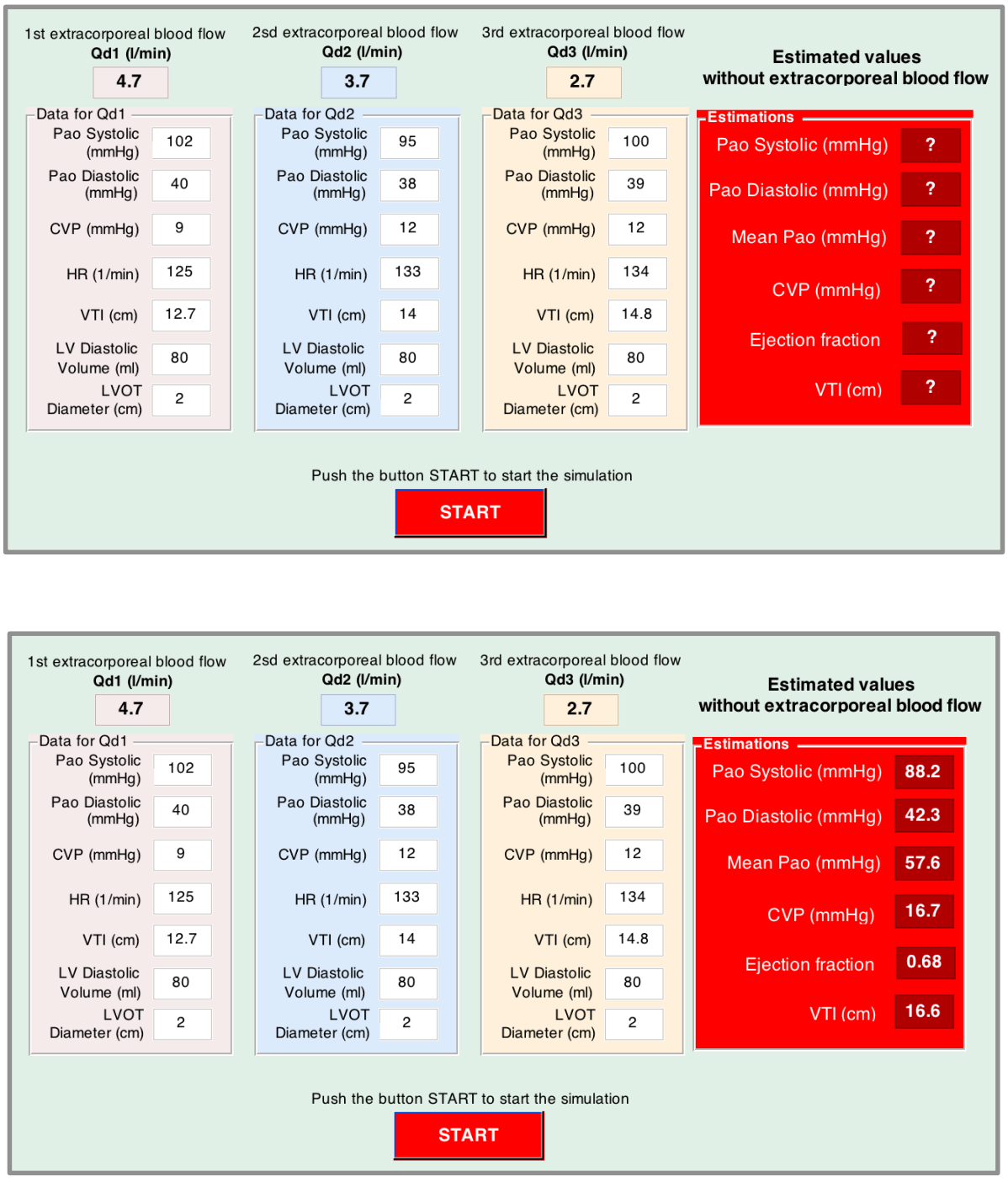

Figure 12.1 – Patient-specific va-ECLS simulator. The clinical data are taken from the weaning test Patient6 T1 (see section 10.4). The upper panel shows the graphic interface before starting the simulation while the bottom panel shows the solution.

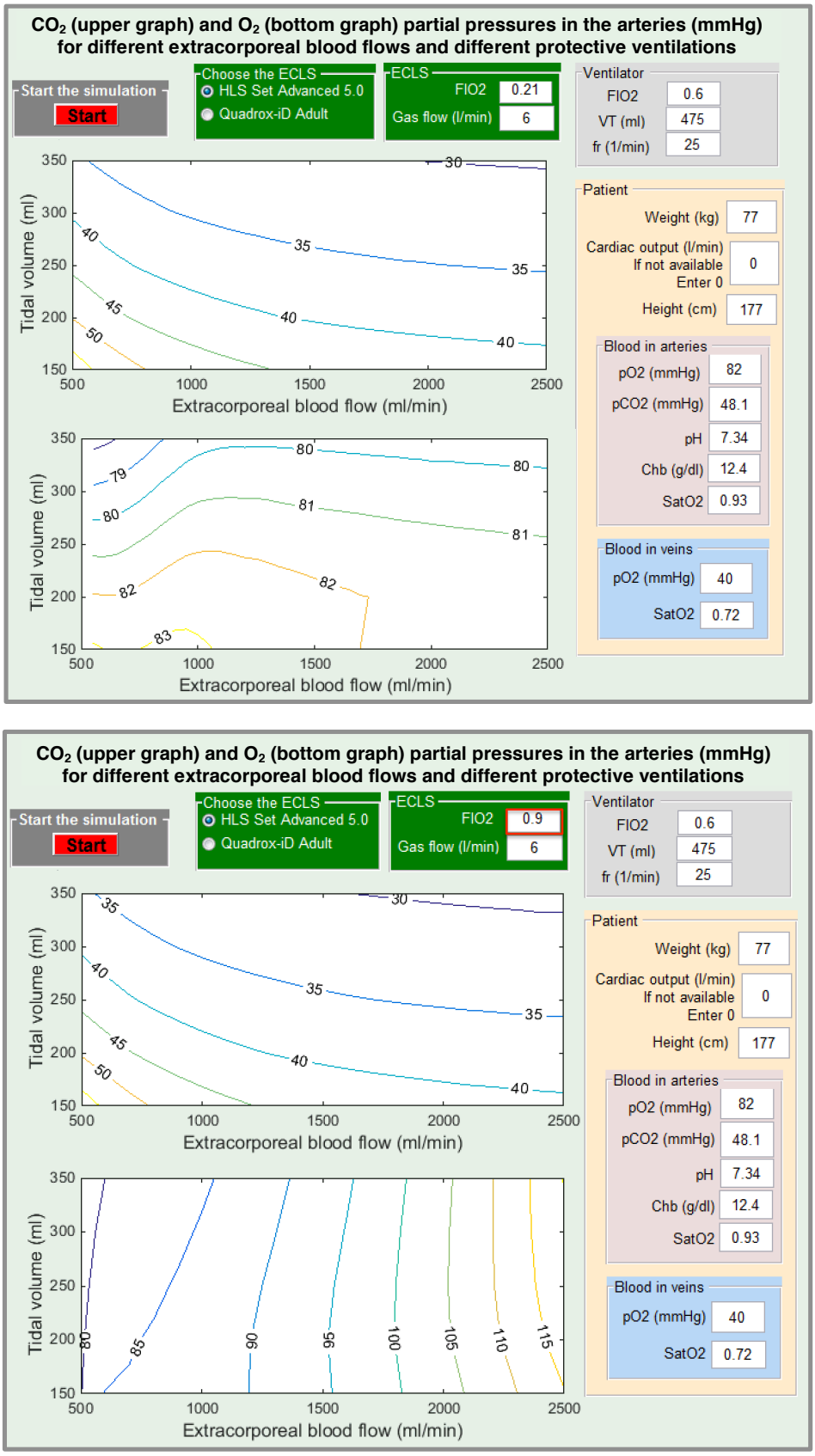

Figure 12.2 – Patient-specific vv-ECLS simulator. The upper panel shows the results for the patient $S1$ (see section 11.3) and the bottom panel shows the results for patient $S1$ if the gas entering the ECLS is enriched with O_2 ($F_{ID,O_2} = 0.9$)

Bibliography

[1] Darryl Abrams, Roberto Roncon-Albuquerque Jr, and Daniel Brodie. What's new in extracorporeal carbon dioxide removal for COPD? *Intensive care medicine*, 41(5):906, 2015.

[2] Admin. Respiratory disease. `https://basicmedicalkey.com/respiratory-disease-4/`, 2017.

[3] Christophe Adrie, Minou Adib-Conquy, Ivan Laurent, Mehran Monchi, Christophe Vinsonneau, Catherine Fitting, François Fraisse, A Tuan Dinh-Xuan, Pierre Carli, Christian Spaulding, et al. Successful cardiopulmonary resuscitation after cardiac arrest as a "sepsis-like" syndrome. *Circulation*, 106(5):562–568, 2002.

[4] Nadia Aissaoui, Aly El-Banayosy, and Alain Combes. How to wean a patient from veno-arterial extracorporeal membrane oxygenation. *Intensive care medicine*, 41(5):902–905, 2015.

[5] Open Anesthesia. Respiratory quotient - energy sources. `https://www.openanesthesia.org/aba_respiratory_quotient_-_energy_sources/`, 2017.

[6] Antonio Anzueto and Luciano Gattinoni. Prone position in ARDS. *Acute Respiratory Distress Syndrome*, 233:313, 2016.

[7] GJ Arthurs and M Sudhakar. Carbon dioxide transport. *Continuing Education in Anaesthesia, Critical Care & Pain*, 5(6):207–210, 2005.

[8] Robert H Bartlett. Extracorporeal life support: history and new directions. In *Seminars in perinatology*, volume 29, pages 2–7. Elsevier, 2005.

[9] J. J. Batzel, F. Kappel, D. Scneditz, and H. T. Tran. *Cardiovascular and respiratory systems: modeling, analysis, and control*, volume 34. SIAM, 2007.

[10] Jerry J Batzel, Franz Kappel, and Susanne Timischl-Teschl. A cardiovascular-respiratory control system model including state delay with application to congestive heart failure in humans. *Journal of mathematical biology*, 50(3):293–335, 2005.

[11] Thomas Bein, Steffen Weber-Carstens, Anton Goldmann, Thomas Müller, Thomas Staudinger, Jörg Brederlau, Ralf Muellenbach, Rolf Dembinski, Bernhard M Graf, Marlene Wewalka, et al. Lower tidal volume strategy (3 ml/kg) combined with extracorporeal CO2 removal versus "conventional" protective ventilation (6 ml/kg) in severe ARDS. *Intensive care medicine*, 39(5):847–856, 2013.

[12] Alona Ben-Tal. Simplified models for gas exchange in the human lungs. *Journal of Theoretical Biology*, 238(2):474 – 495, 2006.

[13] Marcel BONAY1, Romain KESSLER2, and Bruno CRESTANI3. Exploration fonctionnelles respiratoires - splf. `http://www.google.be/url?sa=t&rct=j&q=&esrc=s&source=web&cd=1&cad=rja&uact=8&ved=0CC4QFjAA&url=http%3A%2F%2Fwww.splf.org%2Fs%2Fspip.php%3Faction%3Dacceder_document%26arg%3D2746%26cle%3D892a26500c83bbdad6b8d61bef6282ee2f6bf582%26file%3Ddoc%252FExplorations_Fonctionnelles_Respiratoires_2.doc&ei=gc4-U_fyILDa0QX9qIC4CA&usg=AFQjCNFTJie4nd3GxfR9p4F1STyjlRsr5Q&bvm=bv.64125504,d.d2k`, 2009.

[14] C Brendle, K-F Hackmack, J Kühn, MN Wardeh, T Janisch, R Kopp, R Rossaint, A Stollenwerk, S Kowalewski, B Misgeld, et al. Continuous gas transfer monitoring during extracorporeal membrane oxygenation. *Biomedical Signal Processing and Control*, 31:321–330, 2017.

[15] Daniel Brodie and Matthew Bacchetta. Extracorporeal membrane oxygenation for ARDS in adults. *New England Journal of Medicine*, 365(20):1905–1914, 2011.

[16] Mikael Broman, Bjorn Frenckner, Anna Bjallmark, and Michael Broome. Recirculation during veno-venous extra-corporeal membrane oxygenation-a simulation study. *International Journal of Artificial Organs*, 38(1):23–30, 2015.

[17] Michael Broomé and Dirk W Donker. Individualized real-time clinical decision support to monitor cardiac loading during venoarterial ECMO. *Journal of translational medicine*, 14(1):4, 2016.

[18] DANIEL Burkhoff and JOHN V Tyberg. Why does pulmonary venous pressure rise after onset of lv dysfunction: a theoretical analysis. *American Journal of Physiology-Heart and Circulatory Physiology*, 265(5):H1819–H1828, 1993.

[19] Pedi Cardiology. Icu: postop fontan. `http://www.pedicardiology.net/2012/01/icu-postop-fontan.html`, 2012.

[20] Bartolome R Celli, WATS MacNee, AATS Agusti, Antonio Anzueto, B Berg, A Sonia Buist, Peter MA Calverley, N Chavannes, T Dillard, B Fahy, et al. Standards for the diagnosis and treatment of patients with COPD: a summary of the ats/ers position paper. *European Respiratory Journal*, 23(6):932–946, 2004.

[21] J Geoffrey Chase, Bernard Lambermont, Christina Starfinger, Christopher E Hann, Geoffrey M Shaw, Alexandre Ghuysen, Philippe Kolh, Pierre C Dauby, and Thomas Desaive. Subject-specific cardiovascular system model-based identification and diagnosis of septic shock with a minimally invasive data set: animal experiments and proof of concept. *Physiological measurement*, 32(1):65, 2010.

[22] J Geoffrey Chase, Jean-Charles Preiser, Jennifer L Dickson, Antoine Pironet, Yeong Shiong Chiew, Christopher G Pretty, Geoffrey M Shaw, Balazs Benyo, Knut Moeller, Soroush Safaei, et al. Next-generation, personalised, model-based critical care medicine: a state-of-the art review of in silico virtual patient models, methods, and cohorts, and how to validation them. *Biomedical engineering online*, 17(1):24, 2018.

[23] Pr Bruno Chenuel. Physiologie de la respiration. `http:http://djqmfrancois.free.fr/SEMESTRE2/UE3/Physiologie%20de%20la%20Circulation.pdf`, 2012.

[24] Mabel Chung, Ariel L Shiloh, and Anthony Carlese. Monitoring of the adult patient on venoarterial extracorporeal membrane oxygenation. *The Scientific World Journal*, 2014, 2014.

[25] Benjamin Cuming. Regulation of respiration. `http://intranet.tdmu.edu.ua/data/kafedra/internal/normal_phiz/classes_stud/en/med/lik/2%20course/4%20Cycle%20Physiology%20of%20breathing/02%20%20Regulation%20of%20breathing.htm`, 2004.

[26] Kalyani Dhake. Structure of hemoglobin. `http://www.buzzle.com/articles/structure-of-hemoglobin.html`, 2015.

[27] Anna Dolezalova. *Design of a Model for ECMO*. PhD thesis, Czech technical university in Prague, Poland, 2014.

[28] Pearson Education. Chapter 17 − respiratory system. `http://droualb.faculty.mjc.edu/Course%20Materials/Physiology%20101/Chapter%20Notes/Fall%202011/chapter_16%20Fall%202011.htm`, 2011.

[29] Tone Bull Enger, Alois Philipp, Vibeke Videm, Matthias Lubnow, Alexander Wahba, Marcus Fischer, Christof Schmid, Thomas Bein, and Thomas Müller. Prediction

of mortality in adult patients with severe acute lung failure receiving veno-venous extracorporeal membrane oxygenation: a prospective observational study. *Critical Care*, 18(2):R67, 2014.

[30] Vito Fanelli, Marco V Ranieri, Jordi Mancebo, Onnen Moerer, Michael Quintel, Scott Morley, Indalecio Moran, Francisco Parrilla, Andrea Costamagna, Marco Gaudiosi, et al. Feasibility and safety of low-flow extracorporeal carbon dioxide removal to facilitate ultra-protective ventilation in patients with moderate acute respiratory distress syndrome. *Critical Care*, 20(1):36, 2016.

[31] Niall D Ferguson, Eddy Fan, Luigi Camporota, Massimo Antonelli, Antonio Anzueto, Richard Beale, Laurent Brochard, Roy Brower, Andrés Esteban, Luciano Gattinoni, et al. The berlin definition of ARDS: an expanded rationale, justification, and supplementary material. *Intensive care medicine*, 38(10):1573–1582, 2012.

[32] Micah R Fisher, Paul R Forfia, Elzbieta Chamera, Traci Housten-Harris, Hunter C Champion, Reda E Girgis, Mary C Corretti, and Paul M Hassoun. Accuracy of doppler echocardiography in the hemodynamic assessment of pulmonary hypertension. *American journal of respiratory and critical care medicine*, 179(7):615–621, 2009.

[33] X Garcia, L Mateu, J Maynar, J Mercadal, A Ochagavia, and A Ferrandiz. Estimating cardiac output. utility in the clinical practice. available invasive and non-invasive monitoring. *Medicina Intensiva (English Edition)*, 35(9):552–561, 2011.

[34] Simon Gelman. Venous function and central venous pressure: a physiologic story. *Anesthesiology*, 108(4):735–748, 2008.

[35] David F. Katz George A. Truskey, Fan Yuan. *Transport Phenomena in Biological Systems*. Pearson Prentice Hall Bioengineering, 2004.

[36] E Gnaiger. Calculation of energetic and biochemical equivalents of respiratory oxygen consumption. In *Polarographic oxygen sensors*, pages 337–345. Springer, 1983.

[37] Fred S Grodins, June Buell, and Alex J Bart. Mathematical analysis and digital simulation of the respiratory control system. Technical report, DTIC Document, 1967.

[38] Maquet Getinge Group. Coming soon: Low flow CO2 removal – PALP cardiohelp system. `http://www.ventilacionanestesiapediatrica.com/site/PDF/PALP.pdf`, 2017.

[39] Maquet Getinge Group. Extracorporeal life support PLS system. https://www.maquet.com/globalassets/downloads/products/pls-system/pls_system_mcp_br_10066_en_1_screen.pdf, 2017.

[40] Maquet Getinge Group. HLS set advanced integration meets innovation. https://www.maquet.com/globalassets/downloads/products/hls-set-advanced/hls_set_advanced_mcp_br_10039_en_1_screen.pdf, 2017.

[41] Hervé Guénard. *Physiologie humaine (chapitre 7: la respiration)*. Wolters Kluwer France, 2001.

[42] Simon Habran, Th Desaive, Ph Morimont, Bernard Lambermont, and Pierre C Dauby. Importance of metabolism variations in a model of extracorporeal carbon dioxide removal. In *Engineering in Medicine and Biology Society (EMBC), 38th Annual International Conference of the IEEE*, pages 4264–4267. IEEE, 2016.

[43] Simon Habran, Th Desaive, Ph Morimont, Bernard Lambermont, and Pierre C Dauby. A mathematical model of respiration under protective ventilation and extracorporeal CO2 removal therapy. In *Virtual Physiological Human Conference 2016*. VPH, 2016.

[44] Simon Habran, Th Desaive, Ph Morimont, Bernard Lambermont, and Pierre C Dauby. Minimal model of cardiovascular system assisted by a veno-arterial extracorporeal membrane oxygenation. In *44th ESAO and 7th IFAO-Congress*. ESAO, 2017.

[45] Simon Habran, Thomas Desaive, Philippe Morimont, Bernard Lambermont, and Pierre Dauby. Mathematical modeling of extracorporeal co2 removal therapy. *Medical & Biological Engineering & Computing*, 56(3):421–434, 2018.

[46] Guyton & Hall. *Textbook of Medical Physiology*. Elsevier (Eleventh Edition), 2006.

[47] Christopher E Hann, J Geoffrey Chase, Thomas Desaive, CB Froissart, J Revie, D Stevenson, Bernard Lambermont, Alexandre Ghuysen, Philippe Kolh, and Geoffrey M Shaw. Unique parameter identification for cardiac diagnosis in critical care using minimal data sets. *Computer methods and programs in biomedicine*, 99(1):75–87, 2010.

[48] Ian A Herrick, Lois K Champion, and Alison B Froese. A clinical comparison of indices of pulmonary gas exchange with changes in the inspired oxygen concentration. *Canadian journal of anaesthesia*, 37(1):69–76, 1990.

[49] Sandra T Hinski. *Respiratory Care Clinical Competency Lab Manual (chapter 23)*. Elsevier Health Sciences, 2014.

[50] Peter J. Hunter, Andrew J. Pullan, and Bruce H. Smaill. Modeling total heart function. *Annual Review of Biomedical Engineering*, 5(1):147–177, 2003. PMID: 14527312.

[51] National Cancer Institute. Small cell lung cancer treatment (pdq) - patient version. `https://www.cancer.gov/types/lung/patient/small-cell-lung-treatment-pdq`, 2016.

[52] Yadav Jai. 2015 arterial blood pressure monitoring. `http://omronbloodpressuremonitorpictures.blogspot.be/2015/01/2015-arterial-blood-pressure-monitoring.html`, 2015.

[53] Christian Karagiannidis, Kristin Aufm Kampe, Fernando Suarez Sipmann, Anders Larsson, Goran Hedenstierna, Wolfram Windisch, and Thomas Mueller. Veno-venous extracorporeal CO2 removal for the treatment of severe respiratory acidosis: pathophysiological and technical considerations. *Crit Care*, 18(3):R124, 2014.

[54] D. S. Karbing, S. Kjaergaard, S. Andreassen, K. Espersen, and S. E. Rees. Minimal model quantification of pulmonary gas exchange in intensive care patients. *Med Eng Phys*, 33(2):240–8, 2011.

[55] Dan S Karbing, Søren Kjærgaard, Bram W Smith, Charlotte Allerød, Kurt Espersen, Steen Andreassen, and Stephen E Rees. Decision support of inspired oxygen fraction using a model of oxygen transport. *IFAC Proceedings Volumes*, 41(2):8080–8084, 2008.

[56] David A Kass, W Lowell Maughan, Z Mao Guo, Alan Kono, Kenji Sunagawa, and Kiichi Sagawa. Comparative influence of load versus inotropic states on indexes of ventricular contractility: experimental and theoretical analysis based on pressure-volume relationships. *Circulation*, 76(6):1422–1436, 1987.

[57] James Keener and James Sneyd. *Mathematical Physiology: Systems Physiology*. Springer, 2011.

[58] Roy C. P. Kerckhoffs, Maxwell L. Neal, Quan Gu, James B. Bassingthwaighte, Jeff H. Omens, and Andrew D. McCulloch. Coupling of a 3d finite element model of cardiac ventricular mechanics to lumped systems models of the systemic and pulmonic circulation. *Annals of Biomedical Engineering*, 35(1):1–18, 2007.

[59] Go Woon Kim, Eun Young Choi, and Sang Bum Hong. The treatment of adult respiratory distress syndrome (ards) using extracorporeal membrane oxygenation (ECMO). *Tuberculosis and Respiratory Diseases*, 72(1):1–7, 2012.

[60] R. Klabunde. *Cardiovascular physiology concepts*. Lippincott Williams & Wilkins, 2005.

[61] Richard E. Klabunde. Effects of preload, afterload and inotropy on ventricular pressure-volume loops. `http://www.cvphysiology.com/Cardiac%20Function/CF025`, 2015.

[62] Richard E. Klabunde. Ventricular compliance. `http://www.cvphysiology.com/Cardiac%20Function/CF014`, 2016.

[63] Stephanie Klinzing, Urs Wenger, Peter Steiger, Christoph Thomas Starck, Markus Wilhelm, Reto A Schuepbach, and Marco Maggiorini. External validation of scores proposed for estimation of survival probability of patients with severe adult respiratory distress syndrome undergoing extracorporeal membrane oxygenation therapy: a retrospective study. *Critical Care*, 19(1):142, 2015.

[64] Philippe Kolh. *Cours de physiologie des systèmes*. Presses universitaires de Liège, 2009.

[65] Wilbur YW Lew. Time-dependent increase in left ventricular contractility following acute volume loading in the dog. *Circulation research*, 63(3):635–647, 1988.

[66] Oscar A Linares, William E Schiesser, Jeffrey Fudin, Thien C Pham, Jeffrey J Bettinger, Roy O Mathew, and Annemarie L Daly. In silico ordinary differential equation/partial differential equation hemodialysis model estimates methadone removal during dialysis. *Journal of pain research*, 8:417, 2015.

[67] K Lu, JW Clark, FH Ghorbel, DL Ware, and A Bidani. A human cardiopulmonary system model applied to the analysis of the valsalva maneuver. *American Journal of Physiology-Heart and Circulatory Physiology*, 281(6):H2661–H2679, 2001.

[68] S Magder. Hemodynamic monitoring: Guyton at the bedside. `http://www.criticalcarecanada.com/presentations/2012/guyton_at_the_bedside.pdf`, 2012.

[69] MedlinePlus. Cardiogenic shock. `https://medlineplus.gov/ency/article/000185.htm`, 2017.

[70] MedlinePlus. Septic shock. https://medlineplus.gov/ency/article/000668.htm, 2017.

[71] Medtronic, editor. *Cardiovascular cannula products*. Medtronic, 2009.

[72] Elmi Messai, Abdesselam Bouguerra, Guy Harmelin, Gabriella Di Lascio, Manuela Bonizzoli, and Massimo Bonacchi. A numerical model of blood oxygenation during veno-venous ECMO: analysis of the interplay between blood oxygenation and its delivery parameters. *Journal of clinical monitoring and computing*, 30(3):327–332, 2016.

[73] Ronald D. Miller, Lars I. Eriksson, Lee A Fleisher, Jeanine P. Wiener-Kronish, Neal H Cohen, and William L. Young. *Miller's anesthesia*. Elsevier Health, 2015.

[74] Berno J E Misgeld. Automatic control of the heart-lung machine. *Ruhr-Universität Bochum, Diss*, 2006.

[75] Philippe Morimont, Andriy Batchinsky, and Bernard Lambermont. Update on the role of extracorporeal CO2 removal as an adjunct to mechanical ventilation in ARDS. *Critical Care*, 19(1):1, 2015.

[76] Philippe Morimont, Julien Guiot, Thomas Desaive, Vincent Tchana-Sato, Nathalie Janssen, Dominique Hella, Francine Blaffart, Jean Defraigne, and Bernard Lambermont. Veno-venous extracorporeal CO2 removal improves pulmonary hemodynamics in a porcine ARDS model. *Acta Anaesthesiologica Scandinavica*, 59(4):448–456, 2015.

[77] Philippe Morimont, Bernard Lambermont, Pierre Dauby, and Thomas Desaive. Supernova meeting. Private meeting organized in the University Hospital of Liège, 2018.

[78] Rohit Moudgil, Evangelos D Michelakis, and Stephen L Archer. Hypoxic pulmonary vasoconstriction. *Journal of Applied Physiology*, 98(1):390–403, 2005.

[79] J W Mulholland, W Massey, and J C Shelton. Investigation and quantification of the blood trauma caused by the combined dynamic forces experienced during cardiopulmonary bypass. *Perfusion*, 15(6):485–494, 2000.

[80] NImedical. Cardiac output. http://www.ni-medical.com/clinical-applications/cardiac-output/.

[81] European Society of Intensive Care Medicine. Supernova: A strategy of ultraprotective lung ventilation with extracorporeal co2 removal for new-onset moderate to severe ards. `http://www.esicm.org/research/trials-group/supernova`, 2016.

[82] Petr Ostadal, Mikulas Mlcek, Andreas Kruger, Pavel Hala, Stanislav Lacko, Martin Mates, Dagmar Vondrakova, Tomas Svoboda, Matej Hrachovina, Marek Janotka, et al. Increasing venoarterial extracorporeal membrane oxygenation flow negatively affects left ventricular performance in a porcine model of cardiogenic shock. *Journal of translational medicine*, 13(1):266, 2015.

[83] Sabine Paeme. *Mathematical modeling of the mitral valve. From local to global hemodynamics*. PhD thesis, University of Liège, Liège, Belgium, 2014.

[84] Thore H Pedersen, Vibeke Videm, Jan L Svennevig, Harald Karlsen, Randi Wolden Østbakk, Øystein Jensen, and Tom Eirik Mollnes. Extracorporeal membrane oxygenation using a centrifugal pump and a servo regulator to prevent negative inlet pressure. *The Annals of thoracic surgery*, 63(5):1333–1339, 1997.

[85] Francois Péronnet, Denis Massicotte, et al. Table of nonprotein respiratory quotient: an update. *Can J Sport Sci*, 16(1):23–29, 1991.

[86] Antoine Pironet. *Model-based prediction of the response to vascular filling therapy*. PhD thesis, University of Liège, Liège, Belgium, 2016.

[87] Antoine Pironet, Pierre C Dauby, J Geoffrey Chase, Philippe Morimont, Nathalie Janssen, Bernard Lambermont, S Davidson, and Thomas Desaive. A comparison between four techniques to measure cardiac output. In *Engineering in Medicine and Biology Society (EMBC), 2016 IEEE 38th Annual International Conference of the*, pages 2717–2720. IEEE, 2016.

[88] Antoine Pironet, Pierre C Dauby, Philippe Morimont, Nathalie Janssen, J Geoffrey Chase, Shaun Davidson, and Thomas Desaive. Model-based decision support algorithm to guide fluid resuscitation. *IFAC-PapersOnLine*, 49(5):224–229, 2016.

[89] Antoine Pironet, Paul D Docherty, Pierre C Dauby, J Geoffrey Chase, and Thomas Desaive. Practical identifiability analysis of a minimal cardiovascular system model. *Computer methods and programs in biomedicine*, 2017.

[90] MSE (Australia) PL. ECMO simulation user manual (v5.4). `http://www.ecmosimulation.com/User_Manual/index.html?vv_ecmo_1.htm`, 2010.

[91] Joseph A. Potkay. The promise of microfluidic artificial lungs. *Lab Chip*, 14:4122–4138, 2014.

[92] Mieynn Ramsed. Lung volumes and capacities. `https://fr.slideshare.net/mieynnsara/lung-volumes-and-capacities-35398112`, 2014.

[93] Stephen Edward Rees, Søren Kjærgaard, Per Thorgaard, Jerzy Malczynski, Egon Toft, and Steen Andreassen. The automatic lung parameter estimator (alpe) system: Non-invasive estimation of pulmonary gas exchange parameters in 10-15 minutes. *Journal of clinical monitoring and computing*, 17(1):43–52, 2002.

[94] Stephen Edward Rees, Elise Klæstrup, Jonathan Handy, Steen Andreassen, and Søren Risom Kristensen. Mathematical modelling of the acid-base chemistry and oxygenation of blood: a mass balance, mass action approach including plasma and red blood cells. *European journal of applied physiology*, 108(3):483–494, 2010.

[95] James A Revie, David J Stevenson, J Geoffrey Chase, Christopher E Hann, Bernard C Lambermont, Alexandre Ghuysen, Philippe Kolh, Geoffrey M Shaw, Stefan Heldmann, and Thomas Desaive. Validation of subject-specific cardiovascular system models from porcine measurements. *Computer methods and programs in biomedicine*, 109(2):197–210, 2013.

[96] Abraham Rudolph. *Congenial Diseases of the Heart Clinical-Physiological Consideration*. Wiley-Blackwell, 2009.

[97] Daniel Rüschen, Miriam Rimke, Jonas Gesenhues, Steffen Leonhardt, and Marian Walter. Online cardiac output estimation during transvalvular left ventricular assistance. *Computer methods and programs in biomedicine*, 2016.

[98] Tanaka Sachiko, Hayashi Terumi, Kihara Yasuki, Takenaka Katsu, Akaishi Makoto, Ito Hiroshi, Ishizuka Naoko, Ohte Nobuyuki, Otsuji Yutaka, Fukuda Nobuo, Mikami Taisei, and Mizushige Katsufumi. Standard measurement of cardiac function indexes. *Journal of Medical Ultrasonics*, 33:123–127, 2006.

[99] Fabio Sangalli, Nicolò Patroniti, and Antonio Pesenti. *ECMO-extracorporeal life support in adults*. Springer, 2014.

[100] Eva Sawheny, Ashley L. Ellis, and Gary T. Kinasewitz. Iloprost improves gas exchange in patients with pulmonary hypertension and ARDS. *Chest*, 144(1):55 – 62, 2013.

[101] David Sidebotham, Sara Jane Allen, Alastair McGeorge, Nathan Ibbott, and Timothy Willcox. Venovenous extracorporeal membrane oxygenation in adults: practical aspects of circuits, cannulae, and procedures. *Journal of cardiothoracic and vascular anesthesia*, 26(5):893–909, 2012.

[102] Stefan Silbernagl and Agamemnon Despopoulos. *Color Atlas of Physiology*. Thieme, 2009.

[103] AP Simons, EGHJ Martens, YM Ganushchak, and PW Weerwind. Centrifugal pump performance during low-flow extracorporeal co2 removal; safety considerations. *Perfusion*, 30(1):17–23, 2015. PMID: 24919405.

[104] Michael C Sklar, Francois Beloncle, Christina M Katsios, Laurent Brochard, and Jan O Friedrich. Extracorporeal carbon dioxide removal in patients with chronic obstructive pulmonary disease: a systematic review. *Intensive care medicine*, 41(10):1752–1762, 2015.

[105] Bram W. Smith. *Minimal Haemodynamic Modelling of the Heart & Circulation for Clinical Application*. PhD thesis, University of Canterbury, Christchurch, New Zealand, 2004.

[106] Bram W. Smith, J.Geoffrey Chase, Roger I. Nokes, Geoffrey M. Shaw, and Graeme Wake. Minimal haemodynamic system model including ventricular interaction and valve dynamics. *Medical Engineering & Physics*, 26(2):131 – 139, 2004.

[107] Christina Starfinger. *Patient-specific modelling of the cardiovascular system for diagnosis and therapy assistance in critical care*. PhD thesis, University of Canterbury. Mechanical Engineering, 2008.

[108] Milan Stengl, Lenka Ledvinova, Jiri Chvojka, Jan Benes, Dagmar Jarkovska, Jaromir Holas, Patrik Soukup, Jitka Sviglerová, and Martin Matejovic. Effects of clinically relevant acute hypercapnic and metabolic acidosis on the cardiovascular system: an experimental porcine study. *Critical Care*, 17(6):R303, 2013.

[109] Hiroyuki Suga, Kiichi Sagawa, and Artin A Shoukas. Load independence of the instantaneous pressure-volume ratio of the canine left ventricle and effects of epinephrine and heart rate on the ratio. *Circulation research*, 32(3):314–322, 1973.

[110] Pierpaolo Terragni, Giorgia Maiolo, and V Marco Ranieri. Role and potentials of low-flow CO2 removal system in mechanical ventilation. *Current opinion in critical care*, 18(1):93–98, 2012.

[111] Transonic. Pv catheter positioning guide. https://www.transonic.com/resources/research/csd-2-03-pv-catheter-positioning-guide/, 2017.

[112] Transonic. Scisense pressure catheters. https://www.transonic.com/resources/research/pressure-catheters-brochure/, 2017.

[113] TJ Trueb, NS Cherniack, AF D'souza, and AP Fishman. A mathematical model of the controlled plant of the respiratory system. *Biophysical journal*, 11(10):810–834, 1971.

[114] Willem van Meurs. *Modeling and simulation in biomedical engineering*. Mc Graw Hill, 2004.

[115] Johan Verbraecken, Paul Van de Heyning, Wilfried De Backer, and Luc Van Gaal. Body surface area in normal-weight, overweight, and obese adults. A comparison study. *Metabolism*, 55(4):515 – 524, 2006.

[116] Marian Walter, Sören Weyer, Andre Stollenwerk, Rüdger Kopp, Jutta Arens, and Steffen Leonhardt. A physiological model for extracorporeal oxygenation controller design. In *Engineering in Medicine and Biology Society (EMBC), 2010 Annual International Conference of the IEEE*, pages 434–437. IEEE, 2010.

[117] John B West. *Ventilation/blood flow and gas exchange*. Oxford: Blackwell, 1977.

[118] Nicolaas Westerhof, Nikos Stergiopulos, and Mark IM Noble. *Snapshots of hemodynamics: an aid for clinical research and graduate education*. Springer Science & Business Media, 2010.

[119] Wilson. Circulatory system. https://www.studyblue.com/notes/note/n/circulatory-system/deck/6192406, 2013.

[120] Yongjie Zhang and Chandrajit Bajaj. Finite element meshing for cardiac analysis. *Univ. of Texas at Austin: ICES Technical Report*, 2004.

Part VI

Appendix

Appendix A

Decrease in MR_{O_2} and MR_{CO_2} with temperature

The detailed analysis of the temperature dependence of metabolism is not the purpose of the present paper since the final goal of our approach is to develop a model to be used in the ICU, where temperature is controlled and kept constant. However, in the animal experiments to which the model was compared, the temperature of the animals was decreasing. It was thus necessary to take this effect into account to obtain a good validation of the model, but given our final purpose, a rather rough description of the temperature changes is sufficient.

The decrease in temperature in the experiments during the ECCO$_2$RT is illustrated in Figure A.1 for 3 pigs (for the other pigs, the temperature has not been recorded). Unfortunately it was not possible to estimate the corresponding decrease in parameters MR_{O_2} and MR_{CO_2}. Indeed, the estimation of these parameters requires stabilized (i.e. time independent) data (see subsection 7.2.3), which were not available in the experiments during the ECCO$_2$RT.

To study the metabolism changes with temperature, we made a retrospective analysis of other experiments carried out in our lab (see [88]), for which appropriate data were available. The composition of the gas expired out the ventilator has been recorded continuously for two pigs (pig 1 and pig 2). In a stabilized situation, the CO_2 production by metabolism is equal to the CO_2 extraction by the ventilator and we can write the following equation:

$$MR_{\mathrm{CO}_2} = \dot{V}_A \cdot F_{E,\mathrm{CO}_2}, \tag{A.1}$$

where F_{E,CO_2} is the end tidal CO_2 volume fraction and $\dot{V}_A$ is estimated from the tidal volume and the respiratory frequency given by the ventilator and an assumed dead space fixed equal to 30% of the tidal volume [49]. The O_2 consumption (MR_{O_2}) can be estimated similarly. Figure A.2 and Figure A.3 show the time evolutions of MR_{CO_2} and MR_{O_2} and the time evolution of temperature for the two pigs. We observe on these figures that the temperature, MR_{O_2} and MR_{CO_2} decrease linearly. The decrease in MR_{O_2} and MR_{CO_2} are similar (a little bit larger for MR_{O_2}). Therefore, we use the slope of the linear interpolation of MR_{CO_2}, MR_{O_2} and that of the linear interpolation of the temperature to estimate the decrease in the metabolism production rates with temperature. For pig 1, the rates found are of 0.0138 l/min/°C and 0.0213 l/min/°C for MR_{CO_2} and MR_{O_2} respectively and, for pig 2, the rates found are of 0.0125 l/min/°C and 0.0275 l/min/°C for MR_{CO_2} and MR_{O_2} respectively. The mean value is taken (0.0188 l/min/°C). Then from Figure A.1, we can calculate a mean time rate of change for the temperature of the animals used in the experiments, and we found the value 0.0255°C/min. Finally, from this value and from the value of the metabolism rate of change with temperature, we deduce the following estimation of the time rate of change of metabolism production rates in the experiments: 4.78×10^{-4} l/min^2. This value was used in our simulations for all animals.

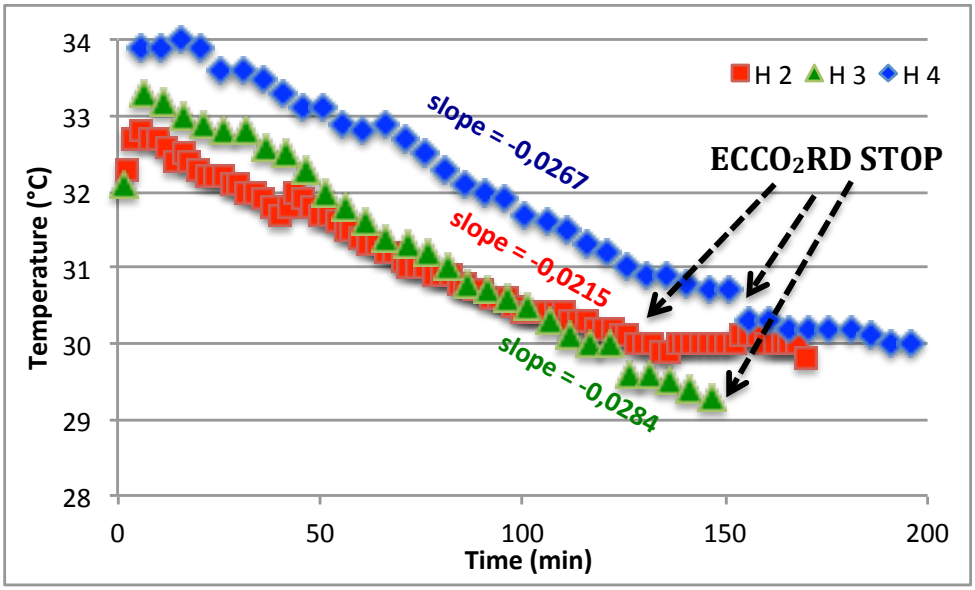

Figure A.1 – Decrease in temperature for 3 pigs (H2, H3 and H4) when the $ECCO_2RD$ is switched on.

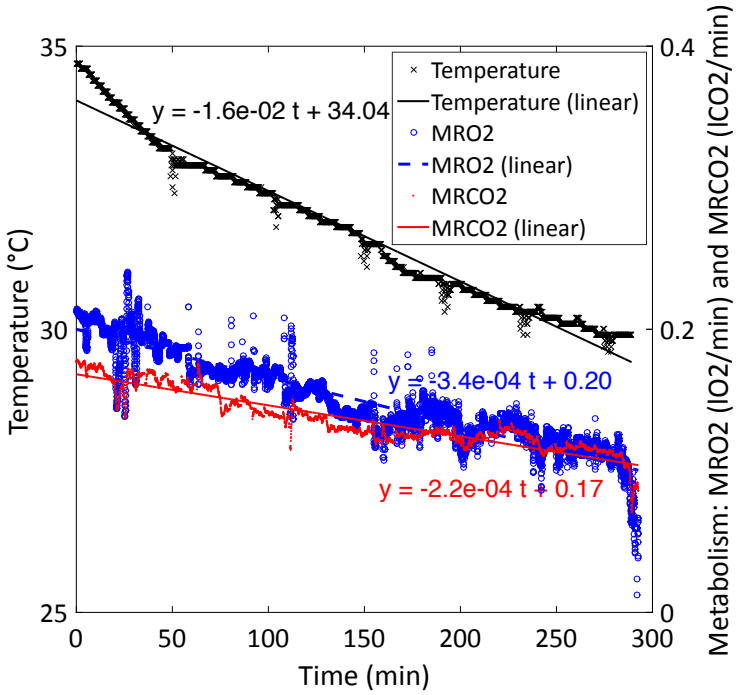

Figure A.2 – Time evolution of MR_{CO_2} and MR_{O_2} and time evolution of temperature for pig 1.

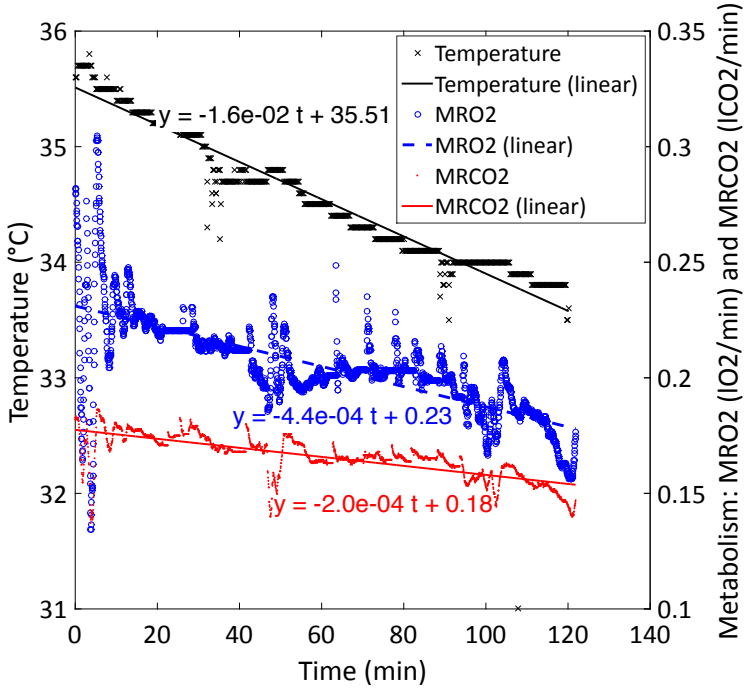

Figure A.3 – Time evolution of MR_{CO_2} and MR_{O_2} and time evolution of temperature for pig 2.

Appendix B

Additional tables and figures

B.1 Pig experiments with a va-ECLS

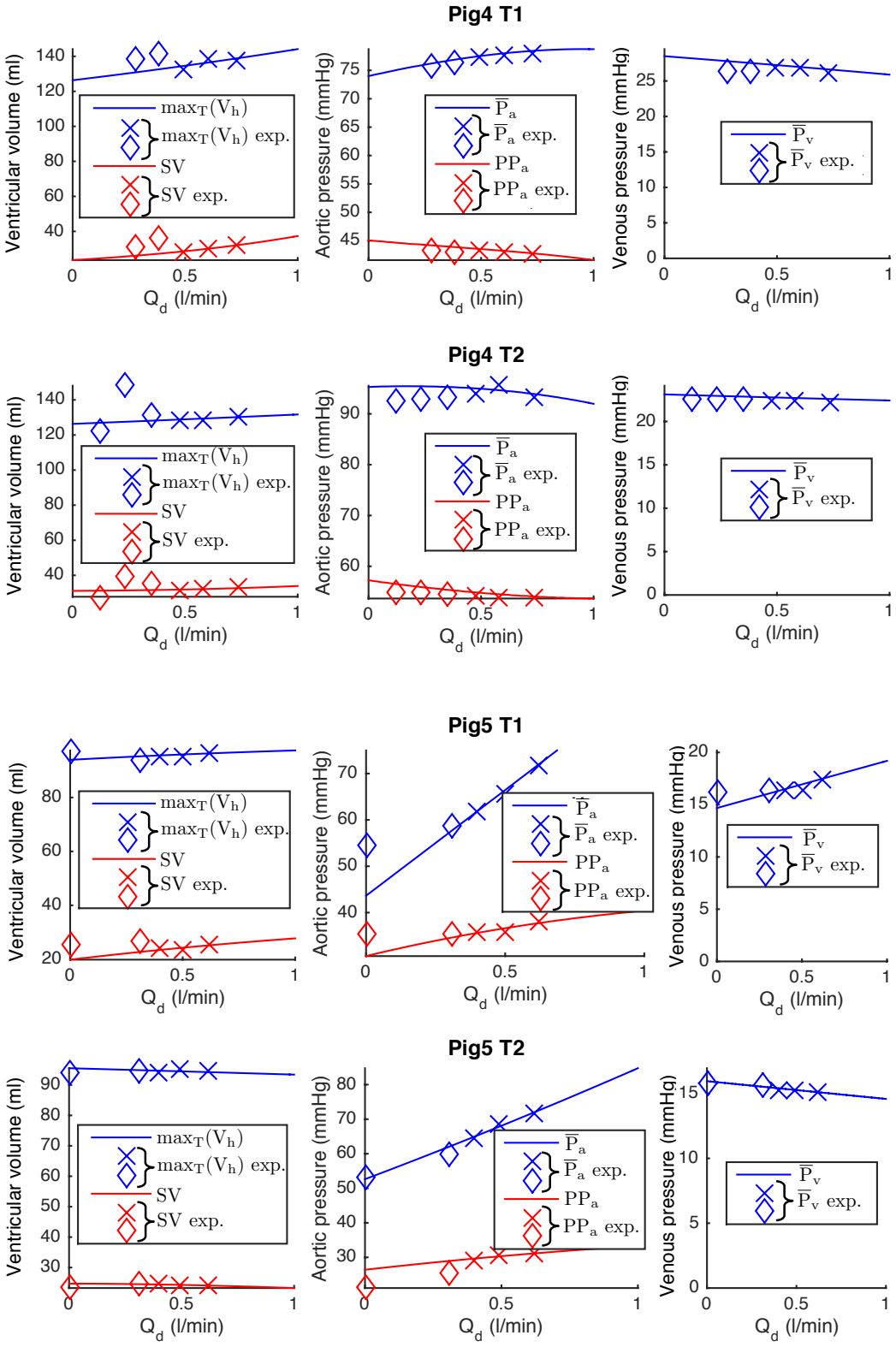

Figure B.1 – Evolution of $\overline{P}_a$, PP_a, $\overline{P}_v$, $\max_T(V_h)$ and SV in terms of different Q_d for the weaning tests Pig4 T1, Pig4 T2, Pig5 T1 and Pig5 T2. The solid lines are the simulations and the crosses and diamonds are the experimental data (the difference between diamonds and crosses has already been explained in Figure 8.1.)

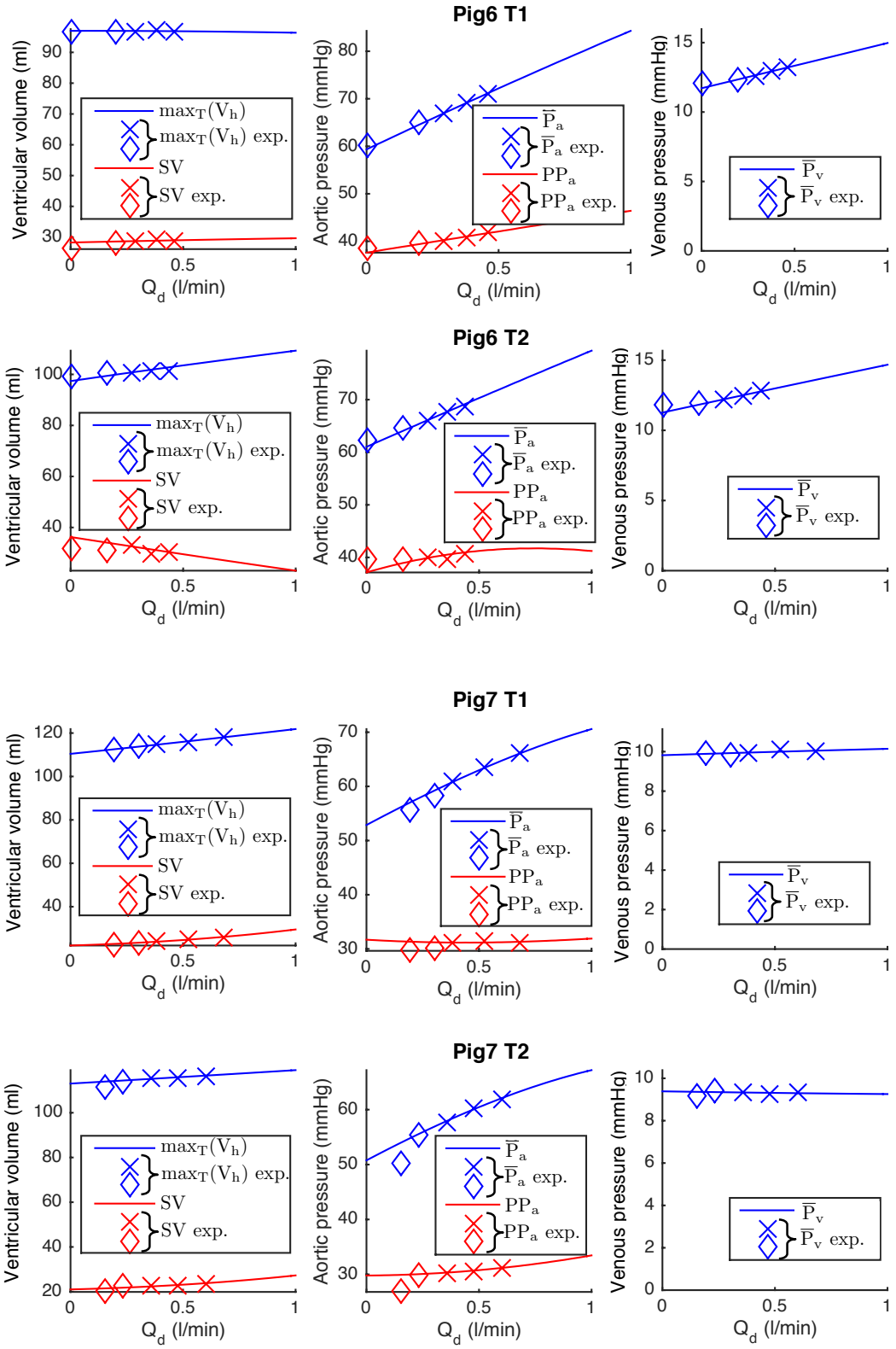

Figure B.2 – Evolution of $\overline{P}_a$, PP_a, $\overline{P}_v$, $\max_T(V_h)$ and SV in terms of different Q_d for the weaning tests Pig6 T1, Pig6 T2, Pig7 T1 and Pig7 T2. The solid lines are the simulations and the crosses and diamonds are the experimental data (the difference between diamonds and crosses has already been explained in Figure 8.1.)

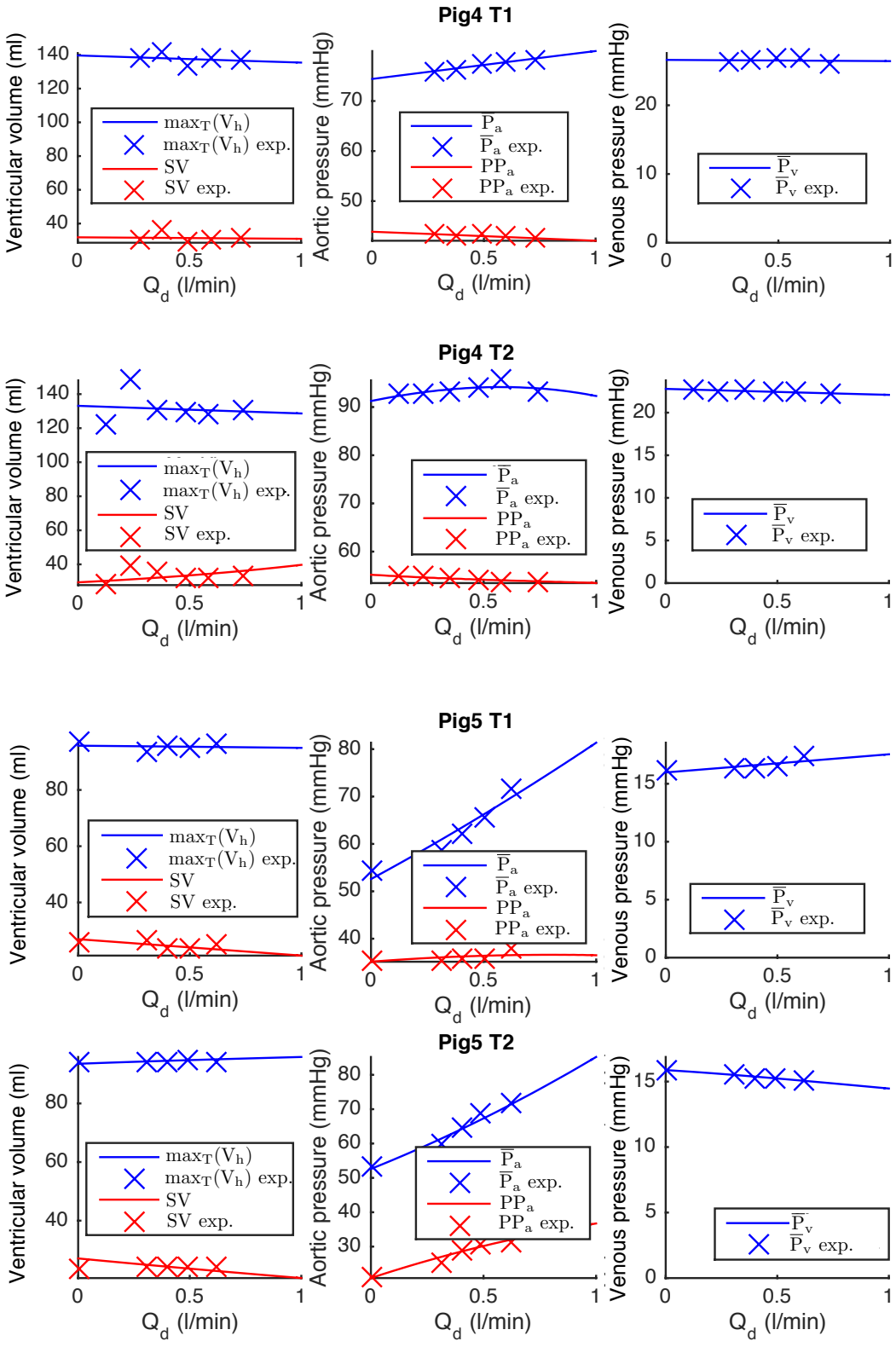

Figure B.3 – Evolution of $\overline{P}_a$, PP_a, $\overline{P}_v$, $\max_T(V_h)$ and SV in terms of different Q_d for the weaning tests Pig4 T1, Pig4 T2, Pig5 T1 and Pig5 T2. The solid lines are the simulations obtained with the parameter identification using the measurements related to all Q_d and the crosses are the experimental data.

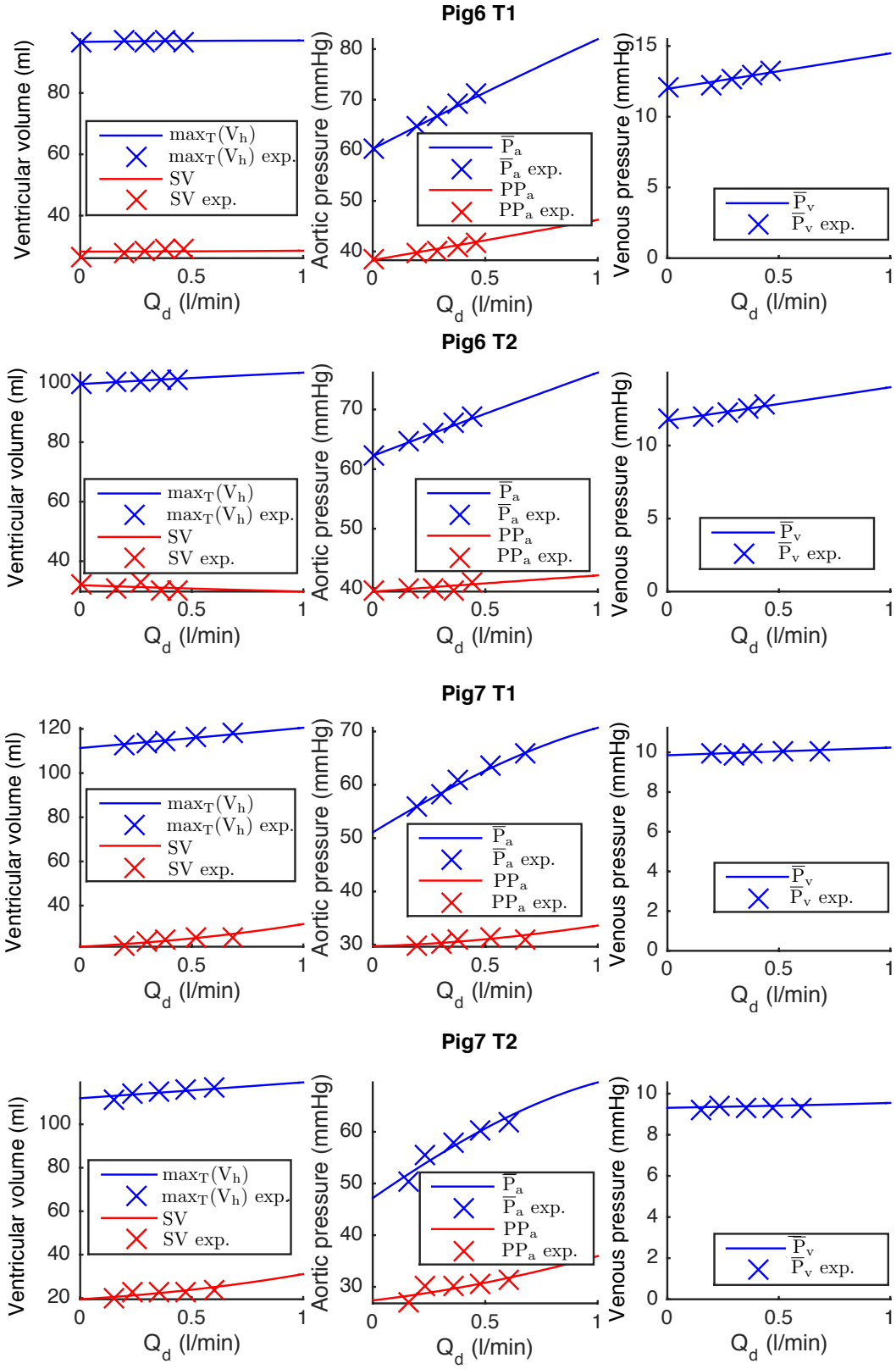

Figure B.4 – Evolution of $\overline{P}_a$, PP_a, $\overline{P}_v$, $\max_T(V_h)$ and SV in terms of different Q_d for the weaning tests Pig6 T1, Pig6 T2, Pig7 T1 and Pig7 T2. The solid lines are the simulations obtained with the parameter identification using the measurements related to all Q_d and the crosses are the experimental data.

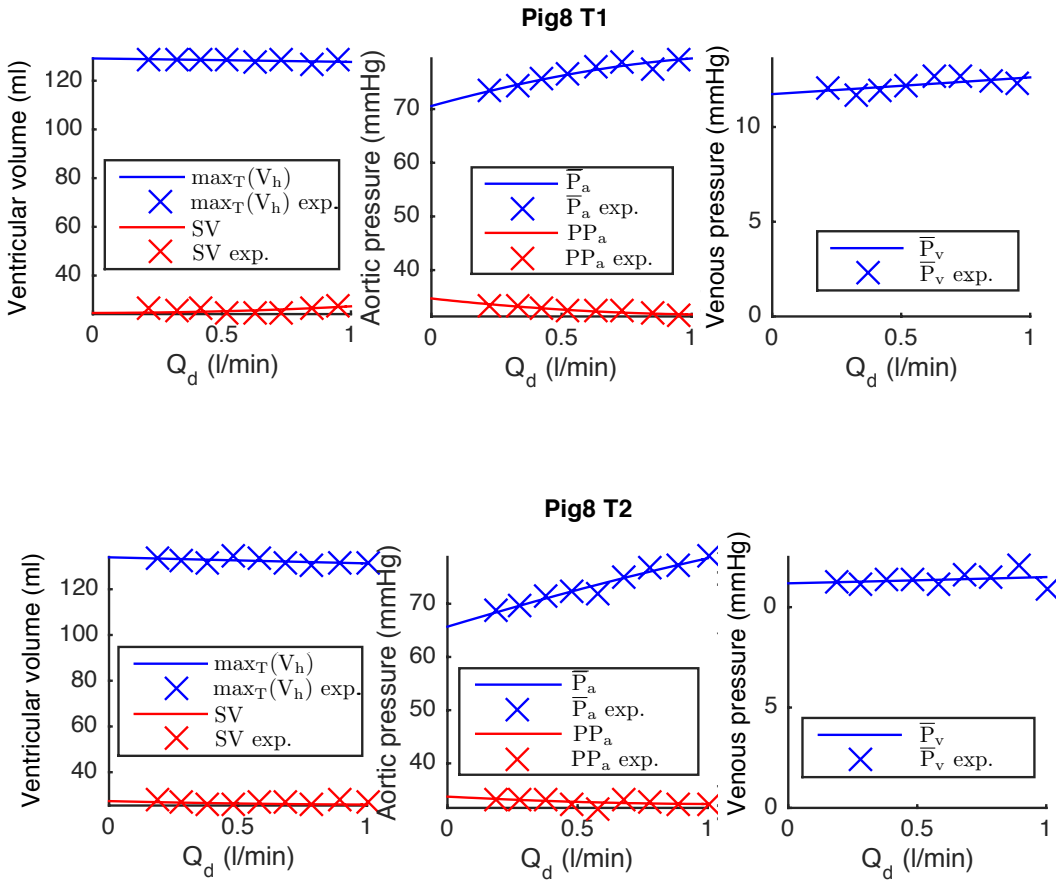

Figure B.5 – Evolution of $\overline{P}_a$, PP_a, $\overline{P}_v$, $\max_T(V_h)$ and SV in terms of different Q_d for the weaning tests Pig8 T1 and Pig8 T2. The solid lines are the simulations obtained with the parameter identification using the measurements related to all Q_d and the crosses are the experimental data.

B.2 Pig experiments with a vv-ECLS

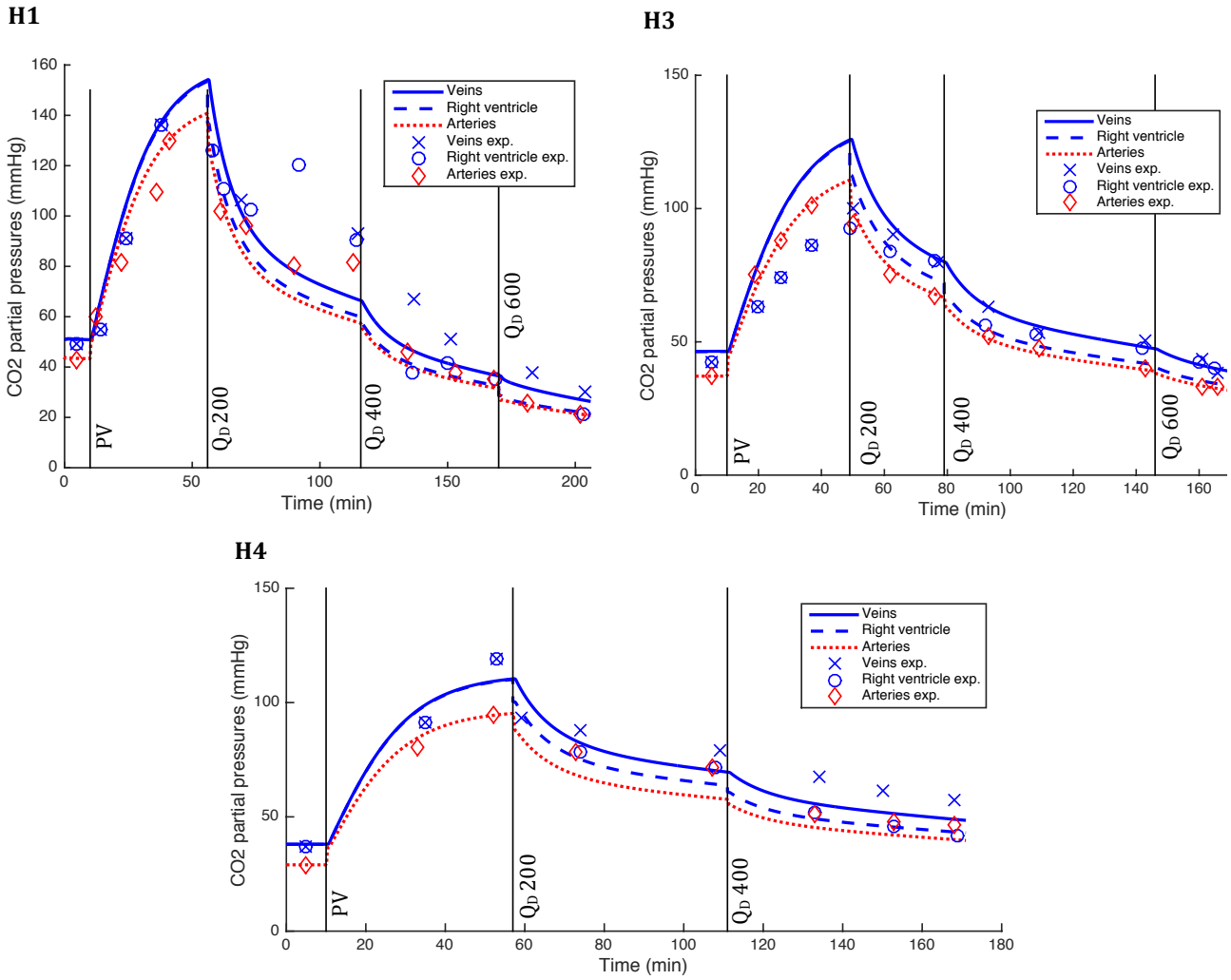

Figure B.6 – Time evolution of calculated (lines) and measured (crosses, circles and diamonds) CO_2 partial pressures in the veins, in the right ventricle and in the arteries for pigs H1, H3 and H4. The labels PV, Q_D 200, Q_D 400 and Q_D 600 mean respectively the start of protective ventilation and blood flow through the $ECCO_2RD$ set to 200, 400 and 600 ml/min.

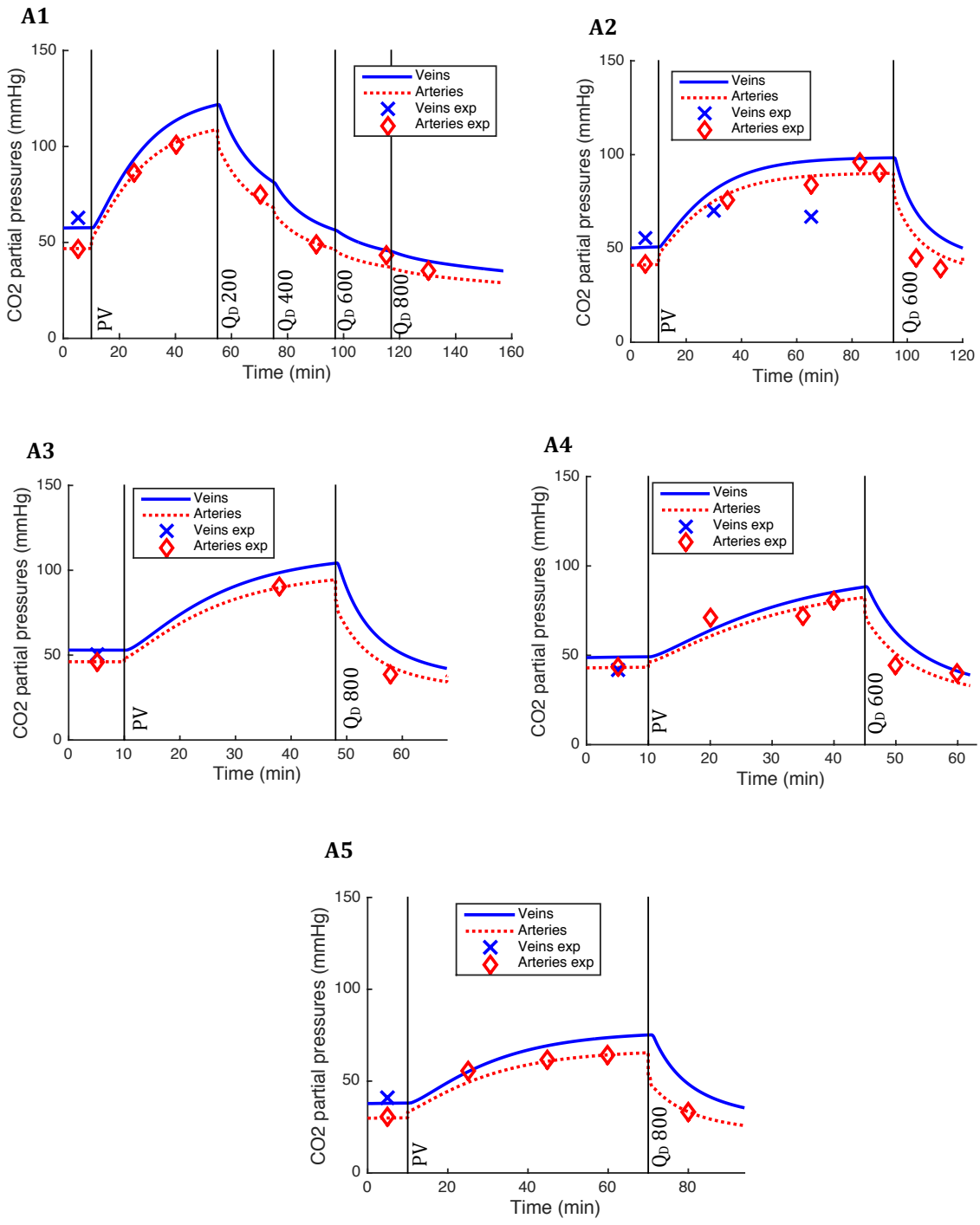

Figure B.7 – Time evolution of calculated (lines) and measured (crosses and diamonds) CO_2 partial pressures in the veins and arteries for pigs A1, A2, A3, A4 and A5. The labels PV, Q_D 200, Q_D 400, Q_D 600 and Q_D 800 mean respectively the start of protective ventilation and blood flow through the ECCO$_2$RD set to 200, 400, 600 and 800 ml/min.

Table B.1 – Identified parameters for *experiments H* (H1 – H4) and *A* (A1 – A6) when transport delays are neglected

	Experiments H ("healthy" pigs)				*Experiments A* (pigs with ARDS)					
Data	H1	H2	H3	H4	A1	A2	A3	A4	A5	A6
	Protective ventilation				**Protective ventilation and ARDS**					
f_s	0.105	0.092	0.081	0.128	0.304	0.436	0.49	0.57	0.409	0.532
$\dot{V}_A$ (l/min)	0.93	1.8	1.695	2.1	1.58	1.92	1.44	1.2	2	2.7

Table B.2 – Errors between the simulations and the measurements during the ECCO$_2$RT for *experiments H* and *A* when transport delays are neglected.

	Experiments H				*Experiments A*						
Data	H1	H2	H3	H4	A1	A2	A3	A4	A5	A6	**Mean** $\pm$ σ
$\overline{\lvert\Delta P_{CO_2}\rvert}$ (mmHg)	13.15 $\pm$ 8.00	10.03 $\pm$ 6.60	6.88 $\pm$ 5.48	7.97 $\pm$ 5.66	5.96	6.03	0.07	5.57	0.79	3.88	**6.03** $\pm$ **3.93**
$\overline{\lvert\Delta P_{CO_2}/P_{CO_2}\rvert}$	0.19 $\pm$ 0.11	0.15 $\pm$ 0.06	0.12 $\pm$ 0.05	0.12 $\pm$ 0.05	0.12	0.14	0.002	0.14	0.02	0.12	**0.11** $\pm$ **0.06**
$\overline{\Delta P_{CO_2}}$ (mmHg)	-13.13 $\pm$ 10.68	-10.03 $\pm$ 5.52	-4.71 $\pm$ 6.29	-6.62 $\pm$ 5.94	-5.96	6.03	-0.07	-5.57	-0.79	3.88	**-3.7** $\pm$ **5.97**
$\overline{\Delta P_{CO_2}/P_{CO_2}}$	-0.19 $\pm$ 0.11	-0.15 $\pm$ 0.06	-0.09 $\pm$ 0.09	-0.11 $\pm$ 0.08	-0.12	0.14	-0.002	-0.14	-0.02	0.12	**-0.06** $\pm$ **0.11**

Table B.3 – Errors between the simulations and the measurements during the $ECCO_2RT$ for *experiments H* and *A* when the cardiac output is equal to 3.21 l/min.

	Experiments H				*Experiments A*						
Data	H1	H2	H3	H4	A1	A2	A3	A4	A5	A6	**Mean** $\pm\ \sigma$
$\overline{\lvert\Delta P_{CO_2}\rvert}$ (mmHg)	13.08 $\pm$ 8.10	10.42 $\pm$ 6.50	6.99 $\pm$ 5.18	7.87 $\pm$ 5.72	5.97	5.26	0.38	5.11	0.07	3.87	**5.90** $\pm$ 4.04
$\overline{\lvert\Delta P_{CO_2}/P_{CO_2}\rvert}$	0.18 $\pm$ 0.11	0.16 $\pm$ 0.06	0.12 $\pm$ 0.05	0.12 $\pm$ 0.05	0.12	0.12	0.01	0.13	0.00	0.12	**0.11** $\pm$ 0.06
$\overline{\Delta P_{CO_2}}$ (mmHg)	-13.03 $\pm$ 10.81	-10.42 $\pm$ 5.55	-4.76 $\pm$ 6.28	-6.29 $\pm$ 6.18	-5.97	5.26	0.38	-4.20	-0.07	3.87	**-3.52** $\pm$ 5.89
$\overline{\Delta P_{CO_2}/P_{CO_2}}$	-0.18 $\pm$ 0.12	-0.16 $\pm$ 0.06	-0.09 $\pm$ 0.09	-0.10 $\pm$ 0.08	-0.12	0.12	0.01	-0.11	0.00	0.12	**-0.05** $\pm$ 0.11

Table B.4 – Errors between the simulations and the measurements during the $ECCO_2RT$ for *experiments H* and *experiments A* when the weigh-based estimation is used for metabolism.

	Experiments H				*Experiments A*					
Data	H1	H2	H3	H4	A1	A2	A3	A4	A6	**Mean** $\pm$ σ
$\overline{\lvert\Delta P_{CO_2}\rvert}$ (mmHg)	10.35 $\pm$ 6.35	7.85 $\pm$ 4.82	5.12 $\pm$ 2.98	6.63 $\pm$ 4.22	3.07	10.04	1.02	11.61	5.93	**6.85** $\pm$ 3.50
$\lvert\overline{\Delta P_{CO_2}/P_{CO_2}}\rvert$	0.17 $\pm$ 0.10	0.12 $\pm$ 0.05	0.08 $\pm$ 0.04	0.10 $\pm$ 0.04	0.05	0.24	0.03	0.27	0.18	0.14 $\pm$ 0.08
$\overline{\Delta P_{CO_2}}$ (mmHg)	-6.31 $\pm$ 11.69	-6.70 $\pm$ 6.79	-1.87 $\pm$ 6.03	-4.66 $\pm$ 5.97	-2.29	10.04	1.02	11.61	5.93	**0.75** $\pm$ 6.91
$\overline{\Delta P_{CO_2}/P_{CO_2}}$	-0.02 $\pm$ 0.20	-0.09 $\pm$ 0.10	-0.02 $\pm$ 0.09	-0.07 $\pm$ 0.08	-0.03	0.24	0.03	0.27	0.18	**0.05** $\pm$ 0.14

B.3 Clinical trials with a va-ECLS

Table B.5 – Values of the 2 coefficients of the linear expressions for each parameter (E_h, SBV, A_h, E_a and R_s) obtained with the parameter identification using the measurements related to all the Q_d.

	Patient1	Patient2	Patient3	Patient4		Patient5		Patient6	
Data	T1	T1	T1	T1	T2	T1	T2	T1	**Mean** $\pm$ σ
Parameter identification									
$E_{0,h}$ (mmHg/ml)	2.84	2.10	1.13	0.91	0.91	2.76	1.94	2.82	**1.93** ±0.85
SBV_0 (ml)	1130	493	834	1092	953	1026	1309	1168	**1001** ±250
$A_{0,h}$ (ml^{-1})	0.050	0.030	0.016	0.027	0.022	0.040	0.034	0.047	**0.033** ±0.012
$E_{0,a}$ (mmHg/ml)	1.80	1.17	1.14	1.18	1.24	1.64	1.94	1.65	**1.47** ±0.32
$R_{0,s}$ (mmHg · s/ml)	1.08	1.37	0.59	0.87	0.81	0.80	0.79	0.43	**0.84** ±0.29
$E_{Sl,h}$ (mmHg · s/ml^2)	-0.012	-0.007	0.000	0.000	-0.003	-0.023	-0.003	-0.002	**-0.006** ±0.008
SBV_{Sl} (s)	-3.540	1.521	-3.597	-4.215	-3.546	-4.334	-4.383	-4.647	**-3.343** ±2.012
$A_{Sl,h}$ (s/ml^2)	-6E-5	2E-5	-5E-5	-1E-4	-1E-4	-2E-4	-6E-5	-8E-5	**-8E-5** ±6E-5
$E_{Sl,a}$ (mmHg · s/ml^2)	0.000	0.038	0.010	0.003	0.004	0.014	0.004	0.007	**0.010** ±0.012
$R_{Sl,s}$ (mmHg · s^2/ml^2)	-0.005	-0.009	0.000	-0.005	-0.003	0.002	-0.003	-0.002	**-0.003** ±0.004

Table B.6 – Errors between the predictions of the mathematical model and the measurements of $\overline{P}_a$, PP_a, $\overline{P}_v$, $\max_{\mathrm{T}}(V_h)$, SV, EF and VTI using the measurements related to all Q_d.

	Patient1	Patient2	Patient3	Patient4		Patient5		Patient6	
Data	T1	T1	T1	T1	T2	T1	T2	T1	**Mean** $\pm\ \sigma$
$\Psi(\mathbf{p}^*)$	910	368	458	526	230	1273	178	453	**549** $\pm$ 367
$\overline{\lvert\Delta PP_a/PP_a\rvert}$	0.035	0.039	0.018	0.012	0.031	0.044	0.009	0.020	**0.026** $\pm$ 0.013
$\overline{\lvert\Delta\overline{P}_a/\overline{P}_a\rvert}$	0.039	0.007	0.024	0.022	0.012	0.024	0.011	0.019	**0.020** $\pm$ 0.010
$\overline{\lvert\Delta\overline{P}_v/\overline{P}_v\rvert}$	0.037	0.127	0.025	0.032	0.061	0.043	0.016	0.050	**0.049** $\pm$ 0.035
$\overline{\left\lvert\frac{\Delta\max_{\mathrm{T}}(V_h)}{\max_{\mathrm{T}}(V_h)}\right\rvert}$	0.003	0.052	0.009	0.042	0.015	0.071	0.036	0.006	**0.029** $\pm$ 0.025
$\overline{\lvert\Delta SV/SV\rvert}$ or $\overline{\lvert\Delta VTI/VTI\rvert}$	0.064	0.033	0.052	0.041	0.022	0.048	0.010	0.030	**0.037** $\pm$ 0.017
$\overline{\lvert\Delta EF/EF\rvert}$	0.062	0.028	0.048	0.079	0.029	0.112	0.034	0.032	**0.053** $\pm$ 0.030
$\overline{\Delta PP_a/PP_a}$	0.009	0.021	0.015	0.011	0.003	0.019	0.006	0.012	**0.012** $\pm$ 0.006
$\overline{\Delta\overline{P}_a/\overline{P}_a}$	0.006	0.002	0.009	0.008	0.000	0.011	0.005	0.006	**0,006** $\pm$ 0,004
$\overline{\Delta\overline{P}_v/\overline{P}_v}$	0,016	0,032	0,016	0,017	0,007	0,018	0,015	0,018	**0,017** $\pm$ 0,007
$\overline{\frac{\Delta\max_{\mathrm{T}}(V_h)}{\max_{\mathrm{T}}(V_h)}}$	0.004	0.011	0.009	0.004	0.003	0.006	0.004	0.005	**0.006** $\pm$ 0.003
$\overline{\Delta SV/SV}$ or $\overline{\Delta VTI/VTI}$	-0.001	0.019	0.010	0.006	0.006	0.012	0.004	0.006	**0.008** $\pm$ 0.006
$\overline{\Delta EF/EF}$	-0.011	0.004	0.001	0.007	0.000	0.017	0.001	0.001	**0.003** $\pm$ 0.008
n	4	4	4	5	4	4	4	6	

B.4 Clinical trials with a vv-ECLS

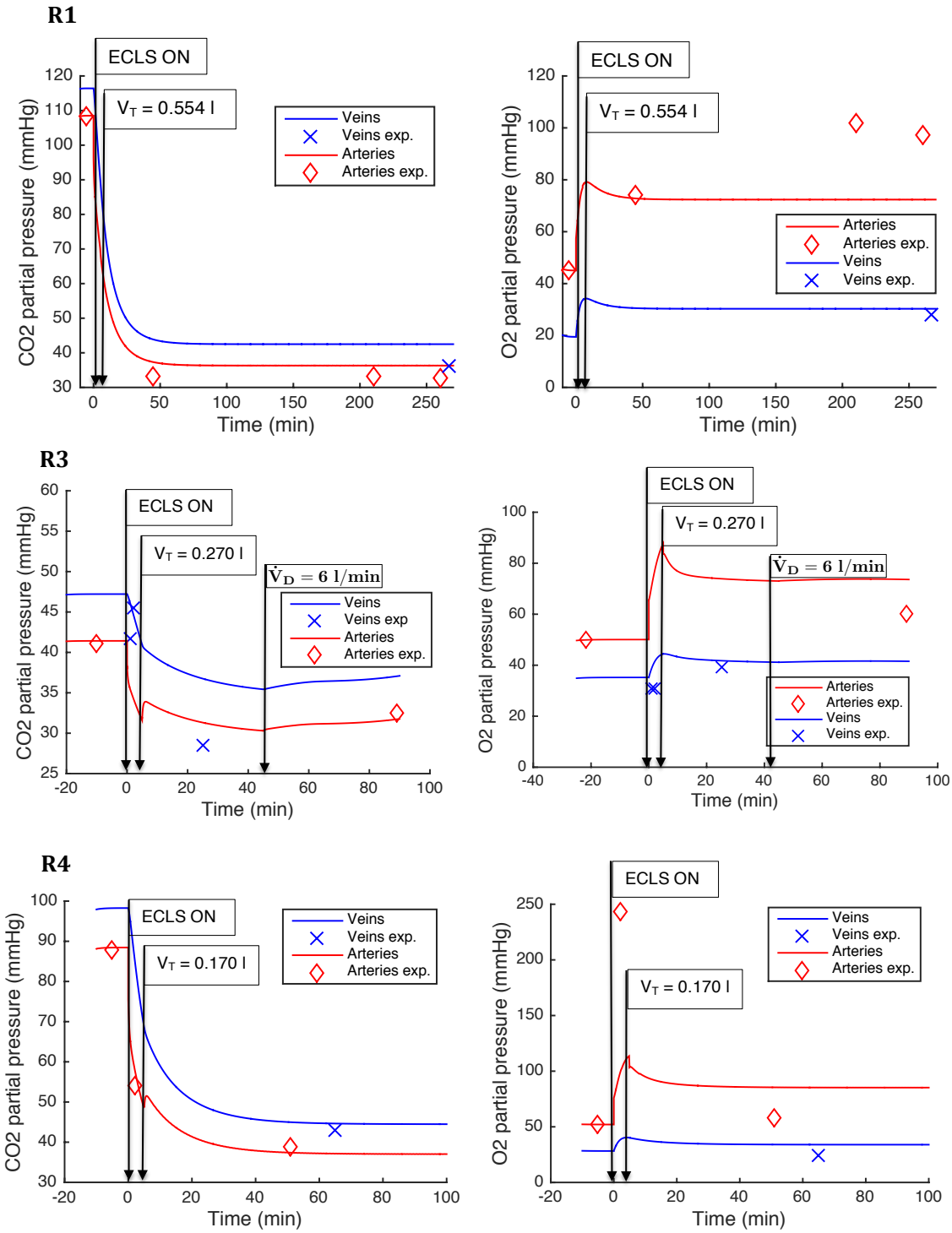

Figure B.8 – Time evolution of calculated (lines) and measured (crosses and diamonds) CO_2 partial pressures in the veins and arteries (left panels) and O_2 partial pressures in the veins and arteries (right panels) for patients R1, R3 and R4. The different phases of observation are delimited by vertical arrows, with the self explaining labels.

Table B.7 – PCO_2 and PO_2 errors between the simulations and the measurements during ECLS for *clinical trial R* and when the dilution is taken into account in our mathematical model. The line m indicates the number of PCO_2 or PO_2 measurements available during ECLST (after the change of ventilator settings).

	CO_2					O_2				
Data	R1	R2	R3	R4	**Mean**	R1	R2	R3	R4	**Mean**
$\overline{\lvert\Delta P\rvert}$ (mmHg)	5.37	4.75	4.25	1.44	**3.95**	18.33	7.50	10.37	20.55	**14.19**
$\overline{\lvert\Delta P/P\rvert}$	0.16	0.09	0.15	0.04	**0.11**	0.20	0.21	0.18	0.44	**0.26**
$\overline{\Delta P}$ (mmHg)	5.37	-4.75	4.25	-0.04	**1.21**	-18.33	7.50	10.37	20.55	**5.02**
$\overline{\Delta P/P}$	0.16	-0.09	0.15	0.00	**0.05**	-0.20	0.21	0.18	0.44	**0.16**
m	4	2	2	2		4	2	2	2	

Table B.8 – PCO_2 and PO_2 errors between the simulations and the measurements during ECLS for *clinical trial S* and when the dilution is taken into account in our mathematical model. The line m indicates the number of PCO_2 or PO_2 measurements available during ECLST.

Data	CO_2	O_2
$\overline{\lvert\Delta P\rvert}$ (mmHg)	1.35 ± 1.24	5.33 ± 4.72
$\overline{\lvert\Delta P/P\rvert}$	0.04 ± 0.03	0.10 ± 0.08
$\overline{\Delta P}$ (mmHg)	0.11 ± 1.89	5.33 ± 4.72
$\overline{\Delta P/P}$	0.00 ± 0.05	0.10 ± 0.08
m	9	9